Electrochemical Society

GLC EXPANDS PRODUCTION WITH GRAPHITE PLANT SERVING WESTERN STATES

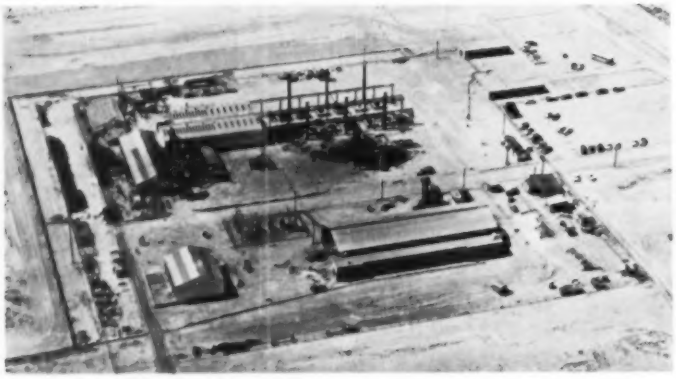

The GLC graphite plant at Antelope Valley, California.

We are glad to inform the electrometallurgical and electrochemical industries in the Western States area that we recently acquired the plant and physical assets of Crescent Carbon Corporation in California.

Carbon and graphite users in the Western States and those overseas in the Pacific area will shortly have a greatly improved source of supply at their command.

Plans now under way at the GLC graphite plant, Antelope Valley, California, call for a substantially increased inventory of electrodes, anodes and mold stock, not only in tonnage but in a variety of shapes and sizes as well. Customers can look forward to faster service on their shipments and to closer cooperation in solving their technical problems.

Technicians from our plants at Niagara Falls, N.Y. and Morganton, N.C. are establishing the most modern production techniques at the Antelope Valley plant, so that its products will meet established GLC standards of quality and uniformity.

As these forward steps are taken, we hope to have the privilege of widening the scope of our service to customers, old and new.

PRODUCTS ELECTRODE GLC DIVISION YOU CAN TRUST ®

GREAT LAKES CARBON CORPORATION

18 EAST 48TH STREET, NEW YORK 17, N. Y.

PACIFIC COAST OFFICE: 671F OAK GROVE AVENUE
MENLO PARK, CALIFORNIA • PHONE: DAVENPORT 3-4152

EDITORIAL STAFF

H. H. Uhlig, Chairman, Publication Committee

Cecil V. King, Editor

Norman Hackerman, Technical Editor

Ruth G. Sterns, Managing Editor

U. B. Thomas, News Editor

H. W. Salzberg, Book Review Editor

Natalie Michalski, Assistant Editor

DIVISIONAL EDITORS

W. C. Vosburgh, Battery

Milton Stern, Corrosion, I

R. T. Foley, Corrosion, II

T. D. Callinan, Electric Insulation

Seymour Senderoff, Electrodeposition

H. C. Froelich, Electronics

Ernest Paskell, Electronics—Semiconductors

Sherlock Swann, Jr., Electro-Organic, I

Stanley Wawzonek, Electro-Organic, II

John M. Blocher, Jr., Electrothermics and Metallurgy, I

A. U. Seybolt, Electrothermics and Metallurgy, II

N. J. Johnson, Industrial Electrolytic

C. W. Tobias, Theoretical Electrochemistry, I

A. J. deBethune, Theoretical Electrochemistry, II

ADVERTISING OFFICE

ECS
1860 Broadway, New York 23, N. Y.

ECS OFFICERS

W. C. Gardiner, President
Olin Mathieson Chemical Corp., Niagara Falls, N. Y.

R. A. Schaefer, Vice-President
The Bunting Brass and Bronze Co., Toledo, Ohio

Henry B. Linford, Vice-President
Columbia University, New York, N. Y.

F. L. LaQue, Vice-President
International Nickel Co., Inc., New York, N. Y.

Lyle I. Gilbertson, Treasurer
Air Reduction Co., Murray Hill, N. J.

I. E. Campbell, Secretary
National Steel Corp., Weirton, W. Va.

Robert K. Shannon, Executive Secretary
National Headquarters, The ECS, 1860 Broadway, New York 23, N. Y.

Manuscripts submitted to the Journal should be sent, in triplicate, to the Editorial Office at 1860 Broadway, New York 23, N. Y. They should conform to the Instructions to Authors, published in this issue, pp. 100C-101C. Manuscripts so submitted become the property of The Electrochemical Society and may not be published elsewhere, in whole or in part unless permission is requested of and granted by the Editor.

Inquiries re positive microfilm copies for volumes should be addressed to University Microfilms, Inc., 313 N. First St., Ann Arbor, Mich.

Journal of the Electrochemical Society

APRIL 1960 **VOL. 107 • NO. 4**

CONTENTS

Editorial

MCA 94C

Technical Papers

The Change in Open-Circuit Potential of the Manganese Dioxide Electrode on Discharge and the Discharge Mechanism. *W. C. Vosburgh and J. H. DeLap* 255

Effect of Adsorption of Polar Organic Compounds on the Reactivity of Steel. *H. F. Finley and N. Hackerman* 259

Mechanism of the Iron-Hydrogen Sulfide Reaction at Elevated Temperatures. *H. Arm, P. Delahay, C. Hudgins, F. Hügli, L. Hulett, and M. Qureshi* 264

Nickel-Aluminum Alloy Coatings Produced by Electrodeposition and Diffusion. *D. E. Couch and J. H. Conor* 272

Effect of Addition Agents on Tungsten Codeposition. *J. S. Sallo and R. D. Fisher* 277

The Mechanism and Efficiency of Electroluminescence in ZnS Phosphors. *F. F. Morehead* 281

Electroluminescence under Pulsed Square Wave Excitation. *R. Zallen, W. T. Eriksen, and H. Ahlburg* 288

Anodization of InSb. *J. D. Venables and R. M. Broudy* 296

Lifetime Preservation in Diffused Silicon. *M. Waldner and L. Sivo* 298

Electrolytic Reduction of Nitro- and Dinitrotetralins. *R. N. Boyd, A. A. Reidlinger, and J. J. Sher* 302

Decomposition of Uranyl Fluoride between 700° and 950°C. *L. M. Ferris and F. G. Baird* 305

Some Properties of Aluminum Nitride. *K. M. Taylor and C. Lenie* 308

Relative Rates of Electromigration of Different Ions of the Same Charge across Permselective Membranes. *R. McClintock, R. Neihof, and K. Sollner* 315

Surface Coverage during Hydrogen and Oxygen Evolution. *P. Rüetschi, J. B. Ockerman, and R. Amlie* 325

A Study of the Factors Affecting the Electrical Characteristics of Sintered Tantalum Anodes. *G. L. Martin, C. J. B. Fincham, and E. E. Chadsey, Jr.* 332

The Growth of Anodic Oxide Films on Germanium. *S. Zwerdling and S. Sheff* 338

Interpretation of Measurements of Potential Decay on Open Circuit. *P. C. Milner* 343

Arsine Evolution and Water Reduction at an Arsenic Cathode. *H. W. Salzberg and B. Goldschmidt* 348

Technical Notes

Creeping Silver Sulfide. *T. F. Egan and A. Mendizza* 353

A New Method for Preparing Hydroxide-Free Alkali Chloride Melts. *D. L. Maricle and D. N. Hume* 354

Brief Communications

Location of Diffused pn-Junctions on Germanium by Electrodeposition of Copper. *R. Glang* 356

Magnetic Gradient at the Surface of Ferromagnetic Substances. *S. Yamaguchi* 357

Overtemperature in Metal Scaling. *D. Caplan* 359

Current Affairs 102C-112C

Published monthly by The Electrochemical Society, Inc., from Manchester, N. H., **Executive Offices, Editorial Office** and **Circulation Dept.,** and **Advertising Office** at 1860 Broadway, New York 23, N. Y., combining the JOURNAL and TRANSACTIONS OF THE ELECTROCHEMICAL SOCIETY. Statements and opinions given in articles and papers in the JOURNAL OF THE ELECTROCHEMICAL SOCIETY are those of the contributors, and The Electrochemical Society assumes no responsibility for them. Nondeductible subscription to members $5.00; subscription to nonmembers $18.00. Single copies $1.25 to members, $1.75 to nonmembers.

Copyright 1960 by The Electrochemical Society, Inc.

Entered as second-class matter at the Post Office at Manchester, N. H., under the act of **August 24, 1912.**

SARGENT

Laboratory Recorders

Designed For Your Specific Laboratory Needs

Model MR

The Model "MR" Recorder

Here is the ultimate in recorders designed exclusively for almost all measurements commonly made in the chemical laboratory. This instrument measures current and voltage and all other quantities which can be transposed into potential or current signals.

The Model "MR" features: 31 Potentiometric Ranges; 9 Chart Speeds, or 27 Chart Speeds with the Sargent Multi-range Attachment; and it is designed for laboratory bench operation.

S-72150 Sargent Recorder
(Pat. Pend.) $1725.00

S-72151 Sargent Recorder
with Multi-Range Attachment, 27 Chart Speeds $1775.00

For complete specifications write for Bulletin R

Model SR

The Model "SR" Recorder

Sargent offers the Model SR to fill the need for a low cost recorder that features: maximum accuracy at a minimum cost; 250 mm width chart; fast balancing speed of 1 second; high sensitivity, high gain amplifier; and square cornering at 10,000 to 50,000 ohms input. This instrument provides the minimum required flexibility at the lowest possible cost.

S-72180 Sargent Recorder
(Pat. Pend.) $675.00

For complete specifications write for Bulletin SR

Designed and Manufactured by E. H. Sargent & Co.

SARGENT SCIENTIFIC LABORATORY INSTRUMENTS • APPARATUS • SUPPLIES • CHEMICALS

E. H. SARGENT & CO., 4647 W. FOSTER, CHICAGO 30, ILLINOIS
DETROIT 4, MICH. • DALLAS 35, TEXAS • BIRMINGHAM 4, ALA. • SPRINGFIELD, N. J.

how do you look at ANODES?

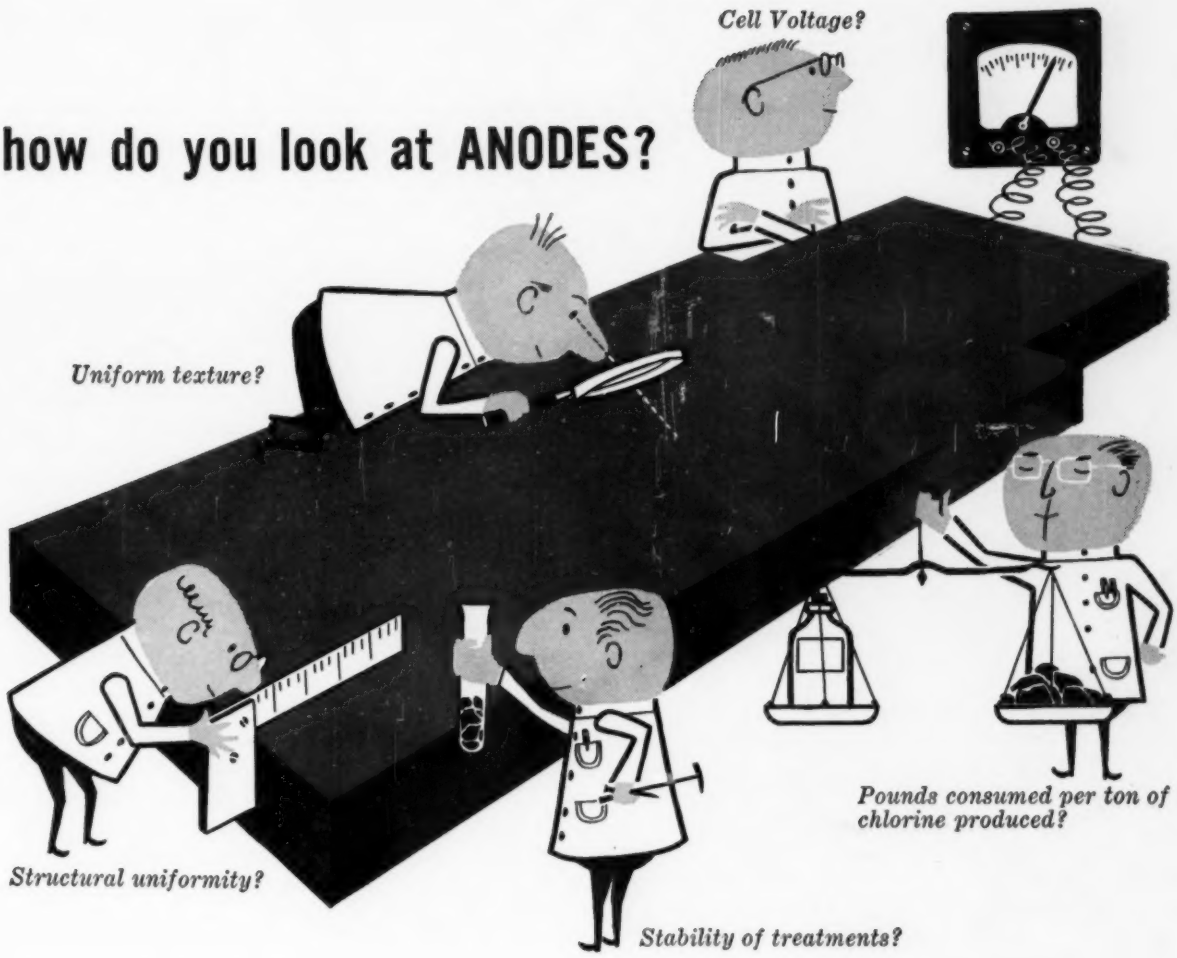

Judged by Cell Maintenance Costs Alone,

the highly stable impregnants used in Stackpole GraphAnode reduce diaphragm clogging to a bare minimum. The graphite is consumed slowly and evenly. Because GraphAnode anodes present uniform, low-porosity surfaces to the electrolyte, the graphite does not slough off to clog the diaphragm or to contaminate the cell.

Judged by Anode Cost and Performance,

Stackpole GraphAnode proves second to none whether you figure in terms of anode life, or in tons of chlorine produced per pound of graphite consumed. You get maximum anode life . . . and with the added advantage of low cell voltages. Stackpole engineers stand ready to offer a convincing demonstration on your equipment.

Stackpole Carbon Company, St. Marys, Pa.

STACKPOLE
GraphAnode®

ELECTROCHEMICAL ANODES FOR DIAPHRAGM, MERCURY, MANGANESE DIOXIDE, & SODIUM CHLORATE CELLS. OTHER TYPES FOR CATHODIC PICKLING, ALUMINUM ANODIZING, AND OTHER USES.

CATHODIC PROTECTION ANODES • FLUXING & DE-GASSING TUBES • SALT BATH RECTIFICATION RODS • ROCKET NOZZLES • RISER RODS • GRAPHITE BEARINGS & SEAL RINGS • ELECTRODES & HEATING ELEMENTS • WELDING CARBONS • VOLTAGE REGULATOR DISCS • "CERAMAGNET"® CERAMIC MAGNETS • ELECTRICAL CONTACTS • BRUSHES for all rotating electrical equipment • and many other carbon, graphite and electronic components.

Editorial

MCA

THE Manufacturing Chemists' Association was founded in 1872 and is the oldest chemical trade organization in the Americas. The principal product of its 17 charter members was sulfuric acid. MCA now has some 177 members in the United States and Canada, representing more than 90% of the chemical industry's production. About half of the membership falls under the U. S. Department of Commerce official category of small business.

The Association's name is seen very frequently in the trade literature and also in the daily press. It is worth while to learn something about an organization of such obvious importance in the chemical industry and, thus, directly or indirectly in the daily life of everyone. Helpful in this direction is "The Chemical Industry Facts Book," published each two years since 1953 by the Association. The fourth edition, published in late 1959 for 1960-1961,[1] contains a wealth of information concerning the nature of the chemical industry; its position in the national economy; its plants, workers, finances, interest in research, development, expansion; and in what respects it is concerned with food, agriculture, clothing, shelter, health, transportation, communications, national defense, chemical and nuclear energy, space flight technology. The book is written in nontechnical language and gives few details; it constitutes a quick and broad survey.

According to the *Facts Book*, there are some 12,500 chemical plants in the United States, and the annual expenditure for new facilities exceeds $1,000,000,000. The industry employs 846,400 workers, of whom 79,200 are scientists and engineers. Of the latter group, about 24,200 are engaged in research and developmental work.

MCA is an extremely active organization whose primary objective is to foster an economic and political climate in which its member firms can prosper. It has some 27 committees which assist a permanent staff of 50 to implement specific programs. Activities range from preparing educational material in science to fighting against any increase in minimum wages required on government contracts (although 90% of chemical workers earn much more than the present minimum).

In the course of its normal activities, the Association has found it both necessary and profitable to make thorough inquiry into methods of protecting the health and safety of chemical workers and all who have contact with chemical products. Its General Safety Committee and its committees on safe packaging and transportation, on precautionary labeling, and on air and water pollution abatement, play important roles in both private and public welfare.

The Association maintains an aid-to-education program designed to improve the teaching of science, to familiarize the public with the nature of the chemical industry, and eventually to attract more qualified workers. An annual "College Chemistry Teacher Awards Program" is conducted. Films showing laboratory experiments, and a variety of literature, are made available. Fundamental research is sponsored at several institutions.

The *Facts Book* is not infallible in its information: The Electrochemical Society is given an address which it left many years ago.

—CVK

[1] Available from Manufacturing Chemists' Association, Inc., 1825 Connecticut Ave., N.W., Washington 9, D. C. Paper bound, 363 pages; $1.25.

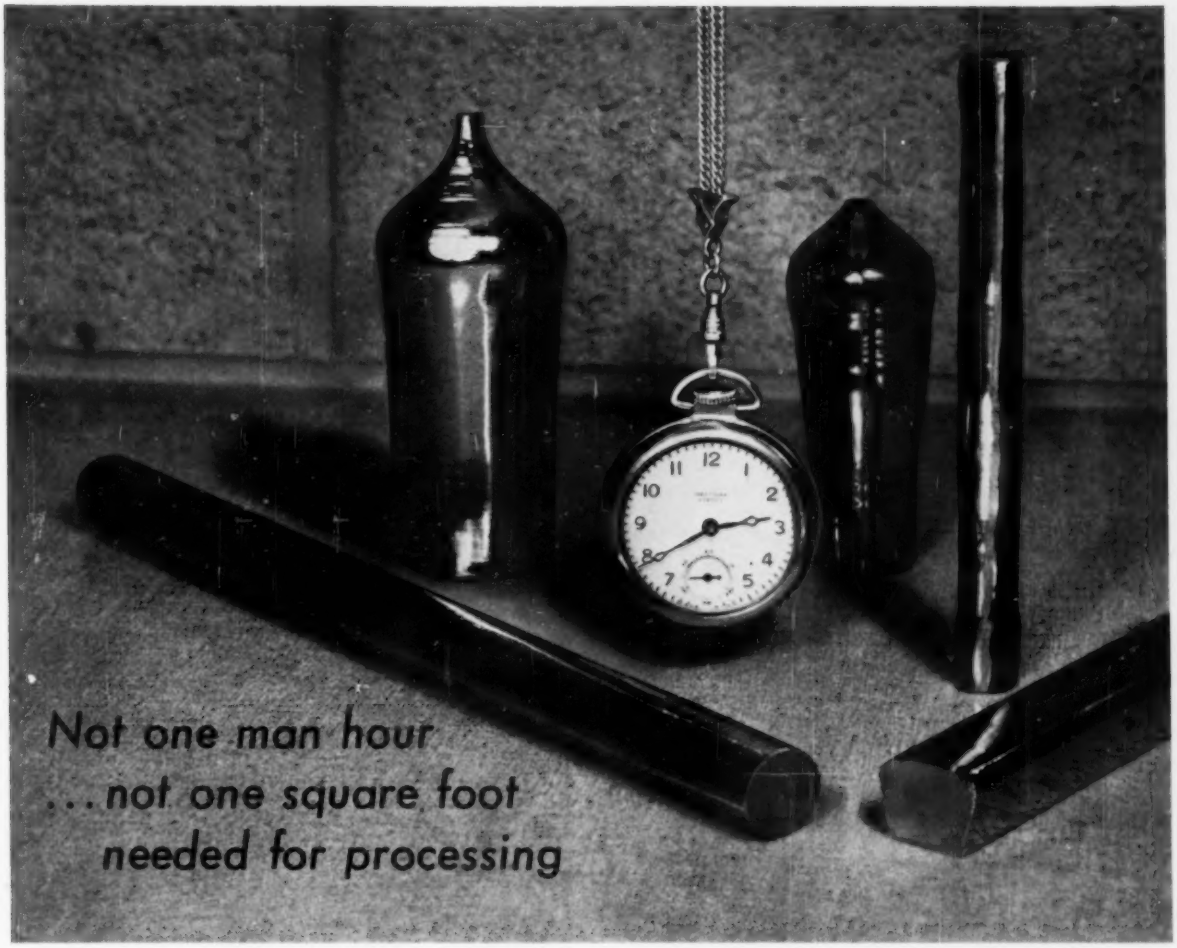

Now Sylvania grows germanium and silicon doped single crystals for you!

Now device makers can concentrate completely on device making! Sylvania grows germanium and silicon single crystals to your most exacting specifications. You not only get a guaranteed quality material ready to use; you're freed of many manpower, space and time problems. You're freed of the cost and trouble of buying and maintaining special equipment, training manpower, and handling scrap. And you can take full advantage of the engineering excellence of the Sylvania staff!

Germanium single crystals are prepared by either the Czochralski or horizontal techniques. Silicon single crystals are produced by both the float zoning and Czochralski methods.

Single crystal slices of either material are also available.

Resistivity, conductivity type, orientation, lifetime, dislocation density, and size are controlled to meet your requirements.

Sylvania know-how makes these crystals available to you at prices that are predictable and attractive. For details, write to the Chemical & Metallurgical Division, Sylvania Electric Products Inc., Towanda, Pennsylvania.

SYLVANIA

Subsidiary of **GENERAL TELEPHONE & ELECTRONICS**

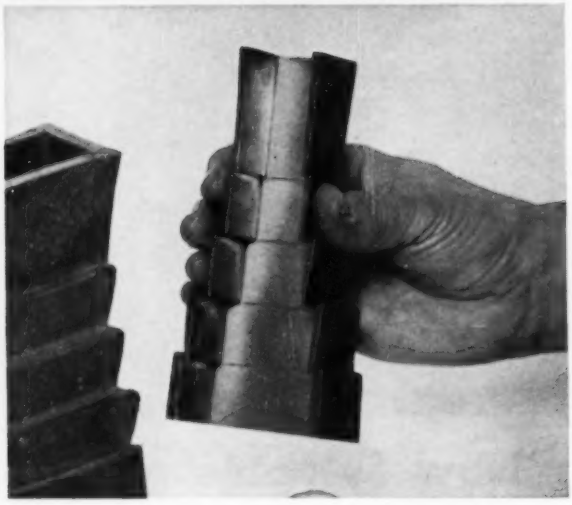

In electrotyping, plating rotogravure rolls, electroforming, "Plus-4" Copper Anodes cut plating costs

ELECTROTYPERS have discovered that, in addition to eliminating the use of bags and diaphragms, they can place "Plus-4" (Phosphorized Copper) Anodes closer to the cathodes to speed up the plating cycle 30% or more with the same power input — and still obtain a smooth deposit. As an alternate, power can be reduced by one-third with an equal reduction in resistance and generation of heat to obtain finished electros in the same plating time. This is an important advantage when thermoplastic plates or molds are used and tanks must run no higher than 95F.

MAKERS OF ROTOGRAVURE ROLLS have found that "Plus-4" Anodes provide a much finer, smoother surface for polishing and etching, and retain the quality of the light tones in runs of over one million impressions on a single set of design cylinders.

In addition, they report significant reductions in cost. One publisher found that he produces superior rolls with less labor and a reduction of 18 to 20% for materials required in the plating process. Another reports he gets a dividend of eight extra rolls for each tank load of "Plus-4" Anodes. And still another has found a 15% saving in over-all costs.

IN ELECTROFORMING operations, "Plus-4" Anodes — by eliminating the most prevalent acid-copper plating difficulties — have made it practical to produce many new products. Their ability to provide a smooth, dense deposit relatively free from growths and blemishes made possible relatively thick shells for molds used in making rubber and plastic articles, and in intricate precision parts for electronic use. Electroformers report operating economies similar to those found in the graphic arts field.

WRITE FOR INFORMATION on how you can obtain a test quantity to supply one tank. Address: The American Brass Company, Waterbury 20, Conn. In Canada: Anaconda American Brass, Ltd., New Toronto, Toronto 14, Ontario. 59106

ANACONDA®

"PLUS-4"® ANODES Phosphorized Copper

Made by The American Brass Company

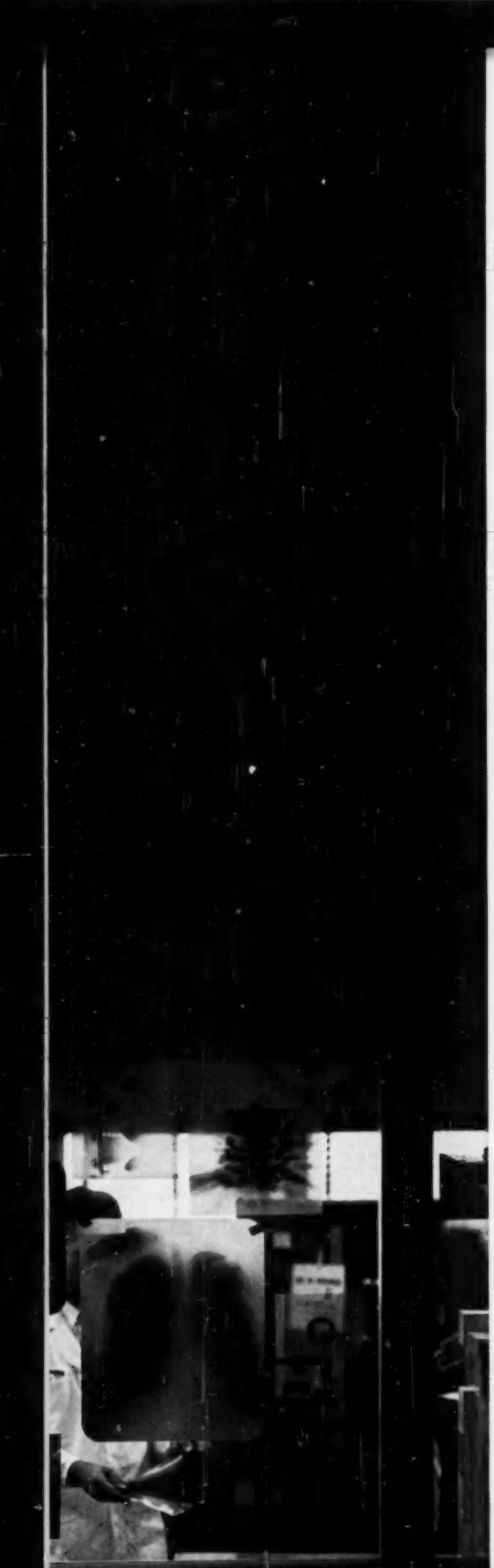

One of a series

Payoff in portable photons

Samarium-145, Samarium-153, Gadolinium-153.
Scientists at the General Motors Research Laboratories began three years ago to measure and re-evaluate the nuclear characteristics of these rare earth isotopes – their half-lives, photon emissions, thermal neutron cross sections.

Conclusion: the radioisotopes had attractive possibilities in industrial and medical radiography, emitting almost pure gamma rays or X-rays (photons) in the low energy range of 30 to 100 kev.

The transition from research to hardware came through two key developments. First, cermet pellets were fabricated using only a few milligrams of the rare earth oxides. Then the irradiated pellets were packaged in special bullet-size holders.

The resulting small, sealed radiographic sources are now being field and laboratory tested. Two excellent applications: "inside-out" checks of hollow shapes inaccessible to X-ray tubes, and radiography of thin steel sections and low density materials such as aluminum or human bone. For example, a recent medical milestone was a chest radiograph of a living person made with a Sm^{153} source. The portable exposure unit to shield the source weighed only 18 pounds.

This isotope radiography program is but one example of the work underway in GM Research's modern isotope laboratory – work that means, through science, "more and better things for more people."

General Motors Research Laboratories
Warren, Michigan

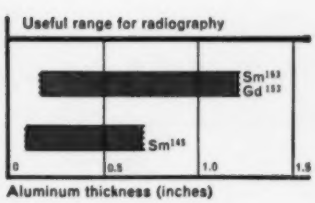

Sm^{153} exposure unit.

Wiley BOOKS

MECHANICAL PROPERTIES OF INTERMETALLIC COMPOUNDS

A Symposium, Sponsored by the Electrothermics and Metallurgy Division of The Electrochemical Society, Inc.

Edited by J. H. Westbrook, *Metallurgist, General Electric Research Laboratory*

The first and only *explicit* treatment of this increasingly important subject to be presented in a single volume. It ranges across the entire field, and includes phenomenology of the mechanical behavior of intermetallics, theoretical and experimental investigations of particular properties, experimental techniques for the preparation and study of intermetallics, and a valuable and timely review of the current literature.

MAKING THIS BOOK OUTSTANDING

1. Gives the only explicit treatment in book form
2. Provides an extremely broad coverage
3. Represents work of the world's leading researchers, including among others, papers by Russians, Japanese, Germans, and British.

1959. 435 pages. $9.50

The Latest Volume—1957 Issue—**SEMICONDUCTOR ABSTRACTS**

Abstracts of the Literature on Semiconducting and Luminescent Materials and Their Applications

Compiled by the Battelle Memorial Institute and sponsored by The Electrochemical Society, Inc. Edited by C. S. Peet.

This volume includes abstracts of the latest information, arranged in four principal divisions. These are elemental semiconductors, compound semiconductors, theory, and general applications. Space precludes a listing of the contents, so it would be best to send for your on-approval copy. Suffice to say that this latest volume is the most inclusive of all the previous books. *1960. 449 pages. In press.*

PROPERTY MEASUREMENTS AT HIGH TEMPERATURES

By W. D. Kingery, *M.I.T.* The first book to cover thoroughly materials and measurements of properties above 1400°C (2550°F). It will be of equal value to researchers, development engineers, and users of materials that must withstand high temperatures. *1959. 416 pages. $16.50*

KINETICS OF HIGH-TEMPERATURE PROCESSES

Edited by W. D. Kingery, *M.I.T.* Covers high-temperature processes in general, and non-metal systems in particular. This book will be a great help in applying these data to actual systems that are often extremely complex. *A Technology Press Book, M.I.T. 1959. 326 pages. $13.50*

STRUCTURE AND PROPERTIES OF THIN FILMS

Edited by Constantine A. Neugebauer, John B. Newkirk, *and* David A. Vermilyea, *all of General Electric Research Laboratory.* The complete record of a recent international conference. It reviews the preparation, growth, and structure of thin films and their mechanical, electrical, optical, and magnetic properties—and their chemical processes at the metal surface. It also includes reports of current research and a transcript of the discussions. *1959. 561 pages. $15.00*

SEND NOW FOR YOUR ON-APPROVAL COPIES

JOHN WILEY & SONS, Inc. 440 PARK AVENUE SOUTH, NEW YORK 16, N.Y.

The Change in Open-Circuit Potential of the Manganese Dioxide Electrode on Discharge and the Discharge Mechanism

W. C. Vosburgh and James H. DeLap

Department of Chemistry, Duke University, Durham, North Carolina

ABSTRACT

Discharge of electrodeposited MnO_2 electrodes for successive short periods at *p*H 8, with time for reattainment of equilibrium, shows that the potential of partially discharged MnO_2 is a linear function of the amount of lower oxide formed over part of the discharge. With this relationship, some previous data on the overpotential of MnO_2 in acid electrolytes are interpreted more simply than before in terms of the discharge mechanism previously proposed. The overpotential is shown to be a linear function of the square root of the current density.

In previous attempts to measure the change in open-circuit potential of the MnO_2 electrode as the result of discharge, the time allowed for recovery from polarization was insufficient (1, 2). This was suspected at the time, but a compensating slow decrease in potential made longer times of doubtful value. The metal anode used in the discharge was probably responsible for much of the decrease (3), and in the present investigation this source of error was avoided. After a small discharge the potential increased for 4 to 40 days, depending on how much the electrode had been discharged previously. The final, nearly constant potential was an approximately linear function of the amount of discharge over the first quarter of the total capacity. The interpretation of some overpotential measurements with acid electrolytes (4) has been reconsidered in the light of this result.

Experimental

Electrodes.—MnO_2 was electrodeposited on graphite rods from a bath of 0.33M $MnSO_4$ and 0.67M H_2SO_4, or from a similar bath containing also 0.3M $(NH_4)_2SO_4$ at 90°C (1, 2, 5). The graphite rods were of 0.48 cm diameter and were covered for a length of 5.1 to 5.2 cm, and on one end, with MnO_2, giving an apparent area of 8 cm^2. Much of the bare portion of the rod was covered with glass sealed to the graphite by glyptal cement for protection from the electrolyte. The current in the electrodeposition was 25 ma (3.13 ma/cm^2) and the time 30 min, giving about 0.2 millimole of MnO_2. The MnO_2 formed in the bath without $(NH_4)_2SO_4$ was probably γ-MnO_2 (6). That deposited in the presence of $(NH_4)_2SO_4$ has been shown to differ in discharge characteristics from γ-MnO_2 (5) and was probably largely α-MnO_2.

After electrodeposition, the electrodes were washed by allowing them to stand in test tubes of 0.01M $(NH_4)_2SO_4$ acidified to *p*H 4.5, this solution being changed daily. Washing was continued until a test for Mn^{++} in the wash solution by oxidation to MnO_4^- with KIO_4 was negative. This usually required 2 to 3 weeks. Each electrode was then immersed in an electrolyte of 1M $(NH_4)_2SO_4$ buffered at *p*H 8 by NH_3. This portion of electrolyte was contained in a 125-ml bottle fitted with a rubber stopper bearing the electrode. By means of a ground-glass joint the electrode was mounted in the stopper in such a way that it could be transferred easily to and from a discharge cell. The stopper also had a hole for the salt-bridge of a saturated calomel electrode, and all of the important potential measurements were made with the electrode in the bottle. Measurements in the discharge cell were used for control only. New electrodes were kept in the bottles with frequent measurements until the potential was decreasing only very slowly; this period was about two weeks usually. The final potential attained was taken as the initial potential of the discharge curve.

Electrodes standing in electrolyte decreased more or less rapidly for a few days and then attained a steady rate of decrease of about 0.1 mv a day which was the same for all electrodes. Although γ- and α-MnO_2 electrodes had nearly the same potential at first, the α-MnO_2 electrodes decreased more rapidly initially and for a longer time, about 10 days. Thereafter the potential was around 70 mv lower than the γ-MnO_2 electrodes, but the slow decrease was at the same rate.

Discharge and subsequent potential measurements.—Tests showed that an electrode could be transferred from one bottle of electrolyte to another of the same electrolyte with no appreciable change in potential. It was concluded that removal of an electrode for discharge and returning it to the same bottle would have no effect other than that of the discharge. It was observed that removal to a discharge cell equipped with 8 graphite rods to act as the anode usually caused a small decrease in potential. The change indicated was considered negligible in comparison with the discharge.

The discharge cell contained about 250 ml of the 1M $(NH_4)_2SO_4$ electrolyte, *p*H 8. The electrode was placed centrally in the cell and was surrounded by 8 graphite electrodes connected together, which formed the anode. A calomel electrode allowed measurement of the changing potential during discharge by a recording potentiometer. A current of 2

Table I. Temperature coefficients of electrodeposited MnO_2 electrodes measured against S.C.E. at 10° to 35°C

Electrode	$\Delta E/\Delta t$, mv/deg C	
	pH 5	pH 8
γ-MnO_2 undischarged	0.07	0.50
γ-MnO_2 discharged 60 ma-min	0.15	0.58
α-MnO_2 undischarged	0.14	0.61
α-MnO_2 discharged 60 ma-min	0.16	0.58

ma from an outside source was passed for the discharge and was regulated by hand.

For discharge an electrode was given a final measurement in the storage bottle and transferred to the discharge cell. A current of 2 ma was passed for a measured time, usually 5 or 10 min. Then the electrode was transferred back to the storage bottle and measured occasionally against a saturated calomel electrode until the potential was increasing less than 1 mv a day. After the first discharge of a new electrode about 4 days was required. In later discharges the times required increased with the amount of total discharge to as much as 40 days. Electrodes of α-MnO_2 required more time than those of γ-MnO_2. All measurements were made at room temperature (in the vicinity of 25°C), and corrections made when necessary for both temperature and pH changes.

Temperature and pH corrections.—For the temperature corrections electrodes in bottles were measured at intervals from 10° to 35°C against a calomel electrode, with about 48 hr allowed at each temperature for the attainment of constancy. In addition to the pH 8 measurements some were made with a 1M $(NH_4)_2SO_4$ electrolyte buffered at pH 5 with pyridine and pyridinium sulfate. The changes in potential per degree are shown in Table I. These are averages for two electrodes which agreed within 0.03 mv/degree at pH 5 and 0.05 mv/degree at pH 8.

The change of potential with pH was determined by transfer of a number of electrodes from one electrolyte to another and measuring after equilibrium was attained. The average change was close to the theoretical 59 mv/pH unit at 25°C.

Test for Mn^{++}.—The solutions in the bottles were tested for Mn^{++} when the electrodes had come to equilibrium. The solution tested was replaced by a fresh portion of electrolyte in the bottle for the next discharge.

Results

The discharge curves determined as above are shown in Fig. 1. The more important are the curves for γ-MnO_2. The solid straight lines are shown to represent the discharges from 10 to 60 ma-min for three electrodes quite well. For a fourth electrode (not shown) which required longer preliminary washing than the others, the first 40 ma-min of discharge was straight. The dashed lines indicate deviations from the straight lines in the first discharge period and after 60 ma-min. No Mn^{++} was found in the electrolytes in which these electrodes were stored for recovery during the first 100 ma-min of discharge. After that an average of 0.12 mg/20 ma-min of discharge was found. Previously (7) in continuous discharges at pH 8 no Mn^{++} was found in the discharge cell until after 150 ma-min.

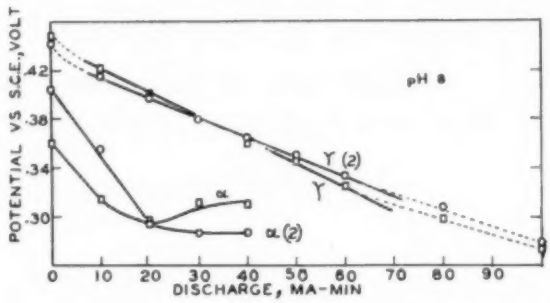

Fig. 1. Variation of equilibrium open-circuit potential with amount of discharge in electrolyte of pH 8; α- and γ-MnO_2. Circles represent averages for two electrodes.

The straight lines for γ-MnO_2 at pH 8 indicate that over a certain portion of the discharge the electrode potential decreases linearly with the increase in lower oxide formed. Deviations from linearity are found at the beginning and below a potential of 0.34 v against the saturated calomel electrode. Within the linear range no Mn^{++} is found in solution, and the entire reduction product remains on the electrode. During the recovery process the product, which is probably formed mainly in the outer portion of the MnO_2 (8, 9), appears to become distributed more uniformly. Even though this process may not have been entirely complete at the time of the final measurements, the amount of product in the surface layer must have been approximately proportional to the total product formed. It has been assumed previously that the electrode potential is determined in part by the composition of the surface layer, but it was thought that the relationship was logarithmic and similar to the Nernst equation (4). The present results indicate a linear relationship over a limited range of compositions. A similar linear relationship is apparent in the data of Kozawa (10) especially in his Fig. 7 showing the decrease in electrode potential when MnO_2 is reduced with varying amounts of Mn^{++}. Ruetschi, Angstadt, and Cahan (11) showed that there is a linear relationship between the potential of a PbO_2 electrode and the surface concentration of adsorbed oxygen.

The formation of Mn^{++} in solution during the later recovery periods (beyond 100 ma-min) after removal of the electrode to another container, does not seem to be in accord with the discharge mechanism proposed by Cahoon and co-workers (12, 13).

In the discharge of α-MnO_2 at pH 8 no Mn^{++} was found for the first 20 ma-min and the potential decreased more rapidly than for γ-MnO_2. The discharge reaction evidently does not penetrate as deeply in α-MnO_2 as in γ-MnO_2, giving a more rapid change in surface composition.

Discussion

The recovery curve.—The straight-line relation between electrode potential and discharge time over a limited range, as shown in Fig. 1, suggests a revision in the interpretation of some previous data (4). It was assumed previously that the electrode

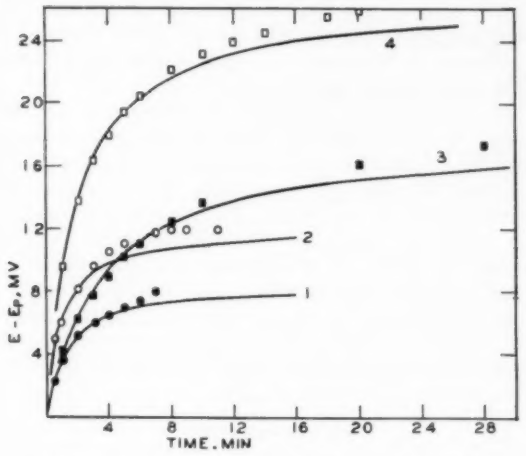

Fig. 2. Decay of polarization in acid electrolytes.

potential is related to the composition of the MnO_2 surface by a logarithmic relation of the form of the Nernst equation (4, 10).

In the discharge of electrolytic MnO_2 electrodes in H_2SO_4 solution containing $MnSO_4$ (4) the potential first decreases, then passes through a minimum and rises to a constant value, indicating a steady state of polarization. The steady state was ascribed to a balance between the lower oxide formed and that dissolved by the electrolyte per time unit. On breaking the circuit a relatively slow rise to a constant open-circuit potential takes place, as shown in Fig. 2.

The amount of polarization shown in Table II of the previous paper (4) was in all cases less than 60 mv, whereas the straight line portions of the γ curves in Fig. 1 extend over about 100 mv. Therefore, a linear relationship between the composition of the surface and the electrode potential may be expected to hold for the polarization in acid electrolytes.

Let E be the variable electrode potential during recovery from polarization, E_c the constant open-circuit potential after recovery, and E_p the closed-circuit potential in the steady state of polarization. If the iR drop and solution concentration polarization are negligible, E_p is also the open-circuit potential at the instant of breaking the circuit. Following the suggestion of Fig. 1, we may write

$$\Delta E = -k' \Delta L \qquad [1]$$

with L defined as a measure of the amount of discharge of product in the electrode surface. It may be somewhat approximate to apply this to the recovery process since the linear relationship may not hold all the way to E_c. However, we shall assume its validity and consider that $L = 0$ when $E = E_c$ which also is an approximation when the solution contains Mn^{++}. Then for the recovery process,

$$E_c - E = k' L \qquad [2]$$

The assumptions made previously that the primary discharge product is a Mn(III) oxide or hydroxide (for which we shall use the formula MnOOH), that the recovery reaction is a disproportionation as in Eq. [3] and that this reaction is rate-controlling are retained. We may add the newer concept that the lower oxide is formed both on and below the surface of the MnO_2 (8).

$$2MnOOH + 2H^+ = Mn^{++} + MnO_2 + 2H_2O \qquad [3]$$

For the velocity of this reaction at constant H^+ concentration we may write

$$-dL/dt = k'' L^2 \qquad [4]$$

This may be somewhat too simple because of the neglect of a reverse reaction, but it seems sufficient for testing the theory. Integration and evaluation of the constant for the condition $L = L_p$ when $t = 0$ gives

$$1/L - 1/L_p = k'' t \qquad [5]$$

with L_p standing for the concentration of product in the surface in the steady state of polarization. Combination of Eq. [2] and [5] gives

$$1/(E_c - E) - 1/(E_c - E_p) = k_1 t \qquad [6]$$

in which $k_1 = k''/k'$.

Equation [6] can be tested by recalculation of the data presented in Fig. 4 and 5 of Yoshiza and Vosburgh (4). Figure 2 gives the results of such a calculation. Curves 1, 2, and 4 represent the same data as the two lower curves of (4): Fig. 4 and the higher of Fig. 5, respectively. Curve 3 represents a different experiment from the lower curve of (4): Fig. 5, but carried out under the same conditions. The lines in Fig. 2 were calculated by Eq. [6] using the experimental values for E_c and E_p and an arbitrary value of k_1 determined for each curve from some of the experimental points. The experimental points shown were taken from recorder curves for the recovery process.

The agreement of the earlier experimental points with the calculated curves is good. The later points deviate from the curves in the direction of too rapid increase in E. It was pointed out above that the equation might not be exact when $E_c - E$ is small. The agreement of the calculated lines and the experimental points is better in curves 3 and 4 than in the corresponding curves of (4): Fig. 5. Curve 2 is not as good as the corresponding one in (4): Fig. 4, but curve 1 may be considered about equal to the lowest (4): Fig. 4 curve, since the earlier points in the latter are not on the curve.

Relation between overpotential and current.—A better test of the above theory is in the relation between overpotential and current in discharges in acid solution. The steady state of polarization in acid electrolytes is enough different from the equilibrium state of the electrode so that Eq. [2] should be a better approximation than for the recovery process.

For the MnO_2 electrode the overpotential has been defined as the difference between the equilibrium open-circuit potential after a discharge and the potential of the steady state of polarization (14). In acid electrolytes the overpotential is not a linear function of the logarithm of the current density (4).

In the steady state of polarization the rate at which lower oxide is formed, $i/\mathbf{F}$ equivalents/sec, can be set equal to the rate at which it is removed

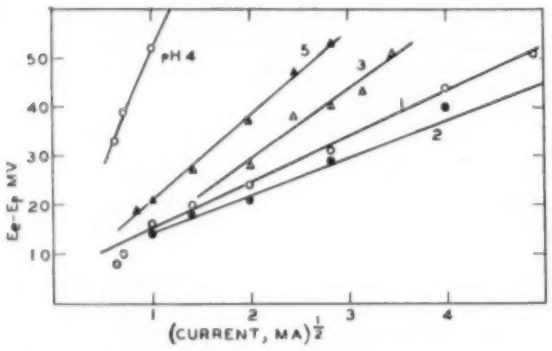

Fig. 3. Overpotential, E_e-E_p, plotted against the square root of the current. Numbers refer to electrolyte compositions (Ref. 4); 1, 1M H_2SO_4; 2, 0.5M; 3, 0.1M; 5, 0.01M; all 0.1M $MnSO_4$. Electrolyte pH 4, acetate buffer and no $MnSO_4$.

from the surface. According to Eq. [4] and the definition of L_p the rate of removal should be equal to $k''L_p^2$. Then

$$i = \mathbf{F}\, k''\, L_p^2 \qquad [7]$$

Combining with Eq. 2 when $E = E_p$ and $L = L_p$

$$i = \mathbf{F}\, k''(E_e - E_p)^2/(k')^2$$

$$E_e - E_p = k_2\, i^{1/2} \qquad [8]$$

Equation [8] predicts a linear relationship between overpotential, $E_e - E_p$, and $i^{1/2}$. Figure 3 shows that this is true over the entire range of currents tried by Yoshizawa and Vosburgh (4). Four different electrolytes, Nos. 1, 2, 3, and 5, give satisfactory straight lines within the limits of error. There was insufficient data for electrolyte 4. An electrolyte of pH 4 gave a slightly curved line. Some of the overpotentials for this electrolyte (not shown in Fig. 3) were so large that the validity of Eq. [1] might be questioned. The data plotted are from (4): Tables II and III.

According to Eq. [8] the lines of Fig. 3 should pass through the origin. However, most of them would pass above the origin, if extended. A constant term in Eq. [8] would be needed to express them. The points of lowest overpotential for the most acid solution in Fig. 3 deviate from the line in the direction to approach $\Delta E_e = 0$ at $i = 0$. This may be connected with the breakdown of the linear relationship between E and oxide composition when the lower oxide component is small.

The data on the growth of polarization of the previous paper have not been recalculated, since these involve the little understood phenomenon of the passage of the electrode potential through a minimum. A recalculation would not be likely to add materially to the older interpretation.

The experimental data and calculations of this paper are in agreement with the assumption made previously that the primary product of the reduction of MnO_2 is a Mn(III) compound formed within the MnO_2 structure, and that its formation is followed by a disproportionation. The assumption of primary reduction to Mn(II) would lead to a linear relationship between overpotential and current, which is not found. However, recent work has shown a linear relation to hold for PbO_2 and TiO_2 electrodes, for which no disproportionation reaction is possible. This work will be reported later.

Acknowledgment

This work was supported in part by a James B. Duke Fellowship and in part by the Office of Ordnance Research. The authors are indebted to Mr. Bruce C. Tyson, Jr., for measurement of the change of potential with pH.

Manuscript received Aug. 14, 1959. This paper was prepared for delivery before the Columbus Meeting, Oct. 18-22, 1959.

Any discussion of this paper will appear in a Discussion Section to be published in the December 1960 JOURNAL.

REFERENCES

1. D. T. Ferrell, Jr., and W. C. Vosburgh, *This Journal*, **98**, 334 (1951).
2. A. M. Chreitzberg, Jr., and W. C. Vosburgh, *ibid.*, **104**, 1 (1957).
3. W. C. Vosburgh, D. R. Allenson, and Stanley Hills, *ibid.*, **103**, 91 (1956).
4. S. Yoshizawa and W. C. Vosburgh, *ibid.*, **104**, 399 (1957).
5. A. Kozawa and W. C. Vosburgh, *ibid.*, **105**, 59 (1958).
6. W. F. Cole, A. D. Wadsley, and A. Walkley, *Trans. Electrochem. Soc.*, **92**, 133 (1947).
7. W. C. Vosburgh, M. J. Pribble, A. Kozawa, and A. Sam, *This Journal*, **105**, 1 (1958).
8. J. Brenet, *Proc. Intern. Comm. Electrochem. Thermodynam. and Kinetics*, 8th Meeting, Madrid, 1956, p. 394.
9. W. C. Vosburgh, *This Journal*, **106**, 839 (1959).
10. A. Kozawa, *ibid.*, **106**, 79 (1959).
11. P. Ruetschi, R. T. Angstadt, and B. D. Cahan, *ibid.*, **106**, 547 (1959).
12. N. C. Cahoon, *ibid.*, **99**, 343 (1952).
13. N. C. Cahoon, R. S. Johnson, and M. P. Korver, *ibid.*, **105**, 296 (1958).
14. A. M. Chreitzberg, Jr., and W. C. Vosburgh, *ibid.*, **104**, 1 (1957).

Effect of Adsorption of Polar Organic Compounds on the Reactivity of Steel

Howard F. Finley[1] and Norman Hackerman

Department of Chemistry, The University of Texas, Austin, Texas

ABSTRACT

Rate studies were made for the oxygen-free reaction between steel powder and 1*N* H_2SO_4, both uninhibited and inhibited. In particular, it was shown that the retardation of the reaction by organic polar compounds was influenced more markedly by molecular structure than by molecular weight or area.

This study is a continuation of the work reported by Hackerman and Cook (1) on the adsorption of polar organic compounds on steel and their effect on its reactivity in acid solution. A comprehensive theory of the general adsorption of organic inhibitors and subsequent inhibition of acid dissolution by polarization of the anodic reaction was given by Hackerman and Makrides (2). The investigations undertaken here were for the purpose of obtaining additional information as a basis for confirming or denying the theory as stated.

Experimental

The essential features of the experimental approach have been described (1). The principle used was to determine gravimetrically the increase in weight of a sample of steel powder on being exposed to a solution of benzene containing the organic inhibitor. The metal used was SAE 1010 steel powder purchased from the Vanadium-Alloys Steel Company. It had a composition of 0.10 C, 0.10 Si, 0.24 Mn, 0.012 P, 0.012 S, and test Fe. It was purchased as powder which passed No. 100 sieve mesh and further sieved, the 140 to 200 range being used.

The benzene was thiophene-free, C.P. grade and was free also from H_2S, CS_2, and SO_3. The polar organic compounds were obtained from several sources. Hexamethylenimine and heptamethylenimine were obtained from Dr. P. D. Gardner, The University of Texas. Diallylamine, 1,4,4, trimethylpiperdine, and 1-benzylpiperdine were obtained from Dr. N. J. Leonard, The University of Illinois; tetrahydrothiophene from Delta Chemical Works, and four alkyl aryl sulfonate salts from Dr. A. H. Roebuck, Continental Oil Company. The remainder of the compounds were of the best grade of Eastman chemicals. In all cases, except for the sulfonate salts, the compounds were liquids and were redistilled. The sulfonate salts were 99.5% pure as received.

In making solutions of the inhibitors, two liters of 0.0100M solution were made and then solutions of 0.005, 0.0025, 0.00125, 0.00063, 0.00031M prepared by dilution of the proper aliquotes.

The relative inhibitor efficiency was determined by measuring the reaction rates in 1*N* H_2SO_4 of the steel powder either untreated or previously exposed to the benzene solutions of the inhibitors. The acid was prepared in 4-liter quantities from stock concentrated C.P. H_2SO_4.

The data are good in general to 5%.

Procedure.—The procedure for determining the amount of polar organic compound adsorbed on the steel has been described (1). There were, however, some modifications made in the method of determining relative inhibitor efficiencies. The apparatus used was essentially the same, with one or two minor alterations, but the technique of treating the data was completely different. Previously the results were compiled as a relative activity based on the time required to liberate 36, 81, and 126 ml of hydrogen gas or the time for the dissolution of 1.6, 3.4, and 5.2% of the metal. Basis time for reaction on clean steel was taken as an average from a number of different runs made on different samples. There are two objections to this procedure. The first is that there is only a relatively small amount of inhibitor on the surface of the steel, and after a short time of reaction it can be expected to be swept away or undermined so that it no longer protects the metal. The second is that unreduced steel powder already has a considerable surface oxide layer, and reaction rates with acid are both low and erratic from sample to sample.

It was believed that the following procedure would eliminate these objections. The powder was reduced in 150-g sample lots under hydrogen for 24 hr at 600° ± 25°C, both inhibited and uninhibited samples being treated alike. Individual curves were run for each sample lot and the inhibited samples were compared with these. Plots were made of volume of hydrogen evolved against time of reaction. The slope of the curve at zero time was obtained by extrapolation and a graphical method. The procedure used was to stand a small mirror on edge on the curve in such a way that the curve was continuous with its reflection. The base of the mirror was then normal to the curve at point of contact. Check values obtained with curves of known slope were never in error more than 2 or 3%. This approach is versatile and readily provides volume vs. time, rate vs. time, and rate vs. volume curves.

[1] Present address: Creole Petroleum Corporation, Cabimas, Edo. Zulia, Venezuela.

The relative inhibitor efficiency, y, was calculated from the equation

$$y = \frac{R_p - R_I}{R_p} \qquad [1]$$

where R_p is the reaction rate at zero time for the plain steel and R_I that for the inhibited steel.

Reaction rate data.—Typical hydrogen evolution data from uninhibited steel samples are shown in Fig. 1. These curves were not immediately amenable to analysis. The data were first plotted as volume vs. square root of the time and seemed to give a fair fit. However, the upper and lower ends of the curves deviated somewhat (Fig. 2). A better fit was obtained by plotting hydrogen volume against the square of the natural logarithm of the time. This is shown for the same data in Fig. 3. The equation for the curves is then

$$V = k_v \ln^2 t + k_i \qquad [2]$$

The rate equation becomes

$$\frac{dV}{dt} = 2k_v \frac{\ln t}{t} \qquad [3]$$

Figure 4 shows the data of the 30°C curve from Fig. 1 plotted as reaction rate vs. time and compared with the function $(k \ln t/t)$ normalized to $(k \ln t/t) = 3.5$ at $t = 2.5$, one of the actual data points.

This time dependence of the hydrogen volume is somewhat difficult to interpret. There was a slight

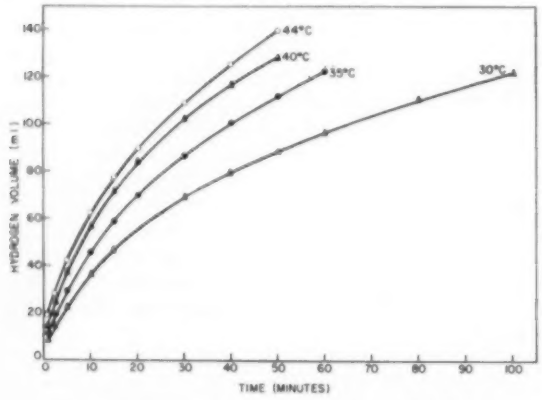

Fig. 1. Hydrogen evolution from steel in 1N H_2SO_4.

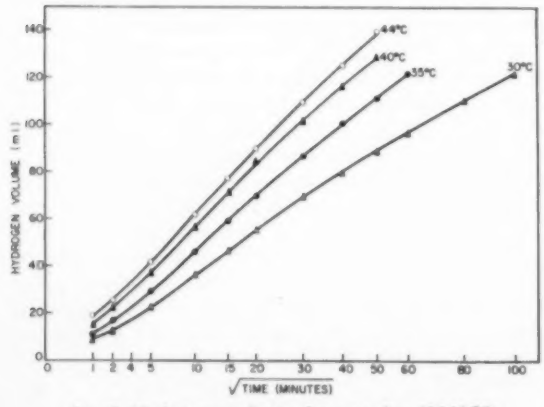

Fig. 2. Hydrogen evolution from steel in 1N H_2SO_4.

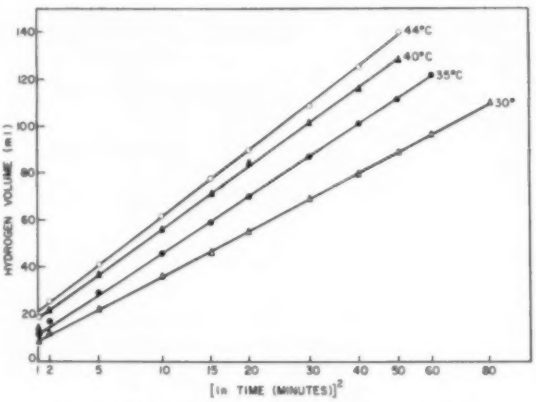

Fig. 3. Hydrogen evolution from steel in 1N H_2SO_4.

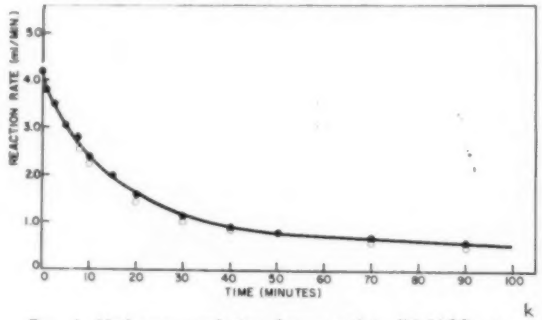

Fig. 4. Hydrogen evolution from steel in 1N H_2SO_4. ○, $\frac{k}{t}$ ln t normalized to $\frac{k}{t}$ ln t = 3.5 at t = 2.5; ●, experimental.

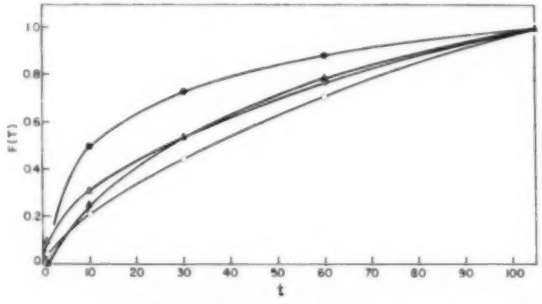

Fig. 5. ▲, $\ln^2 t$; △, $t^{1/3}$; o, $t^{2/3}$; ●, ln t.

increase in pH as the reaction proceeded but nothing of magnitude sufficient to explain the great decrease in reaction rate. Various investigators (3-5) have solved the square root dependence curve in the case of dry oxidation of metals, basing their solution on the diffusion of reactants through the oxide layer formed on the surface of the metal. Figure 5 shows that there is a general similarity between the shape of a $t^{1/3}$ and a $\ln^2 t$ curve. From this the tentative conclusion concerning the latter curve is that it is due to barrier layer formation.

The hydrogen volume-time dependence of the inhibited samples failed to show the same relationship. A typical curve is shown in Fig. 6 compared with a rate curve for plain steel. The rate increases slowly at first, reaches a peak at about 10 min, and then begins to decrease. The final rate is somewhat lower than that for plain steel, but its rate of change with time is about the same.

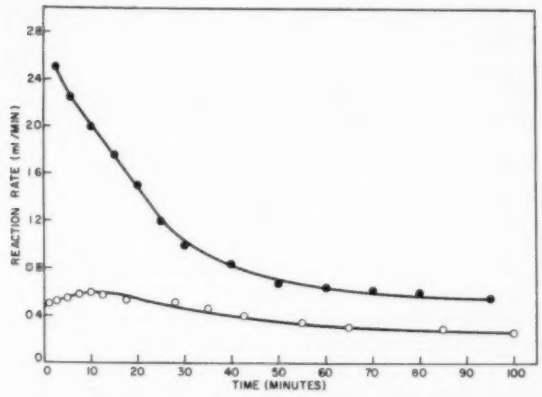

Fig. 6. Hydrogen evolution from steel in 1N H_2SO_4. •, Unhibited; o, inhibited.

The first 10 min the preadsorbed inhibitor is being removed from the surface by undermining, and fresh surface is being continuously exposed. At the same time a barrier layer is forming over the surface of the steel. After about 10 min of reaction the effect becomes predominant and the reaction rate begins to decrease. Thus protection of the steel functions simultaneously through two mechanisms: adsorbed inhibitor and barrier layer formation.

Adsorption and inhibitor efficiency data.—The data for the adsorption of the polar organic compounds are shown in Table I and that for the relative inhibitor efficiencies in Table II. The sulfonate salts were found to be extremely insoluble not only in benzene and water but also in all the usual solvents. For this reason adsorption curves could not be obtained for these compounds. However, they were slightly soluble in 1N H_2SO_4 so that relative inhibitor efficiency curves could be obtained with the inhibitor *in situ*. These data are also given in Table II.

A typical adsorption isotherm and a relative inhibitor efficiency curve are shown in Fig. 7.

The adsorption of the heterocyclic amines, pyrrolidine, piperdine, hexamethlenimine, and heptamethylenimine was not dependent on the number of carbon atoms in the molecule and only slightly on the molecular cross-sectional area. The approximate cross-sectional areas of all compounds studied were determined from Stuart and Briegleb atom models (obtained from Arthur S. LaPine and Company, Chicago), and are given in Table III. Photographs were made of each model with the camera lens in the position of a metal surface atom onto which the polar molecule had adsorbed. Line drawings were made from the photographs and the cross-sectional area calculated assuming that the molecule was free to rotate about the center of its electron density. A plot of the amount of imine adsorbed vs. area is shown in Fig. 8. It is seen that the large molecule adsorbs less but only slightly so. From the areas per molecule and the nitrogen adsorption area of the metal, it was calculated that approximately two layers of inhibitor adsorbed in each case.

There is a marked difference between the adsorption behaviors of these cyclic imines and the high molecular weight aliphatic amines studied earlier (1). Both adsorption data and relative inhibitor efficiency data show that all the imine is irreversibly adsorbed (note the plateaus in Fig. 7). The aliphatic amines adsorbed in every case about the same

Table I. Amount of inhibitor adsorbed (μM/g)

Concentration (molar × 10^3)	10	5	2.5	1.25	0.63	0.31
Pyrrolidine	0.99	0.68	0.61	0.58	0.78	0.80
Piperidine	0.65	0.80	—	0.71	0.68	0.63
Hexamethylenimine	0.68	0.59	0.64	0.61	0.68	0.45
Heptamethylenimine	0.45	0.46	0.49	0.38	0.47	0.41
1, 4, 4 Trimethylpiperidine	0.61	0.60	0.65	0.61	0.52	0.34
1-Benzylpiperidine	0.27	0.25	0.23	0.22	0.19	0.15
Diallylamine	0.97	0.54	0.56	0.44	0.31	—
Tetrahydrofuran	1.42	1.16	1.14	1.11	1.17	1.35
Tetrahydropyran	0.17	0.30	0.34	0.35	—	0.61
Tetrahydrothiophene	0.34	0.56	0.43	0.38	0.21	0.20

Table II. Relative inhibitor efficiency

Concentration (molar × 10^3)	10	5	2.5	1.25	0.63	0.31	0.16
Pyrrolidine	0.43	0.27	0.21	0.14	0.16	0.03	—
Piperidine	0.31	0.42	0.37	0.38	0.27	0.31	—
Hexamethylenimine	0.61	0.57	0.62	0.62	0.55	0.50	—
Heptamethylenimine	0.83	0.61	0.72	0.81	—	0.04	—
1, 4, 4 Trimethylpiperidine	0.51	0.44	0.40	0.46	0.49	0.36	—
1-Benzylpiperidine	0.65	0.66	0.58	0.54	0.45	0.37	—
Diallylamine	0.55	0.32	0.36	0.15	0.06	0.00	—
Tetrahydrofuran	0.37	—	0.38	0.20	0.24	0.03	—
Tetrahydropyran	0.11	0.15	0.16	0.12	—	0.15	—
Tetrahydrothiophene	0.27	0.37	0.40	0.32	0.27	0.11	—
Tetradecyl-benzene Sodium Sulfonate	—	—	—	0.42	0.40	0.41	0.41
Dodecyl	—	—	0.43	0.34	0.31	0.22	0.06
Decyl	—	0.55	0.40	0.37	0.34	0.12	—
Octyl	—	0.61	0.35	0.20	0.04	0.02	—

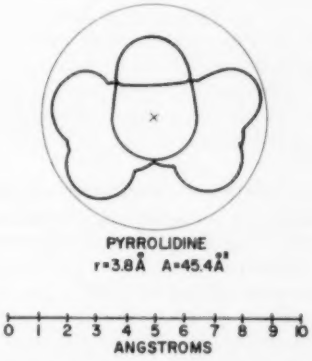

Table III. Molecular areas obtained from maximum radii using atom models

	r (Å)	A (Å²)
Piperidine	4.3	58.1
Hexamethylenimine	4.0	50.3
Heptamethylenimine	5.3	88.2
Tetrahydrofuran	3.4	36.3
1-Benzylpiperidine (Extended)	6.8	145.3
Tetrahydropyran	4.2	55.4
1-Benzylpiperidine (Close-Packed)	5.3	88.2
1, 4, 4 Trimethylpiperidine	4.4	60.8
Tetrahydrothiophene	4.0	50.3
Diallylamine — I = 11.3Å, h = 5.2Å, A = 58.8Å²		

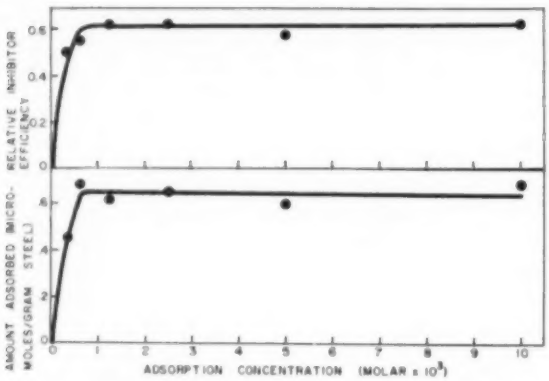

Fig. 7. Inhibitor efficiency of hexamethylenimine (upper); adsorption of hexamethylenimine (lower).

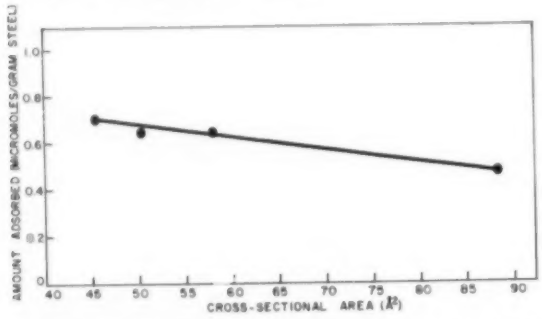

Fig. 8. Point 1-4, pyrrolidine; hexamethylenimine; piperidine; heptamethylenimine.

amount irreversibly and an additional amount, easily desorbed, that increased with the molecular weight of the amine. This difference can be attributed to two things: (*a*) the secondary nitrogen atom of the imines has a greater electron density for coordinating with metal surface atoms, and (*b*) the short, rigid, nearly planar hydrocarbon tails of the imines do not intertwine and lead to physical adsorption. The amines chemisorb less to begin with and their longer, less rigid hydrocarbon tails probably form a loose, haphazard arrangement on top of the chemisorbed layers.

The small amount of adsorption of the 1-benzyl piperdine is due to its large cross-sectional area. In addition the electrophylic phenyl group tends to reduce the electron density on the nitrogen atom. The high degree of adsorption of the tetrahydrofuran is due to its small cross-sectional area. There were evidently areas on the surface available to it that were not available to the other molecules.

Tetrahydrothiophene exhibited a surprisingly small degree of adsorption. However, the compound is extremely volatile. The simple adsorption equipment used in these experiments was not designed for use with volatile compounds.

The relative inhibitor efficiency of the heterocyclic imines is a function of the number of carbon atoms in the ring. This is shown in Fig. 9 and for comparison the data for the n-aliphatic amines taken from Hackerman and Cook's data. The amines also show a linear dependence on the number of carbon atoms for octylamine through tetradecylamine but decidedly less protection for hexadecylamine and octadecylamine. Levine and Zisman (6) found similar behavior for n-aliphatic acids, alcohols, and amines. They noted a marked change in the kinetic coefficient of friction and contact angle for those of 14 or more carbon atoms and attributed this to a transition between monolayers which were liquid condensed and those which were solid.[2] It is seen that the imines increase in efficiency about 20% on the addition of a methyl group, while the amines below hexadecylamine increase by only about 5%.

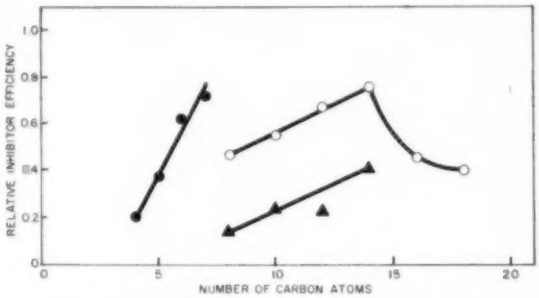

Fig. 9. ●, Heterocyclic imines; ○, aliphatic amines; ▲ alkyl aryl sodium sulfonates.

The imines are relatively good inhibitors. This is in consonance with the fact that secondary amines inhibit better than primary amines. An additional increase in efficiency in going to the tertiary compound can be seen by comparing 1,4,4-trimethylpiperdine with piperdine. It should be noted that there is a greater increase on adding a methyl group to the ring than to the nitrogen atom. Thus,

$$\text{piperdine} < \text{1,4,4-trimethylpiperdine} < \text{hexamethylenimine}$$

The data for the two oxygen compounds is not straightforward. The high relative protection of the tetrahydrofuran is because of the high degree of adsorption observed. The relative inhibitor efficiency of the tetrahydrothiophene was very good even without considering the reduced adsorption of the compound due to its volatility. If the ratio of efficiency to amount adsorbed is considered, the order is

$$\text{tetrahydrofuran} < \text{pyrrolidine} < \text{tetrahydrothiophene}$$

In analyzing the data for the alkyl aryl sodium sulfonates two things must be considered: (*a*) the inhibitor is in the solution and not preadsorbed, and (*b*) the sulfonate salts are very insoluble compared to the other compounds studied. A plot of relative inhibitor efficiency against the number of carbon atoms in the alkyl chain is shown in Fig. 9. Like the amines, the increase is about 5% per methyl group.

Thus we see that homologous series of three types of compounds: heterocyclic imines, aliphatic amines, and alkyl aryl sulfonates exhibit a linear dependence of relative inhibitor efficiency on the number of carbon atoms in the molecule. This cannot be attributed

[2] At first glance, it seems that the sharp drop for hexadecylamine and octadecylamine amine could be ascribed to micelle formation in the solution or to reduced solubility. However, it should be noted that the adsorption increased regularly with molecular weight and what is shown in Fig. 9 is a reduction in effect. Similarly, Levin and Zisman (6) describe a reduction in effect, as did Marsh (7), in connection with a discontinuous change in oil wetting properties. Therefore, the reason could just as well lie in a two-dimensional phase change for instance. In any event, this is a problem which is outside the scope of the present work.

to an increase in barrier layer resistance due to longer chain length on ascending the homologous series, since the amines would then be expected to show a greater effect than the imines. The explanation lies in a more fundamental property of the molecule.

One possible explanation lies in the charge-transfer-no-bond adsorption complex theory advanced by Matsen, Makrides, and Hackerman (8). This postulates that on chemical adsorption a surface complex is formed between adsorbate and adsorbent whose ground state is characterized by a linear combination of wave functions for a no-bond state and a dative state. The dative state lies above the no-bond state by an amount equal to $I_B - (E_A + E_C)$ where I_B is the ionization energy of the adsorbate, a Lewis base, E_A the electron affinity of the metal, a Lewis acid, and E_C the coulombic interaction energy. For a given metal with a series of polar inhibitors, the value of $(E_A + E_C)$ should be constant, but the value of I_B will vary from inhibitor to inhibitor. A lower value of I_B results in a lower value of the energy of the dative state and consequently a lower value of the energy of the ground state. A lower ground state energy is reflected in a stronger bond of chemisorption and a greater relative inhibitor efficiency.

A nucleophylic methyl group tends to increase the electron density on the polar group of organic inhibitors. This is observed as a decrease in ionization potential of each higher member of a homologous series. Data for the compounds studied here are not available, but values of the ionization potentials of some low molecular weight amines were made available by Matsen (9). These values are:

Group	Mono	Di	Tri
Methyl	8.97±0.02	8.24±0.02	7.82±0.02
Ethyl	8.86±0.02	8.01±0.01	7.50±0.02
Propyl	8.78±0.02	7.84±0.02	7.23±?
Butyl	8.71±0.03	7.69±0.03	

A plot of these is shown in Fig. 10. Thus it is seen that the change in ionization energy in ascending a homologous series of amines is about the same per methyl group but that the value of the ionization energy is dependent on whether the amine is primary, secondary, or tertiary.

The inductive effect of a methyl group, with its attendent decrease in ionization potential of the polar group, is thus a possible explanation of the linear dependence of relative inhibitor efficiency on the number of carbon atoms in the molecule. In the heterocyclic imines the change in relative inhibitor efficiency per methyl group is almost 20% reflecting the fact that each carbon in a ring compound is able to exert an inductive effect along both sides of the chain back to the terminal group. The value of 5% for the amines results from the decrease in inductive effect as additional carbon atoms are interspersed in the chain. The same is true for the alkyl aryl sulfonates. The para polarized benzene nucleus.

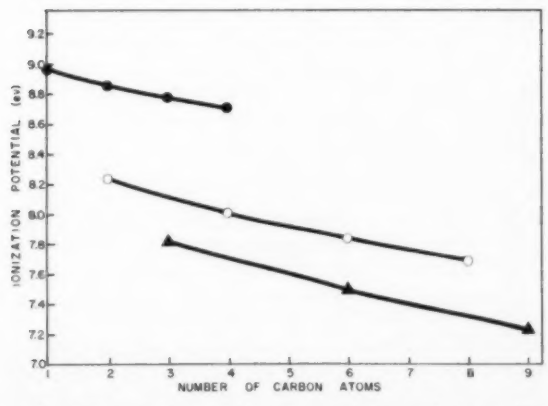

Fig. 10. ●, Primary amines; ○, secondary amines; △, tertiary amines.

hydrocarbon chain + 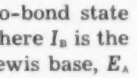 – polar group

is such that the inductive effect is transmitted across it, even though the benzene ring is an electrophylic group.

Conclusions

1. In these experiments the rate of hydrogen evolution from reduced plain steel powder in 1*N* H_2SO_4 is a function of $(\ln t/t)$. Also, the steel was protected by barrier layer formation and by adsorbed inhibitor simultaneously, when the latter was present.

2. The heterocyclic nitrogen, oxygen, and sulfur compounds investigated here exhibit chemisorption under the experimental conditions imposed.

3. Over a range of molecular weights in an homologous series of heterocyclic imines, aliphatic amines, and alkyl aryl sulfonates, the relative inhibitor efficiency is a linear function of the number of carbon atoms in the molecule.

4. A possible explanation of this is the inductive effect of a methyl group with its attendent decrease in ionization potential of the polar group.

Acknowledgment

This research was sponsored in part by the Robert A. Welch Foundation and in part by the Office of Naval Research (Contract Nonr-375(02)). The authors are happy to express their appreciation for this support.

Manuscript received May 29, 1959.

Any discussion of this paper will appear in a Discussion Section to be published in the December 1960 JOURNAL.

REFERENCES

1. N. Hackerman and E. L. Cook, *J. Phys. Chem.*, **56**, 524 (1952); *This Journal*, **97**, 1 (1950).
2. N. Hackerman and A. C. Makrides, *Ind. Eng. Chem.*, **46**, 523 (1954).
3. C. Wagner, *Z. physik. Chem.*, **21B**, 25 (1933).
4. T. P. Hoar and L. E. Price, *Trans. Faraday Soc.*, **34**, 867 (1938).
5. N. F. Mott, *ibid.*, **36**, 472 (1940).
6. O. Levine and W. A. Zisman, *J. Phys. Chem.*, **61**, 1068 (1957).
7. B. E. Marsh, "Corrosion Control with Fatty Nitrogen Derivatives," Paper No. 44, 15th NACE Conference, Chicago, March (1959); Abstract in Corrosion, **15**, 82, January (1959).
8. F. A. Matsen, A. C. Makrides, and N. Hackerman, *J. Chem. Phys.*, **22**, 1800 (1954).
9. From a private communication to Professor F. A. Matsen, University of Texas from K. Watanabe, 1951.

Mechanism of the Iron-Hydrogen Sulfide Reaction at Elevated Temperatures

Hans Arm,[1] Paul Delahay, Charles Hudgins,[2] Fritz Hügli,[3] Lester Hulett,[4] and Mohsin Qureshi[5]

Coates Chemical Laboratory, Louisiana State University, Baton Rouge, Louisiana

ABSTRACT

The mechanism of the iron-hydrogen sulfide reaction was studied in the 500°-760°C temperature range for a total gas pressure of 1 atm. The rate of attack was essentially constant (linear law), and the corrosion scale was composed of two layers: a thin dense layer adjacent to the metal and a porous layer with a coarse crystalline structure. These two features which differentiate this reaction from the iron-sulfur vapor reaction are interpreted on the basis of two main effects: (*a*) partial blocking of reaction sites by hydrogen produced during attack, and occurrence of a reaction at a constant number of reaction sites; and (*b*) continuous recrystallization of the dense scale into a porous scale offering no barrier to transport of reactants. This mechanism is self-regulating.

The following evidence is presented: (*a*) linear Arrhenius plots were obtained; (*b*) essentially the same rate of attack was observed for hydrogen-hydrogen sulfide and helium-hydrogen sulfide mixtures having the same partial pressure of hydrogen sulfide; and the dependence of rate on hydrogen sulfide pressure was accounted for; (*c*) the attack rate was not affected by the coating of specimens with a dense layer of varying thickness obtained by preliminary attack in sulfur vapor; (*d*) the iron-sulfur reaction, which obeys the parabolic law of attack, was inhibited by hydrogen diffusing from the back of the specimen surface; (*e*) recrystallization of the dense layer into the porous one was observed for specimens aged in helium; and (*f*) aging of iron sulfide with a fine crystalline structure (prepared by sulfur attack) in the corresponding hydrogen-hydrogen sulfide equilibrium mixture caused the scale structure to become somewhat coarse.

Discussion of experimental methods covers the following points: (*a*) measurements of the rate of attack with a quartz spring balance in hydrogen-hydrogen sulfide and helium-hydrogen sulfide mixtures; (*b*) techniques for attack in sulfur vapor followed by hydrogen sulfide attack; (*c*) use of a mild steel cartridge containing lithium aluminum hydride in the hydrogen diffusion studies; and (*d*) scale thickness studies.

The iron-hydrogen sulfide reaction at elevated temperatures has two unusual features which distinguish it from most other metal-gas reactions with solid scale formation: (*a*) the rate of attack becomes constant after a short time (a few minutes above 500°C), i.e., the attack follows a linear law; and (*b*) a scale composed of two layers is formed, the layer adjacent to the metal having a fine crystalline structure and the outer layer being of a porous and coarse structure. [See review of previous work in the recent paper of Dravnieks and Samans (1).] In contrast, the iron-sulfur reaction, according to Hauffe and Rahmel (2), follows the normal parabolic law of attack (corresponding to a diffusion controlled process) with formation of a single homogeneous scale having a fine crystalline structure. The same product of attack, iron sulfide, is obtained in both reactions, and yet the kinetics are very different. An interpretation for these differences is given here.

Recent kinetic investigations of this problem were made by Dravnieks and Samans (1) and by Haycock (3). The manuscript of the former authors was available at the onset of our work while Haycock's manuscript became available in the fall of 1958. Dravnieks and Samans postulate a mechanism controlled by a surface reaction which they assume to be the dissociation of hydrogen sulfide at the scale surface. They account for the two-layer scale by assuming two different processes, namely diffusion of sulfide ions in the dense layer and diffusion of ferrous ions in the coarse layer. Haycock postulates mixed control by diffusion of sulfide ions across the dense layer and recrystallization of the dense layer into the porous layer. A linear law is observed when the dense layer reaches a constant thickness. Continuous recrystallization is greatly accelerated by hydrogen produced in the iron-hydrogen sulfide reaction. Haycock concludes from marker experiments that sulfide ion is the diffusing species. This is accounted for by the assumption that the diffusion rate

[1] Postdoctoral fellow, 1957-1958. Present address: Laboratory for Organic Chemistry, University of Bern, Bern, Switzerland.

[2] Predoctoral fellow, 1956-1957. Present address: Development and Research Department, Continental Oil Co., Ponca City, Oklahoma.

[3] Postdoctoral fellow, 1956-1957. Present address: Technical High-school, Winterthur, Switzerland.

[4] Predoctoral fellow, 1956-1958 (part-time) and 1958-1959.

[5] Postdoctoral fellow, 1958-1959. Present address: Department of Chemistry, Muslim University, Aligarh, India.

for ferrous ions is decreased because of the formation of "E-centers." By analogy with other cases (4), Haycock assumes that E-centers are formed by trapping of hydrogen in cation vacancies of the lattice.

Our purpose was to design experiments to discriminate as unambiguously as possible between control by a surface reaction and that by a diffusion process and to determine whether hydrogen plays a role in recrystallization of the dense layer into a coarse layer (not observed when hydrogen is not present). The following studies were made: (*a*) confirmation of the linear law at different temperatures and determination of the heat of activation; (*b*) attack in mixtures of hydrogen sulfide and hydrogen or helium; (*c*) attack of iron in sulfur vapor followed by hydrogen sulfide attack; (*d*) study of the effect of hydrogen on the iron-sulfur vapor reaction, hydrogen being supplied by diffusion through the iron from the unexposed face of the corroding specimen; and (*e*) determination of the scale thicknesses and effect of aging on the two-layer scale.

Experiment (*a*) would give an indication of mixed control by two processes having different heats of activation if a nonlinear Arrhenius plot were obtained. The combination of experiments (*b*), (*c*), and (*d*) should allow discrimination between control by a surface reaction and by diffusion. Experiment (*e*) should provide direct evidence of recrystallization.

Experimental Methods

Attack in Hydrogen Sulfide and Hydrogen Sulfide-Hydrogen or Hydrogen Sulfide-Helium Mixtures

Rates of attack were determined from the increase in specimen weight. The specimen in the lower Vycor reaction chamber (Fig. 1A) was suspended on a fine Vycor fiber attached to a quartz spring (obtained from Worden Laboratories, Houston, Texas). The quartz spring extended only in the upper Pyrex chamber and was essentially at room temperature; i.e., no temperature correction in the calibration was necessary. The elongation of the spring was measured with a cathetometer (Gaertner, Chicago) with an error not exceeding 0.05 mg for specimens weighing approximately 0.5 g.

The chamber with its gas preheater coil was connected to a gas mixing system which could supply hydrogen and mixtures of hydrogen sulfide with either hydrogen or helium. Traces of oxygen in the electrolytic grade hydrogen (Matheson) were removed by passing the gas through a "Deoxo" catalyst cartridge (obtained from Engelhard Industries, Inc., Newark, N. J.). Hydrogen sulfide and helium were used as supplied in tanks (Matheson). The composition of the gas mixtures was constantly controlled (*a*) from the individual flow rates, as measured with differential pressure manometers, in the determination of the heat of activation, and (*b*) by a sensitive thermal conductivity cell in the comparison of attack rates for hydrogen-hydrogen sulfide and helium-hydrogen sulfide mixtures. A gas reservoir with twice the capacity of the reaction chamber was inserted between the chamber and the mixing system. The gas reservoir was used in the initiation of the reaction. The reaction chamber was bypassed during the adjustment of the gas mixture composition.

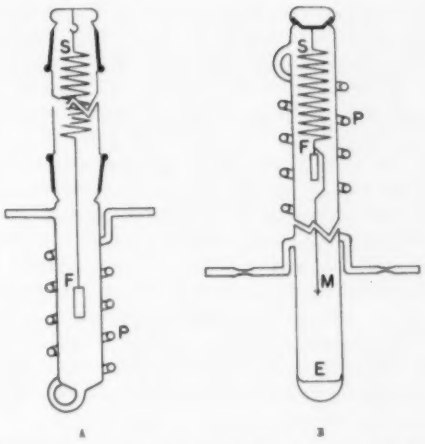

Fig. 1(A). Apparatus for the study of the reaction of iron with hydrogen sulfide and mixtures of hydrogen sulfide and hydrogen or hydrogen sulfide and helium. F, specimen; S, quartz spring; P, gas preheater coil. Fig. 1(B). Apparatus for mixed attack experiments and for hydrogen diffusion experiments. F, iron cartridge or other specimen; S, quartz spring; E, sulfur pool; P, gas preheater coil; M, platinum wire marker.

Specimens were made of spectroscopically pure iron sheets, for which the suppliers (Jarrell Ash Co., Newtonville, Massachusetts) gave the following analysis: 4 ppm Mn; 2 ppm Ni, Si, Mg; 1 ppm Cu, Ag, Na, Li; other metals were not detected spectroscopically. The specimen dimensions of approximately 0.05 x 0.7 x 1.4 cm were determined accurately with a micrometer. Specimens were washed in petroleum ether and acetone before use.

After introduction of the specimen in the reaction chamber the entire flow system was evacuated to a pressure below 1 mm. The absence of leaks was ascertained, and the system was flushed repeatedly with hydrogen and finally evacuated again. Hydrogen then was passed through at a rate of approximately 200 ml/min (linear velocity of approximately 1 cm sec^{-1}), and the furnace was brought to the desired temperature. Reduction of traces of oxide on the specimen followed for 2 hr at 500°C or a higher temperature. After removal of hydrogen by evacuation, the gas mixture was passed through the chamber at the rate of 200 ml/min, and the attack was followed as described above.

Mixed Attack

Experiments in which attack by sulfur vapor was followed by hydrogen sulfide attack involved one difficulty, namely, that to avoid condensation, no part of the apparatus could be colder than the vessel in which sulfur was vaporized. The Pyrex chamber of Fig. 1B was constructed with the upper end open. Sulfur was introduced, and the specimen, suspended on a quartz spring, was hung on an inverted U-rod. The top of the chamber then was sealed. Procedures

for the purging and reduction were the same as for the hydrogen sulfide attack. After reduction of the specimen, the chamber was filled with helium and sealed at the constricted sections of the side arms, the upper part of the chamber being maintained all the time at 575°C. The lower furnace was raised around the sulfur reservoir and heated to 230°C. Vaporized sulfur condensed in the section of the chamber (between the two furnaces), approximately 2 in. in length, which remained cool during the warm-up of the lower furnace. Heater sleeves were slipped over the side arms to avoid sulfur condensation. After the lower furnace reached 230°C, a heater clamp was placed around the exposed midsection, and attack of the specimen was initiated. This method reduced the uncertainty of the zero time to a few minutes.

After the desired increase in weight, as followed by the cathetometer, had been reached, sulfur attack was stopped by removal of the lower furnace, the upper furnace remaining at 575°C. The heater sleeves were removed and the gas flow system, discussed above, was connected to the sidearms with thick-walled Tygon tubing. The system then was evacuated and purged with hydrogen. The hydrogen-hydrogen sulfide mixture of previously adjusted composition was introduced in the chamber by the snapping of the sidearm tips inside the Tygon tubing at the inlet and outlet. Rates of attack were determined from cathetometer readings at a gas flow rate of 200 ml/min.

Influence of Diffusing Hydrogen on the Iron-Sulfur and Iron-Hydrogen Sulfide Reactions

The effect of hydrogen diffusing from the back of the specimen surface during attack in sulfur vapor was studied. The specimen was a mild carbon steel cartridge, 4 x 20 mm with a bore of 2 mm diameter, containing 20 mg of lithium aluminum hydride. The air in the cartridge was flushed with helium while the mouth was crimped together. The cartridge was immediately sealed with an acetylene torch, the lower part of the cartridge being kept cold in water. A platinum wire was attached to the top of the cartridge for suspension purposes, and the wire and sealed portion of the cartridge were masked with a porcelain cement (Saureisen). The cement was allowed to harden in air for at least 24 hr before the cartridge was used. Immediately before use, the cartridge was polished with Behr-Manning 400A sandpaper and jeweler's rouge cloth and then washed with acetone and petroleum ether.

The cartridge and a long platinum wire were suspended on a quartz spring inside a Pyrex tube whose bottom had been filled previously with sulfur (Fig. 1B). This Pyrex tube was provided with an inlet and outlet for hydrogen. The tube then was sealed at the top and placed in a furnace. The cartridge was reduced for 2 hr in a stream of hydrogen, the lower part of the reaction tube remaining at room temperature. After reduction, the furnace was cooled and the tube was removed. The hydrogen remaining in the tube was replaced with helium, and the gas inlet and outlet were sealed off and shortened so that they would not protrude outside the furnace.

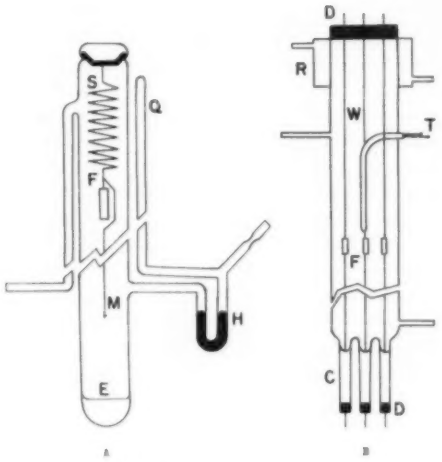

Fig. 2(A). Apparatus for measuring rates of hydrogen diffusion through iron and iron sulfide. S, quartz spring; F, cartridge; E, sulfur pool; M, platinum wire marker; H, differential pressure manometer; Q, tube containing the reference volume of gas at the same temperature as the cartridge. Fig. 2(B). Apparatus for scale studies. F, specimens; W, chromel wires; T, thermocouple; C, detachable casting tubes containing sulfur; D, rubber stoppers; R, cooler.

Sulfur attack followed according to the procedure described in the previous section.

In some experiments with blank cartridges, i.e., without lithium aluminum hydride, the reaction tube was evacuated after hydrogen reduction and kept at a pressure of 0.02 mm for 8 hr to remove the hydrogen which had diffused into the metal.

Experiments on the effect of hydrogen diffusion on hydrogen sulfide attack involved the same procedure as described above for spectroscopically pure specimens except that cartridges were utilized.

Diffusion of Hydrogen in Iron and Iron Sulfide Scale

Rates of hydrogen diffusion through iron with or without ferrous sulfide scale were obtained with the chamber of Fig. 2A. The initial steps were the same as in the preceding section. After reduction, hydrogen was replaced by helium in the chamber. The side arm on the left was sealed off close to the wall of the chamber, and the small sidearm protruding from the U-tube was sealed off at the constriction. Condensation of sulfur was prevented by a specially shaped heater. Sulfur vapor attack was carried out at 500°C all the time. The U-tube was connected, after removal of its heater, to a vacuum system with a thick wall Tygon tube. A small glass bulb containing 5 ml of mercury was also connected near the U-tube and in parallel with the vacuum system. The tip of the sidearm in the Tygon tube was snapped and the reaction chamber was evacuated with the forepump. The sulfur reservoir was sealed off to eliminate subsequent errors in pressure measurements as a result of gas release from the sulfur. Evacuation to 1 μ was continued with an oil diffusion pump. Mercury from the small reservoir was poured through the sidearm and into the U-tube, and the sidearm was sealed. An all glass, completely sealed system with a built-in differential pressure mano-

meter thus was obtained. Pressure variations in the reaction chamber resulting from hydrogen diffusion through the cartridge wall were measured with a cathetometer.

Scale Thickness Studies

A special reaction vessel was designed for scale thickness studies to allow rapid casting of specimens in molten sulfur. Five specimens (only three shown in Fig. 2B) were suspended on chromel wire by means of insulating glass hooks. The wires were strung through rubber stoppers. The casting tubes were filled with sulfur chips which were melted with a clamp heater just before the casting of a specimen. After attack in a hydrogen sulfide-hydrogen mixture, the specimen was lowered into the molten sulfur, and the casting tube was allowed to cool. The five specimens could be cast at different times. The reduction in hydrogen before attack and the attack were conducted as above.

The tendency of the scale to peel off as a result of the temperature change was minimized by the use of curved specimens as suggested by Haycock (3). The scale remained quite adherent on the concave side.

Mounted specimens were cut with a high-speed, glass-cutter's saw. The cross section was polished with graded emery cloths and levigated alumina on a metallographic polishing wheel. A Bausch and Lomb metallographic microscope was used for examination and photography.

Specimens obtained in mixed attack and aging experiments and cartridges from experiments with hydrogen diffusion were mounted in an EPON resin.[6] The procedure was as follows: Add 9 parts EPON 828 to 1 part curing agent (DTA); mix well; pour into mold around the specimen; allow the EPON to cure for 24 hr at room temperature.

Aging of Scale in Hydrogen-Hydrogen Sulfide Mixture

Specimens were attacked in sulfur vapor as in the mixed attack experiments. After attack, hydrogen was introduced in the chamber much in the same way as hydrogen sulfide was introduced in the mixed attack studies, and the pressure in the chamber was adjusted slightly above atmospheric pressure. The equilibrium partial pressure of hydrogen sulfide, in the conditions of this experiment, was quite insignificant in comparison with the hydrogen pressure (see below, influence of diffusing hydrogen on sulfur vapor attack), and this allowed the use of pure hydrogen rather than the equilibrated mixture hydrogen-hydrogen sulfide. After aging, the chamber was allowed to cool slowly to room temperature before the specimens were removed. Specimens then were mounted in the EPON resin.

Mechanism of the Iron-Hydrogen Sulfide Reaction

Postulated Mechanism

The results of attack in helium-hydrogen sulfide mixtures and mixed attack experiments led us to postulate a mechanism for the iron-hydrogen sulfide reaction which was further confirmed by experiments on sulfur attack with hydrogen diffusion and experiments on aging of the scale. The mechanism is as follows:

Hydrogen produced by the iron-hydrogen sulfide reaction remains in large part adsorbed (or associated in some other fashion) with iron sulfide. The number of reaction sites available for attack by hydrogen sulfide is considerably decreased as a result of hydrogen adsorption, and attack occurs at an essentially constant number of reaction sites, i.e., a linear law of attack is observed. Furthermore, diffusion is not rate controlling (at least at sufficiently high temperatures, i.e., above 500°C approximately) because of continuous recrystallization of the scale into a coarse layer which offers no diffusion barrier. The thickness of the thin layer is not sufficient to cause diffusion control.

This mechanism is self-regulating in that a decrease (or increase) in rate would result in a decrease (or increase) in the rate of hydrogen production and, consequently, in an increase (or decrease) in the number of reaction sites. The latter effect then would compensate the initial decrease (or increase) in rate that caused it.

Supporting evidence will now be presented.

General Characteristics and Effect of Temperature[7]

The two essential characteristics of the iron-hydrogen sulfide reaction, linear law of attack and formation of a two-layer scale, are apparent from Fig. 3 and 4. The slope of the log-log plot in Fig. 3 is quite close to unity, i.e., the law of attack is linear. In the early stage of attack (5-15 min) the rate is somewhat larger than the constant rate observed afterwards. This effect causes the slope of the log-log plot in Fig. 3 to be somewhat smaller than unity. The initial high rate possibly results from the difference in the metal and scale areas.

At temperatures below 500°C, plots of the increase in specimen weight vs. time exhibit a marked

[7] This section based on the work of L. Hulett, C. Hudgins, F. Hügli, and M. Qureshi.

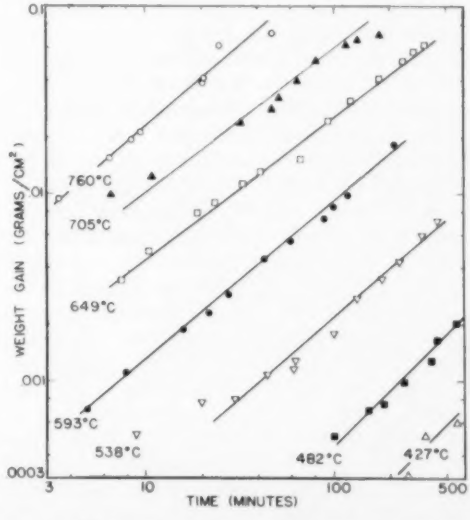

Fig. 3. Weight gain of iron against time for reaction in hydrogen sulfide at 1 atm at different temperatures.

[6] Courtesy of Dr. E. W. Haycock, Shell Development Co., Emeryville, California. Information about EPON resins can be obtained from the Shell Development Co.

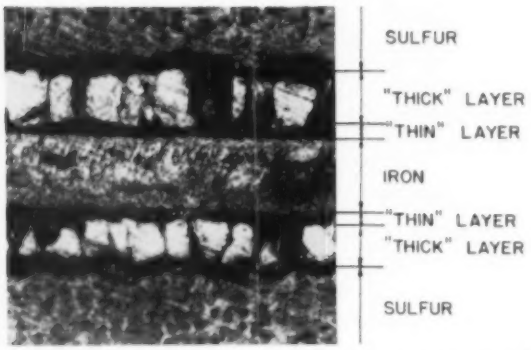

Fig. 4. Photomicrograph of section of specimen after 60 min exposure to hydrogen sulfide at 1 atm and 649°C. Magnification, 200× before reduction for publication.

curvature [cf. Dravnieks and Samans (1) and Haycock (3)] which is probably due to partial diffusion control.

Arrhenius plots for the data on Fig. 3 and similar data for a 4:1 hydrogen-hydrogen sulfide mixture are linear (Fig. 5). Mixed control of kinetics by two processes having rather different heats of activation is ruled out by the linear plot of Fig. 5. The corresponding heat of activation is 30 kcal/mole, as compared to 20 kcal/mole according to Dravnieks and Samans (1) and 12 kcal/mole according to Haycock (3). The variation from 30 to 12 kcal/mole is possibly due to differences in hydrogen coverage. (This point was suggested to us by Dr. Haycock.) Indeed, the values of 30, 20, and 12 kcal/mole were obtained, respectively, in pure hydrogen sulfide at 1 atm, in hydrogen at 1 atm with a relatively low partial pressure of hydrogen sulfide, and in hydrogen at 600 p.s.c. with hydrogen sulfide at 0.6 p.s.c. If one assumes that hydrogen desorption is the rate-determining step, the foregoing heats of activation correspond to the heats for hydrogen adsorption. The values of 30 to 12 kcal/mole then are of the right order of magnitude, and their variation with coverage is in the right direction. Compare for instance with the heat for hydrogen adsorption on nickel which, according to Beeck (5), decreases from approximately 30 kcal/mole near zero coverage to 17 kcal/mole near full coverage. The iron sulfide scale probably behaves as a metal for hydrogen adsorption because of the high density of free electrons (high conductivity of scale).

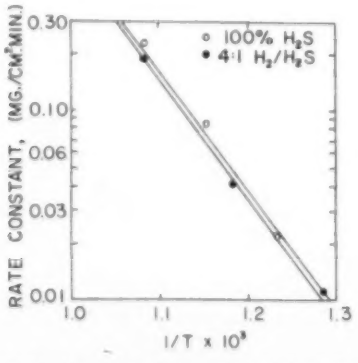

Fig. 5. Arrhenius plots of the rate constant for attack in hydrogen sulfide and in hydrogen-hydrogen sulfide mixture.

Attack in Hydrogen Sulfide-Hydrogen and Hydrogen Sulfide-Helium Mixtures[a]

It is well established that the rate of attack of iron in hydrogen-hydrogen sulfide mixtures depends on the partial pressure of the gases [cf. Dravnieks and Samans (1) and references therein]. The effect can be accounted for by thermodynamics, and there is little doubt that near equilibrium a thermodynamic interpretation holds. Hydrogen, however, might act primarily as a diluting agent in the attack of iron in hydrogen-hydrogen sulfide mixtures not near equilibrium. Essentially the same rate of attack then should be obtained with hydrogen-hydrogen sulfide and helium-hydrogen sulfide mixtures having the same partial pressures of hydrogen sulfide, if variations in hydrogen coverage did not complicate matters. Figure 6 shows that the same rates are indeed observed with mixtures having the same partial pressure of hydrogen sulfide. (Incidentally, the decrease in rate at low partial pressures of hydrogen sulfide is not caused by depletion of reactant.)

These observations preclude interpretation based on a Wagner model for the kinetics of attack, since such a model presupposes equilibrium attainment at the metal-scale and gas-scale interfaces. Very different rates of attack would be obtained for a reaction obeying a Wagner model when hydrogen is replaced by helium, especially for low partial pressures of hydrogen sulfide. The data of Fig. 6 do not eliminate diffusion as a partial or total rate-controlling factor, but it can be concluded from them that equilibrium is not reached at the metal-scale and/or scale-gas interfaces. Of course, departure from equilibrium does not necessarily imply control by a surface reaction since the surface reaction might be too fast to be rate-controlling.

Since, according to our interpretation, the rate of attack depends on hydrogen coverage, Fig. 6 im-

[a] This section based on the work of C. Hudgins, F. Hügli, and L. Hulett.

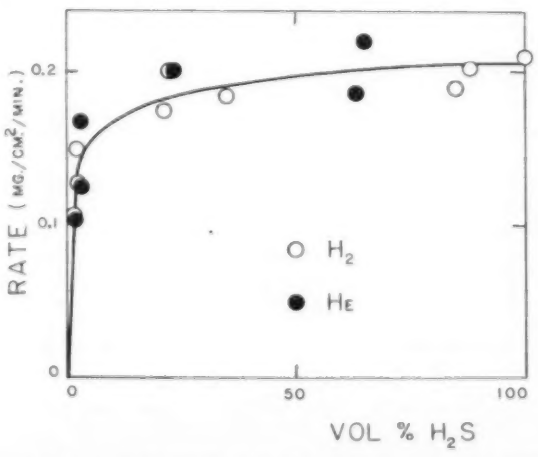

Fig. 6. Rate of attack at 649°C against volume per cent of hydrogen sulfide for mixtures of hydrogen sulfide with hydrogen or helium.

plies that this coverage remains essentially the same when helium is substituted for hydrogen. Of course, coverage by hydrogen for adsorption equilibrium would be affected by such a substitution unless full coverage were achieved for the lowest partial hydrogen pressure. One then must assume that adsorption equilibrium is not reached for hydrogen.

The data of Fig. 6 can be interpreted on the basis of the postulated mechanism. It is assumed (*a*) that the attack rate is proportional to the partial pressure of hydrogen sulfide and (*b*) that the rate is proportional to the number of reaction sites, i.e., the "free area." Thus

$$v = kp(1-\theta) \qquad [1]$$

where v is the attack rate, k a proportionality constant, θ the "coverage" by hydrogen, and p the partial pressure of hydrogen sulfide. The coverage by hydrogen increases with the rate of production of hydrogen, i.e., with v. A rigorous relationship between v and θ would be complicated because it would include the adsorption isotherms for hydrogen and hydrogen sulfide, or kinetic terms corresponding to these isotherms, and possibly other considerations for the interaction between hydrogen and the scale [Haycock's E-centers (3)]. Furthermore, the dependence of θ on p should be considered. This dependence is quite minor for the data of Fig. 6, if the foregoing analysis is accepted. It will suffice for the present purpose to assume without any claim to rigor that

$$\theta = k'v \qquad [2]$$

By elimination of θ from Eq. [1] and [2] there follows an equation in the form of a Langmuir isotherm (but the similarity ends with the form of the equation)

$$v = \frac{kp}{1 + kk'p} \qquad [3]$$

It follows from Eq. [3] that a plot of p/v against p should be linear. This is the case (Fig. 7) for the data of Fig. 6.

Dravnieks and Samans (1) also noted that the dependence of attack on pressure obeys a Langmuir isotherm type of equation, and, in fact, they reported linear plots of p/v against p. Their explanation, however, is different from the one offered here.

Mixed Attack[9]

Rather conclusive proof of the absence of diffusion control was obtained from mixed attack experiments. Data for attack in hydrogen-hydrogen sulfide mixtures (4:1) are given in Fig. 8 for specimens with different initial thicknesses of iron sulfide scale (as obtained by preliminary attack in sulfur vapor). After an initial period, which is interpreted below, the same rate of attack prevails regardless of the thickness of the initial scale of iron sulfide. This conclusion holds even for the experiment in which the initial scale was approximately twice as thick as the scale formed during hydrogen sulfide attack. An interpretation of the iron-hydrogen sulfide reaction based on control by diffusion in the scale is inconsistent with these observations.

[9] This section based on the work of H. Arm, L. Hulett, and M. Qureshi.

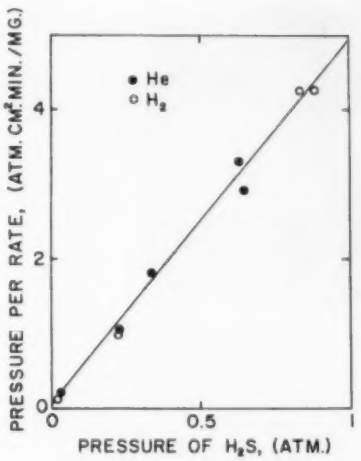

Fig. 7. A verification of Eq. [3] for the data in Fig. 6

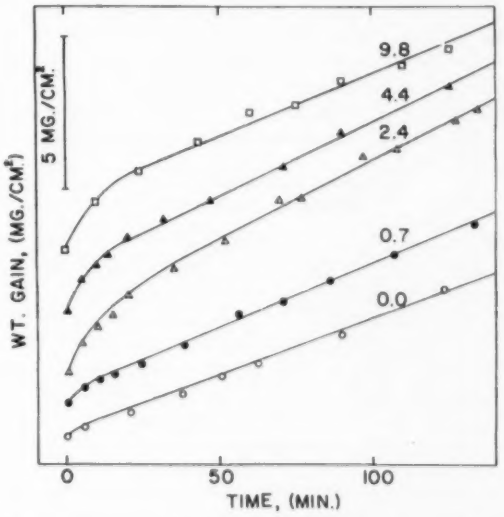

Fig. 8. Increase of weight against time for specimens previously attacked in sulfur vapor. Number on each curve is weight of iron sulfide in mg/cm² formed during sulfur vapor attack. Temperatures: molten sulfur during sulfur vapor attack, 230°C; specimen during sulfur vapor and hydrogen sulfide attacks 575°C; curves are shifted for clarity.

It could be argued that the scale underwent some transformation during the initial hydrogen sulfide attack and that the rate became constant when the thin dense layer obtained in the usual hydrogen sulfide attack was formed. Examination of the scale (Fig. 9) did not confirm this view. The outer scale exposed to hydrogen sulfide was composed of large crystals, but the bulk of the scale had remained quite compact and homogeneous. Furthermore, the initial rate of attack in hydrogen sulfide was higher than the constant value reached at a later stage, and yet the initial scale (formed in sulfur vapor) had a fine crystalline structure.

The initial rapid attack can be interpreted in terms of the postulated mechanism. Thus, the area at the gas-iron sulfide interface before hydrogen

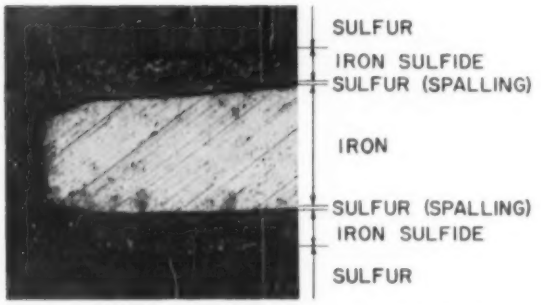

Fig. 9. Photomicrograph of section of specimen after attack by sulfur vapor followed by hydrogen sulfide attack. Temperature: 575°C. Magnification, 200× before reduction for publication.

sulfide attack was larger than for the metallic surface corresponding to the same projected area. Hence, rates of attack by hydrogen sulfide were initially larger than for a metallic specimen without prior sulfur attack. However, the self-regulating mechanism soon brought the rate to a constant value. Note that the curves of Fig. 8 for the three thicker scales appear to be the same, i.e., the initial process was independent of the scale thickness once a sufficiently thick scale had been produced.

Influence of Diffusing Hydrogen on Sulfur Vapor Attack[10]

Since hydrogen, in our interpretation, is supposed to block in part the surface for attack in the iron-hydrogen sulfide reaction, it was thought that a similar effect might be observed in the iron-sulfur vapor reaction if hydrogen were allowed to diffuse from the back of the specimen surface. The data of Fig. 10, obtained by the cartridge technique, confirm this inference. The parabolic law was confirmed for the blank cartridges which had been left in vacuum for 8 hr after hydrogen reduction. An induction period was observed for blank cartridges which had not been vacuum treated, and an even longer induction period was observed for cartridges containing lithium aluminum hydride. In all cases, sulfur attack resumed its normal course after a sufficiently long time. The interpretation is as follows:

Hydrogen produced in the lithium aluminum hydride cartridge diffused toward the outside surface of the cartridge and greatly reduced the attack by sulfur vapor. Nevertheless, an iron sulfide scale slowly built up. The diffusion rate for hydrogen through the compact scale (no leaks!) was lower than through iron, as shown[11] in Fig. 11, and consequently, coverage of the scale by hydrogen decreased as the scale became thicker. This resulted in a progressive increase in rate of attack until the film had become so thick that diffusion was practically stopped. Attack then resumed its normal course. Complete decomposition of lithium aluminum hydride cannot be invoked for resumption of normal attack because of the respective amounts of this substance and diffused hydrogen that were involved.

[10] This section based on work of L. Hulett and M. Qureshi.

[11] One calculates from the rate of diffusion of hydrogen for the cartridge without scale the approximate inner pressure of hydrogen of 2 atm on the basis of the permeability data of Jost (7).

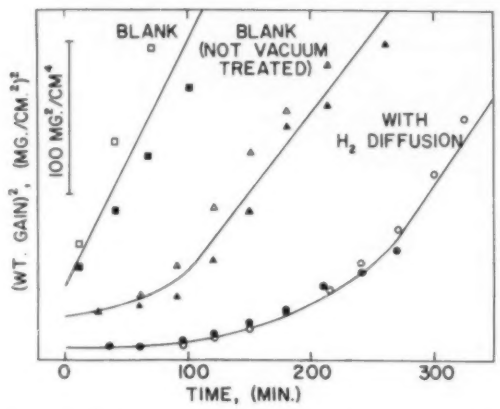

Fig. 10. Plots of the square of the weight gain against time for iron cartridge during attack by sulfur vapor. Temperatures during attack: molten sulfur, 230°C; cartridge, 500°C. Curves are equally shifted at the origin by 20 mg^2/cm^4.

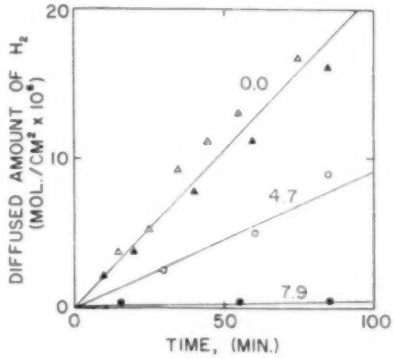

Fig. 11. Data for hydrogen diffusion through iron or iron coated with iron sulfide scale. Number on each line is the weight of iron sulfide in mg/cm^2. Temperature: 500°C.

The same interpretation holds for the blank cartridges which had not been vacuum treated. Hydrogen which had diffused in the metal during reduction then hindered attack in sulfur vapor until it could no longer appreciably cover the scale surface.

Further confirmation of the above interpretation was obtained by similar experiments in which the blank cartridge and a lithium aluminum hydride filled cartridge were attacked in hydrogen-hydrogen sulfide mixture (4:1). The same rate of attack was observed in both cases, and no induction period due to the presence of hydrogen was observed.

An alternative explanation, based on thermodynamic considerations, namely that iron attack by sulfur did not proceed in the presence of hydrogen, is ruled out. Thus, one calculates from the data of Rosenqvist (6) that the equilibrium constant for the reaction $FeS + H_2 \rightleftharpoons Fe + H_2S$ at 500°C is 2×10^{-4}. The amount of hydrogen sulfide formed in one of the experiments was in fact determined by passing the gas through a detection tube used in air pollution studies.[12] A maximum amount of 6×10^{-6} moles of hydrogen sulfide was formed in the reaction chamber. Since the amount of hydrogen sulfide produced is so small, the retarded sulfur attack is

[12] Courtesy of Professor P. W. West, Louisiana State University.

Table I. Thicknesses of the dense layer of iron sulfide produced by attack by a 4:1 hydrogen-hydrogen sulfide mixture at 575°C

Reaction time, min	Thickness, mm × 10^2	Number of determinations
30	1.6	2
140	6.5	1
180	8.0	4
480	7.7	1
540	8.9	1
550	7.7	1
660	7.7	1
720	8.9	1

definitely not due to reduction of iron sulfide by diffusing hydrogen.

Another possible interpretation according to which Haycock's E-centers (3), resulting from the presence of hydrogen in the film, decrease diffusion by cation vacancy does not account for the resumption of attack. Thus, the scale, at least in its inner layer, retained a relatively high concentration of E-centers because of the vicinity of hydrogen supply. This layer would have offered a permanent barrier to vacancy diffusion, i.e., attack would never have resumed unless the film had cracked. The latter explanation, however is invalidated by the very low diffusion rate of hydrogen through the scale (Fig. 11). Of course, one could say that sulfide ion is the diffusing species, but the role of hydrogen then remains unexplained.

Recrystallization of the Scale[12]

It is well established [see Dravnieks and Samans (1) for review of literature] that the thin dense layer reaches an essentially constant thickness. The data on Table I confirm this, but it should be noted that initially (30 min) the thin layer had not reached its constant thickness although a linear law was already observed. This seems to preclude, with other arguments discussed above, control by diffusion through the thin layer.

Since the thin layer reaches a constant thickness, there must be a continuous transformation of the thin dense layer into the porous one (Fig. 4). We observed that aging of the two layer scale in a helium atmosphere causes a progressive disappearance of the dense layer. Since such a transformation is not observed for iron sulfide produced by the iron-sulfur vapor reaction, hydrogen or hydrogen sulfide must be responsible for recrystallization. Haycock (3) suggested a tentative mechanism for the recrystallization process, and he showed that hydrogen greatly enhanced the sintering rate of powdered iron sulfide. Powdered ferrous sulfide with a large initial surface area did not appreciably sinter when left in a vacuum for 5 hr at 500°C. In the presence of hydrogen at the same temperature the surface area was reduced by half after only 2 hr, and the powder had visibly sintered to a porous plug.

Haycock's experiments were corroborated by studies on aging of iron sulfide, prepared by sulfur attack, in the equilibrium hydrogen-hydrogen sulfide mixture (see Experimental Methods). The outer crystalline structure of the scale became somewhat more coarse upon aging (Fig. 12).

[12] This section based on the work of L. Hulett and M. Qureshi.

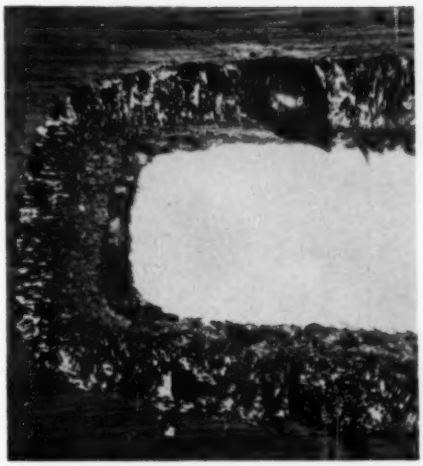

Fig. 12. Photomicrograph of section of specimen, attacked in sulfur vapor at 500°C (vessel with liquid sulfur at 230°C), after a 48-hr aging in hydrogen at a pressure slightly above 1 atm. Note EPON resin around metal contour as a result of scale spalling. Magnification, 200× before reduction for publication.

Conclusion

It is concluded that the linear law of attack for the iron-hydrogen sulfide reaction at elevated temperatures (above 500°C approximately) results from two main effects: (*a*) partial blocking at reaction sites by hydrogen produced during attack, and (*b*) continuous recrystallization prevents the formation of a thick dense scale that would become a real diffusion barrier for sufficient thicknesses. The blocking of reaction sites is self-regulating and the linear law is thus obeyed.

Acknowledgment

The support of the American Petroleum Institute is gratefully acknowledged. The authors are indebted to the following members of the Subcommittee on Corrosion, Division of Refining, of the American Petroleum Institute for helpful discussions: Messrs. E. B. Backensto, E. A. Camp, and R. J. Hafsten. Discussions with Drs. A. Dravnieks and E. W. Haycock were most fruitful. Messrs. E. G. Smith and G. F. Mathes of the Mechanical Engineering Department, Louisiana State University, kindly provided equipment for the photomicrographic studies.

X-ray equipment used in some structure studies was purchased in part with a grant from the National Science Foundation.

Manuscript received July 30, 1959.

Any discussion of this paper will appear in a Discussion Section to be published in the December 1960 JOURNAL.

REFERENCES

1. A. Dravnieks and C. H. Samans, *This Journal*, **105**, 183 (1958).
2. K. Hauffe and A. Rahmel, *Z. physik. Chem.*, **199**, 152 (1952).
3. E. W. Haycock, *This Journal*, **106**, 764, 771 (1959).
4. D. Caplan and M. Cohen, *J. Metals*, **4**, 1057 (1952).
5. O. Beeck, *Advances in Catalysis*, **2**, 151 (1950).
6. T. Rosenqvist, *J. Iron Steel Institute*, **176**, 37 (1954).
7. W. Jost, "Diffusion in Solids, Liquids, and Gases," p. 305, Academic Press, New York (1952).

Nickel-Aluminum Alloy Coatings Produced by Electrodeposition and Diffusion

Dwight E. Couch and Jean H. Connor

National Bureau of Standards, Washington, D. C.

ABSTRACT

Nickel-aluminum alloy coatings were produced by diffusion of aluminum electrodeposited over nickel. The aluminum was plated from baths operated at 25°-1000°C. The alloys were much harder than nickel and were superior to nickel coatings in salt spray, atmospheric exposure, and air oxidation tests. Attempts to codeposit the two metals were not successful.

Nickel-aluminum alloys are very resistant to oxidation in air at temperatures of 500°-1100°C. They are hard and resistant to corrosion at normal temperatures. Alloys of this type have been prepared by metallurgical methods (1, 2) but, because the alloys are brittle, they are difficult to use in the manufacture of intricately shaped objects. Electrodeposited coatings of these alloys should provide valuable protection to other metals. In previous studies (3) coatings of nickel-aluminum alloys were formed by the electrodeposition of aluminum, from a fused cryolite bath, on nickel. Beck (4) used a cryolite bath to form nickel aluminide coatings on nickel-plated molybdenum and identified the various phases of the alloy diffusion layer. Many objects that require coating cannot withstand a temperature of 1000°C at which the cryolite bath is operated; therefore, other baths that may be used at lower temperatures were investigated. Fink and Solonki (5) studied several aluminum chloride alkali chloride baths with a 1 to 1 mole ratio. Collins (6) used a higher aluminum chloride content and obtained smooth deposits. A review of aluminum coating processes was given by Murphy (7).

Electrodeposition of Nickel and Aluminum from Organic Type Baths

All of the known organic-type baths (8-13) for plating aluminum were investigated to see if nickel could be codeposited with aluminum. In general, nickel salts were only slightly soluble in the organic solvents used to prepare the baths and no alloy deposits were produced. Electrodeposition of nickel from other organic solvents also was investigated, since the desired alloy would be predominantly nickel. Ductile nickel deposits could not be obtained from any of the organic baths. Thin, coherent, highly stressed, lustrous deposits were obtained sometimes. These contained only 85% nickel, the remaining 15% probably was occluded organic material. Table I lists organic solvents and nickel salts used in the experiments. Since pure nickel could not be electrodeposited from organic solvents, this approach was abandoned.

The ether-hydride bath (8) was used successfully to produce coatings of aluminum that could be alloyed with nickel. However, an intermediate coating of zinc or copper was required to give necessary adhesion and to prevent blistering of the aluminum

Table I. Organic baths used in the electrodeposition of nickel

Solute:	$NiCl_2$		$NiBr_2$		NiI_2		$Ni(CF_3COO)_2$		$Ni(C_2F_5COO)_2$		$Ni(SCN)_2$	
Solvent	Solubility*	Nature of deposit	Solubility	Nature of deposit	Solubility	Nature of deposit	Solubility	Nature of deposit	Solubility	Nature of deposit	Solubility	Nature of deposit
Formamide	S	Coherent	T	Coherent	T	Black coherent	S	Coherent	T	Coherent	T	Fair
Acetamide	T	Fair	T	Fair	T	Fair	—	—	—	—	—	—
Dimethylformamide	i	None	i	None	T	None	S	Poor	T	Poor	T	Poor
Acetonitrile	T	Poor	S	None	T	None	S	Coherent	S	Fair	i	None
Ethyleneglycol dimethyl ether	T	None	T	Black powder	S	Black powder	S	Black	S	Powder	T	None
Tetrahydrofuran	T	None	T	Black powder	S	Black powder	S	Poor	S	None	T	None
Ethyl ether	i	None	i	None	i	None	—	—	T	Powder	i	None
Tetraethyleneglycol dimethyl ether	T	None	S	Black powder	S	Black powder	S	None	S	Coherent	T	Powder
Xylene	i	None	i	None	T	None	i	None	i	None	T	None
Toluene	i	None	i	None	T	None	i	None	i	None	T	None
Benzene	i	None	T	None	T	None	T	None	i	None	T	None
N-butylamine	T	None	T	None	T	None	S	Black	S	Black	S	Black

* i, Insoluble; T, Trace; S, Soluble.

deposit during the heat treatment at 550°C required to alloy the aluminum with the nickel.

Fused Salt Baths and Conditions of Operation

Several fused-salt baths for the electrodeposition of aluminum were studied, and the following were found to be the most satisfactory: potassium chloride-sodium chloride-cryolite, aluminum chloride-sodium chloride.

The composition and optimum operating conditions for these baths are as follows:

Potassium chloride-sodium chloride-cryolite: sodium chloride, 440 g; potassium chloride, 560 g; cryolite, 150 g; temperature, 700°-800°C; current density, 2-10 amp/dm²; anodes, graphite; container, graphite.

Aluminum chloride-sodium chloride: aluminum chloride (anhydrous), 900 g; sodium chloride, 200 g; temperature, 160°-180°C; current density, 1-4 amp/dm²; anodes, tungsten or graphite; covered container, glass (Pyrex or equivalent).

Potassium chloride-sodium chloride-cryolite bath.—This bath was contained in a graphite crucible and operated at temperatures from 650° to 900°C. At the higher temperature the graphite crucible oxidized rather rapidly, and at 650°C the aluminum diffused into nickel rather slowly. Therefore, most of the deposits were made at 700°-750°C. At this temperature the aluminum deposit was liquid and alloyed with the nickel.

Samples (0.1 x 3 x 6 cm) to be plated were placed in the bath and allowed to heat up to bath temperature before electrolysis. Excellent adhesion was obtained on nickel, iron, and previously prepared Ni-Al alloys. No precleaning of the specimen was necessary. At 700°C an aluminum deposit 6 μ thick could be produced by using a current density of 7 amp/dm² for 5 min. When the electrolysis was continued under these conditions for more than 5 min, the aluminum was electrodeposited faster than it could diffuse into the nickel, and free aluminum was produced on the surface of the sample. Thicker deposits could be produced by using a lower current density for a longer time, or by operating at a higher temperature. Deposits 25 μ thick were prepared at 700°C by the following schedule: 7 amp/dm² for 5 min, 4 amp/dm² for 20 min, and 2 amp/dm² for 90 min.

The cathode current efficiency for plating aluminum on nickel cathodes is shown in Fig. 1. The efficiency was about 90% at 15 amp/dm², but decreased, as the current density decreased. At 0.5 amp/dm² the solution rate of the alloy equaled the deposition rate, thus giving an efficiency of zero. The efficiency at current densities greater than 15 amp/dm² could not be determined because the aluminum deposited more rapidly than it could diffuse into the nickel and was lost as molten aluminum into the bath. Nickel and Ni-Al alloy slowly dissolved in the bath. Nickel dissolved at a rate of about 0.6 mg/cm²/hr, and the Ni-Al alloy dissolved at approximately 1.6 mg/cm²/hr.

Alloy deposits 25 to 75 μ thick[1] produced from the potassium chloride-sodium chloride-cryolite bath contained from 43 to 52% Al. This represents an average composition of 1 mole Ni to 2 moles Al. No attempts were made to identify the separate phases of this alloy system.

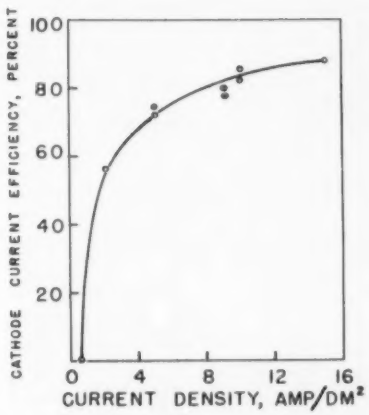

Fig. 1. Cathode current efficiency of aluminum electrodeposited from potassium chloride-sodium chloride-cryolite bath at 700°C.

Occasionally, deposits produced at the higher current densities showed traces of free aluminum on the surface. Excess aluminum was removed with 2.5M aqueous sodium hydroxide. This solution dissolved the alloy at a rate of about 0.005 mg/cm²/hr.

Aluminum chloride-sodium chloride baths.—This bath was operated at a temperature where very little diffusion of aluminum into nickel took place. Therefore, it was necessary to heat the samples after plating to form the alloy. Temperatures of 700°C could be used for thin coatings 5 μ thick, but coatings 25 μ thick melted, and only a small fraction of aluminum diffused into nickel, the remainder formed a metallic bead at the edge. The approximate time required for various thicknesses of aluminum to diffuse into nickel at 700° and 550°C are shown in Fig. 2. Values for 700°C were obtained on flat specimens that were held horizontally to prevent run off of molten aluminum.

If the aluminum chloride-sodium chloride mole ratio was less than 1.5, as in the baths described by Fink and Salonki (5), and operated at 160°-180°C,

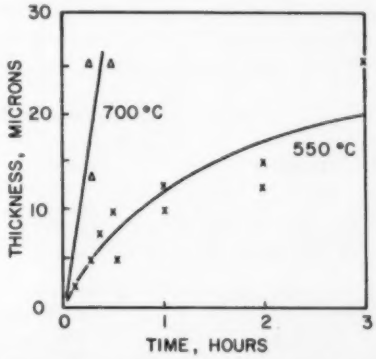

Fig. 2. Time required to completely alloy aluminum with nickel at various temperatures. Aluminum was plated from $AlCl_3$-NaCl bath, or ether-hydride bath.

[1] The thickness referred to here and at all later places in this paper is the thickness of the electrodeposited aluminum as determined by the increase in weight of the sample as a result of the aluminum deposit. Therefore it is not a measure of the actual thickness of the alloy layer formed.

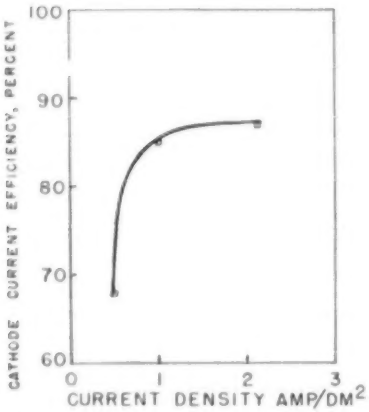

Fig. 3. Cathode current efficiency for electrodeposition of aluminum from an $AlCl_3$-NaCl bath at 170°C.

the maximum thickness of satisfactory deposits was about 5 μ. Thicker deposits were rough and powdery. Electrodeposits up to 25 μ thick were obtained from a bath similar to that given by Collins (6). However tungsten was used for anodes instead of aluminum.

Figure 3 shows the cathode current efficiency of aluminum chloride-sodium chloride bath. Chlorine liberated at the insoluble anode apparently dissolved in the bath in sufficient amounts to slowly dissolve aluminum deposit, thus accounting for the decrease in cathode efficiency at the lower current densities. Moisture that reacted with aluminum chloride produced some hydrogen chloride that attacked the aluminum deposit.

When aluminum electrodeposited from this bath was overplated with a second layer of aluminum, the adhesion was very poor. Aluminum deposits that were allowed to stand in the bath showed surface attack and formation of a thin black film. This film prevented adhesion of the second deposit. Anodic treatment of the panel in the bath caused a similar condition regardless of current density (1-15 amp/dm^2). If the sample was heated to alloy the first aluminum deposit with nickel, a second layer could be deposited with sufficient adhesion to allow heat treatment to alloy it with the first layer.

Codeposition of nickel and aluminum from fused salt baths.—Aluminum and nickel can be codeposited from a bath containing sodium chloride, potassium chloride, cryolite, and nickel chloride at current densities of 100 amp/dm^2 or greater. These deposits contained 30 to 50% Al. Unfortunately, they were produced only as very thin deposits, and attempts to form deposits 25 μ thick resulted in thin coherent layers covered with a black noncoherent material. At current densities of less than 100 amp/dm^2, the deposits contained no aluminum. Nickel anodes were insoluble and were coated with a tan-colored material that was also insoluble in the bath. This was presumably an oxide or oxychloride of nickel. Other fused-salt systems studied are listed in Table II. No alloy deposits were obtained from these baths. Although aluminum could be electrodeposited from most of them, nickel only could be electrodeposited after the addition of nickel salts.

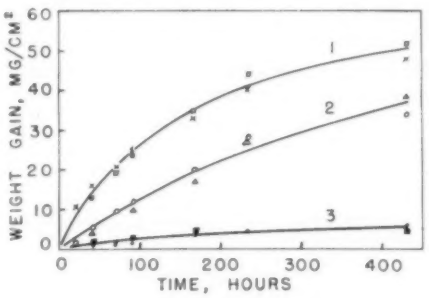

Fig. 4. Oxidation of nickel and nickel-aluminum alloy at 1000°C. Curve 1. □, x, pure nickel, duplicate samples; 2. ○, △, alloy coating, approximately 8 μ, duplicate samples; 3. ●, ■, alloy coating, approximately 25 μ, duplicate samples.

Evaluation of Deposits

Oxidation.—In air at 550°C, Ni-Al alloy coatings on steel oxidized at a slower rate than nickel-coated steel. Similar results were obtained at 1000°C using nickel panels as a basis metal. Nickel panels, 6 x 3 x 0.1 cm, were cut from rolled sheet nickel. Two of these panels were used as controls while five others were plated in the fused aluminum chloride-sodium chloride bath to the following average thicknesses: 8, 8, 10, 25, and 25 μ. Two panels (8 and 10 μ aluminum) were heated in air at 750°C for 30 min and others were heated in helium for 15 hr at 550°C to alloy the aluminum; all panels showed a slight gain in weight of about 3 x 10^{-5} g/cm^2. Oxidation curves are shown in Fig. 4. The oxide of one panel spalled in large flakes when cooled after heating for 20 and 44 hr. This oxide was weighed and added to the total weight gain of the panel. This panel had oxidized at about the same rate as the pure nickel. A coating of

Table II. Fused salt baths used in deposition of nickel and aluminum

Bath composition	Temp, °C	Deposit obtained	Type deposit	Anode used	Anode effect
NaCl-$AlCl_3$	160	Aluminum	Coherent	Nickel	Insoluble
KCl-NaCl-NaCN	600	Nickel	Dendrites	Nickel	Soluble
KCl-NaCl-NaCN-$NiCl_2$	600	Ni^{++} chemically reduced to Ni	—	—	—
NaCl-KCl-Na_3AlF_6-$NiCl_2$	700-800	Nickel	Dendrites	Graphite	Insoluble
NaCl-KCl-Na_3AlF_6-$NiCl_2$	700-800	Nickel	Dendrites	Nickel	Passivated
NaCl-$AlCl_3$-$NiCl_2$	600	Nickel	Dendrites	Nickel	Soluble
KBr-$AlBr_3$-$NiBr_2$	200	Black powder	Powder	Nickel	Soluble
KBr-$AlBr_3$-$NiBr_2$	200	Black powder	Powder	Tungsten	Insoluble
$NaPO_3$-$NiCl_2$-Na_3AlF_6	700-800	Nickel	Dendrites	Nickel	Soluble
KCl-NaCl-$Ni_3(PO_4)_2$-Na_3AlF_6	600	Nickel	Dendrites	Nickel	Soluble

8 μ Al reduced the amount of oxidation at 1000°C about 40%, curve 2, while a coating of 25 μ Al reduced the oxidation by about 80%, curve 3. Heating samples in an inert atmosphere to alloy aluminum with nickel did not affect the rate of oxidation.

The oxide layer that formed on the Ni-Al alloy was gray, while that formed on the nickel was vitreous and black in color. A gray oxide formed on specimens with a coating of 8 μ Al, but after heating about 100 hr at 1000°C, the surfaces of the panels were black. Those specimens with 25 μ Al retained their gray color for 300 to 400 hr before the black nickel oxide covered a significant amount of the surface.

Figure 5 shows that alloy coatings 25 μ thick do not give satisfactory protection to steel at 900°C. The iron diffused through the coating, resulting in rapid oxidation. Thicker coatings are required to protect steel at these temperatures.

Salt spray test.—Salt spray tests were made on steel (6 x 3 x 0.1 cm) coated with Ni-Al alloy. Samples were first nickel plated, then separated into groups in random fashion. One group was used as a control, while the alloy was formed on the other group. In this way the influence of the nickel plating process was minimized. The most corrosion-resistant coatings were produced by plating aluminum from the sodium chloride-potassium chloride-cryolite bath and subjecting these coatings to oxidation at 500°-600°C prior to testing. Rapid temperature cycling of these panels did not affect their corrosion resistance. The coatings were more resistant if the aluminum thickness was less than 50% of the total thickness of the coatings (see Table III). In the salt spray tests, 5 or more samples were used for each thickness tested and the average time required for the first rust to form on the surface is given in Table III.

Evaporated aluminum coatings[2] 0.1 μ thick, which were alloyed with nickel by heating in air, caused a decrease in the corrosion of nickel-plated steel. Although they showed the first rusting at the same time as the control panels (5 hr), the surface area was 7% rusted after 75 hr as compared to 30% on the control panels.

[2] Panel size in these tests were 10 × 15 × 0.1 cm.

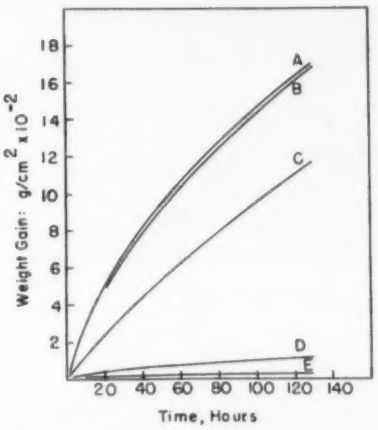

Fig. 5. Oxidation at 900°C in air of alloy-coated steel and nickel. Coatings were prepared in cryolite bath at 1000°C. Curve A, steel; B, 25 μ of nickel on steel; C, 25 μ of nickel plus 25 μ of aluminum on steel; D, wrought nickel; E, 25 μ of aluminum on wrought nickel.

Sprayed aluminum coatings[2] were also effective in reducing corrosion by salt spray. Although small areas of uncoated nickel could be seen through the sprayed coating, these areas could not be detected after the sample was heated. The sprayed coating was initially about 20-30 μ thick, but after heating for 30-45 min at 550°C, which was sufficient time to produce an alloy layer about 10 μ thick, the samples were treated with 2.5M aqueous sodium hydroxide to remove the excess aluminum. They then were subjected to salt spray tests. These samples showed rust after 30 hr and were 2% rusted after 75 hr. The control[2] samples showed the first rusting after 5 hr and were 30% rusted after 75 hr.

Corrosion studies conducted on atmospheric exposure racks at Washington, D. C., correlated well with the salt spray tests. Steel panels coated with 25 μ Ni and 5 μ Al did not show rust at the end of one year of exposure, while coatings with 12 μ Ni plus 4 μ Al showed traces of rust after eight months of exposure. Nickel-plated control panels tested simul-

Table III. Salt spray tests (20% solution) on 3 x 6 cm steel samples coated with Ni-Al alloy or nickel. The time shown is an average time for 5 or more samples

Thickness, μ		Type bath used to deposit Al	Other treatments	Time in salt spray to first rust,* hr
Nickel	Aluminum			
50	8	$NaCl$-KCl-Na_3AlF_6	Oxidized 90 hr 550°C in air	400
50	8	$NaCl$-KCl-Na_3AlF_6	None	300
25	25	$NaCl$-KCl-Na_3AlF_6	None	100
12	5	$NaCl$-KCl-Na_3AlF_6	None	40
12	5	$NaCl$-KCl-Na_3AlF_6	Oxidation cycled†	60
12	5	$NaCl$-KCl-Na_3AlF_6	Oxidized 90 hr 550°C	70
5	35	$NaCl$-KCl-Na_3AlF_6	None	20
12	5	$AlCl_3$-$NaCl$	Heated to form alloy	30
50	None	—	None	20
25	None	—	None	10
12	None	—	None	5

* Samples were inspected after 5 hr, 20 hr, and every day thereafter.
† Samples were heated at 550°C for 10 min, then cooled to room temperature 10 min, then reheated to 550°C. This cycling was repeated for 24 hr, then they were salt spray tested 24 hr, then oxidation cycled 24 hr, etc.

Fig. 6. Nickel-aluminum alloy formed by plating 25 μ of aluminum over nickel and heating at 550°C to alloy aluminum with nickel. Magnification 200X before reduction for publication.

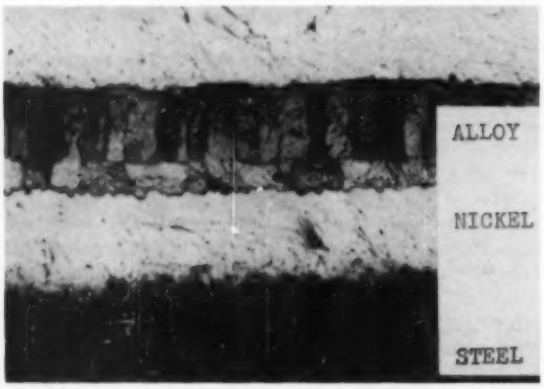

Fig. 7. Nickel-aluminum alloy produced in sodium chloride-potassium chloride-cryolite bath at 700°C. This deposit was heated 2 hr at 1000°C after plating. Magnification 500X before reduction for publication.

taneously with the above samples showed rust after four months and one month, respectively.

Metallographic examinations.—Figure 6 shows a deposit prepared from low-temperature fused aluminum chloride-sodium chloride bath at 160°C, then alloyed with nickel by heating at 500°-600°C for a few hours. Figure 7 shows a deposit produced from potassium chloride-sodium chloride-cryolite bath, after heating for 2 hr at 1000°C. No structure could be developed on the alloy in the as-plated condition.

The Knoop hardness of the Ni-Al alloy produced from the chloride-cryolite bath was 620 for thin films and 700-725 for thicker coatings (50 μ). The hardness of deposits produced from the all-cryolite (3) bath varied from 611 to 788.

The coatings were brittle, and, if 25 μ thick, they could be separated from the basis metal by repeated bending. Thin coatings 5 μ thick fractured when bent, but did not separate from the basis metal. Results of bending samples of two different thicknesses around a 0.6 cm diameter rod are shown in Fig. 8.

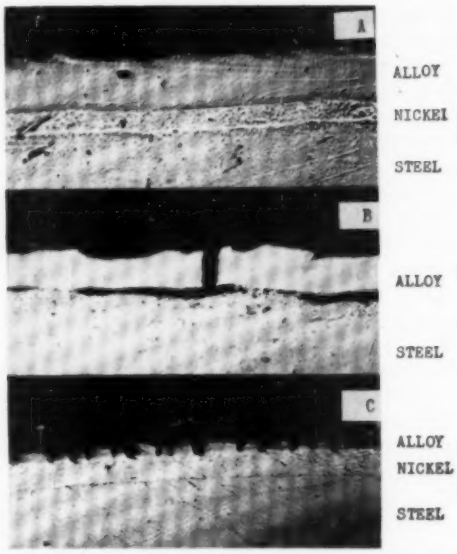

Fig. 8. Nickel-aluminum alloy over steel. A, 50 μ nickel and 40 μ aluminum formed by plating 3 separate deposits of aluminum; B, effect of bending deposit "A" 90 degrees over a 0.6 cm diameter rod; C, effect of bending a deposit of 12 μ nickel and 5 μ aluminum to 90 degrees over a 0.6 cm diameter rod. Magnification 200X before reduction for publication.

Acknowledgment

This research was supported by the United States Air Force under Contract No. DO 33(616)-57-10, monitored by the Materials Laboratory, Wright Air Development Center, Wright-Patterson Air Force Base, Ohio.

Manuscript received Sept. 3, 1959. This paper was prepared for presentation at the Ottawa Meeting, Sept. 28-Oct. 2, 1958.

Any discussion of this paper will appear in a Discussion Section to be published in the December 1960 JOURNAL.

REFERENCES

1. J. H. Westbrook, *This Journal*, **103**, 54 (1956).
2. E. M. Grala, NACA Tech. Note 3660 (1956), Lewis Flight Prop. Lab., Cleveland, Ohio.
3. D. E. Couch, H. Shapiro, and A. Brenner, *This Journal*, **105**, 485 (1958).
4. W. Beck, *ibid.*, **106**, 783 (1959).
5. C. G. Fink and D. N. Solonki, *Trans. Electrochem. Soc.*, **91**, 203 (1947).
6. F. R. Collins, *Iron Age*, January 17, **169**, 100 (1952).
7. N. F. Murphy, *Metal Finishing*, **50**, 76 (1952).
8. D. E. Couch and A. Brenner, *This Journal*, **99**, 234 (1952).
9. J. H. Connor and A. Brenner, *ibid.*, **103**, 657 (1956).
10. F. H. Hurley and T. P. Weir, *ibid.*, **98**, 203 (1951).
11. A. C. Doumas and N. F. Murphy, *Tech. Proc. Am. Electroplaters' Soc.*, **43**, 162 (1956).
12. M. A. Miller and C. D. Baker, U.S. Pat. 2,763,605, Sept. 18, 1956.
13. K. Ziegler and H. Lehmkuhl, *Angew. Chem.*, **67**, 424 (1955).

Effect of Addition Agents on Tungsten Codeposition

J. S. Sallo[1] and R. D. Fisher

Magnetic Research Department, The National Cash Register Company, Dayton, Ohio

ABSTRACT

Small quantities of certain addition agents will prevent the codeposition of tungsten with iron, nickel, or cobalt. Data are presented comparing addition agent concentration with the amount of tungsten in a nickel-tungsten codeposit. Polarographic data indicate that addition agents which prevent tungsten codeposition are capable of being adsorbed at a Hg cathode and form complexes with the codepositing metal ion. These complexes are more readily reduced than is the original codepositing species. The cathode potential of the deposition process is lowered to a more positive potential by the addition agent. Structural studies show that the deposit does not consist of alternate layers of tungsten and codeposited metal as is required by the catalytic reduction mechanism. It is shown that the addition agent effect can be explained by a mechanism of codeposition involving complex formation.

Many claims have been made for the deposition of pure tungsten from aqueous tungstate solution (1-3). Subsequent investigation of these processes has shown that the deposits always contain iron, nickel, or cobalt (codepositing metal ion) (4), and that deposition ceases when these impurities are exhausted from the plating solution. When no such impurities are present in the plating solution, oxides of tungsten may be deposited at the cathode; however, under these conditions reduction of tungstate to tungsten has not been observed.

Many baths have been developed for the codeposition of tungsten with iron, nickel, or cobalt. The most successful of these are the complex ammoniacal baths which have been developed by Brenner (5) and by Holt (6). Brenner's baths allow the codeposition of sound Ni-W deposits containing 20% tungsten. Iron-tungsten deposits containing 50% tungsten can be plated from such baths. Two mechanisms have been proposed to explain the codeposition process. These are the catalytic reduction mechanism and the complex formation mechanism.

The catalytic reduction mechanism proposes that laminations observed in the codeposits are alternate layers of tungsten and the codeposited metal (iron, nickel, or cobalt) (7). The codeposited metal acts as a catalytic surface on which, in the presence of hydrogen, the tungstate anion is reduced chemically and electrochemically to metallic tungsten. When a layer of tungsten has covered this catalytic surface, the deposition ceases and the formation of a fresh layer of catalytic codeposited metal begins.

The complex formation mechanism describes the codeposition as taking place from some complex of tungstate and the codepositing metal ion (7). The function of the codepositing metal ion is to provide a reducible tungstate complex. The major disadvantage of the complex formation mechanism is that no complex of tungstate with ions of iron, nickel, or cobalt has been observed.

The effect of addition agents on tungsten codeposition and data indicating that the codeposits are solid solutions are discussed in this paper.

[1] Present address: Minneapolis-Honeywell Regulator Company, Research Center, Hopkins, Minnesota.

Experimental

Deposition studies.—All chemicals used were C.P. reagent grade and were not further purified.

The plating bath used for the nickel tungsten deposition was as follows: $NiCl_2 \cdot 6H_2O$, 28 g/l (0.12 mole/l); $Na_2WO_4 \cdot 2H_2O$, 32 g/l (0.036 mole/l); NH_4Cl, 50 g/l (0.94 mole/l); sodium citrate, 100 g/l (0.39 mole/l); H_2O and NH_4OH to 1 liter at a pH of 8.5. For the iron-tungsten and cobalt tungsten codeposits 0.12 mole/l of $FeCl_2 \cdot 4H_2O$ or $CoCl_2 \cdot 6H_2O$, respectively, were used in place of $NiCl_2 \cdot 6H_2O$.

The cathodes for deposition were 0.003 in. thick sheets (2 x 2 in.) of phosphor bronze to which were welded copper wires for electrical contact. The copper contacts were kept well above the solution level. The cathodes were cleaned cathodically in an alkaline medium, followed by an acid dip (1:1 HCl), and a distilled water rinse. Sheets or rods of pure tungsten were used as anodes. The temperature of the bath was controlled at 90° ± 0.5°C by means of a glascol heating mantel. The current density was 2 amp/dm^2. The volume and pH of the solution were maintained by continuous addition of a NH_4OH, H_2O solution through a peristaltic action pump.

In the studies leading to the determination of the minimum concentration of addition agent required to prevent tungsten codeposition completely, a fresh plating system was used for each addition agent concentration. In the studies showing the decrease of tungsten content in the nickel-tungsten deposit with increasing addition agent concentration, successive additions of the addition agent were made to a single plating system.

Cathode potential studies.—Cathode potentials were determined at varying current densities on the following three baths:

1. $NiCl_2 \cdot 6H_2O$, 28 g/l (0.12 mole/l; NH_4Cl, 50 g/l (0.94 mole/l); and sodium citrate, 100 g/l (0.39 mole/l) H_2O and NH_4OH to a pH of 8.5.

2. Same as 1 except 32 g/l $Na_2WO_4 \cdot 2H_2O$ (0.036 mole/l) added.
3. Same as 2 except 0.1 g/l (0.0013 mole/l) thiourea added.

Cathode potentials during deposition from the above baths were determined by the direct method. The cell consisted of a 2-liter beaker with a heating mantle and contained a platinum cathode (0.95 x 1.01 x 0.022 cm) and two platinum anodes (2.2 x 2.2 x 0.022 cm). The distance between the anodes and cathode was 4.75 cm. The flat platinum cathode was coupled with an external Beckman saturated calomel electrode by means of a bridge made from 6.3 mm Pyrex tubing with one end drawn out to a capillary tip 1 mm in diameter and 1 cm long. The tip was bent at 90° and placed near the face of the cathode. To measure the potential, a L&N type K-3 potentiometer supplied a balancing emf, and a Kintel Microvoltammeter served as a Null detector. The potentials were measured commencing with the initial static potential emf. The readings of the emf were taken at various current densities. The current was measured with a Simpson milliammeter (Model 373). Sufficient time (2-3 min) was allowed for each measurement to enable the potentials to reach a steady value. Individual determinations were reproducible within ± 5 mv. No correction was made for the *IR* drop between the capillary tip and the surface of the cathode. Also, a nonuniform current density results with a parallel electrode system since the current density is highest at the edges. These factors and others make the absolute cathode potential measurements somewhat uncertain. The *p*H and volume of each bath were maintained by continuous additions of NH_4OH and H_2O, and temperature was controlled at 90° ± 1°C.

X-ray diffraction.—X-ray diffraction was performed on a North American Phillips type diffractometer. In all cases copper K α radiation was used, the potential was 35 kv, the current was 20 ma, the scanning rate was 2°/min, and the Geiger counter voltage was 1385. The time constants were 8, 2, and 16 sec for nickel, tungsten, and nickel-tungsten, respectively.

X-ray fluorescence.—The plated samples were analyzed for Ni, Co, Fe, and W, respectively on a Norelco x-ray spectrograph. The unit was operated with a W x-ray tube at 50 kv and 50 ma. Fixed count operation was employed, i.e., the times were recorded to obtain 512,000 counts for Ni; 256,000 counts for Co; 128,000 counts for Fe; and 32,000 counts for W. These readings were converted to counts/second for each element. A LiF crystal was used and first-order peaks of the elements were used as follows: Ni $K\alpha_1$ at 48.61° 2θ, Co $K\alpha_1$ at 52.74° 2θ, Fe $K\alpha_1$ at 57.45° 2θ, and W $L\alpha_1$ at 42.99° 2θ.

Since the use of a W x-ray tube means that a W count will be produced even if the sample is free of W (background), the point at which no W appears in the deposit for each series of samples was double-checked using a Norelco x-ray spectrograph employing a Mo x-ray tube, operating at 50 kv and 40 ma. In this case a NaCl crystal was used and a scan was made over the W $L\alpha_1$ peak in the second order (at 63.13° 2θ). The absence of W in the end-point samples was confirmed for all series.

Several nickel-tungsten samples were prepared in accordance with the instructions of previous workers (5). These were used as standards for the x-ray spectrometer. The graph of % W in the deposit vs. addition agent concentration is shown in Fig. 1.

Since the composition of the standard was not checked by chemical analysis, the accuracy of the values given is doubtful. However, the relative values of the concentrations in different specimens are probably valid.

Polarographic studies.—The polarographic studies were carried out using a L&N "polarotron" and a type-E electrochemograph. Polarograms were determined in a 1M NH_4OH, 0.2M NH_4Cl supporting electrolyte with 0.005% gelatin. Chemicals were C.P. grade.

Results

Many of the addition agents which were studied in this program were found to prevent the codeposition of tungsten with iron, nickel, or cobalt. These are thiourea, thiosulfate ion, thiocyanate ion, thioacetamide, and water soluble substituted thioureas. Among the addition agents which have no effect on the composition of tungsten codeposits are gelatin, saccharine, and urea. No criteria for the structure required of an addition agent for the prevention of tungsten codeposition can be established at this time; however, all successful addition agents investigated contained sulfur.

The effect of varying quantities of sodium thiosulfate, potassium thiocyanide, and thiourea on the approximate composition of the nickel-tungsten codeposit is shown in Fig. 1. The cut-off concentrations of other addition agents which prevent tungsten codeposition are shown in Table I. These cut-off concentrations were determined by an x-ray fluorescence unit with a molybdenum source.

It has been observed that the concentration of thiourea necessary to prevent tungsten deposition increases with increasing current density. That is, increasing the current density decreases the effectiveness of the thiourea. This decrease in effectiveness with increasing current density may be explained by the desorption of the thiourea with increased negative potential, or it may be due to in-

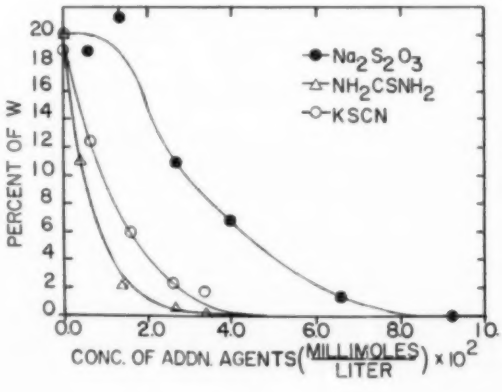

Table I. Effect of addition agents on W codeposition

Addition agent	Deposition of W ceases,* mg/l	Bath
$Na_2S_2O_3$	9.24	Ni-WO_4
KSCN	5.12	Ni-WO_4
NH_2CSNH_2	3.0	Ni-WO_4
NH_2CSNH_2	9.0	Co-WO_4
$Na_2S_2O_3$	29.5	Co-WO_4
KSCN	5.76	Co-WO_4
NH_2CSNH_2	20.0	Fe-WO_4

* Results were obtained by x-ray fluorescence using an x-ray unit containing a molybdenum tube.

creased decomposition of the thiourea with increased negative potential. The latter seems more likely since depletion of thiourea has also been observed. For example, a deposit was made from a bath containing the minimum quantity of thiourea (3 mg/l) required to prevent tungsten codeposition with nickel for a period of 4 hr at 2 amp/dm^2. After this period, a fresh deposit was then made from this bath and tungsten was found in the deposit. The thiourea concentration necessary to prevent W codeposition increases with Ni, Co, and Fe, respectively. In all cases investigated the concentration of addition agent necessary to prevent tungsten codeposition is larger when cobalt is the codepositing metal rather than nickel.

The potential required for the deposition of the tungsten alloys is more noble than the potential required for the deposition of the metal (Fe, Ni, or Co) by itself (8-10). According to data published by Markwell and Holt (11), a criterion for tungsten deposition is that the dynamic cathode potentials of the codepositing ion (Ni, Co, Fe) solutions, with and without tungsten ion, must be within 85 mv of each other. Therefore, it was of interest to determine the effect of thiourea on the cathode potentials of nickel and nickel tungstate solutions. The cathode potential, E_c (vs. SCE) at 2 amp/dm^2 of pure nickel solution was −1100 mv, while the solution containing nickel and tungstate ions had a cathode potential of −970 mv. When 0.1 g/l of thiourea was added to the nickel-tungstate solution, the cathode potential was −880 mv. This value is 90 mv below the cathode potential of the nickel-tungstate solution and 200 mv below the cathode potential of the nickel solution (Table II).

The polarographic method was employed to study the addition agent effect. The half-wave potential ($E_{1/2}$) of the cathodic nickel waves was determined in 1M NH_4OH, 0.2M NH_4Cl, supporting electrolyte and using 0.05 g/l of gelatin as a maxima suppressor. The results of these polarographic measurements are given in Table III. All effective addition agents cause a shift in the half-wave potential of the Ni wave. This is attributed to complex formation between the addition agent and the nickel species.

Except for the thiosulfate, the effective addition agents are seen to form complexes which are more easily reduced than is the original nickel species. This conclusion was also confirmed for thiourea by cathode potential studies.

Since, in general, complex formation makes an ion more difficult to reduce and shifts $E_{1/2}$ to a less

Table II. Cathode potential measurements

Plating bath	E_c*
Nickel	1.1
Nickel-tungstate	0.970
Nickel-tungstate-thiourea	0.880

* Potentials are given vs. a saturated calomel electrode at 2 amp/dm^2.

Table III. Polarographic half-wave potential

Metal ion and complexing agent	$E_{1/2}$ volts
Ni	1.04
Ni + thiourea	1.017
Ni + thioacetamide	0.987
Ni + allylthiourea	1.015
Ni + urea	1.033
Ni + sodium thiosulfate	1.075
Ni + thiosemicarbazide	0.897
Ni + KSCN	1.030

Test solution contained 4.2 × 10^{-5}M Ni^{++}, 2½ cc of 0.2% gelatin solution, 20 cc 5M NH_4OH, 20 cc 5M NH_4Cl, and 0.5 g of each complexing agent per 100 cc solution. $E_{1/2}$ vs. saturated calomel electrode.

noble potential, the observed behavior in this case probably results from the high overvoltage normally associated with the reduction of $Ni(H_2O)_x^{++}$ or $Ni(NH_3)_x^{++}$.

The suppression of the polarographic maximum, as by gelatin, occurs by adsorption of a surface active species at the cathodic mercury drop. Table IV indicates the effectiveness of addition agents as suppressors of the maximum of the cathodic nickel wave. All results are in the absence of gelatin or any other known surface active material. Therefore, it is concluded that all effective addition agents are adsorbed at the cathode. However, there is no quantitative correlation between their effectiveness as maxima suppressors and as tungsten deposition inhibitors.

The catalytic reduction mechanism states that the structure of the deposit consists of alternate layers of tungsten and the codeposited metal. If this is the case, x-ray diffraction should show a phase of nickel and a phase of tungsten, and the diffraction pattern obtained should consist of the superimposed diffraction patterns of pure nickel and pure tungsten. It has been reported that the diffraction pattern of the codeposit is that of a solid solution (5); however, the x-ray data which led to this conclusion was not published. Results obtained in the present investigation are shown in Table V. It is clear from the table that no tungsten phase is present. Instead the codeposit contains only nickel peaks shifted in the direction expected for a solid solution of tungsten in nickel. That the codeposit is a solid solution of tungsten in nickel, and not alternate layers of nickel and tungsten, is thereby confirmed.

Discussion

The addition agents which were found to prevent tungsten codeposition with nickel have several features in common. They all contain at least one sulfur atom, lower the cathode potential of the deposition process, can form bulk complexes with the co-

Table IV. Polarographic adsorption data

Complexing agent	Molar conc. × 10^3	Approximate % adsorption[a]
1-allyl-2-thiourea	5.17	100
Thiosemicarbazide	5.50	96
Thioacetamide	6.77	67
Thiourea	6.60	25
Sodium thiosulfate	4.02	31
Potassium thiocyanate	6.20	22
Urea	8.30	0
Gelatin	—	100[b]

[a] $\% \text{ Adsorption} = \dfrac{(H_n - I_4) - (H_s - I_4)}{H_n - I_4} \times 100$

H_n is height of the maximum of Ni wave without the complexing agent; H_s is height of the maximum of Ni wave in the presence of the complexing agent; I_4 is height of the Ni wave in the presence of gelatin.

[b] Arbitrarily set at 100% adsorption.

Table V. X-ray diffraction data

Ni (f.c.c.)		Ni-W (f.c.c.)		W (b.c.c.)	
d-spacings[a]	Relative intensity[b]	d-spacings	Relative intensity	d-spacings	Relative intensity
2.034(111)	100	2.047(111)	100	2.235(110)	100
1.763(200)	68	1.779(200)	20		
1.245(220)	11	1.252(220)	12	1.580(200)	15
1.0628(311)	17	1.0726(311)	12	1.291(211)	9.5
1.0168(222)	4.8	1.0292(222)	7.6	1.1190(220)	9.5
0.8824(400)	2.4	0.8837(400)	4.5	1.0004(310)	7.4
0.80808(331)	4.8	0.81712(331)	9.1	0.8461(321)	5.3
		0.79990(421)	9.1	0.7918(400)	1.1

[a] Distance between lattice planes in angstrom units.

[b] Obtained by subtracting background and setting most intense peak at 100.

depositing metal ion, and are adsorbed at a dropping mercury cathode. The addition agents which were found to have no effect on the composition of the codeposit were either not adsorbed (i.e., urea) or formed no complexes (i.e., gelatin) with the codepositing metal ion.

It is likely that the formation of a complex between the codepositing species and the addition agent is essential for the prevention of tungsten codeposition. All such complexes are more easily reduced than is the original nickel species, as is shown by the shift to more noble values of the half-wave potentials and of the dynamic cathode potentials. It has also been shown that all addition agents which prevent tungsten codeposition are capable of being adsorbed at the mercury cathode. The fact that very small quantities of addition agent prevent the codeposition and the observed depletion of the addition agent supports the hypothesis that this adsorption is also essential for the prevention of codeposition. As further evidence for this, it has been observed that tungsten will deposit normally from a solution containing 3 mg/l of thiourea (enough to completely prevent codeposition) provided an excess (0.8 g/l) of gelatin is added. This indicates a competition for adsorption between gelatin and thiourea and further demonstrates that adsorption of the addition agent is essential for the prevention of tungsten codeposition.

If one may assume that the behavior of the plating solution at a tungsten alloy electrode is not grossly different from that of the polarographic solution at a mercury cathode, then a plating mechanism consistent with these observations can be formulated. It would involve the adsorption of the addition agent at the cathode and its formation of complexes with the codeposition metal ion[2] as it approaches the cathode. During the formation of this new complex, the original complex between the codepositing ion and the tungstate ion dissociates, and tungsten deposition is prevented.

The x-ray diffraction data negate the mechanism involving alternate layers of the two metals, as does the lack of any periodicity in the plating voltages (12).

Acknowledgments

The authors wish to thank Dr. D. A. Norton, Dr. W. E. Keiser, and Mr. M. Fornoff of The National Cash Register Company and Mr. G. Rappaport, Inland Manufacturing Company, for performing the x-ray diffraction and x-ray fluorescence studies. They are also indebted to Dr. H. J. Modi for many stimulating discussions.

Manuscript received Feb. 2, 1959. This paper was prepared for delivery before the New York Meeting, April 27-May 1, 1958.

Any discussion of this paper will appear in a Discussion Section to be published in the December 1960 JOURNAL.

REFERENCES

1. M. L. Holt and L. Kahlenberg, *Metal Ind.*, **31**, 94 (1933).
2. L. F. Yntema, *J. Am. Chem. Soc.*, **54**, 3775 (1932).
3. C. G. Fink and F. L. Jones, *Trans. Electrochem. Soc.*, **59**, 461 (1931).
4. M. L. Holt, *ibid.*, **66**, 453 (1934).
5. A. Brenner, P. Burkhead, E. Seegmiller, *J. Research Nat. Bur. Standards*, **39**, 351 (1947).
6. M. H. Lietzke and M. L. Holt, *J. (and Trans.) Electrochem. Soc.*, **94**, 252 (1948).
7. M. L. Holt and L. E. Vaaler, *ibid.*, **94**, 50 (1948).
8. W. E. Clark and M. H. Lietzke, *This Journal*, **99**, 245 (1952).
9. L. N. Goltz and V. N. Kharlamov, *J. Appl. Chem., USSR*, **9**, 640 (1936).
10. H. Offermanns and M. V. Stackelberg, *Metalloberfläche*, **1**, 142 (1947).
11. D. R. Markwell and M. L. Holt, *J. Electrochem. Soc.*, **104**, 488 (1957).
12. Z. A. Solovyerva and A. T. Vagramyan, Reports of the Academy Science of USSR, Division of Chemical Science 1954, No. 2, 230-235.
13. T. P. Hoar and I. A. Bucklow, *Trans. Inst. Met. Finishing*, **32**, 186 (1955).

[2] This is, at present, not distinguishable from complex formation followed by selective adsorption of the addition agent codepositing metal ion complex.

Correction

In the article by R. Weil and R. Paquin entitled "The Relationship between Brightness and Structure in Electroplated Nickel" which appeared in the February 1960 JOURNAL, on page 88 in Table II the data for the quantity of reflection light and the eye evaluation brightness group for Specimen 3006a belong to Specimen 3006b and vice versa.

The Mechanism and Efficiency of Electroluminescence in ZnS Phosphors

F. F. Morehead, Jr.[1]

Lamp Research Laboratory, General Electric Company, Nela Park, Cleveland, Ohio

ABSTRACT

This work describes the application of a model of the electroluminescent process to the photon emission and power consumption of insulated electroluminescent phosphors as a function of voltage and frequency. The model represents an extension of one described earlier. The model leads to a convenient summary of such data and an increased understanding of their significance. An upper limit to the efficiency of impact electroluminescence in insulated particles is proposed on the basis of the implications of the model.

One of the difficulties encountered in correlating data for electroluminescence in ZnS phosphors is that there does not exist an adequate model of the process. The lack of such a model makes impossible a convenient summary of the variation of brightness and power dissipation with voltage, frequency, and temperature. Comparisons of the properties of the electroluminescence of different phosphors are difficult to describe in meaningful terms and even more difficult to relate to differences in the fundamental properties of the phosphors. The purpose of this work is to present as complete an approach to an adequate model based on the collision excitation mechanism as is possible at present.

This model, to be described in the following section, is consistent with the relevant experimental data reported in the literature (1-6) although not in entire agreement with their interpretation [cf. (2, 3)]. The major premise is that of delayed recombination, which, despite alternative suggestions (7) remains unambiguously demonstrated (1, 2, 6). Further, the model is a straightforward extension of work by the present writer (1) with some changes suggested by consideration of efficiency. It is similar in concept but more detailed and more accurate than one described by Lehmann (5).

Finally, the model yields a phenomenological approach toward estimating maximum efficiencies that can be achieved with electroluminescence produced by impact ionization. The primary consideration is the relation between the way in which light emission and power consumption increase with voltage in insulated particles.

A Model of the Electroluminescence Process

The principal features of this model have been described previously (1); the same notation will be retained. The electrons participating in the electroluminescence process in a given particle are divided into two populations: n_o "mobile" electrons, which emerge from and return to a "high-field region" in each voltage cycle and N_T "trapped" electrons in the particle bulk which do not succeed in returning to this region. The origin of the high-field region in which carrier acceleration and impact ionization occur is discussed in a following section. It is assumed that all of the participating electrons have been ionized from the lattice and that the resultant holes are localized in the high-field region at N_s recombination centers, so that

$$n_o + N_T = N_s \qquad [1]$$

Of the n_o mobile electrons a fraction α recombine at the emission (recombination) centers and a much larger fraction β are trapped. These βn_o electrons are field-ionized by the succeeding voltage half-cycle and accelerated such that $F\beta n_o$ ionizing collisions occur, where $F \sim e^{-\frac{\text{constant}}{E}}$ and E is the effective field in the high-field region. We have then

$$\alpha + \beta = 1 \qquad [2]$$

and

$$\alpha n_o = F\beta n_o \qquad [3]$$

to maintain a steady-state condition with respect to ionization and subsequent recombination. We further define Ψ as the fraction of the total number of electrons, $n_o + N_T$, which are in the particle bulk at the beginning of a voltage half-cycle, and which fraction returns to the high-field region

$$\Psi = n_o/(n_o + N_t) = n_o/N_s \qquad [4]$$

The fraction α is of course proportional to the number of ionized recombination centers, which, as mentioned above, are localized in the high-field region

$$\alpha = N_s X \qquad [5]$$

where X is a capture cross section for these centers relative to trapping.

With the assumption $\alpha << \beta$, algebraic combination of Eq. [1], [2], [3], [4], and [5] gives the following

$$\begin{aligned} \alpha &\sim F \\ n_o &\sim \Psi F/X \\ B/f \propto \alpha n_o &\sim \Psi F^2/X \end{aligned} \qquad [6]$$

where B/f is the light emission/voltage cycle.

[1] Present address: Research Laboratory, International Business Machines Corp., Poughkeepsie, N. Y.

Trapping and retrapping in the phosphor bulk delays the return of the ionized electrons to the recombination region, which return is facilitated by a field opposite in direction to the ionizing field. Ψ is then a function of the frequency and amplitude of the voltage and of the temperature. The form of this function has been given in previous work (1) for a sinusoidal voltage V of frequency f

$$\Psi = 1 - e^{-\mu}$$
$$\mu = k_\mu \frac{V}{f^{n_0}} e^{-E_{01}/kT} \qquad [7]$$

For a distribution rather than a single trap depth E_{01}, a weighted sum of terms of the form $e^{-E_{01}/kT}$ applies.

Application of the above model to the electroluminescence brightness (time-averaged for photons) yields

$$B = B_e f \Psi F^2 \qquad [8]$$

where B_e is a constant.

The motion of the n_e mobile electrons as well as that of the N_T trapped electrons under the influence of the applied field leads to an increase in both the real and imaginary capacitance of the cell C′ and C″ over the value of these constants in the absence of a carrier-producing process in the insulated phosphor particles C'_o and C''_o. The power dissipated by the cell W, the stored power VAR, and the cell current i are given by

$$W = \omega C'' V^2$$
$$VAR = \omega C' V^2$$
$$i = \omega \mid C \mid V \qquad [9]$$

where

$$C = C' + iC''$$

The increase in C′ and C″ arising from the electroluminescence process is proportional to the increase in the two populations of electrons, n_e and N_T, so that we can write

$$C' = C'_o + \bar{C}'_1 n_e + \bar{C}'_2 N_T$$
$$C'' = C''_o + \bar{C}''_1 n_e + \bar{C}''_2 N_T \qquad [10]$$

where $\bar{C}'_1$ and $\bar{C}''_1$ are constants containing geometric and mobility or polarizability factors and $\bar{C}'_2$ and $\bar{C}''_2$ are similar constants of lower magnitudes representing the more limited excursions of the trapped electrons. One should emphasize here that the lossy motion of a trapped electron is conduction between traps rather than displacement within a trap. The designation "trapped" simply indicates electrons which do not succeed in returning to the recombination region within a half-cycle. Substituting in Eq. [10] from [6] gives

$$C' = C'_o + C'_1 \Psi F + C'_2 (1 - \Psi) F$$
$$C'' = C''_o + C''_1 \Psi F + C''_2 (1 - \Psi) F \qquad [11]$$

The model thus leads to the expectation of a fairly direct correlation between photon brightness B and power consumption W.

Experimental Technique

A demountable cell was used for most experiments consisting of a circular copper block for one electrode and a circular conducting glass plate for the other. The latter makes contact at its periphery with a metal ring attached through an insulator to the copper electrode, providing a fixed separation of the electrodes. The phosphor powders were mixed with a viscous liquid, #1254 Aroclor (a chlorinated biphenyl, Monsanto Chemical Company), to give a desired volume loading. The mix first was deposited on the conducting glass plate, freed of admixed air in a vacuum chamber, and then pressed against the copper electrode, which was covered with a ¼ mil Mylar film to elminate electrolytic processes that might otherwise occur in the liquid medium. The experimental results reported below are not corrected for the effect of the Mylar film, since this correction does not significantly alter the results relative to the purposes of this work.

The cells were operated by means of a wide range oscillator, a 60 w audio amplifier, and a transformer. This combination of units provides up to 450 v rms above 100 cps to beyond the 5 kc frequency to which the measurements were limited to avoid a significant contribution of the resistance of the conducting glass to the power absorption. For measurements at lower frequencies a d-c amplifier which was limited to below 250 v rms was used.

The power consumption and current were measured with a Model 102 electronic wattmeter (John Fluke Engineering Co.) which was checked periodically against known resistances and capacitances.

Cell brightnesses were measured with a 1P21 photomultiplier tube whose output current was read with an electrometer. In each case the output of the photomultiplier was compared with the cell brightness in footlamberts as measured with a Photo Research Corporation "Spectra" brightness spot meter (Model UB) at each of the frequencies employed.

To obtain the cell output in lumens, the brightness in footlamberts was multiplied by the cell area in square feet. To convert the photomultiplier output to a relative photon count in those cases in which the wave-length distribution of the electroluminescence shifts with frequency, several procedures were used. The emission spectra of a ZnS,ZnO:Cu,Cl phosphor were measured at 100 cps and 5 kc, and plotted as relative amount of radiant power (for equal frequency intervals) $dW/d\nu$ vs. photon energy $h\nu$. The S-4 response of the 1P21 photomultiplier was obtained in response for equal radiant power at each photon frequency R_ν. The following integral gives the relative photomultiplier response/photon/second for the particular emission spectrum characteristic of the frequency f

$$(PMR)^{h\nu}_f = \frac{\int \left(\frac{dW}{d\nu}\right)_f R_\nu \, d\nu}{\int \left(\frac{dW}{d\nu}\right)_f \frac{d\nu}{\nu}}$$

For the phosphor described above we had from numerical integration of the above

$$\frac{(PMR)^{h\nu}_{5\text{ kc}}}{(PMR)^{h\nu}_{100\text{ cps}}} = 1.44$$

which is the correction factor by which the photo-

multiplier readings at 5 kc must be divided to obtain the number of photons emitted relative to 100 cps.

Similar calculations give the relative photomultiplier response/watt for each frequency

$$(\mathrm{PMR})^{w}_{f} = \int\left(\frac{dW}{d\nu}\right)_{f} \mathrm{R}\nu\, d\nu \;\Big/\; \int\left(\frac{dW}{d\nu}\right)_{f} d\nu$$

such that for the ZnS,ZnO:Cu,Cl

$$\frac{(\mathrm{PMR})^{w}_{5\ \mathrm{kc}}}{(\mathrm{PMR})^{w}_{100\ \mathrm{cps}}} = 1.42$$

The luminous equivalent of the emission at each frequency can be calculated in similar fashion with the use of the standard eye response curve, which equivalents are 296 lpw for 5 kc and 395 at 100 cps. The ratio of the sensitivity of the photomultiplier in lumens/unit deflection at 100 cps to that at 5 kc will therefore be

$$\mathrm{SR}(100\ \mathrm{cps},\ 5\ \mathrm{kc}) = 1.42\,\frac{395}{296} \sim 1.9$$

This value compares reasonably well with the sensitivity ratios for this phosphor (ZnS,ZnO:Cu,Cl) measured directly as described above with the brightness spot meter, about 1.75 ±0.2. Thus as a rough rule of thumb, one can estimate the correction necessary to convert photomultiplier outputs to relative photon counts as being approximately

$$[\mathrm{SR}(f_1,f_2)]^{0.6}$$

As a final procedure a set of filters were arranged to cover the electroluminescent cell in such a fashion as to give a linear photon count response (when combined with the S-4 1P21 response) in the wavelength range of 4400 to 5600Å. Calculations of the relative cell area assigned to each filter were based on their measured transmission curves. Satisfactory agreement with the results of the above procedures was obtained.

Experimental Results

Figure 1 shows the agreement of the measured photon emission of an electroluminescent cell of a

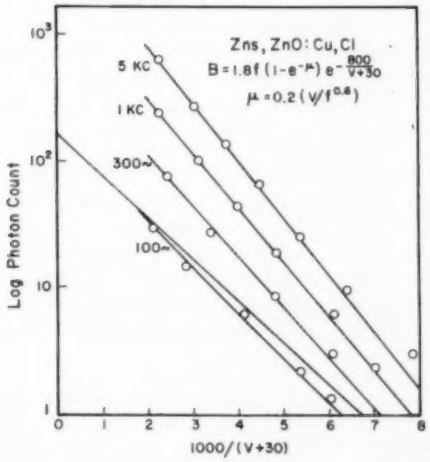

Fig. 1. Log photon count vs. $\dfrac{1000}{V + V_o}$ for ZnS, ZnO:Cu, Cl

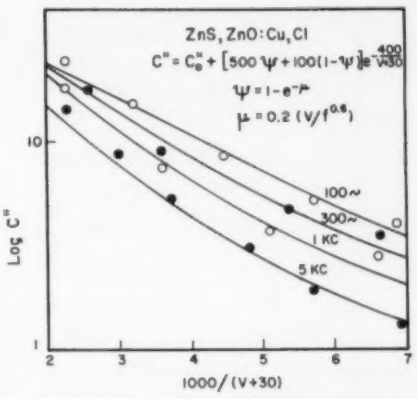

Fig. 2. Log imaginary cell capacitance vs. $\dfrac{1000}{V + V_o}$ for ZnS, ZnO:Cu, Cl.

ZnS,ZnO:Cu,Cl phosphor as a function of voltage and frequency with the form dictated by the model, Eq. [8]. The ionization efficiency F has been given the form

$$\mathrm{F} = e^{-\frac{c}{V+V_o}} \qquad [12]$$

The reasons for choosing this form are given in the following section. The straight lines are not exactly the theoretical curves but are drawn through calculated points at $\dfrac{1000}{V + 30} = 2$ and $\dfrac{1000}{V + 30} = 6$ for each frequency. The heavy line is the relation between emission and voltage that would obtain at 100 cps for $\Psi = 1$. Figure 2 shows the agreement of the measured values of the imaginary cell capacitance in $\mu\mu$f with the form predicted by the model, Eq. [11]. Ψ and F are taken from the light measurements (Fig. 1) and C''_o, C''_1, and C''_2 then chosen to give a good fit of the solid (calculated) lines with the experimental points. (C''_o is about 15 $\mu\mu$f in most cases.) Higher losses than those expected invariably are experienced at the highest voltages. This extra consumption is believed due to nonelectroluminescent processes, possibly associated with the presence of moisture (5).

Variation of cell thickness d and phosphor volume loading N_p give within experimental error the expected changes in the various parameters, viz.

$$B_2 = fB_{o1}\frac{d_2}{d_1}\frac{N_{p2}}{N_{p1}}(\Psi)e^{-\frac{2c_1(d_2/d_1)}{V+V_{o1}(d_2/d_1)}}$$

$$\frac{d_2}{d_1}C''_2 = C''_o(N_{p2}) + \left(\frac{N_{p2}}{N_{p1}}\right)\left[C''_{11}\Psi + C''_{21}(1-\Psi)\right]\frac{c_1(d_2/d_1)}{e^{V+V_o(d_2/d_1)}}$$

$$\Psi = 1 - e^{-\mu}$$

$$\mu = k_{\mu 1}\frac{d_1}{d_2}\frac{V}{f^{0.6}}$$

where the subscripts 1 and 2 refer to the parameters appropriate to cells of thicknesses d_1 and d_2 and phosphor volume loadings N_{p1} and N_{p2}.

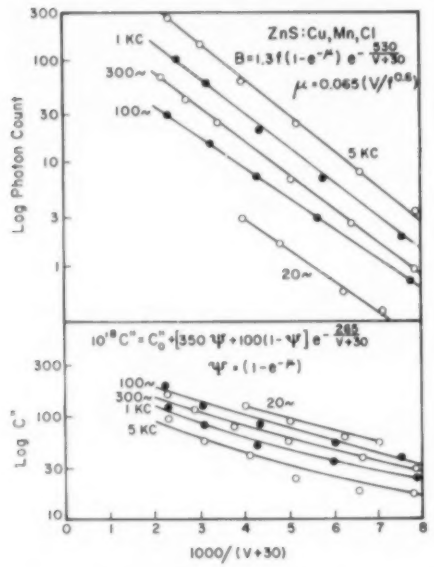

Fig. 3. Log photon count and log imaginary cell capacitance vs. $\frac{1000}{V + V_o}$ for ZnS:Cu, Mn, Cl.

Figure 3 shows the agreement of the model with the brightness and power data for a yellow-emitting ZnS:Cu,Mn,Cl phosphor. There is, of course, no shift in the emission spectrum with frequency. The green- and blue-emitting centers are impact ionized as in the previously described phosphor, but on recombination, the excitation energy is transferred to the yellow-emitting Mn-center, by means of a quantum mechanical resonance process (8, 9). The ground state and excited state of the Mn center are both thought to be below the top of the valence band, so that direct collision excitation rather than ionization of this center can occur (2). This latter mode of excitation of this center occurs significantly only at much higher currents than those characteristic of "normal" ionization electroluminescence and dominates only in cells that allow continuous current flow at very low frequencies or for d-c voltages.

A further distinction of the Mn-phosphor is the very low value obtained for k_μ in the expression for Ψ. This difference results in a much larger contribution of the N_T trapped electrons (a lower value of Ψ) to the power consumption of the cell, which increases rapidly with frequency. Thus if one measures a maximum phosphor efficiency (neglecting C''_o) of 6.0 lpw at 100 cps and 100 v, the equations shown in Fig. 3 predict a maximum efficiency of 8.4 lpw at 20 cps and 80 v. The solid lines shown in Fig. 3 for photon emission and C" at 20 cps were plotted on the basis of measurements made between 100 cps and 5 kc. The agreement with the experimental points shows that one may accurately extrapolate on the basis of the model outside of the actual range of measurements. By contrast, if one measures a maximum phosphor efficiency of 6.0 lpw at 100 cps and 140 v for the ZnS,ZnO:Cu,Cl phosphor, one can expect a maximum efficiency of only about 6.2 lpw at 20 cps and 100 v on the basis of the model and the experimentally determined parameters.

The reason for the low value of k_μ for the Mn-phosphor is not wholly understood. There is no evidence for the presence of deep traps, which would give a lower value at room temperature to $k_\mu = k_{\mu_o} e^{-\Pi_o/kT}$, in either the thermoluminescence or the temperature dependence of the electroluminescence. The answer perhaps lies in a greater concentration of traps with consequently greatly increased retrapping and a slower rate of return at a given applied voltage and frequency. Similar consideration may also apply to the Ni-quenched phosphor discussed below.

ZnS:Cu, Al phosphor have even higher values of k_μ at room temperature than those coactivated with chlorine. A value as high as $k_\mu = 0.66$ has been measured, giving a very nearly linear frequency response to the phosphor at the higher voltages. A further advantage of the phosphor is the absence of color shift with frequency (2).

Interesting variations in the model parameters are produced by firing longer at higher temperatures to yield a higher mean particle size. One such ZnS,ZnO:Cu,Cl phosphor gives the following results (a correction for the greater cell thickness required to accommodate this phosphor has been made)

$$B = 0.32 f \Psi \left[e^{-\frac{255}{V+20}} \right]^2$$

$$C'' = C''_o + [500\Psi + 250\ (1 - \Psi)]\ e^{-\frac{255}{V+20}}$$

$$\Psi = 1 - e^{-\mu}$$

$$\mu = 0.18 \left(\frac{V}{f^{0.6}} \right)$$

A comparison of this phosphor with the usual ZnS,ZnO:Cu,Cl under a microscope shows the former to have roughly twice the average particle size of the latter The change in the parameters contained in the expression for photon emission (cf. Fig. 1) as a result of the increased particle size correlates reasonably well on the basis of Lehmann's work (10). He found that B_s (Eq. [8]) varied inversely as the square of the mean particle size. The present results correlated on this basis with a size ratio of 2.3.[3] His experiments also show that the equivalent of the threshold voltage c (Eq. [12]) varied inversely with the 0.7 power of the mean particle size. Lehmann's analysis of the latter constant is in terms of the 1.0 power rather than 0.7, but the former value cannot explain phenomenologically the decrease in maximum efficiency with increasing particle size which he observed, and 0.7 is in better agreement with his data than 1.0. From the ratio of the c-values then, one obtains a particle size ratio of $\left(\frac{400}{255} \right)^{\frac{1}{0.7}} = 1.9$, in reasonable agreement with the above figure.

Lehmann's analysis was based on the following relation between brightness, voltage, and frequency

$$B = A f \exp\ (-\sqrt{G/V}$$

while we have been using an expression which, at sufficiently low frequencies, reduces to

$$B = B_o f \exp(-2c/(V + V_o))$$

Although no attempt at a rigorous mathematical analysis has been made, it has been the experience of the present author that, at low frequencies, a set of data which fits the equation used by Lehmann above will also be consistent with the second expression above, with the following approximate relations between the constants

$$B_o = 0.10\ A;\ 2c = 0.12\ G;\ V_o = 0.05\ (2c) = 0.006\ G.$$

Therefore any functional relationship between the constants A and G and parameters such as particle size, cell thickness, etc., will also apply, within a constant factor, to the constants B_o and c.

The coarse phosphor is also considerably less efficient than the normally sized phosphor, by a factor of about 1.6. On the basis of the model discussed above one would predict this for at least two reasons. First, the variation of c inversely as the 0.7 power rather than 1.0 power of the mean particle size indicates that a smaller fraction of the total voltage appearing across the particle is concentrated in the high field for large particles than for small. Hence proportionally more useless energy is dissipated in the low field volume by the "mobile" electrons. Second, the relative value of C''_2 to that of C''_1 is greater for the larger particles, indicating, quite reasonably, that in large particles the trapped electrons are subjected to displacements over larger distances within the high-field region in their unproductive agitation by the applied field.

The invariance of C''_1 with particle size suggests that the polarizability per available conduction electron at $V = \infty$ (the number of which is proportional to B_o) varies directly as the square of the particle size. k_μ is also relatively invariant with particle size, which tends to confirm its association with the average field in the phosphor particles rather than the high-field region. It should be realized, however, that the above analysis is based mostly on data from a single phosphor sample.

The introduction of a killer such as Ni into a phosphor of the ZnS,ZnO:Cu,Cl type produces a quenching of the emission which depends on frequency alone (11). To determine the value of k_μ associated with such a phosphor one can use the change in slope at a particular voltage of ln B vs. $\frac{1}{V + V_o}$ (Fig. 1, 3) as a function of voltage, viz.

$$\frac{d \ln B}{d\left(\frac{1}{V + V_o}\right)} = \frac{d \ln \Psi}{d\left(\frac{1}{V + V_o}\right)} - C$$

$$= \frac{(V + V_o)^2}{V} \frac{\mu}{e^\mu - 1} - C \qquad [14]$$

$$\mu = k_\mu \frac{V}{f^{0.6}}$$

[2] That exact agreement is not to be expected is shown by the somewhat different particle size correlations reported by Goldberg (11).

The results of such an analysis on a ZnS,ZnO:Cu,Cl, Ni phosphor are

$$B = \frac{B_o}{Q}(\Psi)\, e^{\frac{710}{V+30}}$$

$$C'' = C''_o + [500\,\Psi + 150\,(1 - \Psi)]\, e^{-\frac{355}{V+30}}$$

$$\mu = 0.1 \frac{V}{f^{0.6}}$$

f:	100	300	1000	5000 cps
$1/Q$:	1.0	1.17	1.60	2.0

The value of $1/Q$ has arbitrarily been set at 1.0 for 100 cps. The addition of the Ni has also had the effect of reducing the value of k_μ (more traps?) as well as quenching the emission at the lower frequencies, compared to the ZnS,ZnO:Cu,Cl phosphor (Fig. 1, 2). Thus a Ni-quenched phosphor can be sublinear, as well as superlinear or linear with frequency at a fixed voltage.

The analyses of the phosphors described above, other than the Ni-quenched material, have been made on the assumption of the absence of quenching. Using Eq. [14] to determine k_μ for ZnS,ZnO:Cu,Cl yields a value of 0.16, compared with 0.2 (Fig. 1), suggesting a small but significant amount of quenching. Trace amounts of Fe, Ni, or Co are undoubtedly present in this phosphor.

It should be mentioned also in this section that for all the phosphors examined, the dependence of the real part of the cell capacitance on voltage and frequency was such that, within experimental error, $C'_1 \sim C''_1$ and $C'_2 \sim C''_2$. Thus of the total energy absorbed by a conduction electron falling through a given potential, roughly half is stored as potential energy and returned to the field on field reversal.

Efficiency of Electroluminescence in Insulated Particles

The efficiency η with which the insulated electroluminescent phosphor converts the electrical power it absorbs from the applied field into luminous flux is proportional to (Eq. 8, 9, 11)

$$\eta \propto \frac{B}{W} = \frac{B f \Psi F^2}{\omega V^2 F[C_1'' \Psi + C''_2(1 - \Psi)]} \qquad [15]$$

The power absorbed by the cell dielectric and phosphor in the absence of electroluminescence, $\omega C''_o V^2$, has been neglected, since we wish here to estimate the limiting efficiency of the electroluminescence process alone.

For most phosphors, at sufficiently low frequencies, $C'' \Psi >> C''_2 (1 - \Psi)$ so that

$$\eta \propto \frac{F}{V^2} \qquad [16]$$

Maximum efficiency then occurs at that voltage V_m for which

$$\frac{d \log F}{d \log V} = 2 \qquad [17]$$

The form of the maximum phosphor efficiency obtainable from insulated particles can be written

$$\eta_m = \frac{n_o (2.5\epsilon) F_m}{n_o (V_o\, \epsilon)} \qquad 400 \text{ lpw} \qquad [18]$$

2.5ϵ is the energy of a typical visible photon; V_o the voltage through which a typical "mobile" electron falls; $F_m = F(V_m)$. (Acceptable "white" luminescence with a luminous equivalent greater than 400 would be difficult to achieve.) One-third is a reasonable guess for the value of $2.5/V_o$ at η_m. V_o is the product of two factors: the average field over the path of the electrons and the mean path of the electrons. Both factors are assumed proportional to the applied field V, so that Eq. [18] is in fact dimensionally consistent with [15] and [16]. For most phosphors the average field across the cell, and hence across the phosphor in a liquid dielectric (5), is about 1.5 v/μ peak at the voltage of maximum efficiency. For $V_o = 3 \times 2.5 = 7.5$ v, the mean path of the electrons in this field is 5 μ, which is not unreasonable. If, as indicated above, half the absorbed energy is stored and later returned to the field, and in the absence of competing, nonradiative recombinations, an upper limit to the maximum phosphor efficiency may be set at

$$\eta_m = \frac{2}{3} F_m \qquad 400 = 267\ F_m \qquad [19]$$

The value of F_m depends on the form of the voltage dependence of $F(V)$. If we apply the usual form $F = \exp(-\text{const}/\sqrt{V})$, which is presumed to arise from the formation of an exhaustion layer (Eq. [2]), we have $F_m = e^{-4} \sim \frac{1}{50}$, which, substituted in Eq. [19], gives $\eta_m < 5.3$ lpw. Measurements have been published which exceed this by approximately a factor of three (10). If these are correct, then the expression $F = \exp(-\text{const}/\sqrt{V})$ does not give a reasonable characterization of the voltage dependence of F. Furthermore, the formation of an exhaustion layer requires the movement of a considerable quantity of charge before an ionization field is obtained, so that the maximum efficiency of such a process would have an even lower limit than 5.3 lpw. For these reasons, consideration of the formation of an exhaustion layer was eliminated from the model description.

Application of the form $F = \exp(-\text{const}/V)$ yields $F_m = e^{-2} \sim \frac{1}{7}$ or $\eta_m < 38$ lpw, a value high enough to explain efficiency obtained experimentally thus far. Such a voltage dependence can arise from, among other possibilities, the intrusion of elongated "spikes" of a conducting phase, such as Cu_2S, into the ZnS phosphor particle interior (13). The field at the tip of such an intrusion can easily be an order of magnitude greater than the average field. The ratio of the high field at the tip of the spike to the average field is given roughly by the ratio of the length of the spike to its cross-sectional diameter (14). This ratio undoubtedly increases with particle size. In such a case the value of the exponential constant c in the expression for $F = \exp -(c/V)$ is a monotonically decreasing function of particle diameter a, $c = c(a)$, and the effective value of F that applies to the rather wide particle size distribution encountered with elcctroluminescent phosphors is an integral or summation of the form

$$F = \sum_i f_i e^{-\frac{\bar{c}(a_i)}{V}} \qquad [20]$$

where the subscript i applies to a narrow range of particle sizes of mean diameter a_i and relative frequency f_i. The form $\exp(-\text{const}/\sqrt{V})$ has been shown to approximate the behavior of Eq. [2] except at the highest applied voltage (15), which makes it possible to use $\exp(-\text{const}/\sqrt{V})$ to describe the dependence of electroluminescence brightness on voltage. A more suggestive approximation to Eq. [20] is (16-18).

$$F = e^{-\frac{c}{V+V_o}} \qquad [21]$$

where the relative value of the constant V_o is considered as simply a measure of the dispersion of a_i, particularly in the direction of larger than average particles. (Much smaller than average particles do not contribute much to brightness or power absorption at voltages in the neighborhood of maximum phosphor efficiency; only a small fraction of the particles that are absorbing power will be operating at the voltage of maximum efficiency for that fraction, so that the effective value of F_m will be less than e^{-2}. In fact, application of Eq. [17] to Eq. [21] for $V_o \cong 0.10c$, true for the phosphors described above, yields

$$F_m = e^{-2.7} \sim \frac{1}{15}$$

Therefore to test the "limit" of about 38 lpw, one would have to use a phosphor of both uniform and small particle size since, as indicated in the discussion of the coarse phosphor, smaller particles concentrate a larger fraction of their total voltage across the high-field region, and on the basis of this model would be expected to operate more efficiently.

Finally, it should be mentioned that for the relations developed earlier in this paper between photon emission and power consumption to apply accurately to the assembly of particle sizes present in a typical electroluminescent phosphor, one must hope, applying Eq. [20] to [8] and [11], that the following is a good approximation

$$\frac{\sum_i f_i e^{-\frac{2\bar{c}(a_i)}{V_1}}}{\sum_i f_i e^{-\frac{2\bar{c}(a_i)}{V_2}}} \sim \left[\frac{\sum_i f_i e^{-\frac{\bar{c}(a_i)}{V_1}}}{\sum_i f_i e^{-\frac{\bar{c}(a_i)}{V_2}}} \right]^2$$

for any values of V_1 or V_2 within the range of interest.

Acknowledgment

The writer wishes to thank the following persons for many helpful suggestions as well as the preparation of most of the phosphors: Dr. I. L. Smith, Dr. M. Aven, Dr. R. M. Potter, and Mrs. M. S. Jaffe.

Manuscript received Oct. 15, 1959.

Any discussion of this paper will appear in a Discussion Section to be published in the December 1960 JOURNAL.

REFERENCES

1. F. F. Morehead, Jr., *This Journal*, **105**, 461 (1958).
2. P. Zalm, *Philips Research Repts.*, **11**, 353, 417 (1956).
3. W. A. Thornton, *Phys. Rev.*, **102**, 38 (1956).
4. G. F. Alfrey and J. B. Taylor, *Proc. Phys. Soc.*, **B68**, 775 (1956).
5. W. Lehmann, *J. Optical Soc. Am.*, **48**, 647 (1958); *This Journal*, **103**, 24 (1956).
6. J. F. Waymouth and F. Bitter, *Phys. Rev.*, **95**, 941 (1954).
7. E. E. Loebner and I. J. Hegyi, Enlarged Abstracts, Electronics Division, The Electrochemical Society, Philadelphia Meeting, p. 45 (1959), not published.
8. H. C. Froelich, *J. Optical Soc. Am.*, **43**, 320 (1953).
9. D. L. Dexter, *J. Chem. Phys.*, **21**, 836 (1953).
10. W. Lehmann, *This Journal*, **105**, 585 (1958).
11. P. Goldberg, *ibid.*, **106**, 34 (1959).
12. W. Lehmann, *Phys. Rev.*, **101**, 489 (1956).
13. W. Lehmann, *This Journal*, **104**, 45 (1957).
14. K. Maeda, *J. Phys. Soc., Japan*, **13**, 1352 (1958).
15. W. Lehmann, Enlarged Abstracts, Electronics Division, The Electrochemical Society, Philadelphia Meeting, p. 18 (1959), not published.
16. W. Lehmann, *This Journal*, **103**, 667 (1956).
17. B. T. Howard, H. F. Ivey, and W. Lehmann, *Phys. Rev.*, **96**, 799 (1954).
18. G. Destriau and H. F. Ivey, *Proc. IRE*, **43**, 1911 (1955).

SYMBOLS

a — Fraction of n_e "mobile" electrons that recombine with emission each half-cycle.

β — Fraction of n_e "mobile" electrons that are trapped in high-field regions each half-cycle.

ϵ — Electron charge.

η — Electroluminescence efficiency.

μ — A constant in expression for Ψ: $\mu = k_\mu \dfrac{V}{f^{0.6}}$

Ψ — $\dfrac{n_e}{n_e + N_T} = (1 - e^{-\mu}) = \Psi$

ω — $2\pi f$

a — Effective particle diameter

B — Photon emission/cycle, arbitrary units.

B_∞ — Photon emission/cycle extrapolated to $V = \infty$.

$c, \bar{c}$ — A constant in one expression for $F = e^{-\frac{c}{V + V_e}}$ for the cell; $F = e^{-\frac{\bar{c}}{(V + V_e)a}}$ for particles of a given diameter.

C_e', C_e'' — The real and imaginary parts of the cell capacitance in absence of electroluminescence.

C'_1, C''_1 — Constant coefficients in expression for real and imaginary capacitance contributed by "mobile" electrons.

C'_2, C''_2 — The same for "trapped" electrons.

d — Cell thickness.

E — Effective ionizing field.

E_o — Trap depth.

F — Probability of impact ionization of a secondary electron by a primary electron in high-field region.

f — Frequency in cps.

f_i — Relative frequency of occurrence of particles of mean diameter a_i.

i — Cell current

k_μ — A constant in expression for μ.

n_e — Number of electrons that return to the high-field region each half-cycle.

N_+ — Steady-state number of ionized centers in high-field region.

N_T — Steady-state number of electrons that remain trapped in phosphor bulk.

$(PMR)_f^{1P}$ — The 1P21 photomultiplier response to a given number of photons/second distributed according to emission spectrum of a given phosphor at frequency f.

$(PMR)_f^{w}$ — Same for a given radiant power.

Q — Quenching factor by which the emission expected in the absence of quenching is divided.

R_r — Relative response of the 1P21 photomultiplier for equal radiant power at each photon frequency.

$SR(f_1, f_2)$ — Response of the 1P21 photomultiplier to a given number of lumens emitted by a phosphor at a frequency f_2 relative to that at a frequency f_1.

T — Absolute temperature.

V — The rms voltage.

V_e — A constant in the expression for F.

V_e — Potential through which a typical electron falls in the electroluminescence process.

N_r — Fraction of cell volume occupied by phosphor.

VAR — Stored power, $VAR = \omega C' V^2$.

W — Consumed power, $W = \omega C'' V^2$.

X — A constant proportional to capture cross section of the ionized activators.

Electroluminescence under Pulsed Square Wave Excitation

R. Zallen,[1] W. T. Eriksen, and H. Ahlburg

Research Division, Raytheon Company, Waltham, Massachusetts

ABSTRACT

The slow return of an electroluminescent cell to its equilibrium state following a field excitation has been studied for a blue-green emitting Zn(S,O):Cu,Cl phosphor and for a yellow-emitting ZnS: Mn,Cu phosphor. The light pulse emitted upon the rise of a square voltage pulse was measured as a function of repetition rate and of temperature between —130° and 150°C. Relaxation times encountered varied between 10^{-3} sec and 10^{5} sec. The temperature dependence of the relaxation rate exhibits effective activation energies of about 0.4, 0.7, and 0.6 ev, respectively, for the blue, green, and yellow emission bands. The results do not seem to favor the mechanism of delayed recombination. An alternative mechanism is suggested whereby the number of filled deep donors is assumed to control the electroluminescence emission via the number of field-ionizable electrons available for collision-excitation of centers. Observations were also made on some other effects associated with square wave excitation.

A complete picture of the microscopic processes involved in the light emission from insulated zinc sulfide crystals under high electric fields (1) has not yet been established firmly, although various models have been more or less successful in accounting for different aspects of the phenomenon. The present work was undertaken to obtain further insight into the nature of electroluminescence.

This paper describes some observations on the electroluminescence of two zinc sulfide phosphors under pulsed d-c voltage excitation and their interpretation in the light of proposed mechanisms. Square wave voltage excitation is in some ways simpler than the extensively studied sine wave excitation and yields information not readily obtainable from studies of brightness wave forms under sinusoidal voltages.

When a square wave pulse is applied to an electroluminescent cell two pulses of light emission are generally observed (2-5), one upon application of the external field and the other upon removal of that field. The first light pulse reaches its maximum shortly after the voltage rise is completed, then decays in roughly exponential fashion until the inception of the second light pulse at the removal of the voltage. A typical time dependence of luminescence and applied voltage is shown in Fig. 1.

In this work measurements were made of the emitted light pulses and their decay characteristics as a function of the two time parameters of the pulsed square wave voltage excitation: pulse width and repetition interval. These effects were studied in the temperature range of —130° to 150°C. The yellow emission band of a manganese-activated phosphor and the blue and green emission bands of a copper-activated phosphor (isolated by means of optical interference filters) were studied. The voltage dependence of emission intensity was checked and found to fit closely to exp $[-b/V^{1/2}]$ as has been widely observed for sine wave excitation (2).

[1] Present address: Gordon McKay Laboratory, Harvard University, Cambridge, Mass.

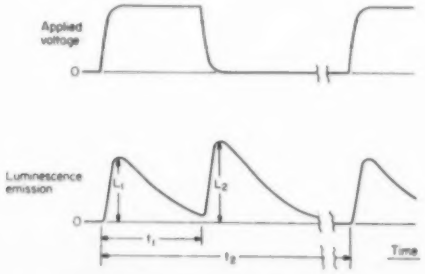

Fig. 1. Typical brightness waveform under square wave voltage excitation: t_1 = pulse width; t_2 = repetition interval; L_1, L_2 = peak intensities of the two light pulses.

Experimental

The preparation of the phosphors is shown in Table I and the panel construction in Fig. 2. Chlorine was included as a charge compensating coactivator in the copper-activated phosphor. Monovalent copper ions substitutionally replacing zinc ions in the crystal are more easily incorporated if chlorine is present simultaneously to substitute for sulfur (6). It has also been proposed (7) that chlorine promotes the formation of sulfur vacancies thought to be necessary for luminescence in ZnS. Preparation of the manganese-activated phosphor did not require

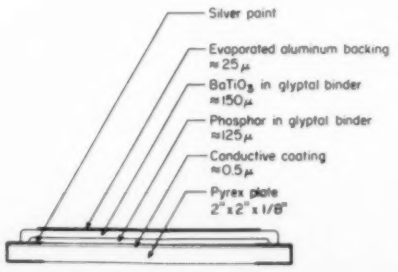

Fig. 2. Construction of the electroluminescent cells

Table I. Phosphor preparation

Phosphor	Zn(S, O): (Cu, Cl)	ZnS: (Mn, Cu)
Activation	0.005 g atom Cu/mole ZnS 0.02 g atom Cl/mole ZnS 0.4 mole ZnO/mole ZnS	0.0025 g atom Cu/mole ZnS 0.0125 g atom Mn/mole ZnS
Firing Temp., Time, Atmosphere	900°C 24 hr air	1100°C 1 hr dry H_2S
Post-Firing Washing Procedure	1. hot acetic acid (20%) 2. water 3. NaCN solution (3%) 4. water 5. methanol	1. NaCN solution (3%) 2. water 3. methanol
Drying Temp., Time, Atmosphere	125°C 16 hr air	125°C 16 hr air

a coactivating halide flux since manganese replaces zinc as a divalent ion in the lattice so that charge compensation is unnecessary (8). Some copper was also included in this phosphor since it has been found to promote electroluminescence (9). The numbers given for the thickness of the various layers are representative. A rough check on the measured phosphor layer thickness was given by the capacitance of the panels which was about 10^{-9} farads in each case. The phosphor powder was mixed with a binder and sprayed onto the conductive surface of a Pyrex plate serving as the transparent electrode. A second layer of binder containing powdered barium titanate was applied to the back of the phosphor layer. This insulating layer was found to be useful in preventing breakdown across thinner portions of the phosphor layer without sacrificing much of the voltage drop across the latter due to the large dielectric constant of barium titanate. An aluminum backing evaporated onto the barium titanate layer served as the rear electrode. Silver paint around the edges of the glass plate allowed contact to be made between the conductive coating electrode and a copper strip pressed against the front of the plate. The aluminum electrode was held against the surface of a copper block kept at ground potential, which also served as the thermal reservoir used in controlling the temperature of the phosphor.

The experimental arrangement is shown schematically in Fig. 3. Tektronix units of the 160 series provided the square wave signals which were fed into an amplifier capable of delivering outputs up to 2000 v with a rise time in the vicinity of 10 μ sec. An RCA 6199 photomultiplier was used to monitor the luminescence. The time dependence of the exciting voltage and of the emitted light were displayed on a Tektronix 545 oscilloscope equipped with a dual trace preamplifier.

The panel was enclosed in a stainless steel chamber fitted with a quartz window for viewing the luminescence. A copper rod connected to the copper block in contact with the panel's aluminum backing led outside the housing through a Teflon insulator. This rod could be immersed in a refrigerant or in a heating coil to vary the temperature of the electroluminescent cell. Temperature was measured by an iron-constantan thermocouple with one junction located on the surface of the copper block next to the panel.

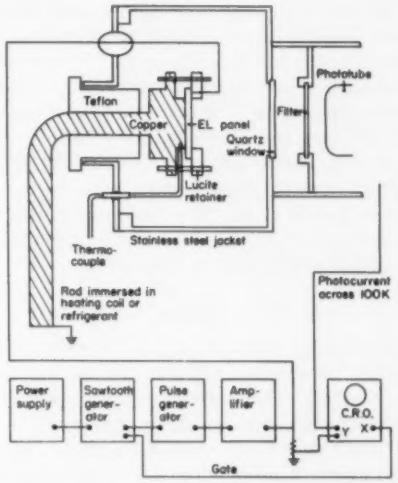

Fig. 3. Schematic diagram of the experimental arrangement.

Procedure and Measurements Performed

The aluminum backing electrode was kept at ground potential while the transparent electrode was driven back and forth between ground and a high negative potential. By means of a Balzers graduated interference filter serving as a crude spectrometer in the visible it was determined that the yellow-orange emission of the manganese panel consisted of the characteristic single broad band peaked around 5800Å. The copper-activated panel exhibited the well-known blue-green emission which changes in spectral content with varying operating conditions, e.g., becomes bluer with increasing frequency. The overlapping emission bands of this phosphor were separated by two Balzers interference filters transmitting 4610Å and 5300Å with peak transmissions of 30% and half widths of 100Å. Because of the reduction in intensity in selecting such narrow spectral ranges for investigation, the measurements on the Zn (S,O): Cu,Cl panel were made at higher exciting voltages and greater phototube sensitivity than were used in the measurements on the ZnS: Mn, Cu panel.

Detailed measurements were made on the variation of the two peak intensities, L_1 and L_2, with the repetition interval t_2, and with temperature. 400-v pulses of 10 msec duration were used in the ZnS: Mn, Cu studies, 700-v pulses of 1 msec duration for

the Zn (S,O):Cu, Cl. The pulse widths chosen were the smallest times needed to allow the first light pulse to decay to a value small relative to L_2. The output photocurrent of the photomultiplier was passed through a 10^5 ohm resistor and displayed on the oscilloscope. When L_1 and L_2 were widely different ($L_1 << L_2$), the signal was fed into both channels of a dual trace preamplifier with each channel set at a scale convenient for measuring one of the peak heights. For long repetition intervals the peak heights were taken from a photograph of the scope trace.

Measurements were made of the decay of the second light pulse after removal of the applied field (L vs. t from L_2 on). For the ZnS: Mn, Cu panel, 400-v pulses of 10 msec duration and 10 cps repetition rate were used in making these measurements. For the Zn (S,O): Cu, Cl panel, 700-v pulses of 1 msec duration and 10 cps repetition rate were used. The delaying sweep circuit of the oscilloscope was employed for these measurements. This decay characteristic was studied at various temperatures.

Qualitative observations were made on the brightness wave forms of the luminescence emission with very small pulse widths. This turned up some interesting effects which will be discussed.

Results

Luminescence emission occurs on the rise and on the fall of the applied voltage, giving the two light pulses L_1 and L_2. For a given voltage amplitude and for the low duty cycles normally employed ($t_1 << t_2$), it was found that L_1 depends on t_2 and L_2 on t_1. This is to be expected if the dominant factor in determining the state of a phosphor at a particular temperature is the time elapsed from the last preceding excitation, i.e., the last preceding voltage shift (3). Thus it is not surprising that the second light pulse is insensitive to the repetition interval and that the first light pulse is unaffected by the duration of the applied voltage following it.

Figures 4 and 5 are log-log plots of the variation in peak intensity of the first light pulse with repetition interval for the two phosphors at several temperatures. Figure 5 consists of the two sets of curves for the green and the blue emission of the copper-activated phosphor. Any small drift in either the applied voltage amplitude or the phototube sensitivity would be expected to change both L_1 and L_2 by the same factor. In order to compensate for such variations the data are normalized by plotting the peak height ratio, L_1/L_2, as the dependent variable.

In all cases the peak height ratio is of the order of unity for small t_2 and falls off as t_2 increases. At low temperatures the drop-off is slower than at high temperatures. At −125°C this variation is well frozen out, with very little change in L_1/L_2 occurring in times less than an hour. For the manganese-activated panel the ratio falls until a terminal value of the order of 10^{-1} to 10^{-2} is attained at a particular value of t_2, and then remains constant. For the copper-activated panel the ratio falls to 10^{-3}, the limit of measurement, without exhibiting any saturation effect. The blue emission of this panel possesses a faster decrease of L_1 with t_2 than does the green emission, al-

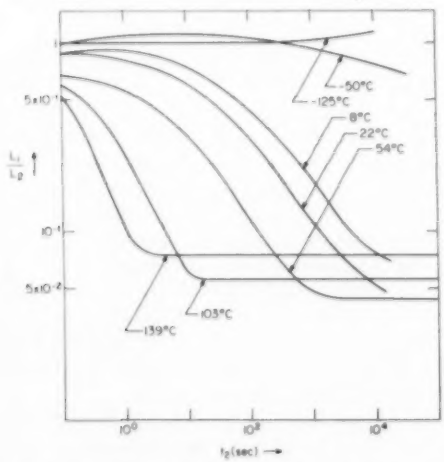

Fig. 4. Peak intensity of the first light pulse vs. repetition interval for the ZnS:Mn,Cu panel.

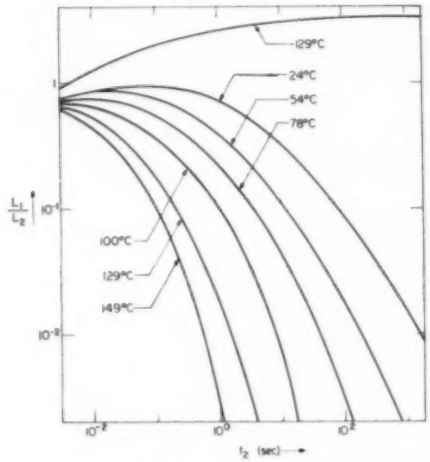

Fig. 5a. Peak intensity of the first light pulse vs. repetition interval for the Zn(S,O):Cu,Cl panel; green emission.

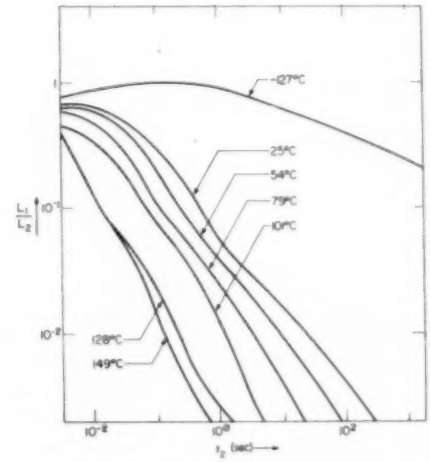

Fig. 5b. Peak intensity of the first light pulse vs. repetition interval for the Zn(S,O):Cu,Cl panel; blue emission.

though the latter decay seems to catch up with the former at very long repetition times. Waymouth and Bitter (4) measured the integrated light output of a blue-green phosphor upon removal of an applied voltage of long duration. They observed a slow decay with increasing duration time similar to that reported here for increasing repetition time, with the blue decay occurring more quickly than the green decay. Their results are compared to ours in the following section.

The temperature dependence of L_1 (t_z) is interesting since such a thermally controlled process can yield information on energy levels of electrons involved in the excitation or recombination processes taking place in electroluminescence. An analysis and interpretation of this temperature dependence is discussed in the next section.

Figures 6 and 7 show the time decay of the second light pulse upon removal of the applied field for the two phosphors at three of the temperatures studied, the latter figure giving both the blue and the green decays of the Zn (S,O): Cu,Cl panel. The ZnS: Mn, Cu data do not exhibit any appreciable systematic temperature shift whereas the Zn (S,O): Cu,Cl curves exhibit a minor systematic change with temperature. The initial slope of the decay at −125°, 25°, and 150°C gives decay rates of 17, 14, and 8 x 10^3 sec^{-1}, respectively, for the blue and 11, 8, and 5 x 10^3 sec^{-1} for the green emission. In addition to this decrease of the initial rate of decay, these curves also become more exponential in shape (linear on a semi-log plot) with increasing temperature so that after long times the emission is lower and the decay rate greater for high temperatures than for low. This produces the cross-over of the decay curves shown in Fig. 7. The initial decay rate of the ZnS: Mn,Cu data is 0.9 x 10^3 sec^{-1} and the shape of this decay does not change with temperature.

Figure 8 shows some brightness waveforms obtained by application of voltage pulses of short duration. For the manganese-activated phosphor, equal increments of emission occur at the rise and fall of the applied voltage except with pulse widths less than about 0.5 msec for which the second increment becomes smaller than the first. Nudelman and Matossi (5) report a very similar behavior for the blue component of a ZnS: Cu,Pb phosphor with a critical pulse width of 0.7 msec. The blue emission of our copper-activated phosphor also exhibits equal increments of emission, but at pulse widths down to 0.2 msec. For the green emission of their phosphor, Nudelman and Matossi report equal peak heights at the voltage rise and fall for pulse widths greater than 0.7 msec. Our observations are similar, except that the critical time observed is about 0.2 msec.

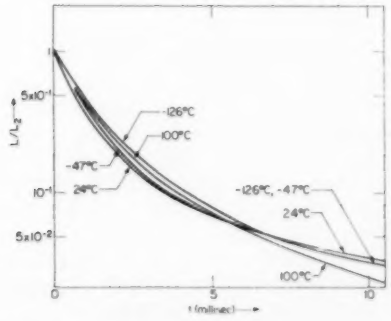

Fig. 6. Decay of light emission L on removal of the applied voltage for the ZnS:Mn,Cu panel.

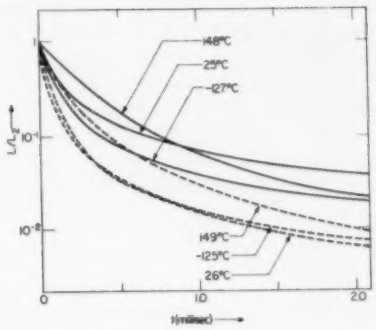

Fig. 7. Decay of light emission L on removal of the applied voltage for the Zn(S,O):Cu,Cl panel. Green emission: solid lines; blue emission: dashed lines.

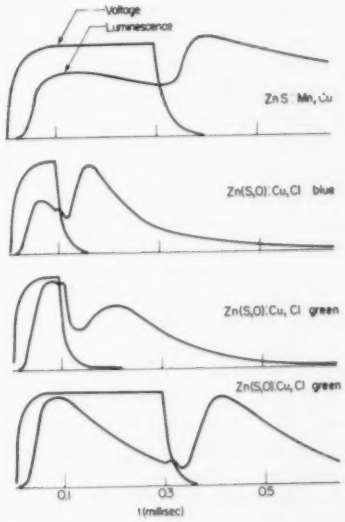

Fig. 8. Brightness waveforms using short pulses

Some interesting effects were observed in the Zn (S,O): Cu,Cl panel. The blue emission exhibits a very small peak preceding the build-up of the second light pulse. This stimulation peak appears at small repetition intervals and is insensitive to pulse width. The green emission also reveals this effect. In addition, however, at short pulse widths this emission shows a sharp dip upon the start of the voltage drop. This quenching dip precedes the build-up of the second light peak but follows the stimulation peak. Some representative brightness waveforms are shown in Fig. 8. The two effects are independent. The stimulation peak is most noticeable at short repetition times and long pulse widths, but as the pulse width is reduced the quenching dip becomes dominant. Nudelman and Matossi observed stimulation peaks, but for the green emission only. They did not find quenching dips in their phosphor.

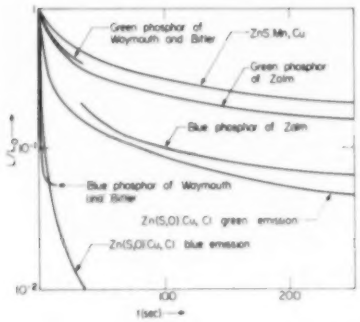

Fig. 9. Room temperature data on the dependence of the emitted light L after an elapsed time t from the preceding voltage shift. L_∞ is the value of L for $t = 0$.

Both of these effects were absent in our manganese-activated phosphor.

Discussion

In Fig. 9 the room temperature curves of Fig. 4 and 5 are replotted on semi-log paper along with some data of Waymouth and Bitter (4), and of Zalm (2), who also noticed this slow return of an electroluminescent cell to its original state following a field excitation. These curves demonstrate that this decay does not follow an exponential law. Rather, the log-log plots are suggestive of the power-law decays encountered in phosphorescence (10). Such decays may be accounted for in terms of the emptying of a collection of filled traps of various depths. For example, it has been shown (11) that a uniform trap distribution, that is, an equal number of traps of all depths, gives a decay with a t^{-1} dependence at long times. It is interesting that the blue emission decay approximates this hyperbolic relationship at the higher temperatures. A trap distribution varying exponentially with trap depth, that is, $dN_t/dE = A \exp[-\alpha E]$, gives a decay going as t^{-n} for long times (11), where $n = \alpha kT + 1$. If a t^{-n} law is assumed and compared with the steepest slopes encountered in Fig. 4 and 5, n is found to vary linearly with temperature from 0° to 150°C, going from 0.7 to 1.8 for the green emission, from 0.5 to 1.2 for the blue emission, and from 0.4 to 0.8 for the yellow emission. These observations suggest that the mechanism responsible for the behavior of L_t with time and temperature is the thermal release of trapped electrons (or holes). The existence of traps in zinc sulfide phosphors has been widely demonstrated by means of glow curves and other methods (12).

The above reasoning may be summarized by the following syllogistic argument: (*a*) temperature dependent phosphorescence has been accounted for in terms of electrons thermally ejected from traps; (*b*) the decay curves of L_t vs. t_2 resemble reported temperature dependent power-law phosphorescence decays; (*c*) therefore, the present measurements may reasonably be explained by the thermal release of trapped electrons.

In order to characterize the temperature dependence of the data, the following method has been employed. A particular value of L_1/L_2 is first selected, and then the value of t_2 corresponding to this level of the peak height ratio is noted for each of the various temperatures studied. The reciprocal of this arbitrarily defined relaxation time is plotted against reciprocal temperature on semi-log paper (hoping, of course, to obtain a straight line). This calculation is repeated for several choices of peak height ratio. The rationale for this procedure is the assumption that the extent to which the phosphor has retrogressed toward its equilibrium condition at a particular time following a field excitation is more or less defined by the value of L_1/L_2 at that time. The reciprocal of the time needed for the relaxation to proceed to a given stage is then taken as a measure of the rate of the relaxation process.

The results are shown in Fig. 10 and 11. Despite the crudeness of the approach and the expected complexity of the actual trap distributions, reasonably good straight lines were obtained. The activation energies corresponding to the slopes of the lines are listed in Table II. The effective trap depths obtained fall in the range of 0.3–0.5 ev for the blue emission, 0.5–0.8 ev for the green emission, and 0.6 ev for the yellow emission. For each emission band the effective trap depths increase with decreasing choices of L_1/L_2. Thus the deeper traps control the later stages in the relaxation process, which is reasonable as it is to be expected that the shallow traps empty first.

Before resuming this discussion of the role of traps in this phenomenon, a brief digression on the nature of the electronic states of the luminescence centers involved may be useful. It is generally agreed that the manganese centers give rise to perturbed ionic states lying well below the top of the valence band (13). Accepting the collision-excitation hypothesis, a ground-state electron interacts with a conduction electron accelerated to optical energies by the electric field in a localized high-field region of the crystal and is raised to a bound excited state from which it drops back to the ground state after a characteristic time, giving off a photon

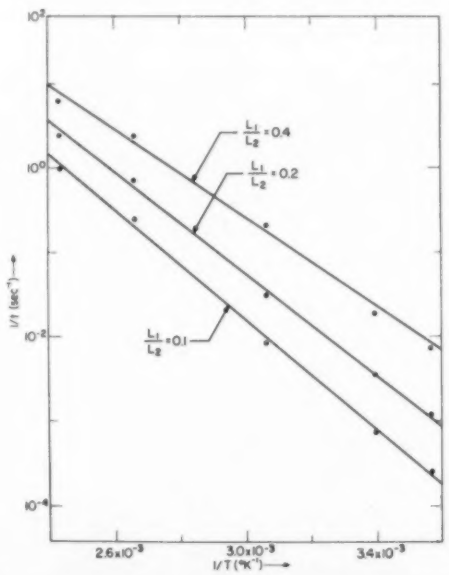

Fig. 10. Temperature dependence of the ZnS:Mn,Cu relaxation time.

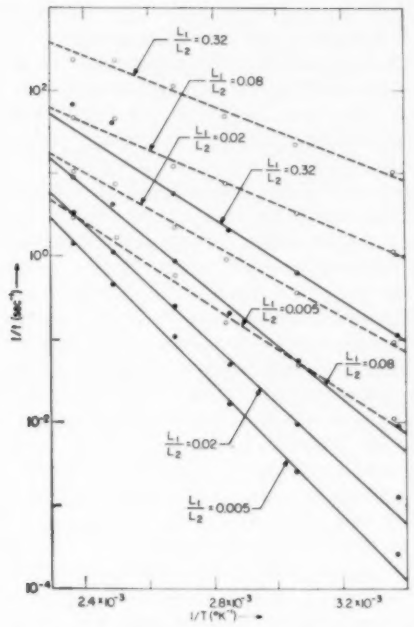

Fig. 11. Temperature dependence of the Zn(S,O):Cu,Cl relaxation time ———— green emission; - - - - -, blue emission.

Table II

Phosphor	Emission band	L_1/L_2	Activation slope in ev
ZnS: Mn, Cu	Yellow	0.4	0.52
		0.2	0.60
		0.1	0.64
Zn(S, O): Cu, Cl	Blue	0.32	0.30
		0.08	0.33
		0.02	0.43
		0.005	0.51
Zn(S, O): Cu, Cl	Green	0.32	0.49
		0.08	0.64
		0.02	0.71
		0.005	0.78

in the process. Ionization does not occur. This picture is consistent with our observations on the yellow emission band. The temperature independence of the decay of the light pulse (Fig. 6), as well as the absence of stimulation or quenching effects, indicates that bound states are involved. The equal increments of emission on the rise and fall of the external field may be understood on the basis of equal effective fields [the field at the voltage fall is due to polarization charges (3-5) to be discussed later] exciting equal numbers of centers which are simply added to the excited centers left over from previous excitations. This latter statement contains the assumption that the number of centers excited at any time is a small fraction of the total so that the number available for excitation remains essentially constant.

In copper-activated zinc sulfide, it is generally assumed that the emission process for both green and blue bands involves transitions between perturbed crystal states lying within the forbidden gap, and either conduction electrons (14) (Schön-Klasens model) or valence band holes (15) (Lambe-Klick model). The green emission exhibits equal peak heights with rise and fall of voltage, as well as sharp quenching dips upon field removal which may be due to charge carriers being swept out of a region in which they had been participating in radiative recombination with ionized activators. In addition, the shape of the light pulse decay is temperature dependent (Fig. 7). These observations favor the belief that excitation of the green centers involves ionization and production of mobile charge carriers. The situation is ambiguous for the blue band since this emission resembles that of the manganese in giving equal increments upon field application and removal, while it possesses a temperature dependence of the light pulse decay similar to that of the green band.

It has been reported (3) that an internal polarization is present which develops upon application of an external field and which decays upon removal of that field with a time dependence similar to that observed for L_1 vs. t_2. This polarization may result from the trapping of charge carriers in regions removed from their place of origin due to migration under the action of the field. It shall be assumed that both this internal polarization and the L_1 dependence arise from the same trapping mechanism within the phosphor.

Waymouth and Bitter (4) propose the trapping scheme shown in Fig. 12 in terms of the Schön-Klasens model. Upon application of the field, electrons are collision-ionized from activator centers into the conduction band whence they are swept by the field to another part of the crystal. Here they are held until field removal, whereupon they return and recombine radiatively with the empty activator centers. During the interim, however, the ionized centers may thermally release their trapped holes to the valence band where they may subsequently be retrapped by deeper quenching centers. Electron-hole recombination occurring at these quenching centers is assumed to be nonradiative at high temperatures, while at low temperatures light of longer wave length is emitted. This process reduces the light pulses emitted in the blue and green bands upon removal of the field, and also accounts for the temperature quenching of the photoluminescence.

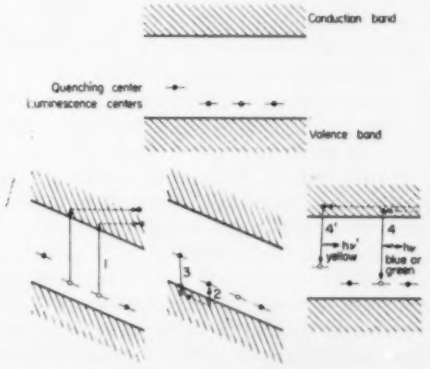

Fig. 12. Schon-Klasens model applied to electroluminescence (after Waymouth and Bitter).

Waymouth and Bitter, from temperature dependence measurements of L_2 vs. t_1, obtained activation energies of 0.29 and 0.21 ev for the green and blue bands, respectively, which they interpret as giving the separation between the vacant activator levels and the top of the filled band. Garlick and Gibson (16), from measurements of temperature quenching, obtained 0.95 ev for green-emitting ZnS:Cu and 0.59 ev for yellow-emitting ZnS:Mn. Activation energies observed here are about 0.7 ev, 0.4 ev, and 0.6 ev for the green, blue, and yellow bands, respectively.

Although this model is consistent with observations on the decrease of the burst of light emitted on removal of an applied field with increasing time of application of that field, there remain some objections to it. It does not appear to account for the decay of the light pulse emitted on aplication of the field with increasing time elapsed from the previous field excitation (our measurements of L_1 vs. t_2). As mentioned above, it seems likely that excitation of the green luminescence band, with emitted radiation (transition 4 in Fig. 12) of about 2.4 ev photon energy, involves ionization of an electron into the conduction band (or a hole into the valence band). Since the band gap of zinc sulfide is about 3.8 ev (17), the depth of the traps involved (transition 2 in Fig. 12) should be about 1.4 ev, much greater than observed values. This failure of the measured activation energies to give the band gap when added to the energy of the emitted radiation contradicts the picture shown in Fig. 12. It is tempting, but doubtful, to explain this discrepancy by invoking Schön's hypothesis of widely different energy levels for thermal and optical processes (18).

In connection with Fig. 12, it may be worthwhile to mention the related concept of delayed recombination proposed by several workers (2, 3). According to this model, electrons removed from ionizable activators by collision excitation on application of a high field are quickly swept to the positive side of the crystal where they are held until removal of the field releases them for radiative recombination with empty centers. Thus excitation of luminescence centers is thought to occur only on the rise of an applied d-c voltage pulse while luminescence emission occurs primarily at the fall of the voltage as only then may electrons return to recombine with ionized centers. Frequently quoted evidence for this theory is the observation that $L_1 << L_2$. However, Fig. 4 and 5 reveal that $L_1 << L_2$ only for long repetition intervals and high temperatures. Over wide ranges of operating conditions, e.g., for t_2 up to an hour at −125°C, L_1 and L_2 are approximately equal. These measurements do not favor delayed recombination. In addition the delayed recombination mechanism is not applicable to activators for which the excited state is a bound perturbed ion state and the electron is never physically removed from the center, e.g., manganese.

In view of the difficulties with this model, we will propose a mechanism by which we hope to account for, among others, these experimental findings: (*a*) the light pulse emitted on application or removal of voltage decays with the time elapsed from the preceding field excitation (voltage shift); (*b*) temperature dependence of (*a*) resembles the emptying of trap distributions of depths between 0.3 and 0.8 ev; (*c*) there is a component of internal polarization which builds up and decays in synchronism with the above effect.

When an external field is applied to a phosphor, there is evidence (3) that large voltage drops are concentrated across small regions of the phosphor due to the existence of barrier layers or rectifying junctions. It is in these high field regions that electroluminescence takes place. Electrons are field-ionized from deep traps and then accelerated to optical energies by the field. Some of these "hot" electrons collide with activator centers and lose all or part of their kinetic energy in raising electrons to excited states from which radiative transitions back to the ground state may later occur. It is natural to assume that the number of luminescence centers excited will be proportional to the concentration of energetic free electrons which, in turn, should strongly depend upon the number of "loose" electrons (electrons thermally excited to or injected into the conduction band, or electrons in traps shallow enough to be directly ionized by the field) originally present to initiate the process. It is hypothesized here that the experimental facts listed above are due to time variations in this population of loose electrons. Thus we consider changes in the number of centers excited rather than changes in the efficiency of the radiative recombination to be the dominant factor.

It is proposed here that the light emissions L_1 and L_2 are independent luminescence events produced by separate excitations at the rise and fall of applied voltage, and that a difference in their intensities reflects a difference in the number of centers excited in each case. Application of the external field establishes a space charge as electrons are swept out of the high field region. The time required for the development of this polarization is of the order of the critical pulse width mentioned earlier (5). Some of the free electrons produced by the applied field are trapped in a normally unoccupied trap distribution. When the external field is removed, part of the polarization charge decays quickly in a time similar to the build-up time. However, that portion of the space charge consisting of electrons in deep traps decays very slowly at a rate determined by the thermal release of trapped electrons. This accounts for the last of the experimental facts listed above, viz., the "frozen-in" component of polarization observed by Waymouth and Bitter.

Consider an electroluminescent phosphor in an equilibrium condition ($t_2 \rightarrow \infty$) at a certain temperature. Application of a field finds a certain number of loose electrons available for acceleration and collision-excitation of luminescence emission L_1. Let us denote this value of L_1 for a first voltage application, i.e., L_1 for $t_2 \rightarrow \infty$, as $L_1°$. Removal of the external field momentarily leaves an unopposed polarization field which causes a second excitation of luminescence, L_2. However, this field finds a larger number of field-ionizable electrons as traps were

filled on the voltage rise. This increases the resultant number of hot electrons to take part in collision-excitation. Thus we may understand the situation whereby $L_1 << L_2$ without recourse to delayed recombination.

A second similar voltage pulse applied after a short time finds the same nonequilibrium concentration of loose electrons so that for short repetition intervals we find $L_1 \approx L_2$. A voltage pulse applied after a considerable elapsed time ($t_2 >> t_1$) will find the phosphor partially relaxed towards thermal equilibrium so that $L_1^\circ < L_1(t_2) < L_2$. From Fig. 4 and 5 we note that L_1° is about one-twentieth of L_2 for the manganese-activated phosphor, while for the copper-activated phosphor L_1° is below the limit of measurement, i.e., less than one-thousandth of L_2. Thus we may interpret (*a*) in terms of a return to thermal equilibrium of the number of field-ionizable electrons via the thermal emptying of an overpopulated trap distribution. The temperature dependence mentioned in (*b*) then follows naturally from Boltzmann statistics. These trapped electrons comprise the slowly decaying component of polarization mentioned above so that this polarization decays in synchronism with L_1, as stated in (*c*).

Although this mechanism accounts for the above experimental behavior it is not without its difficulties, a normal situation among electroluminescence theories. Since L_1 is assumed to vary with the number of occupied deep donors in the crystal, the effect should be largely independent of the particular luminescence center involved for a given host phosphor. However, we obtained different activation energies for the green and blue emissions of the copper-activated phosphor. Further assumptions may be needed to explain these observations in terms of our model. Another objection might be that filling of traps does not seem to occur to any great extent during electroluminescence as evidenced by the very weak glow curves following voltage excitation (9). This result may be due to the fact that electroluminescence is confined to just a small fraction of the phosphor volume. Also, other observations re-emphasize the importance of traps (19).

Summary

Measurements of the temperature-dependent decay of L_1 with t_2 suggest a process involving the thermal emptying of donors of depths between 0.3 and 0.8 ev. This phenomenon has been reported to be correlated with a polarization charge. We therefore attribute the traps to the host crystal rather than to the luminescence centers. The mechanism of delayed recombination does not appear to account satisfactorily for the data. An alternative suggestion is proposed whereby the number of filled deep donors is assumed to control the electroluminescence emission via the number of field-ionizable electrons available for collision excitation of centers.

Manuscript received Oct. 12, 1959.

Any discussion of this paper will appear in a Discussion Section to be published in the December 1960 JOURNAL.

REFERENCES

1. G. Destriau, *Phil. Mag.*, **38**, 700 (1947).
2. P. Zalm, *Philips Res. Repts.*, **11**, 353 (1956).
3. J. F. Waymouth and F. Bitter, *Phys. Rev.*, **95**, 941 (1954).
4. J. F. Waymouth and F. Bitter, *ibid.*, **102**, 686 (1956).
5. S. Nudelman and F. Matossi, *This Journal*, **101**, 546 (1954).
6. F. A. Kröger, *Ergebn. exakt. Naturw.*, **29**, 104 (1956).
7. N. Riehl and H. Ortmann, "Zinksulfid-Luminophore," p. 31, Verlag Chemie, Weinheim, 1957.
8. C. C. Klick and J. H. Schulman, *Solid State Physics*, **5**, 148 (1957).
9. G. F. J. Garlick, *Handb. d. Phys.*, **26**, 99 (1958).
10. H. W. Leverenz, "An Introduction to Luminescence of Solids," p. 254, John Wiley & Sons, Inc., New York (1950).
11. J. T. Randall and M. H. F. Wilkins, *Proc. Roy. Soc. (London)*, **A184**, 390 (1945).
12. W. Hoogenstraaten, *Philips Res. Repts.*, **13**, 515 (1958).
13. W. W. Piper and F. E. Williams, *Solid State Physics*, **6**, 129 (1958).
14. M. Schön, *Z. Physik*, **119**, 463 (1942); H. A. Klasens, *Nature*, **158**, 306 (1946); H. A. Klasens, *This Journal*, **100**, 72 (1953).
15. J. Lambe and C. C. Klick, *Phys. Rev.*, **98**, 909 (1955).
16. G. F. J. Garlick and A. F. Gibson, *J. Opt. Soc. Amer.*, **39**, 935 (1949).
17. W. W. Piper, *Phys. Rev.*, **92**, 23 (1953).
18. M. Schön, Halbleiter-Probleme, **4**, 285 (1958).
19. C. H. Haake, *J. Opt. Soc. Amer.*, **47**, 881 (1957).

Anodization of InSb

J. D. Venables and R. M. Broudy

Research Laboratories, National Carbon Company, Division of Union Carbide Corporation, Cleveland, Ohio

ABSTRACT

The dependence of the constant current anodization curve on crystallographic face and illumination is reported for monocrystalline InSb. It is shown that illumination changes the film formation rate, either increasing or decreasing it depending on certain experimental conditions. Photovoltages similar to those reported for other anodic films have been observed.

The work of Dewald (1) on anodization of InSb indicates that this material is in some ways particularly suited to a study of the general oxidation process. InSb forms in the zincblende structure which, although cubic, does not possess a center of inversion; therefore, opposite directions are not necessarily equivalent. This geometrical polarity, which also can be revealed by etching (2,3), is an important factor in the experiments of Dewald (1) in that he finds that (111) faces anodize at a faster rate than the ($\bar{1}\bar{1}\bar{1}$) faces.[1] In the present account we show the crystallographic dependence of the constant current anodization curves.

In the previous literature, several authors have reported a photodependence of the oxidation process for various materials such as Ta (4-6), Si (7), Cu (8), and Al (6). We have found that photoeffects also exist in the InSb system; several associated phenomena are reported here.

Apparatus

The experimental arrangement is shown in Fig. 1. An appropriately masked sample[2] with either the (111) or ($\bar{1}\bar{1}\bar{1}$) face exposed is made the anode in a 0.1*N* KOH solution held at constant temperature. An electronic constant current source serves as a power supply to provide current densities in the neighborhood of 200 μa/cm^2. Voltages which represent the drop across the anode film are monitored using a reference electrode of InSb connected to a recording voltmeter with a high input impedance.

The samples are x-ray oriented, cut, and then mechanically polished with various grades of alumina down to 0.1 μ which produces a mirror-like finish on the selected face. After masking, they are pre-anodized to 10-20 v and then immersed in concentrated HF which removes the oxide film but does not attack the InSb substrate. This process (pre-anodizing and film removal) is repeated until the anodization curves are completely reproducible.

[1] Allen (2) has made the correlation between anodization rates and etch pits. Pits appear on the ($\bar{1}\bar{1}\bar{1}$) face.

[2] The masking agent used was either polystyrene in toluene (1) or G.E. 1202 baking varnish. The latter is more durable.

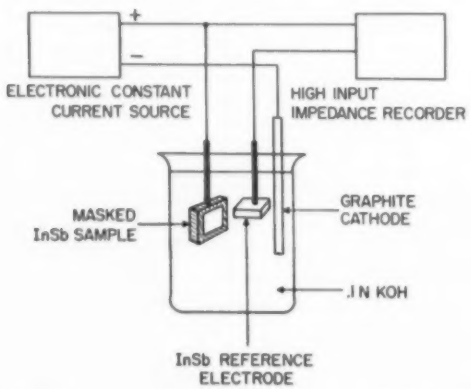

Fig. 1. Experimental arrangement for constant current anodization studies on InSb.

Anodization Curves

In Fig. 2 typical recorder curves of the voltage drop across the film on the (111) and ($\bar{1}\bar{1}\bar{1}$) faces are shown as a function of time at constant current. There are several features of the curves which are of interest: (*a*) the initial region of the two curves is similar and nonlinear, tending to curve upward until the turnover point is reached. The nonlinearity is perhaps a consequence of the formation of space charge in the oxide layers during anodization (9); (*b*) the turnover voltage is different for the two faces and is always greater for the ($\bar{1}\bar{1}\bar{1}$) face than for the (111) face, under identical experimental conditions. This unusual crystallographic dependence indicates that the turnover probably is not a

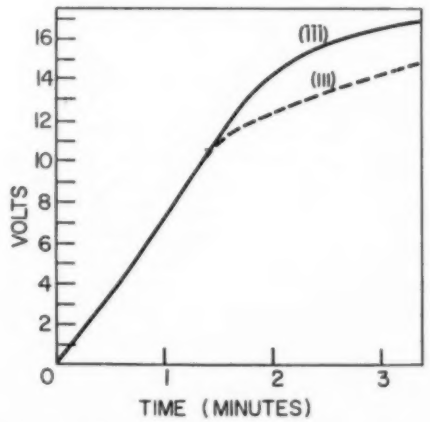

Fig. 2. Constant current anodization curves for (111) and ($\bar{1}\bar{1}\bar{1}$) faces of InSb.

consequence of the structure of the oxide film (porosity, cracks, etc.) but that the metal-oxide interface plays some role in the process.

When a piece of InSb is anodized with both the (111) and $(\bar{1}\bar{1}\bar{1})$ faces exposed, it is observed by means of interference colors that the film thickness is the same on both faces until the turnover region is reached. As anodization continues beyond this point, the interference colors indicate that a thicker film forms on the (111) face than on the $(\bar{1}\bar{1}\bar{1})$. By means of the following experiment we have shown that this is due to a redistribution of current density which takes place when the (111) face reaches its turnover point. The experimental arrangement is shown in Fig. 3. Two InSb samples with {111} faces of equal area but of opposite crystallographic sign are connected to a common constant current supply through separate ammeters. Since the voltage drop across the solution and cathodes is negligible, this is equivalent to anodizing a single sample having both crystallographic faces exposed, except that now the current through each face can be monitored separately. Initially both meter readings are the same; however, as soon as the (111) face reaches its turnover voltage for the currents involved, its resistance ceases to increase. Eventually most of the current flows through the (111) face producing a thicker film on it than on the $(\bar{1}\bar{1}\bar{1})$ face. Apparently this redistribution occurs because the electric field required for ion flow cannot be maintained across the film on the $(\bar{1}\bar{1}\bar{1})$ face after the (111) face attains the turnover voltage.

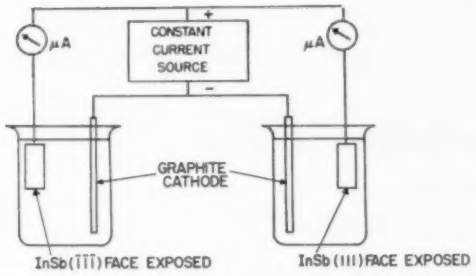

Fig. 3. Experimental arrangement to monitor current through (111) and $(\bar{1}\bar{1}\bar{1})$ faces separately.

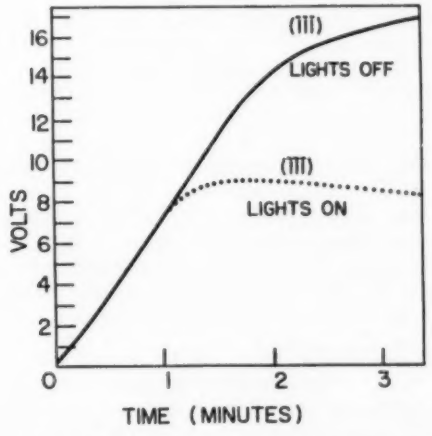

Fig. 4. Effect of illumination on constant current anodization curves.

Photoanodization

When a sample undergoing anodization is irradiated with visible light of wave length shorter than approximately 5200Å, it is observed that the initial part of the anodization curve remains unaffected but that the turnover voltage is decreased. The illumination from a 300-w slide projector produces the effect shown in Fig. 4. Accompanying this reduction in turnover voltage under the two sets of experimental conditions described below, there occurs a change in the film formation rate.

Condition No. 1.—The exposed face of an InSb sample is illuminated evenly and anodized under constant current conditions beyond the turnover point. The relative thickness of the film formed is measured using the step gauge method described by Dewald (1). The film is removed with HF and the sample, now in total darkness, is anodized again using the same value of current for the same length of time. Step gauge measurements show that the illuminated film is thinner than the one formed in darkness, indicating that the efficiency of film formation is lowered when the sample is illuminated.

Condition No. 2.—In this experiment, only half of the exposed InSb face is illuminated during anodization. The process is carried out past the turnover point and it is observed that the above situation is reversed. At first glance it appears that here the light increases the efficiency of film formation since the illuminated section is now thicker than the dark section. We have shown, in an experiment similar to the one discussed in the previous section, that this is actually due to a redistribution of current density which takes place when the illuminated section reaches the turnover. Figure 5 depicts the experimental arrangement. Two identical faces are anodized, one with illumination and the other without. The two samples are connected to a common constant current supply through separate meters.

Again it is observed that initially both meter readings are the same; however, as soon as the illuminated face reaches the light-induced turnover voltage its resistance ceases to increase with time and most of the current flows through that face. This produces a film on the illuminated face which is considerably thicker than the one which is formed

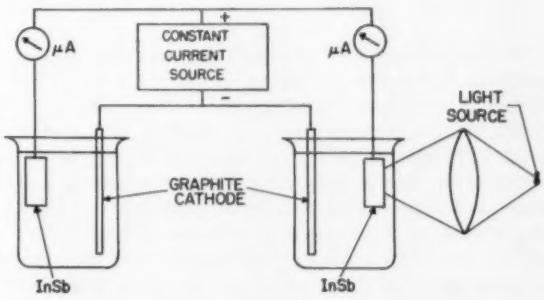

Fig. 5. Experimental arrangement to monitor current through illuminated and nonilluminated faces of InSb separately.

in darkness. A device which utilizes this photoanodization effect to record an image projected on the face undergoing anodization has been described elsewhere (10).

Photovoltages

When InSb of any orientation is anodized beyond the turnover point (it makes no difference whether the turnover is light-induced or not) and then removed from the circuit, it is found that a voltage appears across the film when illuminated. This photovoltage, which incidentally has the same polarity as the anodizing voltage, saturates at approximately 1.5 v and is similar in many respects (time constants, decay, internal impedance, etc.) to photovoltages found in Ta_2O_5 films by van Geel, Pistorius, and Winkel (8). Because of this similarity, no further description is given here. We do wish to point out, however, that the photovoltage demonstrates the existence of light-induced carriers (electrons or holes) in the system. We speculate that perhaps it is these carriers which serve to lower the film forming efficiency during photoanodization by providing electronic (or hole) conduction in addition to the ionic current.

Summary

The phenomena observed during our preliminary studies on the InSb anodic system have been presented at this time because of their unique character. No attempt has been made to interpret the data theoretically since several questions which are raised by this initial work remain to be clarified. For example, we do not know whether the crystallographic dependence of anodization rate as observed by Dewald (1) exists during the initial stages of the anodic process or occurs only near the turnover point as our initial experiments seem to indicate. In addition it is not known why the turnover occurs at all or why illumination changes the turnover point; it is possible that space charge effects which have been discussed by Dewald (9) and light-induced space charge effects which were hypothesized by Vermilyea (11) may be responsible for the observation phenomena.

Acknowledgments

The authors wish to thank Dr. R. G. Lye, Dr. W. Ware, and Dr. S. Senderoff for many helpful discussions of this work. They are also indebted to R. E. Hart, Jr. for his help in sample preparation.

Manuscript received Aug. 13, 1959.

Any discussion of this paper will appear in a Discussion Section to be published in the December 1960 JOURNAL.

REFERENCES

1. J. F. Dewald, *This Journal*, **104**, 244 (1957).
2. J. W. Allen, *Phil. Mag.*, **2**, 1475 (1957).
3. J. D. Venables and R. M. Broudy, *J. Appl. Phys.*, **29**, 1025 (1958).
4. D. A. Vermilyea, *J. Appl. Phys.*, **26**, 489 (1955).
5. D. A. Vermilyea, *This Journal*, **104**, 212 (1957).
6. W. Ch. van Geel, C. A. Pistorius, and P. Winkel, *Philips Research Repts.*, **13**, 265 (1958).
7. P. F. Schmidt and W. Michel, *This Journal*, **104**, 230 (1957).
8. J. Kruger, *Nat. Bur. Standards (U.S.) Tech. News Bull.*, **47** (March 1958).
9. J. F. Dewald, *This Journal*, **102**, 1 (1955).
10. J. D. Venables and R. M. Broudy, *J. Appl. Phys.*, **30**, 1110 (1959).
11. D. A. Vermilyea, *This Journal*, **104**, 216 (1957).

Lifetime Preservation in Diffused Silicon

M. Waldner[1] and L. Sivo

Semiconductor Products Department, General Electric Company, Electronics Park, Syracuse, New York

ABSTRACT

Minority carrier lifetime in silicon which has been diffused in BCl_3 plus nitrogen at 1100°C may be in excess of 100 μsec. Diffusion at 1200°C may give lifetimes in excess of 25 μsec. The lifetimes are significantly higher than the values obtained by heat treatment without the BCl_3. A similar effect is observed if chlorine or PCl_5 is added to the nitrogen ambient. Some lifetime preservation after extended heat treatment following the BCl_3 treatment indicates that the glassy layer deposited during the treatment plays a significant role in the process.

Several methods for lifetime preservation during the heat treatment of silicon, such as is incurred during a diffusion process, have been reported. These include slow cooling (1), vacuum heat treatment (2), and gettering by a metal-silicon liquid phase on the silicon surface (3). The purpose of this paper is to show that relatively high lifetime may be maintained in silicon that has been diffused with boron, even with fairly rapid cooling, and that the diffusion process, using BCl_3 gas, plays a significant role in this lifetime preservation; furthermore, that chlorine gas or PCl_5 as well as the BCl_3 also give the effect of lifetime preservation.

The use of BCl_3 as a carrier for boron during diffusion has been noted by Fuller and Ditzenberger (4). Moreover, Prince (5) has noted that during the diffusion of boron in such a process lifetime regeneration of previously diffused silicon may be observed on thin samples.

Experimental Procedure

The diffusion and heat treatment were carried out in a dual tube furnace with 1⅛ in. ID quartz tubes. The silicon was in a 5-15 ohm-cm resistivity

[1] Present address: Hughes Products, Semiconductor Division, Newport Beach, California.

range with initial lifetimes in excess of 100 μsec. The silicon wafers were supported either horizontally in a separate quartz half tube or vertically in a slotted quartz holder. The wafers were from 35 to 60 mils thick. One of the quartz tubes was used to run control samples in a nitrogen gas flow of 10 ft³/hr.[2]

Three programs were used during the introduction of the BCl_3. They were as follows: Program A—The samples were introduced into the furnace, with only a nitrogen flow, followed by a BCl_3 flow of 0.04 ft³/hr with 18 ft³/hr of nitrogen, for 30 sec, 0.04 ft³/hr of BCl_3 and 10 ft³/hr of nitrogen for 30 sec, 0.04 ft³/hr of BCl_3 and 4 ft³/hr of nitrogen for 4 min, and 10 ft³/hr of nitrogen only for the rest of the run; Program B—The samples were introduced into the furnace, with only a nitrogen flow, followed by a BCl_3 flow of 0.04 ft³/hr with 10 ft³/hr of nitrogen for 30 sec, 0.04 ft³/hr of BCl_3 with 4 ft³/hr of nitrogen for 4 min, and 10 ft³/hr of nitrogen only for the rest of the run; Program C—A BCl_3 flow of 0.04 ft³/hr with 4 ft³/hr of nitrogen was established before introduction of the samples, which were then held at approximately a 500°C zone of the furnace for 1 min, a 900°C zone for 1 min, and at 1100°C for 4 min, followed again by a 10 ft³/hr flow of nitrogen only for the rest of the run.

The first of these programs, with the high initial nitrogen flow, was chosen to minimize back diffusion of air into the furnace. However, the programs which allowed higher initial BCl_3 concentrations, especially at low temperatures as in program C, gave the best results.

The PCl_5 was introduced by placing several grams of PCl_5 in the quartz tube at a point where the temperature was about 180°C. The PCl_5 gradually sublimed in the nitrogen carrier gas.

The chlorine heat treatment involved a chlorine flow rate of 0.04 ft³/hr for 4 min, mixed with 4 ft³/hr of nitrogen, followed by a chlorine flow rate of 0.01 ft³/hr, mixed with 10 ft³/hr of nitrogen, for the remainder of the run.

In most of the experiments the sample was cooled by turning the furnace off after the heat treatment. The resulting cooling cycle ("slow cool") is shown in Fig. 1. Two other cooling cycles were used. One involved cooling the sample by withdrawing it from the furnace during a 15-min period ("fast cool"); the other was a rapid withdrawal from the furnace ("air quench").

The pellets were prepared for diffusion by soaking in 48% nitric acid (to remove a nickel plate used in preliminary lifetime measurements), followed by three successive etches in "white" etch (4 parts HNO_3, 1 part HF), followed by a soak in HNO_3 and final rinses in deionized water and distilled water.

The lifetime of the samples were determined by a measurement of the photoconductivity decay following excitation of excess carriers by a sparked light source (6). For all but the very short lifetimes, the illumination was through a 1.6 mm thick silicon filter. For measurements on the short lifetime samples either a 0.2 mm filter or no filter were used. Because trapping may have been present in the very low lifetime samples, the true lifetime may in some cases be less than the measured decay times which are given here. On the higher lifetime samples, with junctions, photovoltaic measurements (7) on several samples confirmed the spark data. For two samples an attempt was made to estimate the lifetime from the amplitude of the collected signal in the usual drift mobility experiment (8). These checks indicated that the measured lifetime in the n-type control samples was correct, but that the lifetimes measured on p-type control samples was much too high.

In many of the samples the minority carrier diffusion distance was so great that a very large correction, due to surface recombination, needed to be applied to the measured values. For this reason both the measured decay times and the corrected values are given.

[2] All flow rates are given in air equivalent at 14.7 psi and 70°F.

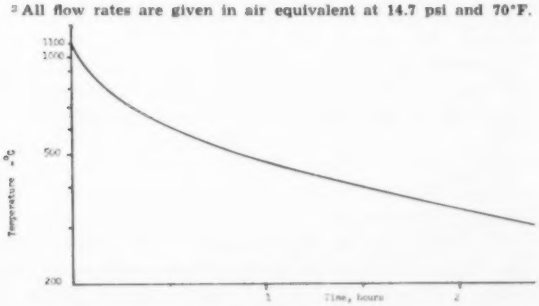

Fig. 1. Slow cool

Experimental Results

Lifetime Preservation

Below are listed the results for a number of experiments with the boron trichloride process, at 1100° for ½ hr, with "slow cooling." The boron diffused junction depth was about 0.04 mil. The control runs listed were run simultaneously with the listed boron diffusion of the same run number.

BCl_3 diffusion, 1100°C for ½ hr, n-type silicon

Run	Program	Material	Measured t, μsec	Corrected t
24	A	M2455	48	125
27	A	M2455	43	80
34	A	M2455	37	60
38	A	M2455	50	120
45	B	M2455	53	150
45	B	FZK59	68	120
47	B	M2455	54	170
47	B	FZK59	65	110
48	B	M2455	240*	240
48	B	FZK59	180*	180
50	B	FZK59	33	42
50	B	M2474	49	95
50	B	M2474	47	100
51	C	M2474	39	80
51	C	M2474	65	200
	Control (vs. BCl_3), 1100°C for ½ hr, n-type silicon†			
34		M2455	4.2	4.2
48		M2455	3	3
48		FZK59	2.6	2.6
50		M2474	3.6	3.6
50		M2474	3.9	3.9
51		M2474	3.7	3.7
51		M2474	4‡	4‡

* Photovoltaic measurement.
‡ Estimated as 5 μsec from drift mobility experiment.
† All but the first measurement were obtained with the 63 mil silicon filter.

Run	Program	Material	Measured t, μsec	Corrected t
BCl_3 diffusion, 1100°C for ½ hr, p-type silicon				
34	A	XP3223	7.8	7.8
38	A	M2592	6	6
48	B	M2592	17	32
50	B	XP3223	10	14
50	B	XP3223	5.6	5.6
50	B	M2592	14.5	22
50	B	M2592	15	31
51	C	XP3223	11.7	16
51	C	XP3223	9	9
51	C	M2592	27	72
51	C	M2592	26.5	70
Control (vs. BCl_3), 1100°C for ½ hr, p-type silicon†				
34		XP3223	3	3
48		M2592	3.7	3.7
50		XP3223	3	3
50		XP3223	2.5	2.5
50		M2592	4	4
50		M2592	3	3
51		XP3223	2.1	2.1
51		XP3223	2.1	2.1
51		M2592	3*	3
51		M2592	2.8	2.8

M2455: n-type Czochralski, 9-13 ohm-cm, approximately 20 dislocations/cm²
FZK59: n-type floating zone, 10-11 ohm-cm, approximately 10^4 dislocations/cm²
M2474: n-type Czochralski, 5-8 ohm-cm
XP3223: p-type floating zone, 5-10 ohm-cm, approximately 2×10^4 dislocations/cm²
M2592: p-type Czochralski, 5-8 ohm-cm, approximately 7×10^3 dislocations/cm²

* No observable lifetime from drift mobility measurement.
† These measurements were made with no filter or a thin filter. At least half of the samples showed evidence of trapping in the shape of the decay curve.

Both high dislocation density floating zone and low dislocation density Czochralski n-type material gave consistently high lifetimes well above those obtained with the control samples. Control sample lifetimes were usually about 4 μsec, although one exceptional value of 14 μsec was observed during the experiment. Some variation would be expected in the control results because of the expected dependence upon cleanliness.

The results with p-type material have been somewhat more erratic. However, use of the program C has resulted in lifetime values comparable to those observed in n-type material. Furthermore, although the listed values for the control lifetimes are similar to those reported for the n-type material, many of these samples showed evidence of trapping. An effort to correlate the results with those of a drift mobility measurement, which was successful with one n-type sample, failed with the p-type sample. Consequently, it is likely that the measured decay times for these control samples are not characteristic of the recombination process but are dominated by trapping effects.

The lifetime in a larger number [36] of diffused junctions on lower resistivity, 0.5 to 1 ohm-cm, n-type silicon was measured by means of the photovoltaic effect. The median lifetime on these samples was in excess of 10 μsec.

The results with chlorine and PCl_5 added to the nitrogen are tabulated below. Slow cooling was used.

Run	Material	Measured t, μsec	Corrected t
11	M2455(n-type)	45	74
11	M2455(n-type)	22.5	76
33	M2455(n-type)	21	26
16	M2455(n-type)	16.5	20
32	M2455(n-type)	21	26
31	XP3223(p-type)	2.9	2.9
32	XP3223(p-type)	7.1	7.1
41	M2455(n-type)	5	5
(Chlorine for 4 min only)			
	Control (vs. chlorine) 1100°C for ½ hr		
11	M2455(n-type)	7	7
11	M2455(n-type)	12.5	14
16	M2455(n-type)	5	5
31	XP3223(p-type)	2.5	2.5
	PCl_5 at 1100°C for ½ hr		
37	M2455(n-type)	29	58
37	XP3223(p-type)	3.1	3.1

For both the chlorine and PCl_5 ambient the lifetimes, at least in n-type material, were higher than those of the control samples. When the chlorine was run only for a few minutes at the beginning of a run, as in run 41 above, no marked lifetime retention was observed. This is in contrast to the results with BCl_3.

In the case of the chlorine treatment, a significant difference in lifetime in several samples run together was noticed. For instance, for three samples placed vertically and directly behind each other in the gas flow at 1100°C the corrected values were 74, 52, and 29 μsec in order from the upstream end. This effect, if present, was much less pronounced with the BCl_3 process. The values in a corresponding experiment with the BCl_3 were 90, 90, and 72 μsec.

The tabulation below shows the results obtained when the diffusion time at 1100°C was extended, or the temperature raised to 1200°C. N-Type material was used.

Time and temperature	Measured t, μsec	Corrected t
2 hr at 1100°C	43	80
2 hr at 1100°C	37	60
21 hr at 1100°C	11.5	13
21 hr at 1100°C	19	24
21 hr at 1100°C Control	3.4	3.4
½ hr at 1200°C	26	38

Lifetimes in excess of those resulting from the heat treatment alone may be obtained during extended diffusion, or at 1200°C. In order to obtain the results quoted at 1200°C it was necessary to apply the boron from the BCl_3 at 1100°C and then raise the temperature to 1200°C. If the BCl_3 is introduced at 1200°C, the adherent glassy deposit otherwise obtained on the silicon surface is not observed. Instead, layers which were cracked and chipped were found.

The effect on the final lifetime of the three cooling cycles which were tried is shown below. N-type silicon diffused for ½ hr at 1100°C, with program A, was used. The fast, 15-min cooling was without

Cooling	t Measured, μsec	t Corrected
Slow cool	48	125
Fast cool	37	90
Air quench	7.5	7.5

serious effect, although the air quench did give much lower lifetime.

Lifetime Regeneration

An experiment was performed on several diffused silicon p-n junctions (provided by F. E. Gentry) to determine the feasibility of lifetime regeneration with the BCl_3 process. These samples had been diffused with gallium to a junction depth of about 3 mils. These samples were run through program C with slow cooling. The low-temperature step changed to 700°C for 1 min. Two samples were subjected to a control cycle with nitrogen ambient only. The photovoltaic method was used to measure the lifetime before and after the processing. Values quoted below may be taken only as relative values for this particular experiment because the boundary conditions imposed by the deeply diffused junctions are not those for which the photo-voltaic equipment was calibrated. Results are tabulated below.

Process	Initial t, μsec	Final t
Program C	1	6.8
	2.7	24.3
	3.6	11.9
	3.0	6.1
Average	2.6	12.3
Control	3.4	2.3
	2.7	2.0

These results substantiate Prince's observation (5) that lifetime regeneration may be obtained in this way.

Discussion

The above data show that lifetimes of 20 to over 100 μsec may be obtained in diffused p-n junctions formed by the diffusion of boron from a BCl_3 carrier. The similar results obtained with PCl_5 and chlorine suggest that the chlorine liberated by the decomposition of the boron trichloride and phosphorus pentachloride plays a part in the process. However, good results can be obtained with BCl_3 even though the gas flows only a few minutes, while with chlorine a continuous flow is necessary. This suggests that the adherent glassy deposit formed on the silicon surface during the BCl_3 flow also plays a part.

Chlorine is known to attack many metals at elevated temperatures. Indeed, during the PCl_5 and chlorine experiments there was some attack even on the silicon. It may be that the chlorine provides an effective in-site etching and cleaning of the presumably contaminated silicon surfaces. Moreover, because of such an etching action, the chlorine may act as an impurity getter at the silicon surface during the diffusion. The results with BCl_3, despite the short application of the gas, suggest that the glassy surface layer may act as an impurity getter, or at least mask the silicon against the in-diffusion of impurities coming from the carrier gas or the walls of the furnace.

As has been described, a BCl_3 program that had beneficial effects on the n-type material did not work as well on the p-type material. It was necessary to modify the process to obtain markedly improved results on p-type material. This suggests that, at least under the conditions of these experiments, an impurity (not necessarily the only one) was present which was particularly effective in reducing the lifetime in the p-type material, and was particularly difficult to remove from the system.

Acknowledgments

The writers wish to thank R. E. Hysell for his assistance and instruction in the lifetime measurements, J. P. Dietz for making the dislocation density estimates, J. E. Greever and D. C. Jillison for supplying the silicon crystals, and J. F. Elliott for discussions of his related work which initially suggested this study.

Manuscript received Sept. 18, 1959.

Any discussion of this paper will appear in a Discussion Section to be published in the December 1960 JOURNAL.

REFERENCES

1. B. Ross and J. R. Madigan, *Phys. Rev.*, **108**, 1428 (1957).
2. A. N. Baker and G. Bemski, paper presented at I.R.E.-A.I.E.E. Semiconductor Device Research Conference, Boulder, Colorado, July, 1957.
3. S. J. Silverman and J. B. Singleton, *This Journal*, **105**, 591 (1958).
4. C. S. Fuller and J. A. Ditzenberger, *J. Appl. Phys.*, **25**, 1439 (1954).
5. M. B. Prince, U. S. Pat. 2,790,940, April 30, 1957.
6. D. T. Stevenson and R. J. Keys, *J. Appl. Phys.*, **26**, 190 (1955).
7. M. Waldner, *Proc. I.R.E.*, **47**, 1004 (1959).
8. J. R. Haynes and W. Shockley, *Phys. Rev.*, **81**, 835 (1951).

Electrolytic Reduction of Nitro- and Dinitrotetralins

R. N. Boyd, A. A. Reidlinger, and M. J. Sher

Department of Chemistry, Washington Square College, New York University, New York, New York

ABSTRACT

The polarographic reduction of mono- and dinitrotetralins was studied in buffered solutions at four different pH values. The reduction became more difficult and was less complete with increase in pH. The relative heights of the multiple waves were interpreted in terms of certain electron changes, and these were checked by coulometric measurements at controlled potentials. The first stage in reduction in the tetralin series appears generally to be a four-electron change as it is in the benzene series.

In the course of other work in this laboratory it was found necessary to prepare most of the isomeric dinitrotetralins. From a search of the literature it became evident that a study of the polarographic behavior of the dinitrotetralins would be a logical extension of the work carried out by Pearson (1) on various dinitro compounds in the benzene series.

For the sake of completeness all four possible dinitrotetralins as well as the two known mononitrotetralins were prepared; 5 x 10^{-4}M solutions of the nitro compounds in 80% ethanol were studied in four buffered solutions. The compounds were also studied by constant potential coulometry to determine the number of electrons associated with each polarographic wave.

Experimental

6-Nitrotetralin (2), 5-nitrotetralin (3,4), 5,6-dinitrotetralin (2), and 5,7-dinitrotetralin (2) were prepared by methods given in the literature.

5,8-Dinitrotetralin.— 5-Aminotetralin (5) was nitrated (2) to give a low yield of 8-nitro-5-aminotetralin. One gram of the nitroamine was stirred into a mixture of 4 ml trifluoracetic acid and 0.5 ml 90% hydrogen peroxide (6); the solution was kept below 50° for 1 hr. At the end of this time the reaction mixture was poured over ice. The solid dinitro product was filtered off and recrystallized from ethanol. Yield, 0.1 g, mp 88.0°-88.1° [Literature: 87-88° (7)].

6,7-Dinitrotetralin.—6-Aminotetralin (3, 4) was transformed by nitration (2) to give 7-nitro-6-aminotetralin. One gram of the nitroamine was oxidized by trifluoroacetic acid and 90% hydrogen peroxide as described previously. The dinitro product was recrystallized from methanol. Yield, 0.3 g, mp 109.0°-109.2° [Literature: 108° (2)].

Polarographic procedure.—The polarograph employed was a Fisher Elecdropode which had been calibrated against a Type K L&N potentiometer. The electrolysis cell was a modified H-type cell. At a drop time of 4.0 sec with an open circuit and using an alcohol solution buffered by acetic acid and sodium acetate, the drop weight was 6.5 mg. The electrolysis cell was immersed in a thermostat maintained at 25°± 0.2°, and a saturated calomel electrode was used as the anode. Dissolved oxygen was removed by bubbling prepurified nitrogen through the solution for 20 min; the gas was previously passed through another sample of the solution under test. The polarographic curves were plotted as the experimentally determined currents minus the blanks. The half-wave potentials were corrected for *IR* drop.

The solutions were made by adding 10.0 ml of the proper buffer solution to 40.0 ml of 95% ethanol which was 6.25 x 10^{-4}M in nitro compound and then adding sufficient 95% ethanol to give a total volume of 50.0 ml. The apparent pH values of the solutions were measured using a Beckman pH meter Model G.

The buffer solutions were the following: for pH 2.1, 0.800M potassium chloride, 0.100M hydrochloric acid; pH 6.4, 4.00M sodium acetate, 3.00M acetic acid; pH 9.4, 1.00M triethylamine, 0.500M hydrochloric acid; pH 11.0, 1.00M phenol, 0.500M sodium hydroxide. All buffers were also made 0.050% in methyl cellulose. C.p. chemicals were used in each case.

Coulometric procedures.—Electrolyses were performed on 2-5 x 10^{-4} solutions of the nitro compounds in 80% ethanol. Initial currents were low due to low solubility of the nitro compounds and were generally of the order of 20 to 50 ma. The reductions were usually allowed to proceed to zero current (or at most 0.1-0.5 ma) and they generally lasted for 2-4 hr.

Electrolyses were carried out at a stirred mercury cathode at pH 2.1. Potentials (vs. SCE) were maintained constant (±15 mv) by means of a Lingane-Jones potentiostat (8) at values which were read from the polarographic curves. Those values were selected which appeared to offer the best chances for step-wise reductions.

The electrolytic cell consisted in the main of a standard three-neck one-liter round-bottom flask to which an extra neck had been added. One neck was fitted with a nitrogen bubbler which extended to the bottom of the flask and a 4-ft length of 6-mm tubing which served as an outlet. The center neck was fitted with the portion of the cell that served as the anode compartment; it consisted of a piece of an 8-in Pyrex test tube to which an 18-mm fritted-glass filter of medium porosity was fused. The anode was a silver gauze in contact with nearly saturated aqueous potassium chloride. A third neck

Table I. Constant potential reduction of nitro- and dinitrotetralins

Compound	pH	E (vs. SCE)	n (coulom.)	n (polarog.)[a]
5-Nitro	2.1	−0.80	6.03	6
6-Nitro	2.1	−0.75	6.21	6
5, 6-Dinitro	2.1	−0.30	3.82	4
		−0.75	11.72	12
6, 7-Dinitro	2.1	−0.22	3.98	4
		−0.80	12.11	12
5, 7-Dinitro	2.1	−0.23	3.91	4
		−0.40	8.11	8
		−0.90	12.21	12
5, 8-Dinitro	2.1	−0.25	3.71	4
		−0.80	11.72	12

[a] Estimated to nearest integral number of electrons from wave heights of the polarographic curves.

was fitted with a glass-sealed platinum wire through which contact was made to the 50 ml of triply distilled mercury which served as the cathode. The remaining neck was fitted with a saturated potassium chloride salt bridge (9) that was in contact with the cathode and led to the same calomel electrode that was used in determining the polarographic curves. Stirring was done by a magnetic stirring motor and a Teflon-covered stirring bar.

A silver coulometer of the usual design (10) was placed in series with the electrolysis cell.

In operation, 500 ml of buffer solution were introduced into the flask and deaerated for 30 min with prepurified nitrogen. The electrolysis of the buffer solution was carried out at −1.03 v (vs. SCE) until the current dropped to approximately 0.2 ma, and then the circuit was opened. Twenty to thirty milligrams of nitro compound were introduced, deaeration was resumed, and stirring was maintained for ½ hr to insure complete dissolution. The coulometer was then placed in series with the cell, and the circuit was closed. The electrolysis was allowed to proceed at the desired potential until the current dropped to a negligible value. It was found necessary to have a vigorous stream of nitrogen bubbling through the cell at all times during an electrolysis in order to prevent atmospheric oxygen from diffusing into the system.

Coulometric values obtained from the nitro- and dinitrotetralins are listed in Table I.

Large-scale reduction of 1,3-dinitrobenzene.—The anode compartment was a 150-ml porous cup, the anolyte was 20% sulfuric acid, and the anode was a carbon rod. The entire assembly was suspended in a 400-ml beaker which served as the cathode compartment. A pool of mercury covering the bottom of the beaker was used as the cathode. Its potential was controlled by a Lingane-Jones potentiostat (8) just as in the coulometric procedure. The cathode compartment was fitted with a nitrogen bubbler. The catholyte was stirred with a Teflon-covered stirring bar and a magnetic stirring motor.

Dissolved oxygen was removed from the catholyte by bubbling nitrogen through the solution for 20 min. Pre-electrolysis of the catholyte, consisting of 250 ml of the buffer solution (pH 6.4), was carried out at −0.60 v (vs. SCE) until the current dropped to a negligible value (2 ma). This took about 20 min. The circuit was opened and 1,3-dinitrobenzene (1.5 g) was introduced, and nitrogen was bubbled through the cell for 30 min. At the end of this time, the circuit was closed again, and the electrolysis was allowed to proceed at −0.50 v vs. SCE (value chosen from the polarogram). The initial current was 0.150 amp, and the electrolysis was allowed to continue until the current dropped to 2 ma.

The solvent was removed at reduced pressure, and the orange-yellow residue was recrystallized twice from benzene. The yield was 0.8 g of N-(3-nitrophenyl)hydroxylamine, mp 119°-119.5° [Literature: 118°-119° (11)].

The same product was obtained from a reduction at −0.55 v (vs. SCE) in which a nickel gauze cathode and a platinum anode were used.

Discussion

Pearson (1) has claimed that the first of the multiple waves obtained from the polarographic reductions of dinitro compounds is usually that corresponding to a four-electron change, the transformation of a nitro group to a hydroxylamino group. Present coulometric data amply confirm this conclusion for the nitro- and dinitrotetralins.

The polarogram obtained by Pearson (1) from *m*-dinitrobenzene is very similar to the one that he obtained from 2,4-dinitrotoluene and to the one obtained in the present work from 5,7-dinitrotetralin. Large-scale electrolytic reductions of *m*-dinitrobenzene at controlled potentials and at pH 6.4 show that N-(3-nitrophenyl)hydroxylamine is indeed the first reduction product, the result of a four-electron change. *m*-Dinitrobenzene rather than a dinitrotetralin was chosen for a test of the coulometric procedure at controlled potentials because it gives an intermediate that is stable enough to be isolated and identified.

It is shown conclusively by coulometry that reductions in acid lead to complete reduction with the formation of polyamines (for a dinitro compound this requires twelve electrons). At pH 9.4 complete reduction becomes more difficult, and the final product may be a bis-hydroxylamine (an eight-electron change) or an aminohydroxylamine (a ten-electron change). At pH 11 the curves are rather diffuse and difficult to interpret simply. The diffuseness may be due to secondary electrode processes involving reduction of condensation products.

It can be seen from Table II that as the pH increases the separation between the component waves also increases. Pearson (1) suggested for the dinitrobenzenes that this was due to a decrease in salt formation in alkaline media, and the same seems to hold in the present case.

It can also be seen that 5-nitrotetralin is more difficult to reduce than 6-nitrotetralin. This is in good agreement with the findings of Pearson (1) that *o*-nitrotoluene is more difficult to reduce than either *m*- or *p*-nitrotoluene. It may also be mentioned that when a mixture of 5-nitrotetralin and 6-nitrotetralin is allowed to react with a limited amount of sodium hydrogen sulfide, only 6-nitrotetralin will be reduced.

Table II. Polarographic reduction of nitro- and dinitrotetralins[a]

Compound	pH 2.1		6.4		9.4		11.0	
	$E_{1/2}$	i_d/C	$E_{1/2}$	i_d/C	$E_{1/2}$	i_d/C	$E_{1/2}$	i_d/C
5-Nitro	−0.36	11.6	−0.60	10.9	−0.81	9.1	?	8.9
	−0.56	16.2	?	15.6				
6-Nitro	−0.35	11.3	−0.56	11.3	−0.76	9.7	?	9.2
	−0.55	14.8	?	15.1				
5, 6-Dinitro	−0.21	9.2	−0.42	8.4	−0.55	8.5	−0.62	8.2
	−0.38	25.4	−0.64	25.2	−0.86	20.9	?	23.5
6, 7-Dinitro	−0.18	8.8	−0.39	8.7	−0.50	8.8	−0.56	8.4
	−0.34	25.1	−0.62	22.8	−0.83	21.8	−0.97	?
			?	25.2				
5, 8-Dinitro	−0.19	7.4	−0.37	8.4	−0.49	7.2	−0.55	7.2
	−0.40	23.6	−0.69	24.8	−0.92	21.2	−1.01	20.8
5, 7-Dinitro	−0.20	9.0	−0.41	9.5	−0.58	9.0	−0.72	7.8
	−0.34	18.6	−0.62	18.8	−0.83	17.8	−0.96	16.5
	−0.72	26.9	−1.37	27.5				

[a] The values of $E_{1/2}$ are in volts vs. SCE, and those of i_d/C are in μa/mmole/l. A question mark indicates that the wave is too indefinite to assign values with any degree of certainty.

An examination of Fisher-Hirschfelder molecular models showed that the three atoms of the nitro group in o-nitrotoluene or 5-nitrotetralin cannot so easily lie in the plane of the aromatic ring as in the other isomers. As a result of the probable steric inhibition of resonance, the hindered nitro group should be expected to be more like an aliphatic nitro group which, in general, is the more difficult to reduce (12).

Finally, as might be expected, present results with the dinitrotetralins present a striking concordance with the work of Pearson (1) on *ortho-*, *meta-*, and *para*-dinitro compounds in the benzene series.

Acknowledgment

The authors wish to thank Dr. R. T. Schenck for his suggestions concerning some of the apparatus used in this work. They are also grateful to the Minnesota Mining and Manufacturing Company for the gift of trifluoroacetic acid, and to the Becco Chemical Division of the Food Machinery and Chemical Corporation for the gift of 90% hydrogen peroxide.

Manuscript received Aug. 20, 1959.

Any discussion of this paper will appear in a Discussion Section to be published in the December 1960 JOURNAL.

REFERENCES

1. J. Pearson, *Trans. Faraday Soc.*, **44**, 683 (1948).
2. G. Schroeter, *Ann.*, **426**, 17 (1922).
3. L. K. Chudozilov and V. Vesely, *Rec. trav. chim.*, **44**, 123 (1925).
4. W. M. Cumming and G. Howie, *J. Chem. Soc.*, **1931**, 3176.
5. W. E. Bachmann and R. D. Morin, *J. Am. Chem. Soc.*, **66**, 553 (1944).
6. W. D. Emmons and A. F. Ferris, *ibid.*, **75**, 4623 (1953).
7. L. K. Chudozilov, *Collection Czech. Chem. Communs.*, **1**, 302 (1929).
8. J. J. Lingane and S. L. Jones, *Anal. Chem.*, **22**, 1169 (1950).
9. H. A. Laitinen, *Ind. Eng. Chem., Anal. Ed.*, **13**, 393 (1941).
10. O. F. Steinbach and C. V. King, "Experiments in Physical Chemistry," p. 159, American Book Co., New York (1950).
11. K. Brand, *J. prakt. Chem.*, **74**, 464 (1906).
12. I. M. Kolthoff and J. J. Lingane, "Polarography," 2nd ed., Vol. II, p. 750, Interscience Publishers, New York (1952).

Decomposition of Uranyl Fluoride between 700° and 950°C

L. M. Ferris and F. G. Baird[1]

Chemical Technology Division, Oak Ridge National Laboratory, Oak Ridge, Tennessee[2]

ABSTRACT

The thermal decomposition of uranyl fluoride was studied by a thermogravimetric technique between 700° and 950°C. At temperatures below 900°C, the main decomposition reaction is

$$3\ UO_2F_2 \rightarrow 2/3\ U_3O_8 + UF_6 + 1/3\ O_2$$

In an atmosphere of dry helium, the rate of decomposition was first order with respect to uranyl fluoride. The rate constants, determined with a constant helium flow rate of 270 cc (STP)/min, were $k = 3.72 \times 10^{11} \exp(-71{,}800/RT)$. Sublimation of uranyl fluoride, as a parallel, first order process, occurred at temperatures above 825°C.

Previous investigators (1) have reported that uranyl fluoride undergoes thermal decomposition at temperatures as low as 300°C. Several decomposition products, which include the uranium oxides U_3O_8 and UO_2, and uranium tetrafluoride were found under various conditions, but the data were insufficient to determine the exact stoichiometry. In contrast, preliminary data obtained in this laboratory (2) indicated that uranyl fluoride was quite stable in a dry atmosphere below 700°C. Above this temperature slow decomposition occurred, apparently according to the reaction $3\ UO_2F_2 \rightarrow UF_6 + 2/3\ U_3O_8 + 1/3\ O_2$. Further work performed in this laboratory, which supports the preliminary data, is presented in this paper.

Experimental

Materials.— High-purity uranyl fluoride was prepared by the ion exchange method of Higgins, Roberts, Hancher, and Marinsky (3). Details of the method are given in Fig. 3 of their article. The product was quite hygroscopic and initially contained 4.5 w/o (weight per cent) water. During the course of the investigation, the water content increased to about 6.2 w/o. It was demonstrated, however, that complete dehydration could be achieved at 150°-250°C without causing pyrohydrolysis. The purity of the dehydrated uranyl fluoride was 99.4 ± 0.3%. The major impurities were uranium dioxide and uranium tetrafluoride.

All gases used in the study were of high purity. Before use they were dried carefully by passage through ta charcoal bed, held at −196°C, and two Drierite bulbs.

Apparatus.—Weight loss data, used in determining the stoichiometry and rates of decomposition, were obtained with a semi-automatic, recording thermobalance. The thermobalance provided a continuous plot of the sample weight vs. time. Details of this instrument and its operation may be found elsewhere (4).

Procedure.—At the start of each experiment, a 2-g sample of the hydrated uranyl fluoride was weighed accurately into a small platinum basket. This sample was then transferred to the thermobalance reaction chamber where it was dehydrated by heating to about 230°C in a stream of dry helium. Reaction rates were obtained by continuously recording the isothermal weight loss due to decomposition at several predetermined temperatures. A gas flow rate of 270 cc (STP)/min was used in each experiment.

Determination of the Stoichiometry

Prior to initiation of the experimental work, estimates were made of the standard free energy changes of the following reactions which include all the decomposition products reported by other workers (1):

$$UO_2F_2 \rightarrow UO_2 + F_2 \qquad [1]$$

$$2\ UO_2F_2 \rightarrow UO_2 + UF_4 + O_2 \qquad [2]$$

$$3\ UO_2F_2 \rightarrow UF_6 + 2/3\ U_3O_8 + 1/3\ O_2 \qquad [3]$$

$$4\ UO_2F_2 \rightarrow UF_4 + U_3O_8 + 2\ F_2 \qquad [4]$$

$$3\ UO_2F_2 \rightarrow 2\ UO_2 + UF_6 + O_2 \qquad [5]$$

A plot of ΔF° vs. temperature for reactions [1]-[4] is found as Fig. 2, Ref. (2). For reaction [5], ΔF°, in kcal, can be computed from the equation $\Delta F^\circ = 109\text{-}0.085\ t$ where t is °C. The free energy change is positive for all the reactions; however, that for reaction [3] is the least positive of the others and could be expected to be the main reaction in a dry system.

In accordance with the thermodynamics, uranouranic oxide (U_3O_8) was the only decomposition product which could be identified by x-ray analysis at temperatures below 880°C. At 900°C, a small amount of uranium dioxide was present in the product.

Reaction [3] was shown to be the main decomposition reaction by comparison of the calculated weight losses and chemical analyses expected from reactions [1]-[5] with those obtained by decomposing uranyl fluoride at 880°-900°C until constant

[1] Present address: Department of Chemistry, University of Wisconsin, Madison, Wisconsin.

[2] Operated by Union Carbide Corporation for the U. S. Atomic Energy Commission.

Table I. Comparison of calculated[a] weight losses and chemical analyses for reactions [1]-[5] with those determined experimentally

Exp. No.	Temp, °C	Reaction	Weight loss, %	U in residue, %	U(IV) in residue, %	F in residue, %
		[1]	12.34	88.15	88.15	0.0
		[2]	5.19	81.51	81.51	13.01
		[3]	39.25	84.80	28.27	0.0
		[4]	6.17	82.38	41.19	6.57
		[5]	41.56	88.15	88.15	0.0
3[b]	900		40.1	82.1	38.4	2.0
4	900		42.7	79.4	43.5	1.7
5	900		41.8	84.3	32.5	1.6
10	900		43.3	85.3	34.6	0.16
18	880		44.5	70.7[c]	31.6	0.14
19	880		41.4	83.6	38.7	0.10

[a] Weight losses and composition of the residues were calculated for complete decomposition according to reactions [1]-[5].
[b] In each case the decomposition was essentially complete, i.e., the residue had attained a constant weight.
[c] Analysis is obviously low.

weight was obtained (Table I). Reactions [1], [2], and [4] may be eliminated from consideration at the outset on the basis of weight loss alone. Comparison of the uranium (IV) analysis of the residue with that expected from reactions [3] and [5] leaves no doubt that reaction [3] is the main decomposition reaction.

A rapid loss in weight, corresponding to complete dehydration, occurred at temperatures below 250°C. Any further weight loss was attributed to the decomposition of uranyl fluoride. In all cases, the per cent weight loss due to decomposition was slightly greater than expected from reaction [3]. As indicated by the uranium (IV), fluoride, and x-ray analyses, reaction [2] may also have occurred to a slight extent. In most cases the residue was found to be virtually pure U_3O_8; therefore, it was concluded that the excess weight loss was due primarily to simultaneous sublimation of uranyl fluoride. It is important to note that if reaction [2] occurred to a significant extent the weight loss would be less than expected from reaction [3] alone.

Rates of Decomposition in Dry Helium

If it is assumed that the following parallel, first order reactions

$$UO_2F_{2(s)} \xrightarrow{k} 2/9\ U_3O_{8(s)} + 1/3\ UF_{6(g)} + 1/9\ O_{2(g)} \quad [3]$$

$$UO_2F_{2(s)} \xrightarrow{k_v} UO_2F_{2(g)} \quad [6]$$

account for the total loss in weight when a sample of uranyl fluoride undergoes decomposition, the following equation is easily derived

$$\frac{-dw_s}{dt} = (fk + k_v)\, w \quad [7]$$

In Eq. [7], w_s is the sum of the weights of uranyl fluoride and urano-uranic oxide, i.e., the weight of the sample at any time, w is the weight of uranyl fluoride at any time, and f is a stoichiometry factor defined by

$$f = \left[1 - \frac{2/9 M_{U_3O_8}}{M_{UO_2F_2}} \right] = 0.3925 \quad [8]$$

in which M is the molecular weight of the respective compound. Since

$$w = w^\circ \exp\left[-(k + k_v)t\right] \quad [9]$$

Eq. [7] may also be expressed as

$$\frac{-dw_s}{dt} = (fk + k_v)\, w^\circ \exp\left[-(k + k_v)t\right] \quad [10]$$

For convenience, define

$$X = fk + k_v \quad [11]$$

$$Y = k + k_v \quad [12]$$

Then, integration of Eq. [10] with the boundary condition that $w_s = w_s^\circ$ at $t = 0$ yields

$$w_s - w_s^\circ = \frac{Xw^\circ}{Y}\left[\exp(-Y\,t) - 1\right] \quad [13]$$

Rearrangement of Eq. [13] and conversion to common logarithms gives

$$\log\left[\frac{Y(w_s - w_s^\circ)}{Xw^\circ} + 1 \right] = \frac{-Yt}{2.303} \quad [14]$$

Equation [14] contains the two desired quantities, k and k_v, in terms of experimentally measurable quantities, but it cannot be used directly. However, the rate constants may be evaluated by the following method, if the assumptions made above are valid. The quantity X may be computed from the initial slope of a plot of sample weight vs. time, i.e., at $t = 0$, Eq. [10] reduces to

$$\frac{-dw_s}{dt} = Xw^\circ \quad [15]$$

Once X is known, Y may be evaluated from Eq. [14] by successive approximations using the experimentally determined weight-time data. Arbitrary values for Y are used in the calculation of the logarithmic portion of Eq. [14]. This logarithmic quantity is then plotted vs. time. If the value chosen for Y is not the correct one, a curved plot will result. Successive approximations are continued until the plot becomes linear. Then, as required by Eq. [14], the value of Y used in the calculation of the logarithmic term will equal that calculated from the slope of the line. The rate constants k and k_v can then be obtained by solving Eq. [11] and [12] simultaneously.

For the special case where no sublimation occurs, Eq. [14] reduces to

$$\log\left[\frac{w_s - w_s^\circ}{f w^\circ} + 1 \right] = \frac{-kt}{2.303} \quad [16]$$

Here a plot of the logarithmic term vs. time should be linear with k evaluable from the slope.

Figure 1 contains several examples of the type of first order plot which results when the rate of sublimation is negligible, i.e., k_v is approximately zero. The lower curve in Fig. 1 illustrates the marked deviation from linearity which results if

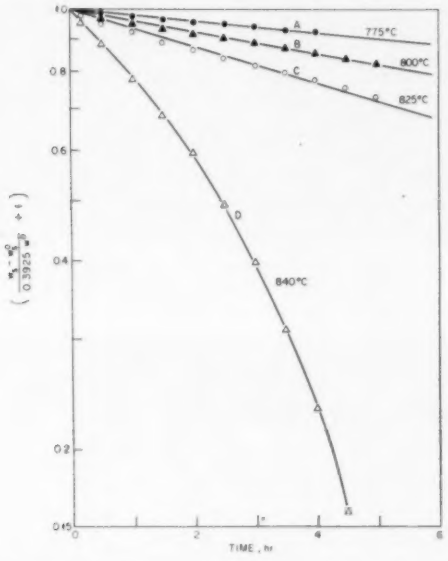

Fig. 1. Decomposition of UO_2F_2, showing a single first-order process below 825°C.

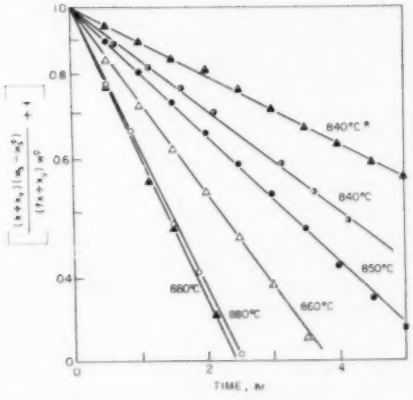

Fig. 2. Representative plots obtained when decomposition and sublimation of UO_2F_2 are considered parallel, first-order processes at temperatures above 825°C.
* Curve plotted from same weight-loss data as the lower curve in Fig. 1.

sublimation is ignored at temperatures above 825°C. Use of Eq. [14] to show that decomposition and sublimation are parallel, first order reactions is illustrated by Fig. 2. It should be noted that the upper curve in Fig. 2 was plotted from the same data used to plot the lower curve in Fig. 1. Table II contains the rate constants obtained over the temperature range of 750°-880°C., while a least squares plot of log k vs. $1/T$ is found in Fig. 3. The temperature dependence of the rate constant for the decomposition reaction is $k = 3.72 \times 10^{11} \exp(-71{,}800/RT)$.

Discussion of Results

Consideration of several other variables would be necessary before a detailed rate expression could be determined. Among the important variables omitted in this study were the effects of oxygen partial pressure, gas velocity, and gas density on the rate of decomposition. The results of preliminary

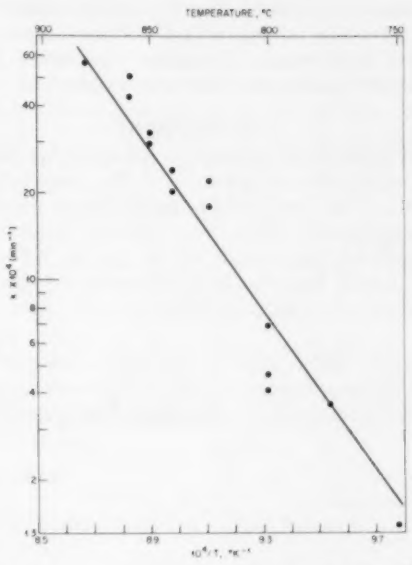

Fig. 3. Rate constants for the reaction 3 $UO_2F_2 \rightarrow$ 2/3 U_3O_8 + UF_6 + 1/3 O_2.

experiments (Table III) indicated that the rate of decomposition decreased with increasing oxygen partial pressure.

An attempt was made to estimate the heat of

Table II. Rate constants[a] for the decomposition and sublimation of UO_2F_2

Exp. No.	Temp.,[b] °C	$10^4/T$, °K^{-1}	$10^4\,k$, min^{-1}	$t_{1/2}$, hr	$10^4\,k_v$, min^{-1}	$k_v/(k_v+k_g)$
8	750	9.78	1.4	82	—	0.0
7	775	9.54	3.6	32	—	0.0
15	800	9.32	6.9	17	—	0.0
1	800	9.32	4.1	28	—	0.0
2	800	9.32	4.7	25	—	0.0
6	825	9.11	18	6.3	0.1	0.005
20	825	9.11	22	5.3	—	0.0
1	840	8.98	20	5.7	9.3	0.32
14	840	8.98	24	4.8	—	0.0
21	850	8.90	32	3.6	11	0.26
22	850	8.90	30	3.8	5.1	0.14
16	860	8.83	43	2.7	7	0.14
17	860	8.83	51	2.2	6.3	0.11
18	880	8.67	56	2.1	27	0.33
19	880	8.67	56.5	2.0	26	0.31

[a] Rates measured in dry helium flowing at 270 cc (STP)/min.
[b] Temperatures were maintained within 5°C of the recorded temperature with a Pyr-O-Vane proportional controller.

Table III. Effect of oxygen partial pressure on the rate of decomposition of UO_2F_2

Initial weight of sample: 2 g; gas flow rate: 270 cc (STP)/min

Gas	Weight loss after 3 hr at 840°C, mg
Helium	320
	320
Air	43
	25
Oxygen	23
	20

sublimation of uranyl fluoride by assuming that the slope of a plot of log k_r vs. $1/T$ was equal to the heat of sublimation. However, the scatter in the values of k_r precluded any such estimation.

Acknowledgment

The authors are pleased to acknowledge Mr. I. R. Higgins for the preparation of the uranyl fluoride, and Mr. J. F. Land for his assistance in performing the experiments. Chemical and x-ray analyses were provided by the groups of Mr. G. R. Wilson, Mr. W. R. Laing, and Mr. R. L. Sherman, of the ORNL Analytical Chemistry Division.

Manuscript received Aug. 13, 1959. This paper was presented before the Nuclear Technology Subdivision, American Chemical Society, Boston, Mass., April, 1959.

Any discussion of this paper will appear in a Discussion Section to be published in the December 1960 JOURNAL.

REFERENCES

1. J. J. Katz and E. Rabinowitch, "The Chemistry of Uranium," Div. VIII, Vol. 5, p. 570, National Nuclear Energy Series, McGraw-Hill, New York (1951).
2. L. M. Ferris, *J. Am. Chem. Soc.*, **79**, 5419 (1957).
3. I. R. Higgins, J. T. Roberts, C. W. Hancher, and J. A. Marinsky, *Ind. Eng. Chem.*, **50**, 285 (1958).
4. L. M. Ferris, *ibid.*, **51**, 200 (1959).

Some Properties of Aluminum Nitride

K. M. Taylor and Camille Lenie

Research and Development Division, The Carborundum Company, Niagara Falls, New York

ABSTRACT

Aluminum nitride crystals in the form of six-sided prismatic needles, up to 0.5 mm in diameter by 30 mm long, and thin plates, 2-3 mm in diameter, have been prepared by vaporization of aluminum in a nitrogen atmosphere at temperatures ranging from about 1800° to 2000°C, and the properties of the crystals determined. Also, an aluminum nitride body, having a density of 98% of theoretical, has been prepared by hot pressing the fine powder, and a study made of its properties.

Aluminum nitride, AlN, consists of 65.81% aluminum and 34.19% nitrogen. Although aluminum nitride was prepared many years ago, its properties have not been well known. Early investigators considered it too unstable, especially with respect to moisture and oxidizing conditions, to be useful as a refractory. More recent work, however, has indicated that aluminum nitride, prepared at high temperature, is relatively inert and, therefore, may have applications as a refractory.

Reconsideration of the potentialities of aluminum nitride as a refractory appears to have started with a publication (1) in 1956 by Kohn and associates of the U. S. Bureau of Mines. These investigators incidentally obtained small crystals of aluminum nitride while working at high temperatures on another project and reported that the crystals were inert to hot and cold mineral acids and alkali solutions. Other recent workers who found aluminum nitride a relatively stable material include Rey (2), Renner (3), and Long and Foster (4). Notwithstanding the considerable recent work on aluminum nitride prepared at high temperature, there is still disagreement on many of its properties such as melting point, hardness, color, and oxidation resistance.

Refractories based on aluminum nitride are not now commercially available, although Rey (2) has prepared aluminum nitride brick by a sintering process and Long and Foster (4) have made laboratory-size crucibles, also by a sintering method. In addition, Johnson (5) has prepared a composite aluminum nitride-cryolite body, and Taylor (6) has used aluminum nitride as a bond for other refractory materials. High density, impervious, essentially pure aluminum nitride ware, however, has not previously been made.

The objects of the present work were to study crystalline aluminum nitride further, especially those properties which are still in dispute, and to prepare and determine the properties of a high-density aluminum nitride body. In the latter instance, hot pressing was chosen as a method of fabrication because preliminary experiments indicated that it would yield ware of maximum density, and, therefore, of optimum physical properties.

Crystalline Aluminum Nitride

Formation of Crystals.—Two methods of forming the crystals were tried: (*a*) heating aluminum nitride powder in a nitrogen atmosphere at high temperatures to induce crystal growth by recrystallization, and (*b*) heating aluminum metal powder in a nitrogen atmosphere to sufficiently high temperatures to vaporize the aluminum and thus form crystals by a vapor phase reaction. The second method was more effective and was used to prepare most of the crystals described in this report.

Sintered aluminum nitride boats and crucibles were used as containers in vaporizing the metal. The reaction was carried out in a horizontal graphite tube resistance furnace or in a vertical induction furnace having a graphite susceptor. In the horizontal resistance furnace, it was possible, using an optical pyrometer with telescope, to follow the origin, growth, and development of the crystals and to measure the corresponding temperatures at the same time.

Fig. 1. Aluminum nitride crystals in the form of six-sided prismatic needles, obtained by nitriding aluminum vapors at 1850°C.

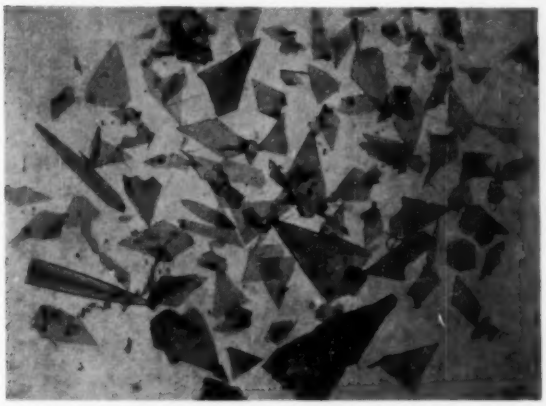

Fig. 2. Plate-like crystals of aluminum nitride formed by heating aluminum nitride powder in nitrogen at temperatures in excess of 1900°C.

It was observed that short, extremely fine filaments of aluminum nitride formed in the range of 1450°-1750°C, while at 1800°-1900°C the crystals were predominantly well-defined six-sided prismatic needles, some of which were about 0.5 mm in diameter and 30 mm long (Fig. 1). Some elongated plates also formed in this temperature range. At 1900°-2050°C, new growth appeared mainly as plates (Fig. 2), while above about 2050°C, previously formed crystals began decreasing in size very slowly due to vaporization. In the case of the prismatic needles shown in Fig. 1, the tapered end was the free end.

Color.—The color of the crystals varied from white to various shades of blue. Rey (2) states that pure aluminum nitride forms blue hexagonal crystals. Long and Foster (4) claim that pure aluminum nitride is water white and that the blue coloration results from the presence of about 7% aluminum oxycarbide (Al_2OC) in the crystals. They report that aluminum oxycarbide is isomorphous with aluminum nitride and that formation of solid solution between the two compounds is very likely. They suggest that Al_2OC results from a reaction between carbon monoxide, incidentally formed in the graphite lined furnace, and aluminum in the sample. In order to test these theories, aluminum nitride crystals were formed in carefully controlled atmospheres of (*a*) nitrogen only, (*b*) in nitrogen containing 0.5-2% of carbon monoxide, and (*c*) in nitrogen containing 1% of methane. Blue crystals formed only when carbon monoxide was present, the shade of blue becoming deeper with increasing amount of carbon monoxide in the nitriding atmosphere; 0.5% carbon monoxide resulted in light blue crystals, while 2% carbon monoxide produced dark blue crystals. Chemical analysis of the crystals showed the presence of carbon and oxygen in an approximately equimolecular ratio. The percentage of carbon varied from a few tenths of a per cent in the light blue crystals to about 2% in the deeper colored crystals. If carbon and oxygen are combined as aluminum oxycarbide, Al_2OC, as stated by Long and Foster (4), then the amount of this compound in the crystals prepared in the present study ranged up to about 14%.

Crystal structure and density.—Both the white and blue crystals have the hexagonal wurtzite structure. Other investigators have reported cell dimensions as follows:

Investigator	Type of material	Cell dimensions a_0	Cell dimensions c_0
Ott (7)	Powder	3.113	4.981
Stackelberg and Spiess (8)	Light gray powder	3.104±0.005	4.96±0.008
Kohn, Cotter, and Potter (1)	Blue crystals	3.10±0.01	4.965±0.01
Paretzkin (9)	Powder	3.114	4.986

In the present investigation, unit cell dimensions were determined by x-ray diffractometer back reflection techniques. Each sample was standardized independently with a spectrographically pure silicon sample. The National Bureau of Standards value of $a = 5.4301$Å for silicon was used.

The following values were obtained for light colored aluminum nitride: $a = 3.111$Å; $c = 4.980$Å.

A sample of the dark blue crystals containing approximately 2% carbon and 2.7% oxygen produced an x-ray diffraction pattern with broader reflections, some of which showed three distinct peaks. Most of these were shifted from the peaks of the light material. Values of 3.11-3.13Å for the *a* dimension and 4.93-4.98Å for the c dimension were obtained, depending on which peak was evaluated. Differences in reflections of the white and blue crystals were not detected when the usual film techniques were used. Possibly the blue samples contained enough pure AlN to overshadow the less prominent shifted reflections. Also, the general broadening would tend to produce the same geometrical center for the reflections of both the white and blue crystals.

The density of aluminum nitride, calculated from the cell dimensions $a = 3.111$Å and $c = 4.980$Å, is 3.26 g/cc.

Melting point.—The literature reports melting points in the range of 2000°-2400°C. Renner (3) observed strong vaporization of aluminum nitride at 2450°C, but no melting. The present investigation confirms Renner's conclusions. The experiments were carried out in a microfurnace (10) at atmospheric pressure in argon. Well-formed prismatic crystals, about 0.2-0.5 mm thick by about 2-5 mm long, were heated in a V-shaped tungsten crucible,

making observations with an optical pyrometer. The crystals were heated to 1800°C in 2-3 min, after which the temperature was increased at the rate of about 200°C/min. Some vaporization could be observed at 2300°C; at 2450°C vaporization was rapid, and after 1 min at 2500°C the crystals had completely disappeared without evidence of melting. In some experiments, crystals were heated to 2450°-2500°C in about 3 min and then immediately allowed to cool. The crystals had partially vaporized, but no evidence of melting was observed.

Hardness.—Hardness values on the Mohs scale ranging from 5 to between 9 and 10 are found in the literature. No accurate microhardness indentations have been reported. However, crystals obtained in the present research were sufficiently large that Knoop indentations could be made readily. All indentations were made with a load of 100 g, the force being applied perpendicular to the *c* or long axis of the crystal. Some indentations were made with the long diagonal of the indenter parallel to, and some perpendicular to the *c* axis of the crystal. Results varied somewhat with the direction, probably because of the anisotropic nature of the crystals. The over-all hardness of aluminum nitride appears to be approximately 1200. This is equivalent to a hardness of slightly higher than 7 on the Mohs scale. Detailed hardness data are seen in Table I.

Oxidation resistance.—Aluminum nitride crystals appear to begin to oxidize in air at about 700°C. This was investigated by heating colorless and blue crystals on a platinum lid in flowing air to various temperatures for 24 hr, and then carefully examining the crystals microscopically after each test. At between 700° and 800°C, the surface of clear transparent crystals became slightly foggy, indicating the beginning of oxidation. The oxidation rate of well-formed crystals, however, was slow even at much higher temperature, because of the formation of a dense adherent aluminum oxide film. Thus, after 24 hr at 1400°C, the cross section of crystals of about 1 mm diameter and 7 mm long showed an oxide surface film estimated to be 40 μ thick. The inside core of the crystal, however, was still clear and transparent.

Tendency to oxidize also was determined by heating 2-3 g samples of the finely milled powder, having an average particle size of about 5 μ, in a flowing stream of air. The weight gain, after 24 hr at 700°C, was 3.2%, corresponding to a conversion of 13% of the compound to aluminum oxide. When a new sample of the same powder was heated 24 hr in air at 800°C, the increase in weight was 9%, corresponding to a conversion of about 36% of the compound to aluminum oxide. In the latter case, x-ray diffraction clearly showed the presence of gamma alumina.

Corrosion resistance.—Crystals of aluminum nitride have been immersed in water at room temperature for several months with no apparent effect on the crystals. Some recent investigators (1, 3, 4) state that aluminum nitride is essentially unaffected by mineral acids. In the present research, it was observed that aluminum nitride crystals were dissolved slowly in a boiling mixture of one part concentrated hydrochloric and one part water. Thus, prismatic needles having a diameter of about 80 μ were dissolved completely in 80 hr. The corrosion rate, based on these experiments, is approximately 170 mils per year.

Table I. Hardness of aluminum nitride crystals

Indentation* No.	Knoop hardness, K_{100}	
	White crystals	Blue crystals
1	1010	920
2	1075	970
3	1010	980
4	1115	1030
5	1000	1050
* Average	1042	990
6	1453	1415
7	1426	1510
8	1454	1450
9	1356	1445
10	1348	1530
* Average	1407	1470
Over-all average	1225	1230

* Indentations 1 through 5 were made with the long diagonal of the indenter parallel to the c axis of the crystal, 6 through 10 were made with the long diagonal of the indenter perpendicular to the c axis.

Hot Pressed Aluminum Nitride

Preparation of hot pressed aluminum nitride.—Aluminum nitride powder was prepared by direct combination of aluminum and nitrogen. Alcoa's No. 101 atomized aluminum powder was mixed with 1% sodium fluoride, which catalyzes the nitriding at low temperatures (11), and heated in purified nitrogen in a refractory crucible. The temperature was raised rapidly to 650°C and then increased slowly over a period of 40 hr to a maximum of 1800°C. In this way a porous sintered agglomerate was obtained. It was reduced readily by dry ball milling in a stainless steel mill with stainless steel balls to a light gray powder with an average particle size of about 5 μ. Chemical analysis of the milled aluminum nitride powder and also the calculated composition, based on this analysis, are shown in Table II. It will be noted that the aluminum nitride content is approximately 96%, and that the chief impurity is alumina. The density of the powder was 3.23 g/cc, compared with a density of 3.26 g/cc as calculated from the cell dimensions of the crystals.

Table II. Aluminum nitride powder
(Pure AlN: 65.81% Al; 34.19% N)

Chemical analysis		Calculated composition	
Al	64.8%	AlN	96.0%
N	32.8%	Al_2O_3	2.1%
C	0.2%	Other compounds	1.9%
Si	0.4%		
Fe	0.1%		
O	1.0%		

Particle size: 0.5 to 25μ
Density: 3.23 g/cc

Table III. Strength and elasticity properties of hot pressed aluminum nitride

Temp, °C	Modulus of rupture, psi	Modulus of elasticity, psi
25	38,500	50×10^6
1000	27,000	46×10^6
1400	18,100	40×10^6

Test specimens, 3 in. in diameter and 3 in. long, were fabricated by hot pressing the milled powder at 2000°C in graphite dies, applying pressures of about 5000 psi. Test bars, 3 x 0.5 x 0.25 in., were cut from the hot pressed pieces with a diamond wheel and then ground to produce smooth parallel surfaces. The test specimens were light gray in color and had a bulk density of 3.20 g/cc or about 98% of the theoretical for pure aluminum nitride. Using a load of 100 g, 10 Knoop hardness indentations gave values ranging from 1005 to 1240, with an average of 1130.

Strength and elasticity.—Data for modulus of rupture and modulus of elasticity at room temperature, 1000° and 1400°C, are presented in Table III. Four specimens, 3 x 0.5 x 0.25 in. were tested at each temperature, pressure being applied perpendicular to the direction in which the bars were hot pressed. These values compare favorably with those for other high-density ceramic materials, especially at high temperatures. For instance, hot pressed alumina is stronger at room temperature, but weaker at 1400°C. The modulus of elasticity of hot pressed aluminum nitride is about the same as that of hot pressed alumina at room temperature, but is higher than that of hot pressed alumina at 1400°C.

Long and Foster (4) reported a modulus of rupture of sintered aluminum nitride at room temperature of 11,500 psi. The exact density of the test specimens was not given but presumably was appreciably lower than that of the hot pressed material reported herein. Rey (2) reported the compressive strength of sintered aluminum nitride brick to be about 3000-4000 psi. Preliminary tests on the hot pressed material indicate a compressive strength of about 300,000 psi.

Thermal conductivity.—The thermal conductivity was measured by a linear flow comparative method, parallel to the direction of pressing, in an atmosphere of stagnant nitrogen, using Inconel as a standard. Values obtained over a temperature range of 200°-800°C are shown in Table IV. These results indicate that aluminum nitride is a good conductor of heat, being intermediate between dense silicon carbide, which is an excellent conductor, and alumina, which is a fair conductor. This is illustrated by the following comparative values for thermal conductivity expressed in cal/cm²/cm/sec/°C obtained by the same method:

Material	At 200°C	At 800°C
Dense SiC	0.24	0.10
Hot pressed AlN	0.072	0.048
Dense Al_2O_3	0.054	0.017

The present data are in sharp contrast to those of Long and Foster (4), who recently reported the thermal conductivity of sintered aluminum nitride at 25°C as 0.0042 cal/cm²/cm/sec/°C. The density of the specimens used by Long and Foster was not disclosed, but the density of some of their test specimens used for determination of electrical resistivity was as high as 2.66 g/cc. It seems probable, therefore, that the difference in density alone is not responsible for the great dissimilarity of the thermal conductivity values, but rather the difference in methods is mainly responsible. According to Kingery and co-workers (12) thermal conductivity at zero porosity can be calculated employing the following simplified relationship of Loeb:

$$k_s = \frac{km}{(1 - P_v)}$$

where k_s is the solid thermal conductivity (zero porosity); k_m, measured thermal conductivity; P_v, volume pore fraction.

Even if it is assumed that the thermal conductivity, $k_m = 0.0042$ cal/cm²/cm/sec/°C, measured at 25°C by Long and Foster, is for a specimen with 40% porosity, the thermal conductivity at zero porosity calculated according to above equation, will be only 0.007 cal/cm²/cm/sec/°C.

The accuracy of the present method has been checked by comparing the results obtained on some standard materials with data from other laboratories as illustrated in the following examples:

Laboratory	Material	Thermal conductivity, cal/cm²/cm/sec/°C at 400°C	at 600°C
Carborundum	Inconel	0.049	0.057
National Bureau of Standards (13)	Inconel	0.049	0.058
Carborundum	Nickel	0.119	0.130
International Nickel Company (14)	Nickel	0.112	0.136

Thermal expansion.—The determination of thermal expansion was made by the dilatometer method, using a silicon carbide dilatometer assembly (15). Thermal expansion was measured parallel to the direction of pressing, on a bar 3 in. long and 0.5 in. in diameter. Values are given in Table V. These

Table IV. Thermal conductivity of hot pressed aluminum nitride

Temp, °C	Cal/cm²/cm/sec/°C	Btu/ft²/in./hr/°F
200	0.072	209
400	0.060	173
600	0.053	153
800	0.048	139

Table V. Thermal expansion of hot pressed aluminum nitride

Temperature interval, °C	Linear expansion, cm/cm/°C
25-200	4.03×10^{-6}
25-600	4.84×10^{-6}
25-1000	5.64×10^{-6}
25-1350	6.09×10^{-6}

check closely the results reported by Long and Foster (4) (4.8×10^{-6} cm/cm/°C in the range 20°-500°C) for the sintered aluminum nitride. The thermal expansion of hot pressed aluminum nitride is in the moderate range for a ceramic, being only slightly higher than that of silicon carbide.

Thermal shock resistance.—The high thermal conductivity and low thermal expansion of hot pressed aluminum nitride are conducive to good thermal shock resistance. Bars, 3 x 0.5 x 0.25 in., heated rapidly to 2200°C in an oxygen-acetylene torch and cooled rapidly, did not crack or spall when the test was repeated consecutively several times. The thermal shock resistance was evaluated also by measuring the loss in strength of hot pressed aluminum nitride bars after 30 cycles of heating in 2.5 min to 1400°C and rapidly cooling to room temperature in an air blast. The modulus of rupture before thermal cycling was 38,500 psi and after thermal cycling, 33,700 psi, or a loss of 12% of the original strength.

Stability in various atmospheres at elevated temperatures.—Test specimens, 0.25 x 0.5 x 0.5 in., were exposed to flowing air, oxygen, dry steam, chlorine, and hydrogen at elevated temperatures. Results are reported in Table VI. The last column shows the percentage of aluminum nitride converted to aluminum oxide or aluminum chloride according to the different conditions of the experiments. As can be seen from these data, the effect of air or oxygen at temperatures up to 1400°C or of steam at 1000°C after 30 hr is slight. At 1700°C in air, however, the rate of oxidation becomes rather rapid. It will be recalled from the discussion of the crystalline material that it was found that oxidation of aluminum nitride in air starts at about 700°C, but that the rate of oxidation is slow even at temperatures as high as 1400°C, because of the formation of a protective oxide coating. This coating also accounts for the slow rate of oxidation of the dense hot pressed material. Figure 3 shows a 0.25 x 0.5 in. cross section of a bar after exposure to air at 1400°C for 24 hr. The oxide layer is approximately 60 μ or 2-3 mils thick. At 1700°C, however, it was noted that the oxide coating tended to crack and no longer protected effectively the aluminum nitride against oxidation. The cracking of the coating at this temperature may be due to the appreciable difference in the thermal expansion of aluminum oxide and aluminum nitride.

Table VI. Stability of hot pressed aluminum nitride in various atmospheres of elevated temperatures
(Test specimens, 0.25x0.5x0.5 in.)

Atmosphere	Temp, °C	Time, hr	Conversion to other compounds, %
Air	1000	30	0.3 Al_2O_3
Air	1400	30	1.3 Al_2O_3
Air	1700	4	10.6 Al_2O_3
Oxygen	1400	30	0.9 Al_2O_3
Dry steam	1000	30	0.3 Al_2O_3
Chlorine	500	30	<0.1 $AlCl_3$
Chlorine	700	30	19.2 $AlCl_3$
Hydrogen	1700	4	nil

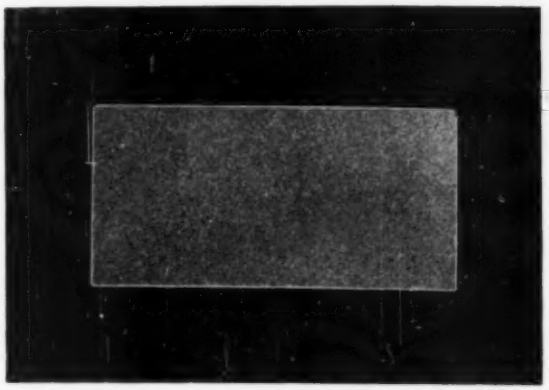

Fig. 3. Cross section of a hot-pressed aluminum nitride specimen showing the protective oxide coating after heating in air 24 hr at 1400°C.

It is of interest to note the difference in the oxidation rate of hot pressed aluminum nitride and the sintered material as reported by Long and Foster (4). Exposure to air for 1 hr at 1200°C of 1-cm cubes of sintered material resulted in a conversion of about 11% of the sample to aluminum oxide, whereas exposure to air for 30 hr at 1400°C of dense hot pressed aluminum nitride specimens of comparable size resulted in a conversion of only about 1% to aluminum oxide.

Table VI also shows that hot pressed aluminum nitride is not appreciably attacked by chlorine at 500°C, but that the reaction rate at 700°C is rapid. Furthermore, hot pressed aluminum nitride is practically unaffected by hydrogen at 1700°C for 4 hr.

Corrosion in water and mineral acids.—As in the case of the crystalline material, hot pressed aluminum nitride is slowly dissolved by hot mineral acids. The results of the corrosion tests are shown in Table VII. Specimens 0.25 x 0.5 x 0.5 in. were heated in a 600 ml volume of water and in the several mineral acids for 72 hr. With the exception of hydrofluoric acid, the tests were made at the boiling temperatures of the liquids. The corrosion rate in boiling water can be considered as low. Although dissolution in the mineral acids is slow, the rate is too great to classify hot pressed aluminum nitride as a corrosion resistant material in these acids. It will be recalled that

Table VII. Corrosion of hot pressed aluminum nitride in water and mineral acids
(0.25x0.5x0.5 in. specimens in 600 ml liquid, 72 hr)

Corrosive liquid	Temp, °C	Corrosion rate, mils/year
Water	100	14
Conc. HCl acid	72	320
1 Conc. HCl acid: 1 H_2O	110	570
Conc. H_2SO_4 acid	305	180
1 Conc. H_2SO_4 acid: 1 H_2O	145	550
Conc. HNO_3 acid	120	150
1 Conc. HNO_3 acid: 1 water	111	200
1 HF: 1 HNO_3 conc. acids	57	160
1 Conc. HF acid: 1 water	57	215

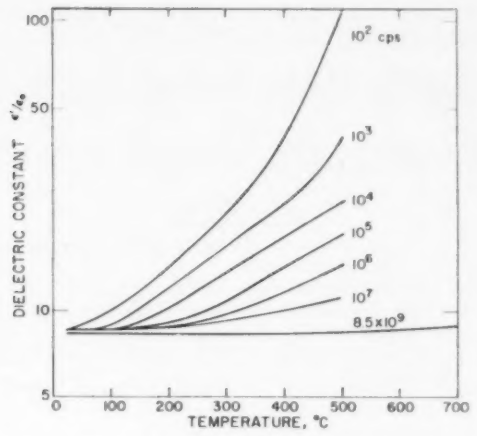

Fig. 4. Effect of temperature on dielectric constant of hot pressed aluminum nitride at several frequencies.

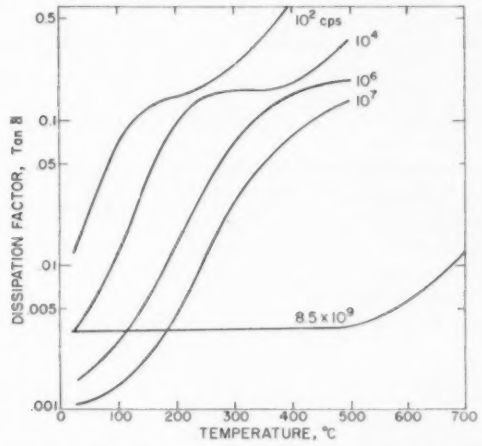

Fig. 5. Effect of temperature on dissipation factor of hot pressed aluminum nitride at several frequencies.

the corrosion rate of single crystals in a boiling mixture of 1 part concentrated hydrochloric and 1 part water was estimated to be about 170 mils per year.

Corrosion in cryolite and aluminum and in boric oxide.—Hot pressed aluminum nitride was heated in an inert atmosphere in a bath consisting of a mixture of molten cryolite and aluminum for 66 hr at 1200°C without visual evidence of corrosion. A piece of hot pressed aluminum nitride, 0.25 x 0.5 x 0.5 in., immersed in molten boric oxide for 4 hr at 1000°C, showed only very slight evidence of attack in the form of faint surface marking and a weight loss of 0.02%. This is equivalent to a corrosion rate of about 25 to 30 mils per year.

Electrical properties.—The electrical properties of hot pressed aluminum nitride appear to be similar to those of alumina, and especially to some of the high density hot pressed aluminas. Dielectric constant and dissipation factor were determined by the Laboratory for Insulation Research at Massachusetts Institute of Technology and also by our own laboratories, the results agreeing fairly closely. Data on dielectric constant are shown in Fig. 4. At room temperature the dielectric constant, over a wide range of frequencies, is about 8.5 compared with between 9 and 10 for many aluminas. The dielectric constant increases rapidly with temperature at low frequencies, less rapidly at high frequencies. At a frequency of 8.5 x 10^9 cps, the change with temperature is only slight. This behavior is also typical of the aluminas.

The dissipation factor at various frequencies and temperatures is shown in Fig. 5. At low frequencies, the dissipation factor increases rapidly with temperature. However, at the frequency of 8.5 x 10^9 cps, the change with temperature up to 500°C is slow. At room temperature the dissipation factor at the various frequencies is between about 0.01 and 0.001, while for the aluminas, the dissipation factor at this temperature is about 0.001 to 0.0001. At high temperatures (400°-500°C) and low frequencies (10^2-10^3 cps) the dissipation factor of hot pressed aluminum nitride and alumina are comparable, while at high temperatures and high frequencies the dissipation factor of the aluminas is appreciably lower.

The volume resistivity of hot pressed aluminum nitride as calculated from the dielectric constant and dissipation factor is shown in Fig. 6. Data for a hot pressed alumina at two frequencies are also shown in Fig. 6 for comparison. At a frequency of 100 cps, the resistivity of hot pressed aluminum nitride is about 2 x 10^{11} ohm-cm at room temperature and 7 x 10^7 ohm-cm at 500°C. Resistivity decreases with frequency; this is also typical for the aluminas and other ceramic insulators.

Summary

Pure aluminum nitride is white. Blue crystals are formed when the metal is heated above 1750°C in nitrogen containing small amounts of carbon monoxide.

Aluminum nitride does not melt under atmospheric pressure in argon, but vaporizes rapidly at about 2400°C. Its Knoop hardness, with a load of

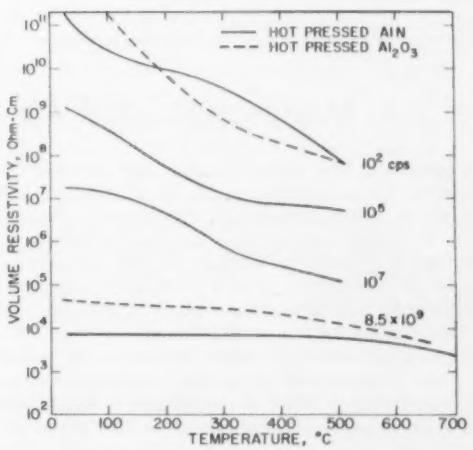

Fig. 6. Effect of temperature on volume resistivity of hot pressed aluminum nitride at several frequencies. Data for a hot pressed alumina at two frequencies are shown for comparison. (Data obtained from Tables of Dielectric Materials Volume V- Laboratory for Insulation Research, Massachusetts Institute of Technology.)

100 g, is approximately 1200, which is equivalent to seven plus on the Mohs scale.

Aluminum nitride starts to oxidize in air at between 700° and 800°C, but in the case of large crystals and the dense hot pressed material, oxidation is slow up to 1400°C because of the protective oxide surface layer formed. It is inert to hydrogen at 1700°C but is attacked by chlorine between 500° and 700°C.

Although aluminum nitride in the crystalline or hot pressed form does not dissolve readily in boiling mineral acids, it is not highly corrosion resistant to these acids. However, it has relatively good corrosion resistance to molten boric oxide and to a mixture of molten aluminum and cryolite in inert atmospheres.

Strength of hot pressed aluminum nitride is lower than that of high-density aluminum oxide at room temperature, but is higher at 1400°C. Compared with most ceramics, it has high thermal conductivity, low thermal expansion, and good thermal shock resistance. Its electrical properties, in many respects, are similar to those of aluminum oxide.

Acknowledgments

The authors are indebted to various members of the Research and Development Division of The Carborundum Company for help in obtaining data and also to Mr. W. B. Westphal of the Laboratory for Insulation Research, Massachusetts Institute of Technology, for measurements of electrical properties.

Manuscript received August 10, 1959. This paper was prepared for delivery before the Philadelphia Meeting, May 1-5, 1960.

Any discussion of this paper will appear in a Discussion Section to be published in the December 1960 JOURNAL.

REFERENCES

1. J. A. Kohn, Perry G. Cotter, and R. A. Potter, *Am. Mineral.*, **41**, 355 (1956).
2. M. Rey, *Silicates Industries*, **22**, 453 (1958).
3. Von Th. Renner, *Z anorg. u. Allgem. Chem.*, **298**, [1-2] 22 (Jan. 1959).
4. George Long and L. M. Foster, *J. Am. Ceram. Soc.*, **42**, No. 2, 53 (1959).
5. A. F. Johnson; U. S. Pat. 2,480,473 (1949).
6. K. M. Taylor, U. S. Pat. 2,839,413 (1958).
7. H. Ott, *Z. Physic*, **22**, 201 (1924).
8. M. v. Stackelberg and K. F. Spiess, *Z. Phys. Chem.*, **A175**, 140 (1935).
9. A.S.T.M. X-ray Powder Data File No. 8-262.
10. W. A. Lambertson and G. Lewis, *This Journal*, **106**, 124 (1959).
11. J. C. Charlton and Ch. C. Evans, British Pat. 784,126 (1957).
12. W. D. Kingery, J. Francl, R. L. Coble, and T. Vasilos, *J. Am. Ceram. Soc.*, **37**, No. 2, 107 (1954).
13. National Bureau of Standards, private correspondence, 1951.
14. Development and Research Division, International Nickel Co., Technical Bulletin T-15, 1949.
15. S. D. Mark. Jr., and R. C. Emanuelson, *Am. Ceram. Soc. Bull.*, **37**, No. 4, 193 (1958).

Manuscripts and Abstracts for Fall 1960 Meeting

Papers are now being solicited for the Fall Meeting of the Society, to be held at the Shamrock Hotel in Houston, Texas, October 9, 10, 11, 12, and 13, 1960. Technical sessions probably will be scheduled on Batteries, Corrosion, Electrodeposition, Electronics (Semiconductors), and Electrothermics and Metallurgy.

To be considered for this meeting, triplicate copies of abstracts (*not exceeding 75 words in length*) must be received at Society Headquarters, 1860 Broadway, New York 23, N. Y., *not later than June 1, 1960. Please indicate on abstract for which Division's symposium the paper is to be scheduled, and underline the name of the author who will present the paper.* Complete manuscripts should be sent in triplicate to the Managing Editor of the JOURNAL at the same address.

Papers submitted for presentation at the meeting become the property of The Electrochemical Society and may not be published elsewhere, in whole or in part, unless permission is requested and granted by the Society. Papers already published elsewhere, or submitted for publication elsewhere, are not acceptable for oral presentation except on invitation by a Divisional program Chairman.

• • •

The Spring 1961 Meeting will be held in Indianapolis, Ind., April 30, May 1, 2, 3, and 4, 1961, at the Claypool Hotel. Sessions will be announced in a later issue.

Relative Rates of Electromigration of Different Ions of the Same Charge across Permselective Membranes

Ruth McClintock, Rex Neihof,[1] and Karl Sollner

Laboratory of Physical Biology, National Institute of Arthritis and Metabolic Diseases, National Institutes of Health, Public Health Service, Bethesda, Maryland

ABSTRACT

A theory is developed which correlates the ratio of the rates of electromigration across permselective membranes of two species of critical exchangeable ions coexisting in solution with the ratio of the rates of spontaneous exchange across the same membrane of the same two species of ions for a third ion in the other solution, and with the bi-ionic potential arising across the same membrane between solutions each containing one of the ions under investigation, at the same activity. The numerous factors which must be considered in electromigration experiments, particularly polarization, are outlined. With solutions in the range of 0.02-0.2*N* and with current densities of about 0.3-1.0 ma/cm², the agreement between the ratios predicted by the theory is closely approached, in many instances within the limits of the experimental errors. At lower current densities, the experimental flux ratios are markedly lower than postulated by the theory, for unknown reasons. At higher current densities, with increasing polarization, there is a gradual decline of these flux ratios, as predicted by theoretical considerations.

In a previous paper we demonstrated the occurrence of greatly different rates of exchange of ions of the same charge across porous membranes of extreme ionic selectivity (permselective membranes) (1). This effect was studied in systems such as System 1 which, in the case of exclusively cation-permeable, anion-impermeable membranes of ionic character, ←⊕→, are represented by:

Solution 1	←⊕→	Solution 2
A^+X^- B^+X^-	Membrane of extreme cationic selectivity	L^+X^-

[System 1]

Here A^+, B^+, and L^+ represent the exchangeable (critical) cations, X^- the nonexchanging, nonpermeating anions. Anionic systems with exclusively anion permeable membranes, ←⊖→, are analogous. Depending on the nature of the membranes, the ratio of the initial rates of simultaneous exchange of univalent ions, A^+ for L^+ and B^+ for L^+, can be as high as 1:100 and more.

These ratios of the rates of exchange, that is, the ratios of the net fluxes of any two species of critical univalent ions coexisting in Solution 1, $(\phi_{A^+}/\phi_{B^+})_{exch.}$, were shown to be correlated to the potentials arising with the same membrane in cells of the type:

Solution 1			←⊕→		Solution 2
Calomel electrode	KCl conc.	c_1 A^+X^-	c_1 B^+X^-	KCl conc.	Calomel electrode

[Cell 1]

(and analogous cells with exclusively anion permeable membranes) (1). The sign and the magnitude of the potential arising in such cells, the so-called "bi-ionic" potential, $E_{bip.}$, as was pointed out by Michaelis (2), are determined by the relative ease with which the two critical ions penetrate the membrane: if in Cell 1 the cations A^+ of Solution 1 penetrate the membrane with greater ease than do the cations B^+ of Solution 2, then Solution 2 will be charged positive; if the converse is true, Solution 2 will be negative.

Expressing this concept quantitatively one may write

$$E_{bip.} = \frac{RT}{\mathbf{F}} \ln \frac{\tau^\circ_{A^+}}{\tau^\circ_{B^+}} \qquad [1]$$

where $\tau^\circ_{A^+}$ and $\tau^\circ_{B^+}$ represent the transference numbers of A^+ and B^+ within the membrane (the superscript ° being used throughout to indicate equality of activities) (3-6). The ratio of these transference numbers is considered to be a quantitative measure of the relative intrinsic abilities of the A^+ and B^+ ions to penetrate across the particular membrane.

If this holds true, the ratio of the transference numbers can be used to predict the ratio of fluxes of A^+ and B^+ ions across the membrane when present at equal activities in Solution 1, and exchanging for a third ion in Solution 2, as in System 1 (1). If this predicted ratio of fluxes derived from the bi-ionic potential is designated $(\phi^\circ_{A^+}/\phi^\circ_{B^+})_{bip.}$, we may write:

$$\left(\frac{\phi^\circ_{A^+}}{\phi^\circ_{B^+}}\right)_{bip.} = \frac{\tau^\circ_{A^+}}{\tau^\circ_{B^+}} \qquad [2]$$

Experimentally it was shown that in most instances these ratios, $(\phi^\circ_{A^+}/\phi^\circ_{B^+})_{bip.}$, agree within the limits of experimental error with the experimentally established ratios of exchange, $(\phi^\circ_{A^+}/\phi^\circ_{B^+})_{exch.}$ (1):

[1] Present address: Chemistry Division, Naval Research Laboratory, Washington 25, D. C.

$$\left(\frac{\phi^{\circ}_{A^+}}{\phi^{\circ}_{B^+}}\right)_{bip.} = \left(\frac{\phi^{\circ}_{A^+}}{\phi^{\circ}_{B^+}}\right)_{ex.h.} \quad [3]$$

If, in systems such as System 1, the ratio of the activities of any two species of exchangeable ions in Solution 1 was not 1:1, the ratios of their initial net fluxes across the membrane, $(\phi_{A^+}/\phi_{B^+})_{exch.}$, were shown to agree satisfactorily, usually within the limits of the experimental error, with the corresponding ratios derived from the bi-ionic potentials, $(\phi^{\circ}_{A^+}/\phi^{\circ}_{B^+})_{bip.}$, times the ratios of the activities of the two ions under consideration, $a_{A^+}[1]/a_{B^+}[1]$, according to the equation:

$$\left(\frac{\phi_{A^+}}{\phi_{B^+}}\right)_{exch.} = \frac{a_{A^+}[1]}{a_{B^+}[1]}\left(\frac{\phi^{\circ}_{A^+}}{\phi^{\circ}_{B^+}}\right)_{bip.} \quad [4a]$$

Combining Eq. [3] and [4a], we may write the expanded equation:

$$\left(\frac{\phi_{A^+}}{\phi_{B^+}}\right)_{exch.} = \frac{a_{A^+}[1]}{a_{B^+}[1]}\left(\frac{\phi^{\circ}_{A^+}}{\phi^{\circ}_{B^+}}\right)_{bip.} = \frac{a_{A^+}[1]}{a_{B^+}[1]}\left(\frac{\phi^{\circ}_{A^+}}{\phi^{\circ}_{B^+}}\right)_{exch.} \quad [4b]$$

Analogous considerations were shown to apply to systems with more than two species of critical ions in Solution 1.

After the ratios of the rates of spontaneous exchange across permselective membranes of coexisting species of ions of the same charge were thus correlated satisfactorily with the bi-ionic potentials arising with these ions across the same membranes, the next obvious step was to test whether analogous correlations exist with the ratios of the migration in an electric field of ions of the same charge across permselective membranes. This electromigration could be studied in cells such as Cell 2, which is essentially System 1 provided with electrodes:

	Solution 1		Solution 2	
		$\leftarrow\oplus\rightarrow$		
Anode	c_1 A^+X^- c_1 B^+X^-		c_2 L^+X^-	Cathode

Cell [2]

This matter, mentioned briefly at an earlier occasion (7), is the subject of the present communication.

When a positive current is passed through Cell 2 from left to right, A^+ and B^+ ions are transported simultaneously from Solution 1 through the membrane into Solution 2, the total number of equivalents of ions moved being identical with the number of faradays passed through the cell.

If the ratio $(\phi^{\circ}_{A^+}/\phi^{\circ}_{B^+})_{bip.}$ and the closely similar ratio $(\phi^{\circ}_{A^+}/\phi^{\circ}_{B^+})_{exch.}$ represent a measure of the ratio of the intrinsic competitive propensities of these two ions to penetrate across the membrane, the ratio in which the current is transported by the A^+ and B^+ ions across the membrane in Cell 2 may be expected to be the same, provided $a_{A^+}[1]$ equals $a_{B^+}[1]$. Denoting the ratio of these net fluxes of the A^+ and B^+ ions, which may also be considered as the ratio of their transport numbers in the membranes, as $(\phi^{\circ}_{A^+}/\phi^{\circ}_{B^+})_{elect.}$ we may write:

$$\left(\frac{\phi^{\circ}_{A^+}}{\phi^{\circ}_{B^+}}\right)_{elect.} = \left(\frac{\phi^{\circ}_{A^+}}{\phi^{\circ}_{B^+}}\right)_{bip.} = \left(\frac{\phi^{\circ}_{A^+}}{\phi^{\circ}_{B^+}}\right)_{exch.} \quad [5]$$

If the concentrations of A^+ and B^+ in Cell 2 are not identical, this is taken into account in the same manner as in the case of exchange studies (1) by the use of the more general equation

$$\left(\frac{\phi_{A^+}}{\phi_{B^+}}\right)_{elect.} = \left(\frac{a_{A^+}[1]}{a_{B^+}[1]}\right)\left(\frac{\phi^{\circ}_{A^+}}{\phi^{\circ}_{B^+}}\right)_{bip.} = \left(\frac{a_{A^+}[1]}{a_{B^+}[1]}\right)\left(\frac{\phi^{\circ}_{A^+}}{\phi^{\circ}_{B^+}}\right)_{exch.} \quad [6]$$

or its analogue for anionic cells.

The foregoing derivation of the flux ratio $(\phi_{A^+}/\phi_{B^+})_{elect.}$ implicitly makes the assumption that potentially complicating effects do not arise to a significant extent. Specifically it is based on the assumptions that:

1. the membranes are of ideal ionic selectivity;
2. equilibrium conditions at the membrane-solution interfaces are maintained;
3. the distribution of ions in the membrane has reached a stationary state;
4. polarization does not arise;
5. electrophoretic effects, particularly a coupling of the movements of different ionic species, are absent;
6. spontaneous net exchange of ions across the membranes is absent; and
7. osmosis, due to differences in the activity of the solvent at the two sides of the membrane does not occur.

Assumption 1 means that no significant quantity of noncritical ions penetrates across the membrane, a condition which is readily fulfilled by permselective collodion matrix membranes (8-10).

Assumption 2 implies that the distribution of ions at the membrane-solution interfaces during electromigration corresponds to the equilibrium distribution of ions which would exist without the flow of current, in the absence of any spontaneous net exchange of ions across the membrane. This assumption is closely linked to the problem of membrane polarization which is treated below, Assumption 4.

Assumption 3 states that the distribution of the ions in the membranes under the influence of the electric field has reached a stationary state. This condition would be fulfilled either if such a stationary state is the same as that with no current flowing, or if a current has been passed through the cell prior to the experiment proper for a period long enough to achieve the stationary state. Membranes having ion exchange capacities which are low compared with the total ionic content of Solution 2 would be expected to cause the least error even if Assumption 3, which is not readily tested by an independent method, should not be strictly fulfilled.

Assumption 4, that polarization at the membrane-solution interfaces does not arise, can be true only with infinitely weak currents, quite as in the case of metallic electrodes.

While polarization at metallic electrodes has been treated widely in the literature, membrane polarization has not been studied extensively. Polarization at

metallic electrodes is thus a useful starting point in discussing membrane polarization.

Electrode polarization is best known for nominally reversible electrodes in contact with single electrolyte solutions such as $CuSO_4/Cu$. Ordinarily one distinguishes (*a*) *chemical polarization* due to a slow step or steps involved in the discharge of the ions, such as their dehydration, and the deposition of the discharged material in a stable form at the cathode, or to the inverse processes in the anodic dissolution of a metal electrode; and (*b*) *concentration polarization* which is due to the slowness of the diffusion of ions in the solution. There is a decrease of the concentration in the solution in the immediate neighborhood of the cathode where ions are being discharged, and an increase near the anode from which metal dissolves and goes into solution in the form of ions. In a thin layer of solution there is always a concentration gradient from that of the bulk of the solution to the smaller or larger (for cathode and anode, respectively) value at the electrode; diffusion into or from the bulk solution tends to reduce these concentration differences near the electrodes. The layer in which this occurs is commonly referred to as the *diffusion layer*. The thickness of this layer can be reduced by stirring, but it cannot be eliminated entirely. With solutions at room temperature that are stirred thoroughly by ordinary mechanical devices a diffusion layer with an apparent thickness of 20 to 30 μ remains.

Before the ions can reach the cathode they must traverse the diffusion layer from the bulk solution; the rate at which ions reach the cathode is proportional to their concentration in the solution. Concentration polarization at a given current density can be reduced by the use of solutions of higher concentrations and by stirring, or by raising the temperature, but it cannot be eliminated entirely. Concentration polarization is less at lower current densities.

At the phase boundaries between two electrolytic conductors, such as an electrolytic solution and an ionic membrane, *chemical polarization* which involves the discharge of ions obviously does not occur except under the most extreme conditions (11).

Concentration polarization, however, does occur when a current passes across the phase boundary between two ionic conductors if the ratios of the transference numbers of cations and anions in the two phases are not the same, as pointed out first by Nernst and Riesenfeld (12) for the simple case of a uni-univalent electrolyte distributed between two liquid phases. Such polarization consists of an increase in concentration of electrolyte at the one side of the phase boundary and a corresponding decrease at the other. The ratios of the transference numbers, $t^{+[1]}/t^{-[1]}$ and $t^{+[2]}/t^{-[2]}$, are obviously not the same if Phase 1 is an electrolytic solution and Phase 2 an ionic membrane equilibrated with it (12-14).

With permselective membranes the situation is much simpler. In such membranes of practically ideal ionic selectivity either the cations or the anions have a transference number of zero. Only the counter ions of the fixed wall charges, the critical ions of the adjacent solution, move into the membrane phase or are released by it.[2] Thus, with permselective membranes the concentration polarization in a solution containing a single electrolyte is quantitatively the same as if the membrane were a reversible electrode on which the ion under consideration is deposited, or from which it is released by dissolution.

The cells investigated in this paper, such as Cell 2, contain two species of critical ions of the same charge in Solution 1, thus being analogous to electrolytic cells in which an alloy is deposited from a mixed solution. In the two solutions of such cells concentration polarization will arise with respect to all ions according to their respective transport numbers in the solutions and the membrane. Therefore, the degrees of concentration polarization of two ions of the same charge will, in general, be different. In other words, the ratio of the concentration of the two critical species of ions in the solution layers immediately adjacent to the membranes will be different from that in the bulk solution. In cells such as Cell 2, this effect would be disturbing particularly at the phase boundary between Solution 1 and the membrane, where the critical ions move from the solution into the membrane, thereby changing profoundly the most important parameter of the cell. If concentration polarization did not change the ratio of the concentrations of the two permeable ions but only their absolute concentrations, concentration polarization would be of little consequence in the present situation.

Assume, for instance, that the A^+ ions in Cell 2 represent potassium ions and B^+, lithium ions. The former have in free solution about twice the diffusion velocity and ionic mobility of the latter. In ordinary permselective membranes the ratios $(\phi^\circ_{K^+}/\phi^\circ_{Li^+})_{exch.}$ or $(\tau^\circ_{K^+}/\tau^\circ_{Li^+})_{bip.}$ are in most instances about six (1). Although the K^+ ions reach the interface about twice as fast as the Li^+ ions, they are removed by the current into the membrane about six times as fast as the Li^+ ions; thus a relatively stronger depletion of the K^+ ions than of the Li^+ ions would arise in Solution 1 at the membrane-solution interface.

The concentration polarization which we have considered so far is the polarization which arises in the solutions. On the membrane side of the interface, concentration polarization in the classical sense, a decrease or increase in total concentration of electrolyte, cannot occur with membranes of extreme ionic selectivity in which all movable ions are of the same charge. However, another type of concentration polarization may conceivably arise. In our discussion up to now the assumption was made (Assumption 2) that equilibrium with respect to the distribution of ions is always maintained between the surfaces of the membrane and the layers of solution immediately adjacent to it. The question arises whether or not the assumed ion exchange equilibrium on the surface of the membrane is maintained when two competing species of ions of the

[2] This is not true if the degree of polarization is extreme, and the concentration of the electrolyte in the diffusion layer immediately adjacent to the membrane becomes so low that the ions of the water, H^+ or OH^- ions, contribute significantly to the transportation of electricity across the membrane (14). Conditions under which this effect arises are not considered in this paper.

same charge are forced by the electric field into the surface of the membrane. There might be some processes associated with the transition of the ions from the solution into the membrane, such as partial dehydration, which are slow and occur at different speeds with the two species of critical ions under consideration. No information fully pertinent to this point seems to be available. It must be assumed that this type of polarization, if it should exist, would, like all other polarization effects, be more pronounced the higher the current density.

Assumption 5 states that there is no electrophoretic coupling of the movement of the A^+ and the B^+ ions in the membrane. Such a coupling may be visualized as being due to an electro-osmotic movement of liquid in the pores which is caused by the friction between the electromigrating ions and the solvent. With the two species of ions electromigrating in the same stream of liquid, the electrophoretic effect would always tend to equalize the experimentally observable fluxes, thus bringing the flux ratios, $(\phi_{A^+}/\phi_{B^+})_{elect.}$ nearer to unity than those predicted on the basis of the bi-ionic potentials or from exchange studies.

Assumption 6, that there is no significant spontaneous net exchange of ions by diffusion across the membrane, can be realized by the use of membranes of high resistance; the rate of exchange of ions across a membrane, *ceteris paribus*, being inversely proportional to its resistance.

Assumption 7 stipulates that movement of water caused by an inequality of the solvent activities at the two sides of the membrane is absent or negligibly small. The direction of this movement of water would depend on the composition of the two solutions or more correctly on the concentrations in the two layers of solution immediately adjacent to the membrane. If polarization occurs, this would result in a reduced concentration of this layer in Solution 1 and in an increased concentration on the side of the more dilute Solution 2. This effect would tend to alter the osmotically active concentration difference across the tested membrane. The use of fairly dense membranes of low water permeability, such as the permselective collodion matrix membranes, tends to minimize the errors due to osmotic solvent movement (8-10).

The conditions postulated by the various assumptions discussed above, except the absence of electrophoretic effects may be realized experimentally to an adequate extent, primarily by the use of low current densities and solutions which are not too dilute in cells with dense, high resistance membranes. The absence of electrophoretic effects, however, cannot be achieved as a matter of principle, except in the unique and trivial instance of equal mobilities within the membrane of the two competing species of critical ions. The mutual interactions between the two types of electromigrating critical ions, the charged pore walls, and the solvent are inherent in the electromigration experiments, independent of the current density. Only the experiments can show whether the simple theoretical approach which has led to Eq. [5] and [6] is justified by the facts.

A study somewhat similar to the present has been published by Bergsma and Staverman (15). Using technical membranes of fairly high water content, they found rather unsatisfactory agreement between theory and experiment. Gregor and Wetstone (16) and Bilberg and Brun (17) have briefly touched the same subject. From a more practical point of view some phases of the problem of the simultaneous electromigration of ions across membranes were taken up by Di Benedetto and Lightfoot (18) and by Partridge and Peers (19).

Design of the Experiments

The experiments were designed not only to fulfill adequately the requirements of the assumptions outlined above, but also to permit ease and accuracy of analysis. Pairs of ions were chosen which do not interfere analytically with each other. Further, to facilitate accurate measurement of concentration changes in the solution into which the ions were transported, Solution 2, the initial concentrations in that solution of the ions under study were made low. Various possible types of cells satisfy these conditions. We chose cells which fulfill the condition described by the Donnan membrane equilibrium:

$$\frac{a_{A^+}^{[1]}}{a_{B^+}^{[1]}} = \frac{a_{A^+}^{[2]}}{a_{B^+}^{[2]}} \qquad [7]$$

In cells with only strong uni-univalent inorganic electrolytes, it is adequate and more convenient to operate with normalities instead of activities, the ratios of which are for practical purposes identical with those of the corresponding activities, for example:

	Solution 1		Solution 2	
		$\leftarrow\oplus\rightarrow$		
Anode	$0.1N$ A^+X^- $0.1N$ B^+X^-		$0.001N$ A^+X^- $0.001N$ B^+X^-	Cathode

[Cell 3]

Before the passage of current, such cells are in equilibrium with respect to the distribution of the critical ions. No spontaneous net exchange of ions between the two solutions can occur until the flow of current has shifted the ratios of their concentrations away from the Donnan distribution.

Although Cell 3 is in equilibrium with respect to the distribution of the ions, it is not in equilibrium with respect to the solvent; there is an osmotic flow of water from Solution 2 into Solution 1. Such an osmotic flow would decrease by the same absolute value the speed of electromigration of the two critical ions across the membrane, and thus would increase the experimental flux ratios above the calculated ones. The influence of osmosis would be most noticeable in long duration, low current density experiments. The osmotic and the electro-osmotic effects in Cell 3 operate in opposite directions and thus tend to cancel.

The following considerations were applied in the detailed planning of the experiments. In order that the concentrations of the ions under study in Solution 1 and therefore also the ratio of their concentrations remain practically unchanged, the volume of this solution should be large and its concen-

tration high compared with that of Solution 2. The volume of Solution 2 should be small, so that a given small amount of electricity passed through the cell would bring about changes in concentration which are large enough to permit accurate analyses. To obtain a large concentration change in a short time with a given current density, it is desirable to have a high ratio of the membrane area to the volume of Solution 2.

To fulfill as far as possible Assumptions 1, 6, and 7 listed in the preceding section, the membranes chosen should be of virtually ideal ionic selectivity, of sufficiently high resistance to prevent significant spontaneous exchange of ions between the two solutions, and dense enough to prevent appreciable osmotic water movement. Further, the membranes should have low ion exchange capacities so that exchange of ions between them and the solutions cannot affect significantly the ratio of the ionic concentration of the solutions.

Permselective membranes except those with very low resistances have satisfactory ionic selectivities in solutions up to about 0.2*N*, they also have low ion exchange capacities (8-10). In general, membranes of higher resistance yield a lower rate of osmotic water movement. However, the resistance must not be so high as to make the exchange studies for the determinations of the $(\phi^\circ_{A^+}/\phi^\circ_{B^+})_{exch.}$ ratios too tedious, or to cause a significant amount of heat to be generated by the flow of the maximum current used. Although the concentrations of both species of critical ions in Solution 1 should be high, the total concentration of Solution 1 can be raised safely only to a certain extent (which depends on the membrane) because the ionic selectivities of the membranes are lower at higher concentrations (8-10).

Also, the current densities used should be low to minimize polarization. However, a certain total quantity of electricity must flow through the cell before analytical data of sufficient accuracy can be obtained. Low current densities therefore necessitate long experimental periods. Under these conditions the danger of a significant spontaneous exchange of ions is increased, due not only to the time factor but also to the less pronounced unidirectional flux of ions in the membrane. The range of current densities used must represent a compromise between these antagonistic requirements.

When a current is passed through Cell 3, the products of electrolysis developed at metallic electrodes, particularly H^+ and OH^- ions, would seriously affect the essential membrane processes. In cells with cation selective membranes and solutions of the halides, the use of silver-silver halide electrodes would considerably ameliorate this situation; however, disturbing electrode processes would still occur with the current densities used in many of our experiments. The difficulties due to electrode processes can be eliminated by using guard membranes of extreme ionic selectivity which separate the electrodes from Solutions 1 and 2 (15, 20). If the tested membrane is cation permeable the guard membranes must be anion permeable, and *vice versa*, as shown in Cells 4a and 4b.

It is evident which ions are transported by the current to and from the different compartments of Cell 4, how contamination of Solutions 1 and 2 from the adjacent electrode compartments is suppressed, and how electroneutrality is maintained in each compartment.

Apparatus and Procedure

The experimental cell, shown schematically in Fig. 1a, consisted of four Lucite sections clamped together by means of four bolts. The compartments so formed, A, B, C, and D, were separated from each other by the tested membrane and two guard membranes, mounted flat between Parafilm gaskets. The exposed area of each membrane was 23.7 cm^2.

The two end sections forming the electrode compartments A and D each had an air hole at the top and a tube at the bottom for introducing or draining

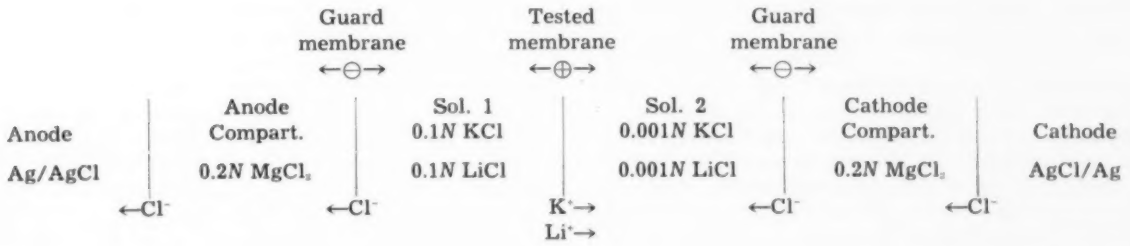

and [Cell 4a]

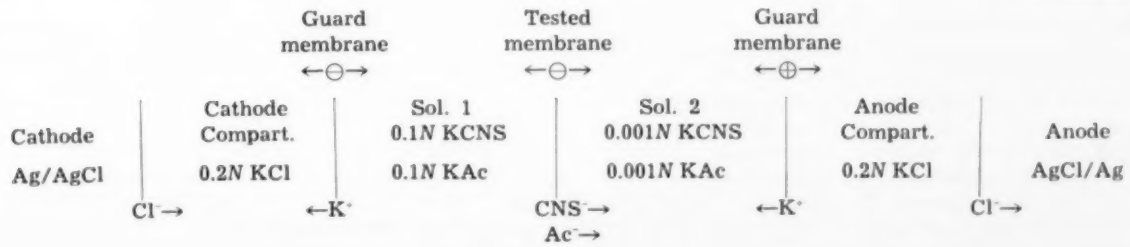

[Cell 4b]

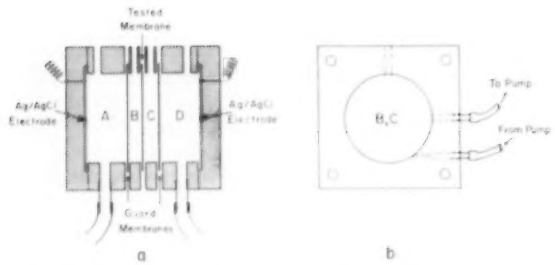

Fig. 1. Cell for the study of the electromigration of ions across membranes (schematic). (a) Cross section through the cell; (b) plastic section forming compartment B or C.

solutions, and contained an electrode, a silver disk on which silver chloride had been deposited by electrolysis from a chloride solution.

The two sections forming compartments B and C on either side of the tested membrane were machined as shown in Fig. 1b. Each had a hole at the top and was provided with a closed loop of polyvinyl chloride (Tygon) tubing. These loops passed through a peristaltic pump which circulated the solutions at a rate of about 100 ml/min. This stirring was vigorous enough that further increases in the rate of circulation made no significant difference in the experimental results. The volume of solution required for filling completely either compartment B or C including the loop of tubing was about 20 ml which, when necessary, was increased to about 200 ml by placing a reservoir in the pumping circuit.

The membranes were cut from the cylindrical parts of test tube-shaped permselective collodion matrix membranes, the preparation and properties of which have been described in detail (8-10). The cation selective membranes contained acidic polyelectrolytes as activating agents, polyacrylic acid (PAA) in the case of weak acid membranes and polystyrene sulfonic acid (PSSA) in the case of strong acid membranes (8). The anion selective membranes were made with basic polyelectrolytes, poly-2-vinyl-N-methyl-pyridinium halide (PVMP) or protamine chloride (9, 10).

The tested membranes had unit area resistances in 0.1*N* KCl, ρ°, from 125 to 300 ohm-cm^2, the guard membranes from 250 to 900 ohm-cm^2. Membranes in these ranges of resistance are known to be of high ionic selectivity as determined from the measurement of concentration potentials or from leak studies, their permeabilities to the critical ions at 0.1*N* being about 400 to 2000 times that of the noncritical ions (8-10). They have ion exchange capacities of 0.4 to 2.0 μeq/cm^2, water contents of 6-13%, and are about 30 μ thick.

For measurement of the *bi-ionic potentials*, $E_{bip.}$, the compartments B and C on opposite sides of the tested membrane were filled with 0.1*N* electrolyte solutions, each containing one of the critical ions to be studied; the electrode compartments were left empty. The solutions, which were stirred continuously, were renewed repeatedly over a period of several hours to establish a stationary state across the membrane (4). Immediately after renewing both solutions again, the potential was measured using saturated calomel half-cells with saturated KCl-agar bridges, and the temperature recorded. This was repeated until successive readings agreed within ± 2%. These potentials were not corrected for the asymmetry of the two liquid-junction potentials at the tips of the bridges. The flux ratio, $(\phi^{\circ}_{A^+}/\phi^{\circ}_{B^+})_{bip.}$ was obtained using Eq. [1] and [2].

For the determination of the ratios of the *rates of exchange*, a reservoir was placed in the pumping circuit of one of the compartments adjacent to the tested membrane, B or C, and filled with Solution 1, a 0.2*N* solution containing equal concentrations of the two critical ions under study. The other compartment, without reservoir, was filled with Solution 2, 0.2*N* NH_4Cl if the tested membrane was cation permeable or 0.2*N* KNO_3 if it was anion permeable. Both solutions were circulated for stirring. A stationary state across the membrane was obtained, as described above, before starting the experiment proper with fresh solutions. The duration of the exchange experiments was chosen so that the concentrations of the critical ions in Solution 2 became sufficient for accurate analysis. The ratio of their concentrations gives the ratio of the exchange fluxes, $(\phi^{\circ}_{A^+}/\phi^{\circ}_{B^+})_{exch.}$. These experimental runs were repeated until two or more runs agreed within 5-10%.

To measure the *electrical fluxes*, the electrode compartments A and D were filled with about 50 ml of 0.2*N* $MgCl_2$ if the tested membrane was cation permeable, or 0.2*N* KCl if the tested membrane was anion permeable. One of the compartments adjacent to the tested membrane, B or C, was provided with a reservoir and filled with the more concentrated solution, Solution 1 [Cell 4]. The compartment on the other side of the tested membrane, without reservoir, was filled with the more dilute solution, Solution 2. Both solutions were circulated for stirring. The membrane was equilibrated with the solutions as described above. Before an experimental run, both solutions were changed, the more dilute solution three times. Finally, a measured volume of the dilute solution was placed in the compartment of Solution 2 and the flow of a direct current of the chosen intensity, 0.042-4.2 ma/cm^2, started. The duration of the experiments, 3-480 min, was adjusted so that the concentrations of the critical ions in the dilute solution increased sufficiently for accurate determination of the concentration changes. The currents passed were 1-100 ma; the total quantity of electricity in the individual runs was 0.2-0.6 x 10^{-3} faraday. The experimental runs at any given current density were repeated, usually two or three times with about 100% variation in their duration. The electrical flux ratios, $(\phi_{A^+}/\phi_{B^+})_{elect.}$, for each experimental run were obtained from the ratios of the increases in concentration of the two critical ions. These ratios were ordinarily reproducible within 15%.

As a routine check for satisfactory performance of the cell, the number of equivalents of critical ions transported was compared with the number of faradays of electricity passed, as determined by an iodine coulometer or as calculated from the magnitude and duration of the current. It also should be mentioned that the membranes did not change significantly during a series of experiments, as indicated

by the constancy of the exchange flux ratios and of the bi-ionic potentials. The sequence in which the experiments were carried out did not influence the results.

In numerous instances the positions of the solutions and the direction of the current were reversed with respect to the tested membrane; with the electrolytes used in the experiments reported below in detail, no significant effect was found.

The analytical determinations of anions were carried out by standard micromethods (21), ordinarily with an estimated error of ±1%. The cations were determined by means of a flame spectrophotometer, the error in analysis being in most cases less than ± 3%, never more than ± 5%.

Before presenting the results of the experiments which were carried out by the methods just outlined, several preliminary tests are described which were made to explore to what extent certain of the conditions assumed in the theoretical development are fulfilled in our experimental cells.

During the course of the electromigration experiments the ratio of the A^+ and B^+ ions in Solution 2 is changed from the Donnan equilibrium distribution shown in Cell 4, and spontaneous back exchange of ions tends to occur, contrary to our assumption.

Back exchange is not readily measured in the presence of the electric field applied in the electromigration experiments. We therefore have tested whether such an exchange of ions might occur in the absence of an impressed electric field. The membranes were of the same types employed in the electromigration experiments, with ρ^* of 175-275 ohm-cm^2. Solutions similar to the final solutions obtained in the electromigration studies were placed in the compartment of Solution 2 and allowed to exchange against Solution 1 while both solutions were stirred. At the end of the exchange periods, 2-16 hr, little or no change in the concentrations of the ions was found. There would have been even less back exchange during the electromigration runs: first, with current flowing, the back exchanging ions would have had to move against an electrical gradient; second, the concentration difference which would cause back exchange is initially zero and would be built up only in course of time. Thus it is certain that back exchange was quantitatively unimportant during the electromigration experiments.

To test whether osmosis due to differences in the activities of the solvent at the two sides of the membrane occurs, the rate of osmotic water movement was measured, as described previously (8-10), with 1.0*N* KCl against water. The same membranes were used as in the back exchange experiments. The rates of osmotic water movement were 2 to 6 mm^3/hr-cm^2. Since the rate of water movement is proportional to the difference in osmolar concentrations, the greatest rate to be expected with the solutions used in our electromigration experiments is approximately one-fourth as much.

The water transported per equivalent of ions moved was also determined for the same membranes. The experimental arrangement was similar to that for the measurement of osmosis, but with the addition of Ag/AgCl screen electrodes on either side of the membrane. The quantity of water transported per faraday depended on the critical ion and the resistance of the membrane. It was independent of the current density and essentially independent of the concentration, in the range of interest here. The values with acidic membranes were 3-4 moles of water per equivalent of K^+ and 6-8 per equivalent of Li^+; for the basic membranes, 4-5 moles per equivalent of Cl^- and 8-10 for Ac^-. The lower figures were obtained with the higher resistance membranes.

The difference in the number of moles of water transported by ions of the same charge may be taken as an indication that an electrophoretic coupling of the movement of such ions exists when they electromigrate simultaneously across a membrane. However, at present it does not seem possible to evaluate this effect quantitatively.

Another aspect of the electro-osmotic transportation of water of interest here is its correlation to the osmotic water movement, the two being opposed in direction to each other in the electromigration experiments. The electro-osmotic effects are proportional to the number of equivalents of ions transported, independent of the duration of the experiment. The osmotic effects, however, are proportional to the time and are thus proportionately less for the shorter experiments at higher current densities. The data indicate that the osmotic and electro-osmotic effects were of the same order of magnitude at the lowest current densities used in our electromigration experiments, 0.042-0.127 ma/cm^2; at the highest current density employed (4.2 ma/cm^2) the electro-osmotic effect was an order of magnitude greater than the osmotic effect.

The effect of the electro-osmotic and osmotic movement of water on the volume and therefore the concentration of Solution 2 must also be considered. At low current densities the two effects, being of about the same magnitude and opposite in direction, tend to cancel and produce little change in the volume of Solution 2. At high current densities where electro-osmosis predominates, a maximum of approximately 6 mM or about 0.1 ml of water is moved into Solution 2 during a single run. This is only about 0.5% of the initial volume of Solution 2, so that the volume change which results from the water movement and the concomitant effect on the concentration of ions in Solution 2 may be neglected.

Results and Discussion

Figures 2-4 summarize our experimental results. In the coordinate graphs the mean values of the ratios of the electrical fluxes for each current density studied are plotted and connected by straight lines. The length of the vertical line at each plotted point indicates the average deviation of the electrical flux ratio from the mean value of replicate experiments. This alternative is used to give an indication of the reproducibility of the experiments, since many more data would be necessary to make possible a meaningful statistical analysis.

To the right of each coordinate graph are two bar graphs, one showing the ratios calculated from

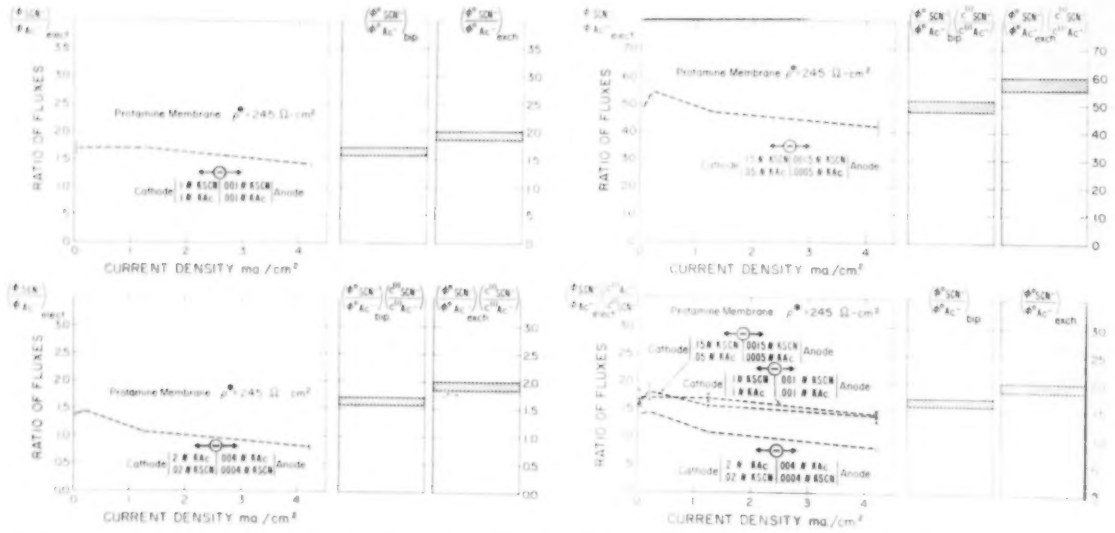

Fig. 2. A comparison of the ratios of fluxes of SCN^- and Ac^- ions (i) as transported by an electric current across an exclusively anion permeable permselective protamine collodion matrix membrane, $(\phi_{SCN^-}/\phi_{Ac^-})_{elect.}$, (ii) as calculated from the bi-ionic potential with the two ions separated by the same membrane, $(\phi^\circ_{SCN^-}/\phi^\circ_{Ac^-})_{bip.}$, and (iii) as measured in the simultaneous exchange of the two ions across the same membrane, $(\phi^\circ_{SCN^-}/\phi^\circ_{Ac^-})_{exch.}$.

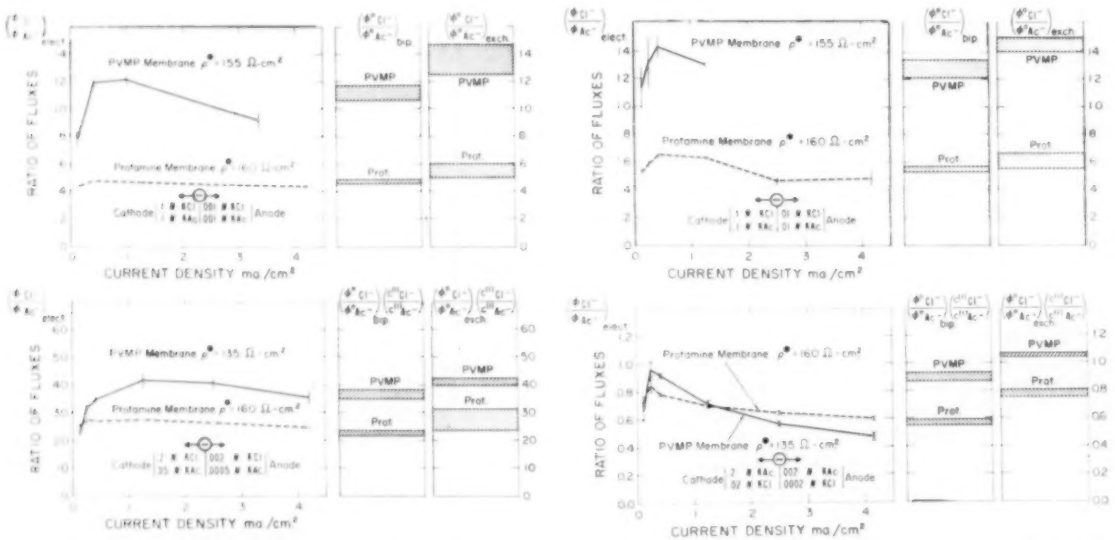

Fig. 3. A comparison of the ratios of the fluxes of Cl^- and Ac^- ions (i) as transported by an electric current across exclusively anion permeable permselective poly-2-vinyl-N-methyl-pyridinium (PVMP) and protamine collodion matrix membranes, $(\phi_{Cl^-}/\phi_{Ac^-})_{elect.}$, (ii) as calculated from the bi-ionic potential with the two ions separated by the same membranes, $(\phi^\circ_{Cl^-}/\phi^\circ_{Ac^-})_{bip.}$, and (iii) as measured in the simultaneous exchange of the two ions across the same membranes, $(\phi^\circ_{Cl^-}/\phi^\circ_{Ac^-})_{exch.}$.

the bi-ionic potentials, and the other, the exchange flux ratios. These graphs have the same vertical scale as the coordinate graphs. In the bar graph of the ratios derived from the bi-ionic potentials, the width of the shaded areas represents the estimated uncertainty in these ratios assuming the measurement of the bi-ionic potential to be accurate within ± 2%. Because the ratio is a logarithmic function of the bi-ionic potential, the width of the shaded areas increases exponentially with the heights on these bar graphs. In the case of the exchange ratios, the width of the shaded areas represents the average deviation from the means of replicate experiments.

Figures 2 and 3 show results obtained with exclusively anion permeable membranes, ←⊖→: Fig. 2 with a protamine membrane and SCN^- and Ac^- as critical ions; Fig. 3 with protamine and poly-2-vinyl-N-methyl-pyridinium (PVMP) membranes Cl^- and Ac^- ions. Figure 4 gives the results with exclusively cation permeable membranes, ←⊕→, polystyrene sulfonic acid (PSSA) and polyacrylic acid (PAA) membranes, with K^+ and Li^+ as critical ions.

A comparison of each pair of bar graphs shows that the flux ratios calculated from the bi-ionic potentials and from the exchange measurements agree

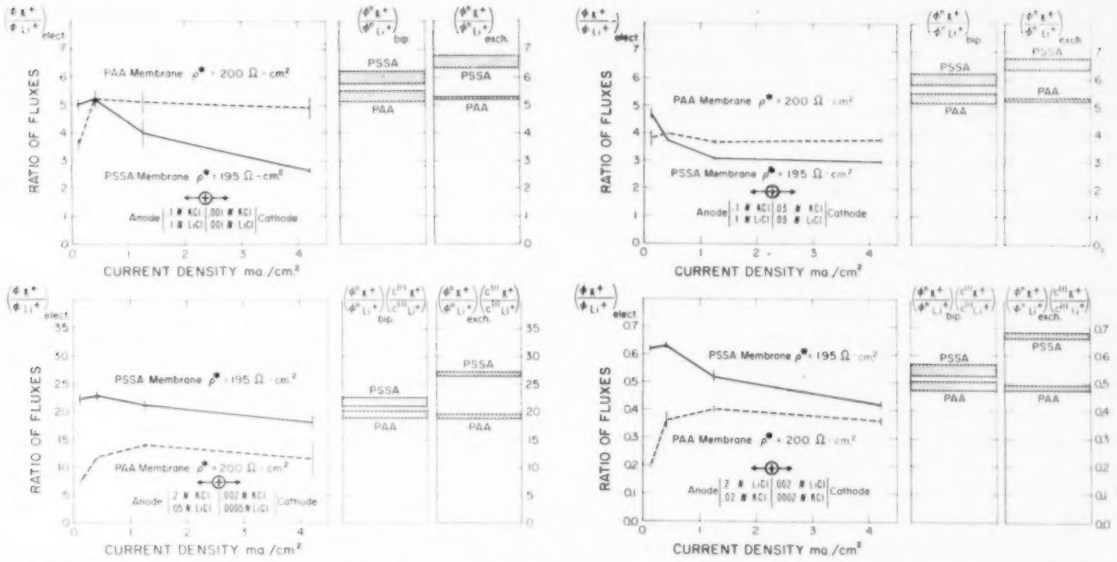

Fig. 4. A comparison of the ratios of the fluxes of K^+ and Li^+ ions (i) as transported by an electric current across exclusively cation selective permselective polystyrene sulfonic acid (PSSA) and polyacrylic acid (PAA) collodion matrix membranes, $(\phi_{K^+}/\phi_{Li^+})_{elect.}$, (ii) as calculated from the bi-ionic potentials with the two ions separated by the same membranes, $(\phi^\circ_{K^+}/\phi^\circ_{Li^+})_{bip.}$, and (iii) as measured in the simultaneous exchange of the two ions across the same membranes, $(\phi^\circ_{K^+}/\phi^\circ_{Li^+})_{exch.}$.

reasonably well with each other, the exchange flux ratios being somewhat higher than the ratios calculated from the bi-ionic potential. The agreement between the two ratios is similar to that reported by Neihof and Sollner (1).

The curves of the ratios of electrical fluxes versus current density in the coordinate graphs of Fig. 2-4 show in the majority of the investigated cells a maximum in the range of current densities of about 0.3-1.0 ma/cm². At higher current densities the ratios of the fluxes are lower, being lower the greater the current density. At current densities less than about 0.3 ma/cm² there is in nearly every cell a significant, in several instances a very marked, drop in the electrical flux ratio. The slope may in many cases be steeper than indicated by the graphs, since the experimental points at low current densities are not close enough together to define exactly the maximum of the curves.

This general shape of the curves is not to be anticipated on the basis of the theoretical treatment. The latter predicts only the observed lowering of the electrical flux ratios as the current density increases, primarily due to polarization and, secondarily, to an increasing preponderance of the electroosmotic over the osmotic liquid movement.

A comparison of the electrical flux ratios at the maxima of the curves with the ratios given by the corresponding bar graphs shows a fairly good quantitative agreement with most of the cells. An extrapolation to zero current of the parts of the curves between about 0.5 ma/cm² and 4.0 ma/cm² would yield an intercept which would show an even better agreement with the bar graphs. This extrapolation, however, seems questionable in view of the drop of the curves at the lower current densities.

The downward slope of the curves toward the side of the lower current densities is contrary to the theoretical expectation. Since this effect occurs quite regularly and is in magnitude far outside the limits of the experimental errors, it must be considered as real. The experiments on spontaneous back exchange reported above preclude an explanation on this basis of the low flux ratios obtained at low current densities. In some instances a spontaneous back exchange with no current passing was not detectable. The greatest back exchange with no current would correspond to less than one-third of the observed decrease in ratios. However, as mentioned previously, any back exchange during the electromigration runs must have been less. Attempts based on the conventional electrochemistry of permselective membranes to explain the lower electrical flux ratios at the lowest current densities have not yet been successful.

That the electrical flux ratios at the maxima of the curves, where polarization is still small, show satisfactory agreement with the theory, seems to indicate that the electrophoretic coupling of the electromigration across the membrane of two species of critical ions is not very marked—the available data are inadequate for any quantitative statement.

Thus the outlined theory seems justified in principle as a first approximation, although it is not adequate to describe the phenomena over more than a very limited area of current densities. Proof is lacking that such agreement between theory and experimental results would be found with membranes of higher porosity, in which each electromigrating ion transports a much greater number of water molecules (22) than in the rather dense membranes used in the present study.

Any more comprehensive and rigorous approach to the problem of the ratios of the electromigration across permselective membranes of two or more species of critical ions coexisting in solution will be confronted not only with the complexity of the membrane processes themselves, but also with the

problem of polarization. Polarization, as indicated by our experimental results, is a most important factor, at all but rather low current densities. The general approach to the theory of irreversible processes given by de Groot (23) and the more specific treatment of membrane processes along analogous lines by Staverman, Kirkwood, Schmid, Schlögl, Spiegler and others yield a useful conceptual framework (24-28). However, the practical obstacles to the use of this approach with experimental cells are formidable. Disregarding polarization in the solutions and assuming no complications such as slow reactions at the membrane-solution interfaces, the situation even with membranes of ideal ionic selectivity is highly complex. With three species of particles, A^-, B^-, and H_2O, which are movable with respect to the membrane, it would be necessary to determine six independent flux constants, which describe the interactions between these particles, in order to know their flux equations (28). However, a given set of constants applies only to a given ratio of A^- and B^- in the membrane and additional data, or permissible assumptions, are needed to describe any different A^-/B^- ratio. Moreover all such constants apply only to the particular membrane under study; different constants pertain to each different membrane.

An approach along these lines to the problem of the ratios of the electromigration across permselective membranes of co-existing species of critical ions is an undertaking of a major magnitude. This prompts us, for the time being, to stop further work in this direction.

Manuscript received Aug. 13, 1959. This paper was prepared for delivery before the New York Meeting, April 27-May 1, 1958.

Any discussion of this paper will appear in a Discussion Section to be published in the December 1960 JOURNAL.

REFERENCES

1. R. Neihof and K. Sollner, *Discussion Faraday Soc.*, **21**, 94 (1956).
2. L. Michaelis and A. Fujita, *Biochem. Z.*, **161**, 47 (1925); L. Michaelis, *Bull. Natl. Research Council (U.S.), No. 69* (1929); *Kolloid Z.*, **62**, 2 (1933).
3. K. Sollner, *J. Phys. Chem.*, **53**, 1211, 1226 (1949).
4. S. Dray and K. Sollner, *Biochim. Biophys. Acta*, **18**, 341 (1955).
5. S. Dray and K. Sollner, *ibid.*, **21**, 126 (1956); **22**, 213, 220 (1956).
6. R. Neihof and K. Sollner, *J. Phys. Chem.*, **61**, 159 (1957).
7. K. Sollner, *Discussion Faraday Soc.*, **21**, 120 (1956).
8. R. Neihof, *J. Phys. Chem.*, **58**, 916 (1954).
9. M. H. Gottlieb, R. Neihof, and K. Sollner, *J. Phys. Chem.*, **61**, 154 (1957).
10. M. Lewis and K. Sollner, *This Journal*, **106**, 347 (1959).
11. K. Sollner, *Z. Elektrochem.*, **35**, 789 (1929).
12. W. Nernst and E. H. Riesenfeld, *Ann. Physik*, (4), **8**, 600 (1902).
13. L. Michaelis, "Die Wasserstoff-ionenkonzentration," Berlin, Springer (1922); English Edition, Translated by W. Perlzweig, "Hydrogen Ion Concentration," Williams and Wilkins Co., Baltimore (1926).
14. A. Bethe and T. Toropoff, *Z. Physik Chem.*, **88**, 686, (1914); **89**, 597 (1915).
15. F. Bergsma and A. J. Staverman, *Discussion Faraday Soc.*, **21**, 61 (1956).
16. H. P. Gregor and D. M. Wetstone, *ibid.*, **21**, 162 (1956).
17. E. Bilberg and T. S. Brun, Universitetet I Bergen, Årbok 1956, Naturvitenskapelig rekke Nr. 11., Bergen 1956.
18. A. T. Di Benedetto and E. N. Lightfoot, *Ind. Eng. Chem.*, **50**, 691 (1958).
19. S. M. Partridge and A. M. Peers, *J. Appl. Chem.*, **8**, 49 (1958); A. M. Peers, *ibid.*, **8**, 59 (1958).
20. T. R. E. Kressman and F. L. Tye, *Discussion Faraday Soc.*, **21**, 185 (1956).
21. Kolthoff and Furman, "Potentiometric Titrations," 2nd ed., John Wiley & Sons, Inc., New York (1931); Kolthoff and Stenger, "Volumetric Analysis," Vol. II, 2nd ed., Interscience Publishers, Inc., New York (1947); Snell and Snell, "Colorimetric Methods of Analysis," Vol. II, 3rd ed., D. Van Nostrand Co., Toronto, New York, and London (1949).
22. C. W. Carr, R. McClintock, and K. Sollner, in preparation.
23. S. R. de Groot, "Thermodynamics of Irreversible Processes," North Holland Publishing Co., Amsterdam (1951).
24. A. J. Staverman, *Trans. Faraday Soc.*, **48**, 176 (1952).
25. T. G. Kirkwood, "Ion Transport across Membranes," H. Clarke, Editor, pp. 119-127, Academic Press, New York (1954).
26. G. Schmid, *Z. Elektrochem.*, **56**, 181 (1952).
27. R. Schlögl, *Z. Physik. Chem.*, N. F. **3**, 73 (1955); R. Schlögl and U. Schödel, *ibid.*, **5**, 372 (1955).
28. K. S. Spiegler, *Trans. Faraday Soc.*, **54**, 1408 (1958).

Surface Coverage during Hydrogen and Oxygen Evolution

P. Rüetschi, J. B. Ockerman, and R. Amlie

Research Center, The Electric Storage Battery Company, Yardley, Pennsylvania

ABSTRACT

The relation between surface coverage and electrode potential during hydrogen and oxygen evolution was studied with inert electrodes of very large surface area. Desorption of gas after interruption of current was followed with micro-volumetric techniques and overvoltage decay was measured simultaneously. The steady-state overvoltage varied linearly with the total amount of hydrogen or oxygen evolved after interruption of current. The true surface area of the electrodes was determined by the BET method, and the capacity was obtained from charging curves. Average effective charges in the double layer per desorbed reacting particle were calculated from these data.

A given (experimentally measurable) over-all Volta potential difference at an electrochemical interface may be established by an infinite number of different charge distributions in the electrode double layer. For the interpretation of transient electrode phenomena (experiments with voltage or current step functions, or a-c techniques) the time-dependence of the charge distribution along the coordinate vertical to the electrode surface, or of the double layer capacity, must be taken into account. Adsorption processes on electrodes are often relatively slow, and it is shown below that considerable time periods may be required to establish steady-state conditions.

Build-up of overvoltage at constant current is generally linear with time over voltage regions extending in some cases over several hundred millivolts if the double layer capacity remains constant during the time period involved (1-6). This is the case if the build-up of the double layer charge is due to accumulation of the same (reacting) species in the same average state (constant distance from electrode interface, constant dipole for adsorption bond) throughout. Changes in the electrode capacity during the charging period (nonlinear charging curves) could result from a variation in specific capacity of a particular species with total Volta potential difference (adsorption state, particularly average distance from the electrode surface varying with potential) or from adsorption of several different species with different specific capacities in such a way that the number of each species in the interface does not vary linearly with over-all Volta potential difference.

The decay of overvoltage after interruption of current becomes, after an initial time period, generally linear with the logarithm of time (1, 4, 6-11). This again can generally be expected only in potential regions where the double layer capacity is constant. This is the case if the number of each species contributing to the charge of the double layer decreases linearly with electrode potential, and if the specific average capacity (adsorption state, distance from electrode surface) is independent of the total Volta potential difference.

Overvoltage in general decays more slowly than expected for an ionic double layer without strong adsorption. The reacting species, maintaining the overvoltage, must be strongly (specifically) adsorbed. Electrodes have the characteristic of maintaining a nonequilibrium concentration of reacting species at the interface over considerable time periods (12). The persistence of nonequilibrium electrode potentials is manifested convincingly by experiments with reversed pulse technique (6). Speculations about the actual configuration of the intermediates (protons, hydrogen molecule ions, atomic hydrogen, surface metal hydrides, molecular hydrogen, for H_2 evolution; and oxygen ions, hydroxyl ions, hydrogen peroxide ions, atomic oxygen, surface oxides, molecular oxygen, for O_2 evolution) on the basis of current-voltage relations only, are not conclusive in view of the fact that (mixtures of) these species might be present in the interface together with foreign inert species, not taking part directly in the reaction. In this connection it is important to point out that there is no such thing as a neutral particle (atom, molecule) in an electrochemical interface. All the surface bonds must have substantial ionic components. This becomes particularly evident from the work function effects of adsorption on solid-gas interfaces (13). The differentiation between atomic and ionic species in the interface is therefore only one of degree and not clear-cut at all. It is the purpose of the present investigation to shed more light on the actual configuration in the electrode interface during hydrogen and oxygen evolution, to study the number and state of adsorbed (activated) species, and to determine the relation between surface coverage and overvoltage. Particular consideration is given to time effects due to slow adsorption phenomena.

Theory

The electrode reaction of gas evolution can be described approximately by the rate equation (13)

$$i = A \exp \{-\alpha Z_i e\, V/kT + \alpha Z_i e\, V_r/kT - (\epsilon^* - \epsilon^\circ)/kT\} \quad [1]$$

where i is the current density, A a factor independent of potential, α the transfer coefficient, $Z_i e$ the

charge of the reacting species in the interface, $V = \psi_I - \psi_{II}$ the Volta potential difference between electrode I and solution II, $V_f = (\psi_I - \psi_{II})_f$ the Volta potential difference at which the number of the reacting species in the interface becomes zero,[1] and $\epsilon^* - \epsilon^\circ$ the covalent adsorption energy of the reacting species.[2] The transfer coefficient α is given by $\alpha = (1/2)(1 - \gamma) = 1/2 - \gamma/2$, where γ is the fraction of the variation of electrode polarization due to inert foreign species according to the theory of Rüetschi (21). The factor A is given by $A = \nu Z_i e \delta n_i$, where ν is a jump frequency and δ the thickness of the reaction zone, and n_i the concentration of the reacting ions in the bulk of the solution (number per cm^3). The instantaneous current, during build-up or decay of overvoltage, is given by

$$i = C\,dV/dt = C\,d(\psi_I - \psi_{II})/dt \qquad [2]$$

where C is the double layer capacity. Combining [1] and [2] and integrating at constant C, one obtains

$$V = \frac{kT}{\alpha Z_i e} \ln \left\{ \frac{tA\alpha Z_i e}{CkT} \exp\left[\frac{\alpha Z_i e V_f}{kT} - \frac{\epsilon^* - \epsilon^\circ}{kT} \right] + \exp\left[\frac{\alpha Z_i e V_o}{kT} \right] \right\} \qquad [3]$$

where $V_o = (\psi_I - \psi_{II})_o$ is the Volta potential difference of the electrode at zero time (beginning of build-up or decay).

If the time t is sufficiently long, the second term in braces can be neglected, and the potential decays on open circuit linearly with logarithm of time.

$$dV/d \ln t = \pm kT/\alpha Z_i e \qquad [4]$$

During constant current charge, the potential increases linearly with time, if C is constant, according to Eq. [2].

$$V = it/C + V_o \qquad [5]$$

In the present paper Eq. [1] to [5] were tested experimentally for hydrogen and oxygen evolution. Deviations from these equations demonstrate the influence of voltage and time effects on the capacity C. Experiments on overvoltage decay were coupled with gas desorption measurements. Such measurements give information about the amount of partially or completely discharged reacting species in the interface.

It should be pointed out here that the behavior of an electrode interface can be described quite accurately with the simple model of a condenser. Each species on the electrolyte side of the interface contributes a characteristic charge to the double layer, and contributes through its specific average capacity in a characteristic way to the total Volta electrode potential difference of the electrode. The total charge is compensated on the electrode side of the interface by an excess or deficiency of electrons, depending on whether the electrode is on the negative or positive side of the zero charge potential. The double layer capacity remains constant only if each species has a constant specific capacity, independent of the total Volta potential difference, and if the number of each species varies linearly with total Volta potential difference.

Equations [1] to [5] imply a reacting species, with charge $Z_i e$, whose energy in the double layer can be compared with its energy in the bulk of the electrolyte. For hydrogen evolution in acid solution, it is convenient to define the proton as reacting species. The charge of the double layer on the solution side in sulfuric acid, e.g., is due to reacting protons, SO_4^{--} ions and overlapping electrons (partially discharged hydrogen ions, or polarized hydrogen atoms). Then $Z_i = 1$, and α is determined by the relative contribution of SO_4^{--} ions and electrons (and conceivably other charged species) to the variation of the electrode potential (21). After having defined the reacting species, Eq. [1] and [4] allow calculation of $\alpha = (1/2)(1 - \gamma)$ from experimental data. A priori, only the product αZ_i can be determined experimentally, but not the individual components γ and Z_i. Only after definition of the reacting species is γ determined. If, in the case of H_2 evolution, the variation in polarization is due to accumulation of reacting protons only, $\gamma = 0$ and $\alpha = \frac{1}{2}$.

For oxygen evolution in acid solution one can define the reacting species as the hypothetical O^{--} ion. On the solution side of the double layer, this ion can be associated with protons (producing OH^- or H_2O), or with overlapping electron holes (producing partially discharged species like O^-, O, O_2^{--}, O_3^-, O_3) or both, producing HO_2^-, and H_2O_2. The charge on the solution side is therefore due to O^{--} and associated foreign species (including SO_4^{--} and ions of the metal). If the variation in polarization due to foreign species were zero, then $\gamma = 0$ and $\alpha = \frac{1}{2}$. If the variation in polarization were due entirely to OH^- ions, each O^{--} is associated with *one* proton and $\gamma = -1$. Since $Z_i = 2$, $(\frac{1}{2})(1 - \gamma)Z_i = 2$ and $\alpha = 1$. To demonstrate that the choice of the reacting species is not arbitrary, one could assume OH^- as the reacting species and variation of polarization due to accumulation of OH^- ions only. Then $Z_i = 1$, $\gamma = 0$, $\alpha = \frac{1}{2}$, and thus $(\frac{1}{2})(1 - \gamma)Z_i = \frac{1}{2}$. This shows that α depends on the choice of the reacting species.

In the following discussion we shall adopt $Z_i = 1$ for hydrogen and 2 for oxygen, since these are the charges actually required to liberate one atom of the gases from their state in the bulk of the solution. The experimental results then yield values for γ, which is a measure of the contribution of foreign species (other than H^+ or O^{--}, respectively) to the variation of polarization for H_2 and O_2 evolution. The factor γ can theoretically assume any value between $-\infty$ and $+1$ (21).

Measurements of build-up of overvoltage at constant current give information about the total capacity of the double layer. Capacity is measured here by the voltage change produced by an external known current. During overvoltage decay, the instantaneous internal current cannot be measured directly, but it is reasonable to assume that it is adequately described by [1].

[1] The potential V_f was denoted V_{if_0} in an earlier theoretical paper (21).

[2] Only changes in $V = \psi_I - \psi_{II}$ are measured in overvoltage studies: $\Delta V = \Delta|\psi I - \psi II| = \Delta\eta$, where η is the overvoltage. In this paper the reference electrodes to which overvoltages are referred are the reversible Pb/$PbSO_4$ and PbO_2/$PbSO_4$ electrodes.

It is necessary to define the term capacity as the charge transferred per unit voltage change. During fast charging, an outer layer of ions is built up at the interface. As time proceeds, part of these ions are brought closer to the interface and are partially discharged. This results in an apparent increase in capacity. Only the gas actually leaving the interface does not contribute anything to the charge of the double layer. In the present paper, the capacities were determined from relatively slow charging curves, which means that they are essentially the capacities for an average adsorption state. On open-circuit decay, an ionic, outer double layer would require theoretically 2 or 4 electronic charges to produce one molecule of H_2 or O_2. Actually, less charge may be required for species already partially discharged in the interface. The amount of gas desorbed in excess of the amount expected for an ionic type double layer is a measure of the number and state of adsorbed and partially discharged reacting species. Thus, even for constant capacity (voltage changing linearly with current-time product) the amount of gas desorbed need not be linear with the amount of electricity passed, nor with the voltage change.

Experimental

To obtain measurable amounts of gas during overvoltage decay, inert electrodes of large surface are required. In the present study, the electrodes were sections of storage battery plates. The electrode for the hydrogen evolution studies consisted of pure metallic sponge lead, with a grid of a lead-calcium alloy (0.075% Ca by weight) and was 7.5 cm high, 3.6 cm wide, and 0.55 cm thick. The total weight of the electrode was 70.00 g. The electrode for the oxygen evolution studies was a PbO_2 sponge plate with a lead-calcium grid alloy (0.075% Ca by weight) and 4.0 cm high, 2.0 cm wide and 0.60 cm thick, weighing 44.02 g. It should be pointed out that PbO_2 is an excellent material for the study of oxygen overvoltage since it cannot be oxidized to a higher oxide and since it has a low electronic resistivity (*ca.* 10^{-4} ohm-cm).

The large-area electrode is shown in Fig. 1 at B. The electrolyte was 5*M* H_2SO_4 prepared from triply distilled water and purified acid. The electrolyte level (E) was adjusted to allow a minimum amount of dead space. Electrode potentials were measured against a sealed mercurous sulfate reference electrode in 5*M* H_2SO_4. The large-area electrodes were polarized by means of a polarizing electrode of pure lead (A). During polarization at constant current, both stopcocks in Fig. 1 were kept open. The electrodes were polarized at small current densities over prolonged time periods prior to the actual experiments on decay and build-up of overvoltage, to remove $PbSO_4$ from the surfaces.

Build-up of overvoltage at constant current and decay of overvoltage on open circuit were followed with an electrometer amplifier (General Radio Voltmeter Amplifier 1230-A) driving a high-speed recorder [Brown-Honeywell Model Y 153 X (19) VX 156] with a precision of 1 mv, current drains of less than 10^{-13} amp, and with a response of 1 mv in 20 msec. Constant current was obtained from an

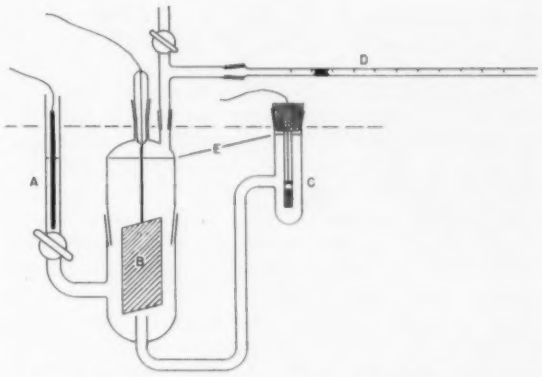

Fig. 1. Cell for overvoltage and gas desorption measurements. A, polarizing electrode; B, large area electrode under study; C, reference electrode; D, capillary; E, electrolyte level.

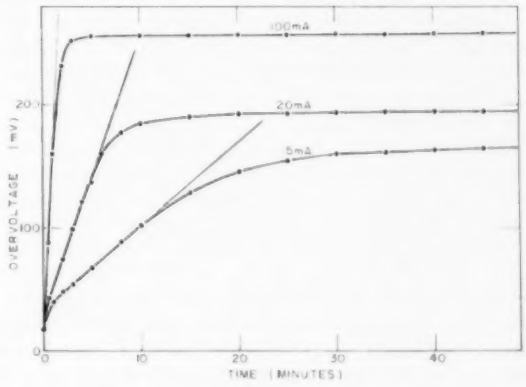

Fig. 2. Build-up of oxygen overvoltage on PbO_2 at constant currents, in 5.0M H_2SO_4 at 30°C.

electronic circuit described earlier (14). To minimize any changes in electrode surface, the electrode potentials were never allowed to reach reversible values. The reversible potential of the $PbO_2/PbSO_4$ electrode in 5*M* H_2SO_4 is 1.704 v vs. H_2 (or 1.111 v *vs.* Hg/Hg_2SO_4) in the same solution. During oxygen overvoltage decay the potential was allowed to reach a value of 1.717 v vs. H_2 (13 mv above the reversible $PbO_2/PbSO_4$ potential). At this point the charging current was switched on again and the constant current charging curves were obtained (Fig. 2). In this manner, specific adsorption effects due to SO_4^{--} ions were minimized. It is known that SO_4^{--} ions are adsorbed on PbO_2 between 1.70 and 2.0 v vs. H_2, and that above this potential adsorption does not change much (15). A similar procedure was followed during hydrogen overvoltage studies on metallic lead. The reversible potential of the $Pb/PbSO_4$ electrode −0.372 v vs. H_2 (or −0.965 v vs. Hg/Hg_2SO_4) in 5*M* H_2SO_4. During decay of overvoltage the potential was allowed to reach a value of −0.392 v vs. H_2 (20 mv more negative than the reversible potential). This decreased the effects of SO_4^{--} adsorption; however, these effects were nevertheless pronounced, which is understandable since the zero charge potential of metallic lead is at about −0.7 v vs. H_2 (16). Only at potentials negative to this value can the polarization be expected to be due predominantly

to accumulation of H^+ ions. In the case of the $PbO_2/PbSO_4$ electrode the zero charge potential in $5M$ H_2SO_4 is at $+1.70$ to $+1.75$ v vs. H_2 (17, 18). This indicates that SO_4^{--} adsorption is less noticeable for the oxygen overvoltage experiments. This was confirmed experimentally. Gas desorption from the electrodes was measured from the displacement of a dibutylphthalate drop in a 1 cm^3 Pyrex capillary, calibrated in units of 1/100 cm^3. After interruption of the polarizing current, the stopcocks were closed instantaneously and the position of the dibutylphthalate drop followed with time. Volume corrections for atmospheric pressure changes were made by simultaneously following a drop in a second capillary attached to a cell with the same dead-space, but without electrodes. The whole system was carefully thermostated to $\pm$ 0.05°C.

At the end of the measurements the electrodes were washed carefully with distilled water and ethyl alcohol and dried quickly in a vacuum desiccator containing $CaCl_2$. The surface areas of the electrodes were determined by standard BET techniques and yielded 35.2 m^2 for the PbO_2 electrode and 15.9 m^2 for the Pb electrode.

Overvoltage studies on porous electrodes can lead to different results from smooth electrodes due to the nonuniform current distribution over the true surface area (19). If the ohmic drop due to current flow in the pores cannot be neglected in comparison with the polarization at the interface, the porous electrode will show different polarization characteristics. According to Ksenzhek and Stender (20) the overvoltage η varies with distance x from the surface of the porous electrode toward the interior according to

$$\eta = 4b \tanh^{-1} [\exp (-x/\sqrt{b/2Si_o\rho}) \tan (\eta_o/4b)] \quad [6]$$

where i_o is the exchange current density, ρ the electrolyte resistivity, S the specific surface area of the porous electrode in cm^2/cm^3, and $b = RT/\alpha$ **ZF** (Tafel slope/2.303); η_o is the apparent overvoltage at the surface of the porous electrode, and η the true overvoltage at the reaction interface. The penetration depth x_o, where the true current density has fallen to $1/e$ of the apparent value, is $x_o = \sqrt{b/2Si_o\rho}$. For our experiments, with $b = 0.05$, $S = 50{,}000$ cm^2/cm^3, $i_o = 10^{-9}$ amp/cm^2, $\rho = 1$ ohm-cm, the penetration depth becomes 22.4 cm. This is 100 times the value of the half-thickness of our porous plates. This shows that pore-structure effects should be negligible in our experiments.

Results

The electrodes were polarized at constant current to a steady-state overvoltage. The corresponding Tafel plots are shown in Fig. 3. Here overvoltage is referred to the reversible $Pb/PbSO_4$ potential for hydrogen evolution, and to the reversible $PbO_2/PbSO_4$ potential for oxygen evolution. These are the stable electrode potentials the electrodes would actually reach on prolonged open circuit. The current densities refer to the total BET electrode surface. Hydrogen overvoltage increases slowly over many hours. If overvoltages are measured over short time intervals, the Tafel slope is 0.120 v i.e.,

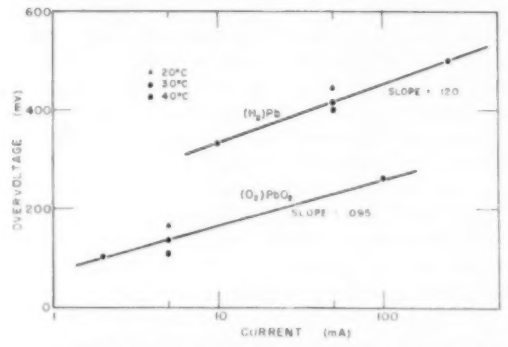

Fig. 3. Tafel curves for hydrogen overvoltage on lead and oxygen overvoltage on PbO_2. Overvoltage measured against reversible $Pb/PbSO_4$ and $PbO_2/PbSO_4$ electrodes, respectively, in 5.0M H_2SO_4 at 20°, 30°, and 40°C.

with $Z_i = 1$, $\gamma = 0$, and $\alpha = \frac{1}{2}$ (Fig. 3). The change in overvoltage from one current density to another is then simply due to accumulation of reacting species only, according to the theory of Rüetschi (21). If, on the other hand, the Tafel curve is taken slowly, allowing longer time periods for each current, the slope increases to 0.160 v in the voltage region of Fig. 3. This means that now slowly adsorbing or desorbing foreign species are contributing to changes in the charge of the double layer (desorption of SO_4^{--} ions), or that the reacting species have a smaller specific capacity (larger distance to the electrode surface) such that for a given number of reacting species in the interface, the electrode potential is higher than before. From the slope 0.160 v one obtains $\alpha = 0.37$ and $\gamma = 0.25$. The latter is the fraction of variation of polarization attributable to desorption of SO_4^{--} or changes in specific capacities of reacting protons (21).

In Fig. 3, oxygen overvoltage has a Tafel slope of about 0.095 v, depending again somewhat on the rate of taking the curve. However, adsorption effects are smaller than for hydrogen on lead, which can be explained on the basis of the relative position of the zero charge potentials. With $Z_i = 2$ one obtains from the Tafel slope $\alpha = 0.32$ and $\gamma = 0.37$. The latter fraction of voltage change from one current to another, is attributable to adsorption or association of foreign species, such as SO_4^{--} (along with the reacting species O^{--}), or changes in specific capacity of reacting species (21). Considering the large surface areas of the electrodes the true current densities are extremely low, in the order of 10^{-6} to 10^{-9} amp/cm^2. However, the exchange currents for hydrogen and oxygen evolution on these electrodes are in the order of 10^{-12} and 10^{-10} amp/cm^2, and therefore the experiments fall into the Tafel region. Measurements of the gas evolved at steady state showed that 97% or better of the current went into gas production, and therefore, no other charging reactions interfered.

Figure 2 shows oxygen overvoltage build-up at constant current. From the slopes of the linear portions one obtains a capacity of 44 farads for the double layer. With a BET surface of 35.2 m^2, this is 125 $\mu F/cm^2$, a relatively high value, which would be even higher if only part of the surface were elec-

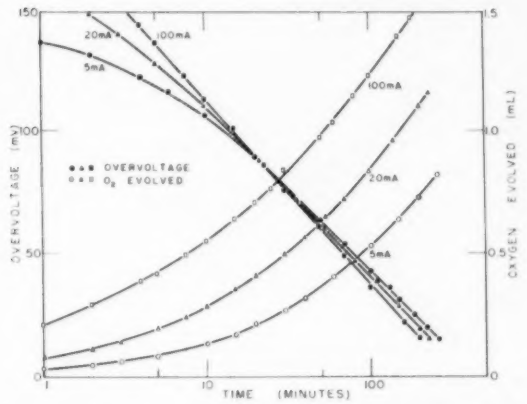

Fig. 4. Decay of oxygen overvoltage on PbO_2 for various prepolarizing currents and oxygen gas desorbed; temperature 30°C.

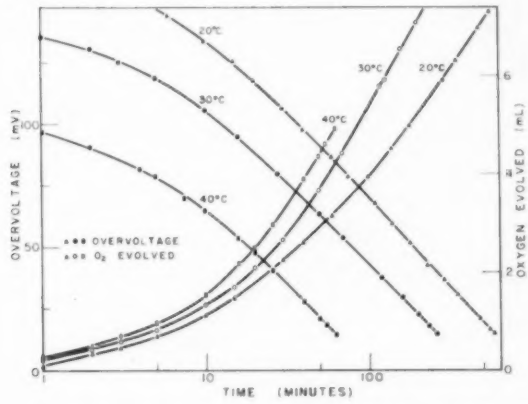

Fig. 5. Decay of oxygen overvoltage on PbO_2 at various temperatures and oxygen gas desorbed. Prepolarizing current 5 ma.

trochemically active. The high value for the capacity indicates strong adsorption of the reacting species. There is a slight bend in the initial portion of the charging curve indicating a small variation in capacity due to a different initial charge distribution.

Figures 4 and 5 show oxygen overvoltage decay on open circuit, and simultaneous gas desorption. Oxygen overvoltage decreases linearly with the logarithm of time, indicating a fairly constant capacity during decay. The decay slope is almost independent of temperature and of prepolarizing current. Figure 4 indicates that at the same temperature (30°C) a given voltage is reached in the same time, independently of prepolarizing current. According to Fig. 5 the desorption rate increases with temperature. In Fig. 6 the logarithm of the gas evolution rate in cm^3/min is plotted against $1/T$ for given overvoltage values. The slopes of the straight lines tend to become less steep with increasing overvoltage. If the rate of O_2 evolution could be set equal to the instantaneous internal current, then the slopes would be, according to Eq. [1], a measure for the term $-\{\alpha Z_i eV - \alpha Z_i eV_f + \epsilon^* - \epsilon^\circ\}/2.303\ k$. A plot of this term against overvoltage should then yield a straight line with a slope of $-\alpha Z_i e/2.303\ k$ $= 5010\ \alpha Z_i$. One could then determine the value of αZ_i by this method, but the accuracy of the measurements is not sufficient to obtain an exact value, although one obtains the correct order of magnitude ($\alpha Z_i = 1 \pm 2$). However, the instantaneous internal current cannot be set equal to the instantaneous gas evolution rate, at 2 electrons per H_2 and 4 electrons per O_2. The slope of the oxygen overvoltage decay curves in Fig. 4 and 5 is about 0.078 v, which is fairly close to the value of the Tafel slope. With $Z_i = 2$ this gives $\alpha = 0.38$ and $\gamma = 0.23$.

In Fig. 7 the results of Fig. 4 have been correlated in such a manner that the total oxygen evolved has been plotted against overvoltage. A voltage of +13 mv above the reversible $PbO_2/PbSO_4$ potential has been chosen arbitrarily for the endpoint of decay. It seems reasonable to assume that at this low value the same state of the electrode surface is reached, independently of prepolarizing current.

Since 1 cm^3 of O_2 at 700 mm Hg and 30°C corresponds to 15.5 amp sec, one can calculate how the voltage should decay, at 2 electrons per oxygen atom, if only a discharge of the double layer capacity of 44 farads were involved. One cm^3 of O_2 evolved should then decrease the potential by 350 mv. In Fig. 7, this theoretical slope has been plotted, marked with 2*e*. Other slopes, corresponding to 1*e* and 0.5*e* per oxygen atom are also indicated. It is

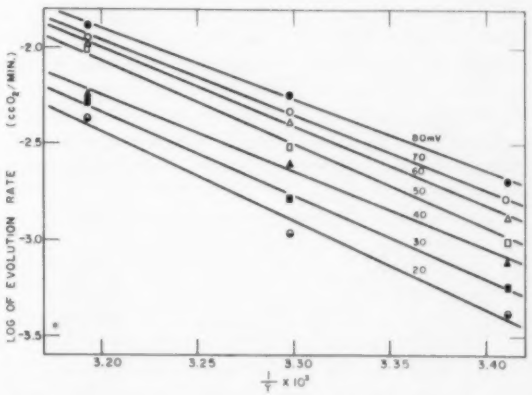

Fig. 6. Logarithm of oxygen gas evolution rates on PbO_2 on open circuit (in cm^3/min) as a function of $1/T$ for various fixed values of overvoltage.

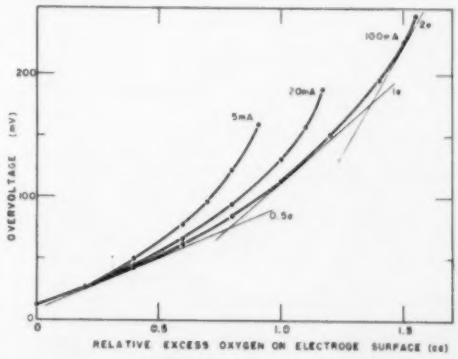

Fig. 7. Oxygen overvoltage decay on PbO_2 as a function of oxygen gas desorbed from the electrode at 30°C.

Table I. Observations on PbO_2 anode

Prepolarizing current, ma	Overvoltage, mv vs. $PbO_2/PbSO_4$	Oxygen atoms desorbed per BET cm^2
100	242	2.12×10^{14}
20	190	1.61×10^{14}
5	158	0.91×10^{14}

interesting to note that for the initial portions of overvoltage decay, the slope approaches the value for 2*e*. However, for later portions, the voltage decay is much smaller, the difference being a measure for the amount of oxygen already partially discharged. A slope of 2*e* could indicate the discharge of 2 OH^- or O^{--} in the outer double layer.

There is another important result in Fig 7. The slope of the plot of the steady-state overvoltage against the total amount of oxygen desorbed gives a straight line. The slope of this line could be interpreted theoretically by postulating the presence of oxygen species with an average charge of about 1*e* per atom in the double layer, although such an interpretation is not rigorous. If the total amount of oxygen desorbed is related to the BET surface of the electrode, one obtains the figures of Table I (1 cm^3 O_2 at 760 mm Hg, 30°C contains 4.84×10^{19} atoms).

Build-up of hydrogen overvoltage on lead at constant current is shown in Fig. 8. From the slope of the linear portion one obtains a capacity of 1.67 farad. With a BET surface of 15.9 m^2, this is 10.5 $\mu F/cm^2$, a small value, indicating that the charges are at considerable distance from the surface. Since the charging was done at relatively low rates, this capacity does probably include some changes in SO_4^{--} adsorption and adsorption capacities due to partially discharged protons.

Figures 9 and 10 give hydrogen overvoltage decay curves and gas evolution curves. Decay of hydrogen overvoltage is nearly linear with the logarithm of time, indicating a nearly constant capacity. The decay slope is almost independent of temperature and prepolarizing current. The temperature has a smaller effect on the rate of desorption than for oxygen. In Fig. 11, the logarithm of the hydrogen evolution rate (cm^3/min) is plotted against $1/T$. The

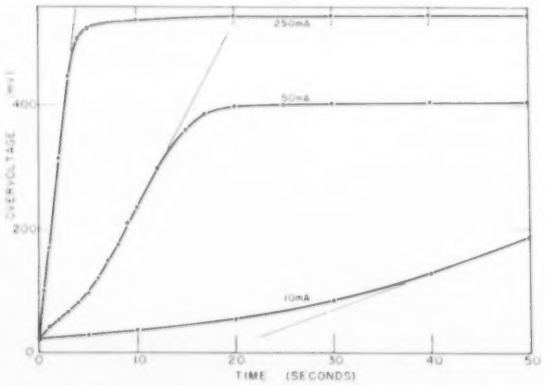

Fig. 8. Build-up of hydrogen overvoltage on Pb at constant currents. Electrolyte 5.00M H_2SO_4 at 30°C.

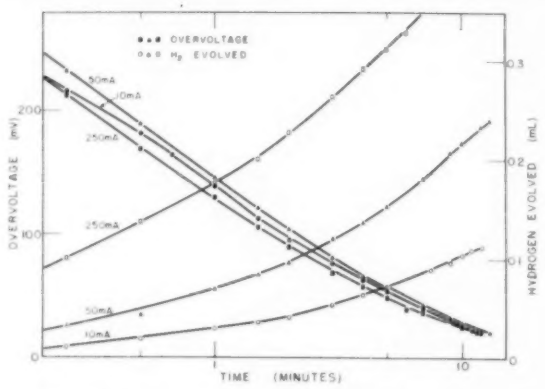

Fig. 9. Decay of hydrogen overvoltage on Pb and hydrogen gas desorbed, for various prepolarizing currents at 30°C.

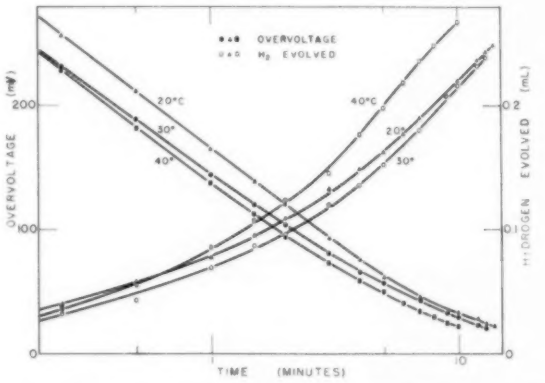

Fig. 10. Decay of hydrogen overvoltage on Pb and hydrogen gas desorbed at various temperatures; prepolarizing current 50 ma.

slopes of the lines are nearly equal but tend to decrease with increasing overvoltage. The variation in the slopes would be a measure for αZ_i if the instantaneous current were equal the rate of gas evolution, which is not exactly the case. One can derive however the right order of magnitude ($\alpha Z_i = 0.5 \pm 1$), although the method is not precise.

The slope of the hydrogen overvoltage decay curves in Fig. 9 and 10 averages 0.145, which is close to the slope of the Tafel curve, when it is taken slowly. The value 0.145 gives with $Z_i = 1$ values for $\alpha = 0.41$ and $\gamma = 0.17$. This shows that the variation in polarization due to foreign species (e.g., adsorption of SO_4^{--} during decay) or the influence of partially discharged hydrogen is not excessive, according to Rüetschi's theory (21).

In Fig. 12 the total amount of H_2 desorbed after interruption of current (to a potential 20 mv more negative than the Pb/$PbSO_4$ electrode) was plotted against overvoltage decay. At the end of decay, the same state of the electrode is reached, independently of prepolarizing current. Since 1 cm^3 of H_2 at 760 mm Hg and 30°C corresponds to 7.75 amp sec at 1*e* per H, one can calculate that 1 cm^3 of H_2 should discharge 1.67 farad by 4.65 v. This theoretical slope between the hydrogen evolved and overvoltage decay is shown in Fig. 12 as a line marked with 1*e*. This is the theoretical decay of the voltage if each

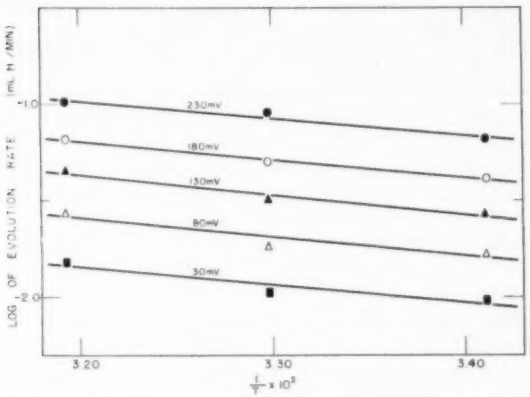

Fig. 11. Logarithm of gas evolution rates on Pb on open circuit (in cm³/min) as a function of 1/T for various fixed values of overvoltage.

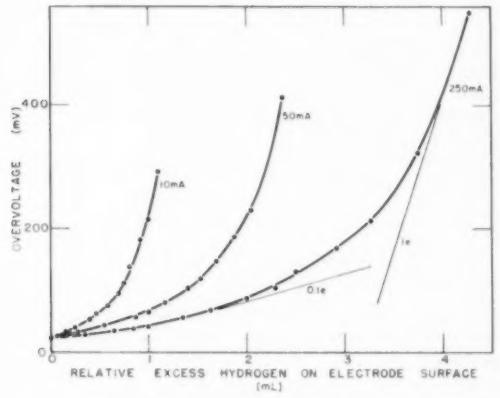

Fig. 12. Hydrogen overvoltage decay on Pb as a function of hydrogen gas desorbed from the electrode at 30°C.

hydrogen atom desorbed were to originate from a proton in a double layer with a capacity of 10.5 μF/cm². For the initial portion of the decay, the voltage decreases according to this theoretical slope. However, for later portions, the potential decreases much less. The difference between the theoretical slope of 1e and the experimental values is a measure of the already partially discharged hydrogen in the surface (overlap of H^+ and electron cloud). This hydrogen contributes to the charge of the double layer only by the heteropolarity of the adsorption bonds. Toward the end of the decay, the potential is determined largely by the adsorption of SO_4^{--} ions, as in the case of the oxygen overvoltage SO_4^{--} become the potential determining species at the reversible potential.[8]

During decay of H_2 and O_2 overvoltages, the potentials approach asymptotically the reversible $Pb/PbSO_4$ and $PbO_2/PbSO_4$ potentials, respectively, while H_2 and O_2 evolution are continuing at a small but steady rate since the $Pb/PbSO_4$ potential is negative to the potential of the hydrogen electrode and the $PbO_2/PbSO_4$ potential positive to the oxygen electrode (self-discharge).

[8] Note that the diffusion of adsorbed gas along the grain surfaces of the porous electrodes to the locations of bubble formation might be interfering with the simple interpretation of the results given in this paper.

Table II. Observations on Pb cathode

Current, ma	Overvoltage, mv, vs. $Pb/PbSO_4$	Hydrogen atoms desorbed per BET cm²
250	553	13.0×10^{15}
50	410	7.2×10^{15}
10	293	3.3×10^{15}

The steady-state overvoltage prior to interruption of current varies, according to Fig. 12, linearly with the total amount of hydrogen evolved. The slope of this line corresponds roughly with the slope of a line calculated for a theoretical discharge of a double layer of 10.5 μF/cm² at 0.5 electron for each hydrogen atom desorbed. This could be interpreted as resulting from a mixture of adsorbed H atoms and protons in the double layer, or the presence of H_2^+. The significant fact is that more hydrogen is desorbed than one could expect from the discharge of a purely ionic type double layer, indicating the presence of partially discharged reacting species.

The total amount of H_2 evolved from the electrode during hydrogen overvoltage decay, down to a potential 20 mv more negative than the $Pb/PbSO_4$ potential, has been correlated to the BET surface. Since 1 cm³ of H_2 at 760 mm Hg at 30°C contains 4.84 x 10^{19} atoms, the figures of Table II were obtained.

Basically, the same laws apply both to hydrogen and oxygen overvoltage. In either case, the electrode potential (overvoltage) seems to be determined essentially by the number of adsorbed activated species at the interface, these species being present in various states of discharge, and by adsorbed foreign inert species, not taking part directly in the electrode reaction (21). Desorption follows a Becker-Zeldovich equation, which is coherent with a Temkin isotherm (13).

Acknowledgments

The authors are indebted to W. J. Burgess and M. L. Block of the Physical Chemistry Division for assistance in BET measurements, and to C. G. Grimes, Director of Research of the Electric Storage Battery Company, for permission to publish this investigation.

Manuscript received June 8, 1959. This paper was prepared for delivery before the Philadelphia Meeting, May 3-7, 1959.

Any discussion of this paper will appear in a Discussion Section to be published in the December 1960 JOURNAL.

REFERENCES

1. E. Baars, *Marburger Sitzungsberichte*, **63**, 214 (1928).
2. A. Frumkin and S. Slygin, *Acta Physicochim., URSS*, **5**, 819 (1936).
3. F. P. Bowden and K. E. W. Grew, *Discussion Faraday Soc.*, **1**, 91 (1947).
4. L. M. Elina, T. I. Borisova, and T. I. Zalkind, *Zhur. Fiz. Khim.*, **28**, 785 (1954).
5. M. Breiter, C. A. Knorr, and W. Volkl, *Z. Elektrochem.*, **59**, 681 (1955).
6. P. Rüetschi, R. T. Angstadt, and B. D. Cahan, *This Journal*, **106**, 547 (1959).
7. G. Armstrong and J. A. Butler, *Trans. Faraday Soc.*, **29**, 1261 (1933).
8. A. Frumkin, *Acta Physicochim. URSS*, **18**, 23 (1943).

9. W. R. Busing and W. Kauzmann, *J. Chem. Phys.*, **20**, 1129 (1952).
10. J. O'M. Bockris and A. K. M. Shamshul Huq, *Proc. Roy. Soc.*, **A237**, 277 (1956).
11. A. L. Pitman and G. W. Work, NRL Reports No. 4844, 4845, 4852, 5031 (1956-1957), Naval Research Laboratory, Washington, D. C.
12. W. Gutt, and D. J. G. Ives, *Proc. Chem. Soc.*, p. 344, Dec. 1957.
13. P. Rüetschi, *This Journal*, **106**, 819 (1959).
14. P. Rüetschi and B. D. Cahan, *ibid.*, **104**, 406 (1957).
15. I. G. Kiseleva and B. N. Kabanov, *Doklady Akad. Nauk SSSR*, **108**, 864 (1956).
16. Y. M. Kolotyrkin and N. Y. Bune, *Zhur. Fiz. Khim.*, **29**, 435 (1955).
17. B. N. Kabanov, I. G. Kiseleva, and D. I. Leikis, *Doklady Akad. Nauk, SSSR*, **99**, 805 (1954).
18. D. I. Leikis and E. K. Venstrem, *ibid.*, **112**, 97 (1957).
19. A. N. Frumkin, *Zhur. Fiz. Khim*, **23**, 1477 (1949).
20. O. S. Ksenzhek and V. V. Stender, *Doklady Akad. Nauk SSSR*, **107**, 280 (1956).
21. P. Rüetschi, *This Journal*, Under consideration.

A Study of the Factors Affecting the Electrical Characteristics of Sintered Tantalum Anodes

G. L. Martin,[1] C. J. B. Fincham, and E. E. Chadsey, Jr.

National Research Corporation, Cambridge, Massachusetts

ABSTRACT

Measurements were made of the electrical characteristics (d-c leakage, capacitance, and equivalent series resistance) of anodically oxidized sintered tantalum pellets, which were made from three tantalum powders of different purities, particle shapes, and particle size distributions. The apparent densities of the pellets after sintering were also measured. The effects of varying the pressed density of the pellets and the time and temperature of sintering were studied systematically, and the results were correlated in the form of empirical relationships.

A tantalum electrolytic capacitor is composed of three basic parts: the tantalum anode, the tantalum oxide dielectric, and the electrolyte which acts as the cathode.

The tantalum anode may be foil, wire, or a sintered porous pellet made from powder. The sintered pellet can give the highest surface area per unit volume and hence the highest capacitance per unit volume of the three types. The tantalum oxide dielectric is formed by anodic oxidation of the tantalum anode. The cathode is an electrolyte, which may be either liquid (e.g., aqueous solutions of sulfuric or phosphoric acids) or solid (e.g., manganese dioxide). References (1-3), for example, give more detailed descriptions of the construction and operation of tantalum capacitors.

This paper reports a study of some of the factors, especially sintering conditions, which affect the electrical properties of porous sintered tantalum anodes and their oxide films. The electrical properties studied were d-c leakage, which is defined as the current which flows when a specified d-c voltage is impressed across the anode and its oxide film; the capacitance, which varies with the surface area and thickness of the oxide film; and the equivalent series resistance (*ESR*), which was calculated from the measured dissipation factor (*D*) using the relationship

$$ESR = \frac{D}{2\pi f C}$$

where *C* is the capacitance (in farads), *f* is the frequency of the a-c signal (in cps), and *ESR* is given in ohms.

[1] Present address: Department of Chemistry, University of Alabama, University, Alabama.

Experimental Techniques

Pressing.—The tantalum powder was pressed into cylindrical pellets of 0.25 in. diameter in a floating-body steel die. No lubricant or binder was used. The pellets all weighed 1.8 g. Annealed 10-mil tantalum lead wires were pressed into the pellets.

Sintering.—The pressed pellets were sintered inside a closed tantalum can, in a modified NRC 2904 resistance-heated vacuum furnace. Temperature was measured with a tungsten-molybdenum thermocouple with the hot junction resting on top of the tantalum can. Temperatures measured in this way were probably lower than the true temperatures of the pellets in the can. The furnace was pumped, through a cold trap, to a pressure of about 5×10^{-5} mm Hg (and a leak rate of less than 10^{-3} mm Hg/min into a volume of about 40 liters) before the power was turned on. At the end of a run, the charge was allowed to cool to about 200°C under vacuum; then argon was admitted. The furnace was not opened to air until the charge temperature was less than 100°C.

Electrical testing.—The sintered pellets were anodized at a constant current of 35 ma/g up to 200 v, in an 0.01% phosphoric acid solution at 92°C. They were held at 200 v for 2 hr. The maximum voltage determined the thickness of the oxide film and hence its capacitance per unit area. At 200 v the thickness of the oxide film is about 0.3 μ (4).

The anodized pellets were washed for ½ hr in de-ionized water and dried in air overnight at room temperature.

Measurements of d-c leakage, capacitance, and dissipation factor were done using 10% phosphoric acid at room temperature as electrolyte.

Direct current leakage was measured after 2 min at 140 v. Capacitance and dissipation factor were measured at 120 cps with a 0.5 v a-c signal, using a modified General Radio 650-A impedance bridge. The signal source was a Hewlett Packard 205 AG audio signal generator, and a Hewlett Packard 400D vacuum tube voltmeter was used as the null detector.

Sinter densities.—The apparent densities of the pellets after sintering were determined by measuring the diameters and lengths of the pellet at several places on the pellet with a pointed end micrometer.

This method was found to give results agreeing well (within 1%) with measurements made by coating the pellets with nail polish and weighing them in air and water.

Materials

Three different tantalum powders were selected for study, and were given the designations E-11, SG-73R, and L-533. As discussed below, there were considerable differences between these powders in chemical purity, particle size distribution, and particle shape.

Chemical purity.—The analyses of the three powders are given in Table I. The impurities showing the widest differences in levels between the powders are O, C, N, Fe, Cr, Si, and Na. In general, SG-73R was the most pure, and L-533 the least pure, of the three powders.

Table I. Analyses of tantalum powders

Impurity	Impurity content, ppm		
	E-11	SG-73R	L-533
O	720	480	930
H	10	10	50
C	25	25	120
N	25	30	750
Fe	100	87	460
Ni	<100	52	25
Cr	61	110	<10
Si	560	81	780
Al	<50	<50	<50
Nb	220	120	140
Na	1500	30	—
Cu	<50	<50	<50
Ti	<50	<10	40
Zr	<50	<50	<50
Mo	<100	<25	<25

< Means below the limit of detection by method used.

Table II. Particle size distribution

Screen mesh	Particle size, μ	Weight per cent in fraction		
		E-11	SG-73R	L-533
+60	>250	—	—	8.6
−60+100	250-150	—	—	8.0
−100+200	100-74	—	—	16.5
−200+325	74-44	12.7	2.5	13.2
−325				
	44-36	1.7	1.0	0.5
	36-30	6.1	4.1	0.3
	30-25	10.5	10.4	1.9
	25-20	14.0	15.7	4.2
	20-15	17.4	24.5	7.4
	15-10	19.7	27.6	18.6
	10-5	13.7	10.6	17.4
	5-0	0.6	0.9	2.0
	Totals	96.4	97.3	98.6

Particle size measurements below 44μ were done using a Roller subsieve particle size analyzer.

Particle size distributions.—These are shown in Table II. Measurements of particle size above 44 μ were done by screen analysis, and below 44 μ by using a Roller subsieve particle size analyzer (5). L-533 differed from the other two powders in having a considerable amount of material in the greater than 74 μ range. In general SG-73R had the lowest average particle size, and L-533 the highest, of the three powders. However, in view of the particle shapes (see below) of L-533, the measurements of particle size for this material are of doubtful significance.

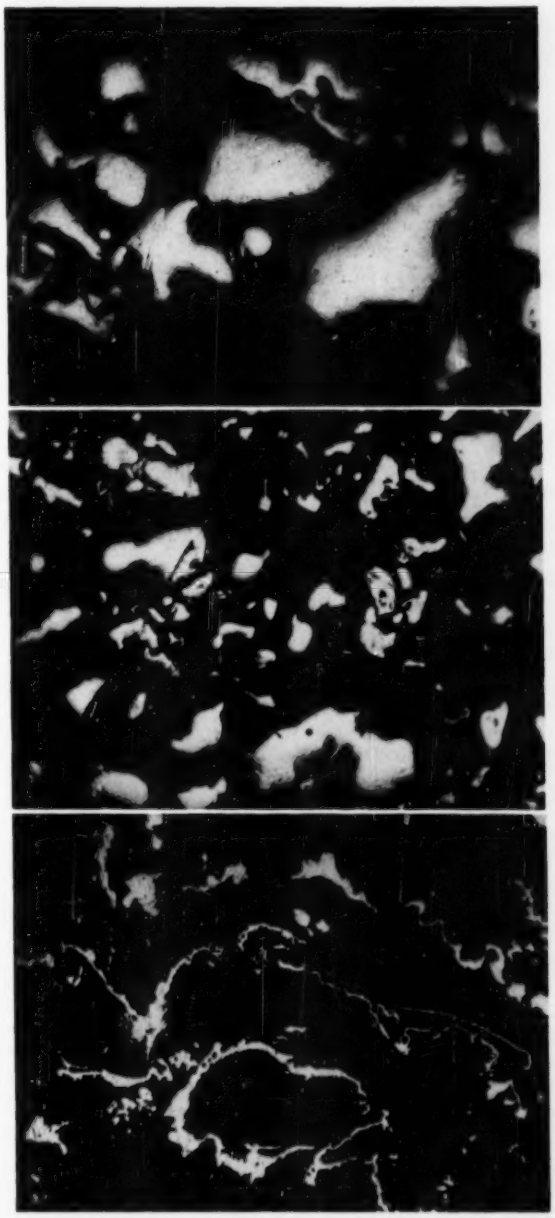

Fig. 1. Particle shape. Photomicrographs of powder particles mounted in plastic, sectioned, and polished. Top, E-11; middle, SG-73R; bottom, L-533.

Table III. Electrical results, sample E-11

Temp, °C	Time, min	D_g = 8.5				D_g = 9.5				D_g = 10.5				D_g = 11.5			
		L	*C*	*ESR*	*L/C*	*L*	*C*	*ESR*	*L/C*	*L*	*C*	*ESR*	*L/C*	*L*	*C*	*ESR*	*L/C*
1750	30	1.0*	12.41*	6*	0.08	0.9	11.75	10	0.08	0.8	10.72	12	0.07	0.8	9.82	15	0.08
	90	1.0*	10.99*	8*	0.09	1.0	10.41	17	0.10	0.8	9.60	21	0.08	0.9	8.51	30	0.11
	180	—	—	—	—	0.7	9.57	20	0.07	0.6	8.43	22	0.07	0.6	7.50	30	0.08
1900	30	1.0**	10.80**	8**	0.09	0.8	10.28	13	0.08	0.8	9.62	13	0.08	0.9	8.63	21	0.10
	90	1.0	10.16	9	0.10	0.7	8.95	12	0.08	0.8	8.13	18	0.10	0.7	7.15	24	0.10
	180	—	—	—	—	0.6	8.03	14	0.08	0.8	7.27	19	0.11	0.7	6.24	31	0.11
2050	30	1.1	9.84	9	0.11	0.8	9.67	12	0.08	0.7	8.86	13	0.08	0.7	7.85	23	0.09
	90	1.0	8.13	10	0.12	0.8	7.62	15	0.11	0.7	6.91	22	0.10	0.6	6.01	31	0.10
	180	—	—	—	—	0.5	6.68	26	0.07	0.5	6.07	32	0.08	0.4	5.03	45	0.08

L is d-c leakage at 140 v, in μa/g; *C*, capacitance at 120 cps, in microfarad/g (200 v formation); *ESR*, equivalent series resistance, in ohm/pellet; D_g, green density, in g/cc.
* Indicates one "wild" pellet out of six.
** Indicates two "wild" pellets out of six.

$$C = 3.75 \times 10^4/T - 3.50 \log (t + 6) - 32.47/(16.6\text{-}D_g) + 3.20 \qquad (T \text{ in } ^\circ\text{K})$$

$$L/C = 0.09 \pm 0.02$$

Particle shape.—Samples of each of the powders were mounted in plastic, sectioned, and polished. Figure 1 shows photomicrographs of the sectioned particles, at a magnification of 500 x before reproduction. The particle shapes of E-11 and SG-73R were somewhat similar, in that the particles tended to be solid and regular in shape. L-533 had several different particle shapes, including hollow hemispheres and "strings." The particle size of such irregular shapes is not measured accurately by screening or by air elutriation in the Roller apparatus.

Results

The results of this study were obtained using the experimental techniques described above. In particular, the electrolyte used for measurement of leakage, capacitance, and equivalent series resistance was always 10% phosphoric acid. However, other work done in these laboratories has shown that, when liquid electrolytes are used, to a first approximation leakage and capacitance are independent of electrolyte. Equivalent series resistance is markedly dependent on the electrolyte, since part of the series resistance is due to the ohmic resistance of the electrolyte in the pores of the anode. Equivalent series resistance therefore varies with the specific resistivity of the electrolyte. The specific resistivity of 10% phosphoric acid at room temperature is about 15 ohm-cm (6, 7).

E-11.—Pellets pressed to three different green densities (9.5, 10.5, and 11.5 g/cc) were sintered at three different temperatures (1750°, 1900°, and 2050°C) for three different times (30, 90, and 180 min).

The electrical results obtained on these pellets are shown in Table III, together with results for a green density of 8.5 g/cc (see below). Each result is the average from four pellets, two from one sinter run and the other two from a second sinter run. The table shows the leakage per gram (*L*, in microamperes), the capacitance per gram (*C*, in microfarads), the equivalent series resistance per 1.8 g pellet (ESR, in ohms), and the leakage divided by the capacitance (*L/C*, in microamperes per microfarad).

It can be seen that both leakage and capacitance decreased as the green density and time and temperature of sintering increased, the over-all change for the range of conditions studied being about a factor of two. As the values of *L/C* show, *L* and *C* changed at the same rate, so that *L/C* was constant at 0.09 ± 0.02 μa/microfarad over the range of conditions.

It was found that the relationship between capacitance and sintering conditions could be expressed in the form of an empirical equation, with independent terms in green density, time, and temperature. This equation is

$$C = 3.75 \times 10^4/T - 3.50 \log (t+6) - 32.47/(16.6\text{-}D_g) + 3.20$$

where *T* is temperature, in °K, *t*, time, in minutes, D_g green density, in g/cc, and *C*, capacitance, in microfarads/g. The average difference between the value of *C* given by this equation and the measured value of C is 1.5%. The maximum difference is 4.9%. These differences are well within experimental error. The expression $(t+6)$ occurs in the term for time because *t* was measured as time at the designated temperature. The additional 6 min is an estimate of the extra effective time due to heating and cooling periods. The density of tantalum metal is 16.6 g/cc, and this number appears in the term for green density.

The equivalent series resistance results showed some scatter which tends to obscure the trends. However, it is clear that *ESR* increased markedly with increasing green density, and also to some extent with time. The effect of temperature is uncertain.

After the results described above were obtained and the capacitance equation derived, the study of E-11 was extended to a lower green density of 8.5 g/cc, at the same temperatures, but for two times only (30 and 90 min). The results are shown in Table III. The agreement between the measured capacitance and the capacitance predicted by the previously derived equation is excellent, the largest difference being 6%. Values of *L/C* also agree with

Table IV. Sinter densities and capacitance per unit volume, sample E-11

Temp, °C	Time, min	Green density, g/cc: 8.5 D_s	8.5 Cvol.	9.5 D_s	9.5 Cvol.	10.5 D_s	10.5 Cvol.	11.5 D_s	11.5 Cvol.
	30	8.98	111	9.72	114	10.54	113	11.41	112
1750	90	9.60	106	10.06	105	10.70	103	11.69	99
	180	—	—	10.34	99	11.04	93	11.93	89
	30	9.53	103	10.05	103	10.80	104	11.54	100
1900	90	—	—	10.59	95	11.34	92	12.03	86
	180	—	—	10.77	86	11.46	83	12.27	77
	30	9.75	96	10.28	99	10.96	97	11.78	92
2050	90	10.46	85	11.05	84	11.73	81	12.20	73
	180	—	—	11.50	77	11.92	72	12.77	64

D_s is sinter density (g/cc) and Cvol. is capacitance per unit volume (microfarads/cc).

those previously found; however, a different kind of result was obtained with a few pellets sintered at the less severe sintering conditions. One, or at most two, of six pellets sintered under the same conditions started to "gas" violently during anodization, and on measurement were found to have leakages of the order of 400 μa/g. These values were termed "wild" leakages and are not included in the averages in the table. The reasons for this phenomenon are not clear, but it is associated with lower green densities and lower times and temperatures of sintering (see also the results for L-533 below).

The results for equivalent series resistance appeared to follow the same trends as those previously obtained.

The apparent densities of the pellets after sintering were measured for the pellets studied electrically. Results are shown in Table IV, together with the values for capacitance per unit volume, which were obtained by multiplying the capacitance per gram by the sinter density in g/cc. For practical purposes, in the manufacture of capacitors, the capacitance per unit volume is the important parameter, rather than the capacitance per unit weight.

The sinter density increased with time and temperature of sintering and also with green density, but the difference between green density and sinter density became less as the green density increased. The capacitance per unit volume was almost independent of green density, except at the highest green density (11.5), where there was some decrease. The capacitance per unit volume decreased with increasing time and temperature of sintering.

SG-73R.—A similar study to that made on E-11 was made with SG-73R, except that the data were not as complete and sinter densities were not measured.

The electrical results are shown in Table V, where the values are the averages from six pellets.

The trends of leakage and capacitance were very similar to those for E-11, and L/C was again found to be constant, although the value of 0.07 ± 0.01 μa/microfarad for SG-73R was slightly lower than that for E-11 (0.09 ± 0.02). The capacitance values could be expressed by an equation, in terms of green density, time, and temperature, of the same form as that used for E-11. The average difference between the values of capacitance given by this equation and the measured values was 2%. The maximum difference was 5.1%. The equation is $C = 4.83 \times 10^4/T - 3.72 \log (t + 6) - 46.56/(16.6\text{-}D_g) + 1.19$.

The measurements of equivalent series resistance showed less scatter than that found for E-11, partly because experimental technique had been improved. The equivalent series resistance increased with increasing green density and time, and slightly with increasing temperature.

L-533.—The study of L-533 was made over a range of green densities (7.0 to 10.5 g/cc) extending lower than that used for E-11. Only times of 30

Table V. Electrical results, sample SG-73R

Temp, °C	Time, min	D_g = 8.5 L	C	ESR	L/C	D_g = 9.5 L	C	ESR	L/C	D_g = 10.5 L	C	ESR	L/C	D_g = 11.5 L	C	ESR	L/C
1750	90	1.0	12.05	8.3	0.08	0.9	11.17	8.7	0.08	0.7	10.02	12.1	0.07	—	—	—	—
	30	0.9	11.47	7.6	0.08	0.85	10.75	9.1	0.08	—	—	—	—	—	—	—	—
1900	90	0.8	10.59	8.2	0.08	0.7	9.37	10.2	0.07	0.6	8.45	14.1	0.07	0.5	7.12	23.8	0.07
	180	0.6	9.24	9.6	0.07	0.55	8.38	12.3	0.07	—	—	—	—	—	—	—	—
	30	0.8	10.67	9.1	0.08	0.7	10.18	11.0	0.07	0.6	8.96	12.5	0.07	—	—	—	—
2050	90	0.6	8.60	9.4	0.07	0.55	8.02	12.0	0.07	—	—	—	—	—	—	—	—
	180	0.5	7.96	10.1	0.06	0.4	6.89	15.0	0.06	—	—	—	—	—	—	—	—

L is d-c leakage at 140 v, in μa/g; C, measured capacitance at 120 c.p.s, in microfarad/g (200-v formation); ESR, equivalent series resistance, in ohm/pellet; D_g, green density, in g/cc.

$C = 4.83 \times 10^4/T - 3.72 \log (t + 6) - 46.56/(16.6D_g) + 1.19$ (T in °K)

$L/C = 0.07 \pm 0.01$

Table VI. Electrical results, sample L-533

Temp, °C	Time, min	D_g = 7.0				D_g = 8.0				D_g = 9.5				D_g = 10.5			
		L	*C*	*ESR*	*L/C*	*L*	*C*	*ESR*	*L/C*	*L*	*C*	*ESR*	*L/G*	*L*	*C*	*ESR*	*L/C*
1750	90	—	—	—	—	1.7*	14.78	10	0.12	1.3	11.88	17	0.11	1.2	9.54	29	0.13
1900	30	—	—	—	—	1.6*	15.66	11	0.10	—	—	—	—	—	—	—	—
	90	—	—	—	—	1.4	11.59	13	0.12	1.3	9.53	24	0.14	3.1	7.77	41	0.40
2050	30	2.5*	14.02	12	0.18	1.7	12.36	12	0.14	1.5	10.36	25	0.14	—	—	—	—
	90	—	—	—	—	1.2	9.75	15	0.12	1.0	7.66	35	0.13	6.4	5.66	63	1.13

L is d-c leakage at 140 v, in μa/g; *C*, capacitance at 120 cps in microfarad/g (200-v formation); *ESR*, equivalent series resistance, in ohm/pellet; D_g, green density, in g/cc.
* One or more pellets had "wild" leakages.
$C = 8.04 \times 10^4/T - 7.34 \log (t + 6) - 94.0/(16.6\text{-}D_g) + 0.40$ (T in° K)
L/C not constant.

and 90 min were used. Electrical results are shown in Table VI, each number being the average from four pellets.

As with E-11 and SG-73R, the capacitance decreased with increasing green density, time, and temperature. However, leakage did not follow the same trend over the whole range of conditions, so that while *L/C* was essentially constant at 0.12 ± 0.02 μa/microfarad for green densities of 8.0 and 9.5, there was a definite increase in *L/C* at a green density of 10.5 and higher temperatures. There were also pellets showing "wild" leakage at the lower green densities and times and temperatures. These were not included in the averages.

The capacitance measurements fitted the same form of equation relating them with green density, time, and temperature as that found to apply for E-11 and SG-73R. The equation is

$$C = 8.04 \times 10^4/T - 7.34 \log (t+6) - 94.0/(16.6\text{-}D_g) + 0.40$$

This equation does not fit the data quite as well as did the equations for E-11 and SG-73R, the average and maximum differences between the measured and calculated capacitances being 3.4% and 9.2%, respectively. This may be due in part to the less complete data used in deriving it.

The equivalent series resistance increased with increasing green density, temperature, and time.

The results of sinter density measurements and the values of capacitance per unit volume derived from them and the capacitances per unit weight are shown in Table VII. Unlike E-11, the capacitance per unit volume of L-533 changed markedly with green density, decreasing with increasing green density. Capacitance per unit volume also decreased with increasing time and temperature.

Comparison of Results

Leakage.—The most significant differences between the leakage results for the three powders were, first, the constancy of *L/C* for E-11 and SG-73R compared with the increase in *L/C* for L-533 at higher green densities and temperatures, and second, the conditions at which the phenomenon of "wild" leakage occurred. Some pellets of E-11 had "wild" leakages at a green density of 8.5 and lower temperatures and times, whereas, under the same conditions, no pellets of SG-73R showed "wild" leakage. L-533 gave "wild" leakages only at green densities below those studied for the other two powders.

Capacitance.—For all three powders the relationship between capacitance and sintering conditions could be expressed by an empirical equation of the form

$$C = A \times 10^4/T + B \log (t + 6) + C'/16.6\text{-}D_g + D$$

There were, however, considerable differences in the values of the coefficients A, B, C′, and D for the three powders. These coefficients (shown in Table VIII) are a measure of the sensitivity of the capacitance to changes in sintering conditions. It can be seen that the capacitance of E-11 is the least sensitive to changes in conditions, and that of L-533 is the most sensitive. SG-73R is much closer in sensitivity to E-11 than to L-533, but is more sensitive

Table VII. Sinter densities and capacitance per unit volume, sample L-533

Temp, °C	Time, min	Green density, g/cc							
		7.0		8.0		9.5		10.5	
		D_s	Cvol.	D_s	Cvol.	D_s	Cvol.	D_s	Cvol.
1750	90	—	—	10.00	148	11.41	136	12.15	116
1900	30	—	—	9.50	149	—	—	—	—
	90	—	—	9.91	115	11.18	107	11.86	92
2050	30	8.76	123	9.89	122	11.17	116	—	—
	90	—	—	10.47	102	11.78	90	12.45	70

D_s is sinter density (g/cc) and Cvol. is capacitance per unit volume (microfarad/cc).

Table VIII. Comparison of capacitance equations

General form of equation:
$$C = A \times 10^4/T + B \log (t + 6) + C/(16.6\text{-}D_g) + D$$

Sample	A	B	C'	D
E-11	3.75	−3.50	−32.47	+3.20
SG-73R	4.83	−3.72	−46.56	+1.19
L-533	8.04	−7.34	−94.0	+0.40

C is capacitance, in microfarad/g (200-v formation); T, temperature, in °K; t, time, in minutes; D_g, green density, in g/cc.

to changes in temperature and green density than is E-11.

Figures 2, 3, and 4 show the changes in capacitance of the three powders with changing temperature (at constant time and green density), time (at constant temperature and green density), and green density (at constant time and temperature), respectively. Those graphs show not only the relative sensitivities of the capacitance of the powders to changes in conditions as described above, but also the effects of each of the separate variables

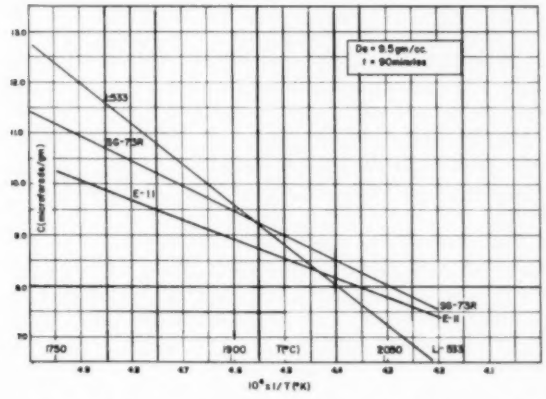

Fig. 2. Capacitance vs. temperature at constant time and green density.

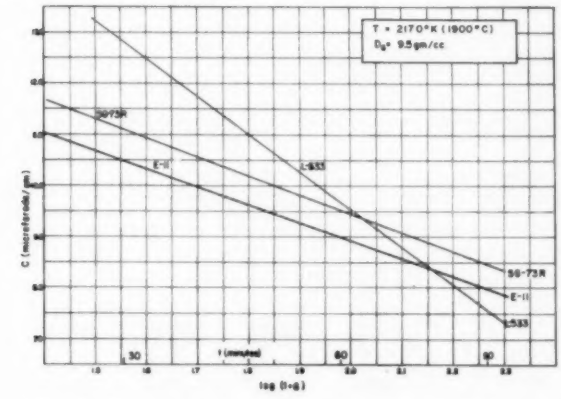

Fig. 3. Capacitance vs. time at constant temperature and green density.

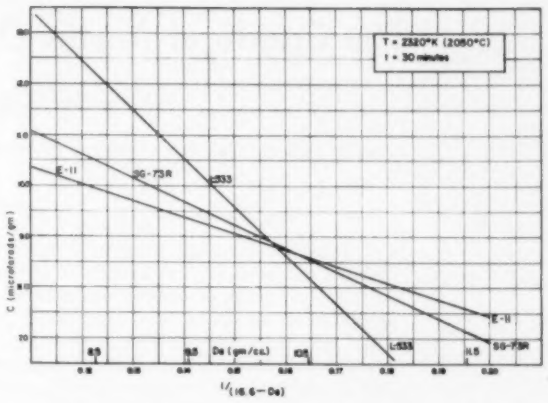

Fig. 4. Capacitance vs. green density at constant time and temperature.

(time, temperature, and green density) relative to each other. The changes in capacitance due to the separate effects of the over-all changes in each variable were approximately equal, over the ranges studied.

Equivalent series resistance.—The equivalent series resistance increased with green density and time for all three powders. It increased with temperature for SG-73R and L-533, but the effect of temperature for E-11 is uncertain. The *ESR* of L-533 was the most sensitive of the three powders to changes in sintering conditions, and also the highest in magnitude for a given set of conditions.

Conclusions

No attempt has been made to give speculative interpretations of the observed results, since it is thought that speculation could be more misleading than helpful when discussing such complex systems. Much more experimental work is needed in this field before, for example, any meaningful physical interpretation could be given for the form of the general capacitance equation, or the phenomenon of "wild" leakage could be explained. It is hoped that such work will be forthcoming.

Manuscript received June 22, 1959. This paper was prepared for delivery before the Philadelphia Meeting, May 1-5, 1959.

Any discussion of this paper will appear in a Discussion Section to be published in the December 1960 JOURNAL.

REFERENCES

1. M. Whitehead, *Bell Lab. Record*, **28**, 448 (1950).
2. R. L. Taylor and H. E. Haring, *This Journal*, **103**, 611 (1956).
3. D. A. McLean and F. S. Power, *Proc. IRE*, **44**, 872 (1956).
4. L. Young, *Proc. Roy. Soc.*, **244A**, 41 (1958).
5. P. S. Roller, *J. Am. Ceram. Soc.*, **20**, 167 (1937).
6. H. E. W. Phillips, *J. Chem. Soc.*, **95**, 59 (1909).
7. C. M. Mason and J. B. Culvern, *J. Am. Chem. Soc.*, **71**, 2387 (1949).

The Growth of Anodic Oxide Films on Germanium

Solomon Zwerdling and Sumner Sheff[1]

Lincoln Laboratory, Massachusetts Institute of Technology, Lexington, Massachusetts

ABSTRACT

Thick uniform germanium dioxide films of controlled thickness have been grown anodically on both n- and p-type germanium. The electrolyte used was a 0.25*N* solution of anhydrous sodium acetate in glacial acetic acid. The composition of the films was established by gravimetric and spectrometric methods. From the current efficiencies and the other parameters of the electrolysis, certain significant properties of the oxide films were calculated, i.e. differential formation field during growth, resistivity, and thickness. Furthermore, it was possible to determine changes in these quantities by evaluating them for different intervals of the electrolysis.

The presence of a thick oxide film on a germanium substrate is considered of importance in understanding the surface properties of semiconductors. Such specimens could be used for physical measurements involving electronic interactions between the oxide layer and the substrate, e.g., the influence of various gaseous ambients on the surface conductivity. Anodic electrolysis was selected to produce these films, since it readily permits obtaining pertinent electrochemical data for the films including differential formation field during growth, resistivity, and thickness. Furthermore, the oxidation rate may be controlled readily, and the films may be formed at room temperature, so that the electrical characteristics of the substrate are unaltered.

Anodic oxide film growth on electrodes has been studied rather extensively for metals in aqueous electrolytes (1-8), and several theories (4, 9-11) have been proposed according to which the formation current density should be dependent exponentially on the electric field across the oxide film. The data obtained for these systems have been essentially in agreement with theory. In recent years, the experiments have been extended to semiconductors, including germanium (12), indium antimonide (13), and silicon (14). In this paper, we will present the detailed results obtained for the electrochemical parameters of the anodic oxide film formation on germanium in a nonaqueous electrolyte.

Experimental

Apparatus.—The experiments for producing the oxide films were performed at room temperature in a three compartment electrolytic cell with the same electrolyte in all three compartments. The experimental arrangement is shown schematically in Fig. 1. Current was obtained from an electronically stabilized current supply having an equivalent source voltage of 100 kv. The anode was grounded and its voltage relative to a reference platinum electrode in the same electrolyte was measured and recorded continuously by a very high input impedance electronic potentiometer. The circuit was designed so that the current could be monitored on the same apparatus without interrupting the circuit.

Samples.—The samples were Ge wafers (approximately 2 × 1 × 0.1 cm) carefully lapped with No. 600 and No. 800 silicon carbide followed by a 1.5 min CP-4 etch.[2] Surfaces were examined in intense oblique light and were reprocessed if not satisfactory. For repeated anodic oxidations with the same electrode, only a 0.5 min CP-4 etch was used. Tygon paint (air-dried, then baked at 70°C overnight) was used to protect the lead soldered to the anode which was only partially immersed in the electrolyte.

The geometrical areas of the electrodes were determined to ± 1% by means of an optical comparator capable of reading dimensions to within 0.005 cm. A surface roughness factor of 1.3 was assumed based on measurements reported by Law (15). The depth of immersion of the Ge anode was determined from the boundary line of the oxidized portion of the electrode observed after the removal of the oxide film by immersion in 0.01*N* sodium hydroxide (aq.).

Electrolyte.—A large number of experiments showed that it was apparently impossible to grow oxide films on germanium using aqueous electrolytes, due to the appreciable solubility of the formed

[2] CP-4 consists of concentrated HNO_3 (5 parts by volume), glacial CH_3COOH (3 parts), 48% HF (3 parts) and Br_2 (0.06 part).

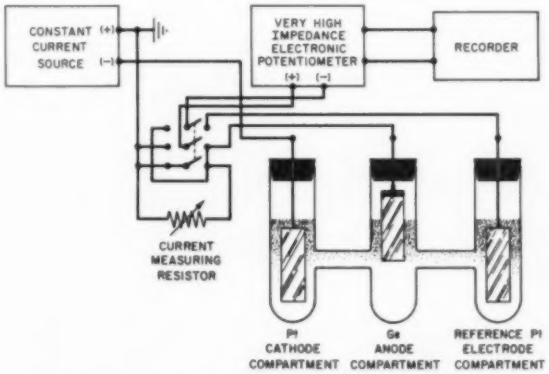

Fig. 1. Schematic diagram of electrolysis apparatus

[1] Present address: Semiconductor Division, Raytheon Manufacturing Company, Newton, Mass.

GeO_2 in water. Among many electrolyte systems tried a solution of anhydrous sodium acetate in glacial acetic acid (A.R.) was found suitable and it was employed in the present study. The optimum composition for producing satisfactory oxide films over the current density range from 50-400 $\mu a/cm^2$ was found to be 0.25*N* and it was employed throughout.

Anodically formed GeO_2 is essentially insoluble in the electrolyte (less than 0.2 γ/ml) as shown by a colorimetric procedure described below. The electrolyte had a specific conductivity of 43.7 $\mu mho\text{-}cm^{-1}$ at 24.3°C.[a]

Analytical.—A method for the determination of the amount of oxidized Ge in the anodic films was developed by a modification of the oxidized hematoxylin photometric procedure described by Newcombe, *et al.* (16). The modifications involved (*a*) dissolving the oxide film on the electrode by a 10-sec immersion with stirring in 0.01*N* aqueous sodium hydroxide, neutralizing with 0.04*N* aqueous sulfuric acid, and making up to standard volume with phthalate buffer of pH = 3.2, (*b*) using 10 ml aliquots of this solution to determine the Ge concentration, and (*c*) allowing 60 min for the reaction time between the Ge and the hematoxylin. The 10-sec immersion time was experimentally found sufficient to remove completely even the thickest film grown and make negligible any contribution due to further oxidation and dissolution of the electrode. A calibration curve was obtained by using β-GeO_2 standard solutions prepared by dissolving a weighed quantity of the oxide in 0.01*N* aqueous sodium hydroxide, neutralizing, and diluting to volume with the same reagents as above. Optical density measurements were made on a Beckman Model DU Spectrophotometer to a precision of ± 0.002 unit standard deviation.

Determination of Oxide Composition

A study was made in order to determine the composition of the anodic films. Since the electrolysis was performed in glacial acetic acid, the possibility that the films were germanium tetraacetate was investigated. This compound had been synthesized by Schmidt, *et al.* (17) and was reported to be soluble in benzene and acetone. These anodic films were found to be insoluble in those reagents.

To test the assumption that the films were GeO_2, experiments were performed to determine the stoichiometric ratio of germanium to oxygen. The ratio was calculated from the weight loss of germanium anodes after the film had been removed by dissolution in aqueous sodium hydroxide and from the amount of germanium found in the resulting solution. The films were grown on p-type germanium at 100 $\mu a/cm^2$ for 10 hr. They were freed of sodium acetate by ten 5-min rinsings in fresh portions of glacial acetic acid, and of acetic acid by pumping in a vacuum desiccator for several hours. Radiotracer experiments using Na^{22} tagged electrolyte indicated that this rinsing procedure was sufficient to remove completely all sodium ions possibly adsorbed on the film. By counting the aqueous sodium hydroxide solutions containing the dissolved film grown in the tagged electrolyte, it was found that no significant amount of sodium was incorporated in the film. Prior to weighing, the films were equilibrated at atmospheric pressure in a desiccator for 30 min. Weighings were made on a microbalance to a precision of ±2γ. A stoichiometric ratio of 1:2 corresponding to the empirical formula GeO_2 was found.

X-ray diffraction patterns were taken of the powder obtained by mechanically removing the film material grown on Ge anodes. A diffuse pattern was obtained indicative of an amorphous powder. After recrystallization from redistilled water, the diffraction pattern contained only the lines associated with the hexagonal form of GeO_2.

The composition of the anodically formed film was investigated further by determining its infrared absorption spectrum. Transmission measurements were made using two oxidized electrodes in series, corresponding to four film thicknesses, in the radiation beam. The spectral region from 2-20 μ was scanned. This was possible since bulk germanium is transparent in this region. Only the absorption bands of GeO_2 (18) were found and are shown in Fig. 2(a) and (b), thus confirming that the films were germanium dioxide.

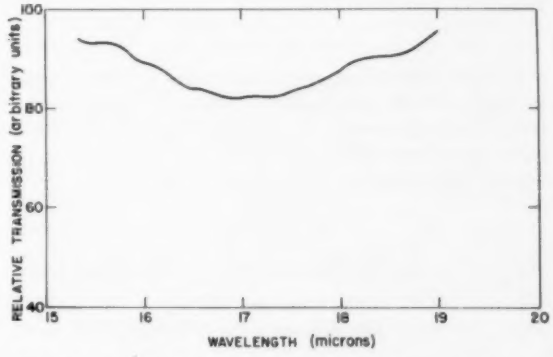

Fig. 2(a). Infrared transmission of GeO_2 films produced anodically on germanium (16 to 18μ band).

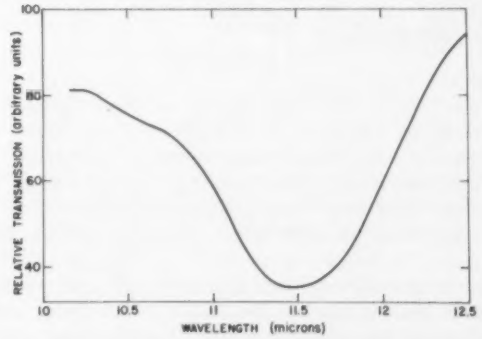

Fig. 2(b). Infrared transmission of GeO_2 films produced anodically on germanium (11.5μ band).

[a] A small quantity of the electrolyte was refluxed at 120°C for 1 hr with 0.6% of its weight of acetic anhydride to dehydrate it further. The resulting solution had a specific conductivity of 42.4 $\mu mho\text{-}cm^{-1}$ at 27.5°C as contrasted to a value of 49.5 $\mu mho\text{-}cm^{-1}$ for the original solution. Attempts to grow uniform oxide films on Ge anodically with the refluxed electrolyte were unsuccessful. Further investigations with this electrolyte may elucidate the reaction mechanism of the anodic oxidation.

Electrochemical Considerations of Film Growth

Certain pertinent properties of the oxide films were calculated from the parameters of the electrolysis, i.e., the total current, the anode area, and the increase of voltage across the oxide with time as the film grew thicker.

The differential oxide formation field at any thickness is defined as

$$E_d = dV/dx = dV/\beta dq_f \quad [1]$$

where E_d is the differential oxide formation field, v/cm; V the potential across the film, v; x the film thickness, cm; and β the centimeters of film thickness formed per amp-sec/cm^2 of charge q_f passed leading to oxide formation.

The thickness of the oxide film at any time t is given by

$$x_t = x_o + \beta q_f \quad [2]$$

where β is taken to be a constant, and x_o is the thickness prior to electrolysis. The density of the oxide formed on the Ge anode was assumed to be that of bulk hexagonal GeO_2 (4.28 g/cm^3) (19), so that a calculation for β yielded 6.35 x 10^{-5} cm^3(amp-sec)$^{-1}$, and for the average thickness of a GeO_2 layer 3.4Å. The current efficiency for oxide formation ϵ is defined as

$$\epsilon = i_f/I \quad [3]$$

where i_f is the oxide formation current density and I the total current density. If the current efficiency is a constant during a given electrolysis interval in the anodic oxidation of Ge to GeO_2, then

$$\epsilon = 4FM_{Ge}/Q \quad [4]$$

where F is the Faraday constant, M_{Ge} is the number of moles of Ge anodically oxidized, and Q is the total charge passed during that interval. If the electrical resistivity of the oxide ρ_{ox} is a constant during the same interval, from Ohm's law,

$$\rho_{ox} = E_d/I \quad [5]$$

Since $i_f = dq_f/dt$, Eq. [3] may be combined with Eq. [1] to give

$$E_d = dV/\beta i_f dt = (1/\beta\epsilon I)\, dV/dt \quad [6]$$

and with Eq. [2] to give

$$x_t = x_o + \beta\epsilon It \quad [7]$$

Alternatively, the thickness of the film may be determined from

$$x_t = W_{Ge}\, G/D \quad [8]$$

where W_{Ge} is the quantity of oxidized Ge on the surface in g/cm^2, G is the gravimetric factor for GeO_2/Ge, and D is the density of GeO_2 in g/cm^3.

Because of the experimental method used, the current efficiency could be obtained only as an average over an interval of electrolysis. Therefore, it was only possible to evaluate the differential field for those intervals during which the current efficiency was constant. Since the electrolyses were performed at constant current density, such intervals would be expected to exhibit a linear rise of voltage with time. As the potential across the oxide was the only component of the measured anode potential that was expected to contribute primarily to its increase with time as the oxide grew thicker, the rate of increase of the latter was taken equal to the rate of increase of potential across the oxide dV/dt. This increase was assumed to be due only to the increase in the film thickness and not to any changes in the oxide already formed.

It was necessary to consider the possibility of the formation of a p-type "inversion" layer at the surface of n-type Ge when anodized in the sodium acetate-glacial acetic acid electrolyte. The effect was not observed in the electrolyses performed except at the highest current density used. For this case, the anode voltage rose abruptly to abnormally high values when the current was turned on, and within 1 min had fallen to the value normally obtained with p-type germanium under the same conditions. During further electrolysis, the behavior of the anode voltage with time remained normal. Evidently, the oxide film formed within 1 min of electrolysis was sufficiently thick to destroy the "inversion" layer by preventing the electrolytic double layer from affecting the normal electron and hole densities at the surface of the germanium substrate. Furthermore, an accumulation of electrolytic oxidation products near the anode might also have contributed to the rise of anode potential with time. It is likely, however, that this did not occur since the potential of a platinum anode substituted for the germanium was found to remain constant during prolonged electrolysis.

Results and Discussion

As a consequence of the above considerations, the criteria adopted for a successful anodic oxide film growth experiment were: (*a*) the film grown should be of uniform thickness as evidenced by the uniformity of the color it produced by optical interference in white light, and (*b*) for all intervals following the initial shorter one, the anode voltage should increase uniformly with time at constant current density.

For current densities between 66 and 240 μa/cm^2, uniform films appearing blue and yellow, respectively, in white light were obtained. The anode voltage vs. time curves satisfied criterion (*b*), although the onset and duration of the intervals varied with the current density. Plots of corrected anode potential vs. electrolysis time for both n- and p-type germanium are shown in Fig. 3.

The correction was chiefly due to the IR drop in the anolyte included in the measured voltage and depended on the geometry of the experimental cell. By substituting a platinum anode for the germanium and electrolyzing at various current densities in the range studied, these corrections were evaluated, the largest being about 4.5 v at the highest current density. The curves show the different linear intervals for the different current densities. The values of dV/dt which were used in calculating E_d from Eq. [6] for the different linear intervals were obtained from these curves. The current efficiencies for the different linear intervals were calculated from the charge passed during each interval

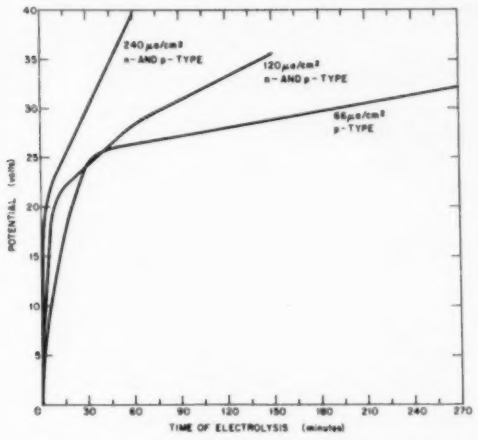

Fig. 3. Potential of Ge anodes vs. a reference Pt electrode during growth of anodic oxide films in 0.25N sodium acetate in glacial acetic acid (corrected for IR drop in electrolyte).

and from differences in the amounts of oxidized germanium found in films grown at the same current density for times equal to those at the beginning and end of each interval. From such differences, the values for M_{Ge} in Eq. [4] were obtained. It was established that the current efficiency actually was constant throughout a linear interval, by dividing each of two such intervals into two parts and obtaining the current efficiency for these parts. The results for two samples of both n- and p-type germanium are shown in Table I. The uncertainty of the efficiency determinations for the total interval in each case was ± 5%. Since the determinations for the intermediate intervals involve smaller differences between relatively large quantities of oxidized germanium than in the case of the corresponding total intervals, the uncertainty for the former was ± 10%. Consequently, within this experimental error the current efficiency was constant throughout a linear interval.

A comparison was made between the anodic oxidation parameters of the (111), (110), and (100) faces of p-type Ge with resistivities of approximately 30 ohm-cm. Experiments were performed for periods of 6 hr at various current densities in the range of interest. The results indicated that, within experimental error, there were no differences between the anodic oxidations of the various crystallographic planes.

Table I. Current efficiency for anodic oxidation of germanium

Material	Total current density, μa/cm²	Specimen	Interval, min	Current efficiency, %
n-type Ge (30 ohm-cm)	120	1	60-105	11
			105-150	11
			60-150	11
		2	60-105	12
			105-150	11
			60-150	11
p-type Ge (30 ohm-cm)	66	3	60-150	17
			150-270	16
			60-270	16
		4	60-150	17
			150-270	16
			60-270	17

The results of a series of determinations of the anodic oxide growth parameters for n- and p-type Ge of 30 ohm-cm resistivity, electrolyzed at the indicated current densities are shown in Table II. For the p-type Ge, the (111) face was used, and for the n-type Ge, the (111) and (100) faces were used. The values reported are the averages of determinations with each electrode as well as with different samples cut from adjacent sections of the same ingot. The current densities for repeated experiments could be reproduced only to within ± 3% on account of the partial immersion technique used for the Ge anodes. The reproducibility of the determinations of dV/dt was ± 5%, so that the values for E_d, ρ_{ox}, and i_f are reported with an uncertainty of ± 8%. Within this experimental error, both n- and p-type Ge showed the same behavior during anodic oxide film growth.

The average current efficiency values obtained for the oxidations during the initial nonlinear intervals at the various current densities were all approximately the same, about 24-26%. The duration of these nonlinear intervals was shorter the greater the corresponding current density. However, for the later intervals, there is a tendency for the efficiency to decrease with increasing current density. It is interesting to note that in all cases, the first pronounced change in slope occurred at a potential between 20 and 24 v (see Fig. 3). This might indicate a change in the anodic process which could arise from the onset of increased electron and/or "hole" conductivity in the oxide due to the field across it, or to a heating effect by the current passing. Since the current efficiency of oxide formation for any current density, following the change of slope, is less than during the initial interval as is evident from Table II, it follows that the electronic conductivity increases at this point probably accompanied by a decrease in ionic conductivity in the oxide since the total current density remains constant.

For the measurements taken at a current density of about 120 μa/cm², the values of the current efficiency and dV/dt are smaller for the third interval than they are for the second interval, but in approximately the same proportion. Consequently, the related values for E_d and ρ_{ox} are about the same for these intervals.Furthermore, the three different current densities employed resulted in E_d values for the later intervals that were approximately proportional to the respective current densities. Therefore, the corresponding resistivities, ρ_{ox} are again about the same. This indicates that the oxide films grown were alike.

Using the assumption for the oxide density stated earlier, the thicknesses of the oxide films were found to range from 220 to 1240Å. The amounts grown for specific intervals are shown separately in Table II.

Table II. Anodic oxide growth parameters for n- and p-type germanium in 0.25N sodium acetate in glacial acetic acid

Interval, min	Area, cm²	Total current density, μa/cm²	Oxidized Ge, micromole/cm²	Current efficiency, %	$10^8\ dV/dt$, v/sec	$10^{-8}\ E_f$, v/cm	$10^{-10}\ \rho_{ox}$, ohm-cm	Thickness x_f, A
			p-type Ge, (30 ohm-cm)					
0-60	2.12	66	0.16	26	—	—	—	390
60-270	2.12	66	0.35	16	0.47	0.70	1.1	850
								1240
0-20	2.09	120	0.10	25	—	—	—	230
20-60	2.09	120	0.14	19	2.3	1.6	1.3	340
60-150	2.19	120	0.19	11	1.4	1.7	1.4	460
								1030
0-10	2.17	240	0.09	25	—	—	—	220
10-60	2.17	240	0.22	10	5.5	3.5	1.4	530
								750
			n-type Ge, (30 ohm-cm)					
0-20	2.42	120	0.10	26	—	—	—	240
20-60	2.42	120	0.15	19	2.1	1.4	1.2	360
60-150	2.56	120	0.19	11	1.3	1.6	1.3	460
								1060
0-10	2.41	240	0.09	24	—	—	—	220
10-60	2.41	240	0.21	11	5.5	3.3	1.4	510
								730

In conclusion, we have shown that relatively thick oxide films may be grown on germanium by anodic electrolysis in the nonaqueous electrolyte system: sodium acetate-glacial acetic acid. It was not possible to deduce a simple relationship between the formation current density and the differential formation field in this case, as is usually found for metal-aqueous electrolyte systems. Likewise, no definite relationship between these parameters was reported for an analogous semiconductor nonaqueous electrolyte system by Schmidt and Michel (14) who studied the anodic formation of oxide films on silicon in a solution of 0.04*N* potassium nitrate in N-methyl acetamide. Similar curves for the increase in anode potential with time were obtained in their study and ours. Anodic oxide films on indium antimonide have been grown in the aqueous electrolyte 0.1*N* potassium hydroxide by Dewald (13) where, although the potential vs. time curves were similar to those found for Ge and Si, the data obtained could be fitted empirically to the relationship $i_f \propto \exp(E_f)$. In this work on InSb, it was indicated that the interpretation of the kinetic parameters derived from the experimental data was difficult, since the necessary mathematical formulations of the detailed theory of the oxidation of such a binary intermetallic electrode have not yet been developed. The interpretation of the data for the more complex system of a semiconductor electrode in a nonaqueous electrolyte must also await further theoretical and mathematical developments.

Acknowledgment

The authors wish to thank Dr. Harry C. Gatos of this Laboratory for many helpful discussions and assistance with the preparation of the manuscript. The x-ray measurements and crystallographic orientations were performed by Mr. Joseph W. Sanchez. The radiotracer experiments were performed with Mr. J. A. Kafalas, to whom the authors express their thanks.

Manuscript received July 2, 1959. The work reported in this paper was performed by Lincoln Laboratory, a center for research operated by Massachusetts Institute of Technology with the joint support of the U.S. Army, Navy, and Air Force.

Any discussion of this paper will appear in a Discussion Section to be published in the December 1960 JOURNAL.

REFERENCES

1. J. J. Polling and A. Charlesby, *Proc. Phys. Soc.*, **67**, 3-B, 201 (1954).
2. H. A. Johansen, G. B. Adams, Jr., and P. Van Rysselberghe, *This Journal*, **104**, 339 (1957).
3. L. Young, *Trans. Faraday Soc.*, **50**, 153 (1954).
4. A. Guntherschultze and H. Betz, *Z. Physik*, **92**, 367 (1934).
5. A. Charlesby, *Proc. Phys. Soc.*, **66**, 317 (1953).
6. R. D. Misch and E. S. Fisher, *This Journal*, **103**, 153 (1956).
7. P. E. Lake and E. J. Casey, *ibid.*, **105**, 52 (1958).
8. G. B. Adams, Jr., P. Van Rysselberghe, and M. Maraghini, *ibid.*, **102**, 502 (1955).
9. N. F. Mott, *Trans. Faraday Soc.*, **43**, 429 (1947).
10. N. Cabrera and N. F. Mott, *Repts. Progr. in Physics*, **12**, 163 (1948-1949).
11. J. F. Dewald, *This Journal*, **102**, 1, (1955).
12. S. Zwerdling and S. Sheff, *ibid.*, **103**, 61C (1956).
13. J. F. Dewald, *ibid.*, **104**, 244 (1957).
14. P. F. Schmidt and W. Michel, *ibid.*, **104**, 230 (1957).
15. J. T. Law, *J. Phys. Chem.*, **59**, 543 (1955).
16. H. Newcombe, W. A. E. McBryde, J. Bartlett, and F. E. Beamish, *Anal. Chem.*, **23**, 1023 (1951).
17. H. Schmidt, C. Blolm, and G. Jander, *Angew. Chem.*, **A59**, 233 (1947).
18. W. Kaiser, P. H. Keck, and C. F. Lange, *Phys. Rev.*, **101**, 1264 (1956).
19. W. Zachariasen, *Z. Kryst.*, **67**, 226 (1928).

Interpretation of Measurements of Potential Decay on Open Circuit

Paul C. Milner

Bell Telephone Laboratories, Incorporated, Murray Hill, New Jersey

ABSTRACT

Observations of the change in electrode potential as a function of time on open circuit have proved a useful method for the study of electrode kinetics and double-layer capacitances. The interpretation of such observations may be complicated by capacitative effects resulting from competing faradaic processes. Consideration of these effects is included in a theory of open-circuit decay. In certain cases such effects are virtually indistinguishable from double-layer capacitances and they may be of surprising importance. The analysis of decay measurements is also considered, and a new method is described.

In view of recent interest in the decay of overpotential on open circuit in studies of electrode kinetics and of double-layer capacitances, it is pertinent to re-examine the theoretical basis for interpretation of observations. The simplicity of the measurement and its applicability to large electrodes should be recognized. Former interpretations of potential-decay data have depended on very simple theories. This has, in a number of cases, proved inadequate or led to erroneous results.

Early observations of hydrogen overpotential decay made by Baars (1) and Bowden and Rideal (2) were simply explained by Butler and Armstrong (3, 4) in terms of the discharge of a capacitor (electrical double layer) by a faradaic current which is an exponential function of the potential (Tafel current). On this basis, explicit potential-time relations are readily derivable and have been given by a number of authors (5-11). Where the faradaic reaction has equal anodic and cathodic Tafel slopes, expressions valid throughout the whole potential range have been derived (11, 12), and the situation near the equilibrium potential has also been considered (9, 13). When diffusion is a factor in the faradaic process, Grahame (10) and Scott (14) have shown the extreme complexity to be expected in any analysis of decay measurements.

The more general situation, in which more than one faradaic process occurs, is treated here. It has been approached only by Lukovtsev and Temerin (15) in their treatment of the discharge of the nickel oxide electrode by oxygen evolution without consideration of the electrical double layer.

General Equations

For any electrode

$$i_{ext} - \Sigma i_f = dq_{dl}/dt = C_{dl}\, dE/dt \qquad [1]$$

where i_{ext} is the external current, Σi_f is the sum of the currents for faradaic processes at the electrode, q_{dl} is the charge on the electrode side of the electrical double layer, t is the time, C_{dl} is the differential capacitance of the electrical double layer, and E is the potential of the electrode, measured with respect to an unpolarized reference electrode (Gibbs-Stockholm sign convention). In any given electrode system, C_{dl} is a function of potential, but its variation over short ranges of potential is generally small, and it may be treated as a constant to a good approximation. By analogy with mercury (16), C_{dl} may be expected to be of the order of 20 μf/cm^2 of true electrode surface.

The potential-time relation to be observed for any electrode can therefore be determined if the current-potential relations for the faradaic processes are known. Although the rates of many faradaic processes are influenced strongly by mass transport phenomena, such complex effects will be neglected here and all phases will be assumed homogeneous. The resulting simplification will be only an approximation to the state of affairs in a system where mass transport is important. Since sufficient homogeneity of a phase can be assured by adequate mixing, and since the extent of inhomogeneity in a real system depends markedly on geometrical as well as electrochemical considerations, the treatment given here will omit any specific discussion of these factors. The current-potential relation for a faradaic process is then determined entirely by activation control.

Close to the equilibrium potential E_e, the faradaic current intensity is given by

$$i_f = i_o n\mathbf{F}(E - E_e)/RT \qquad [2]$$

where i_o is the exchange current intensity (17) and n the number of electrons passed when the rate-determining reaction occurs once. Both i_o and E_e are dependent on the concentrations of reacting species.

At potentials considerably removed from E_e, the current intensity is given by the Tafel equation

$$i_f = \pm i_o \exp[\pm\alpha\mathbf{F}(E - E_e)/RT] \qquad [3]$$

where α is the anodic or cathodic transfer coefficient (17) and the upper signs are used for anodic processes, the lower for cathodic. The Tafel slope is $\pm 2.303\, RT/\alpha\mathbf{F}$.

Normally, investigations of electrode kinetics are made in systems which are buffered in an electro-

chemical sense. Hydrogen and oxygen evolution are usually studied in fairly acidic or basic electrolytes to prevent significant changes in *p*H during the course of an experiment. Problems associated with mass transport and ohmic solution effects are also reduced by this procedure. The faradaic current for a reaction in a system which is electrochemically well-buffered with respect to that reaction is then given by [2] or [3] with both i_o and E_e constant.

However, the electrochemical buffering of a system with respect to one reaction often precludes the buffering of the system with respect to competing reactions which may occur. For example, it is possible to examine the kinetics of silver deposition in solutions containing both silver and hydrogen ions in large quantity, but the process of hydrogen evolution at silver electrodes cannot be studied in solutions containing appreciable quantities of silver ion without great difficulty.

In such a case, it is customary to buffer the system with respect to the reaction of interest and to eliminate as far as possible all other reactants. Even then, the measured steady-state current-potential relations will not refer to the desired reaction unless all the remaining possible reactions are either at equilibrium or so slow for kinetic reasons that they may be disregarded. Very slow reactions may be neglected in general, but it is necessary to consider the possibility of remaining unbuffered reactions which are at equilibrium under steady-state conditions.

For example, during hydrogen evolution at any metal electrode in an acid solution, there exists a finite equilibrium quantity of metal ion in solution at any given steady-state hydrogen overpotential. A change in potential changes the amount of metal ion required for equilibrium and results in a faradaic current corresponding to oxidation of, or reduction to, the metal. Current-potential relations for such an unbuffered reaction are complex, depending on the potential, the exchange current for the reaction, and the concentration of metal ion, all of which are interrelated and time dependent. However, if the unbuffered reaction is characterized by an inherently large rate constant, the process may be considered to take place under conditions close to thermodynamic reversibility, and a considerable simplification becomes possible.

In this case, the faradaic current may be related to the potential by

$$i_f = dq_f/dt = (dq_f/dE_e)(dE_e/dt) \qquad [4]$$

where dq_f is the positive charge carried by the faradaic process from electrode to electrolyte in time dt. Two classes of faradaic processes are of interest.

The equilibrium potential for the metal-metal ion couple $M = M^{z+} + ze^-$ is given by

$$E_e = E^\circ + (RT/z\mathbf{F}) \ln a \qquad [5]$$

where a is the activity of M^{z+} and E° is the standard electrode potential. If the activity can be approximated by the molarity c, the activity change resulting from a faradaic process is

$$da = dc = dq_f/z\mathbf{F}V \qquad [6]$$

where V is the volume of the solution in liters. With the assumption that E is not significantly different from E_e, i.e., that the electrode substantially maintains thermodynamic reversibility with respect to the metal-metal ion reaction, the faradaic current is given by

$$i_f = (z^2\mathbf{F}^2V/RT) \exp [z\mathbf{F}(E - E^\circ)/RT](dE/dt) \qquad [7]$$

For the reaction: reduced species = oxidized species + ze^-,

$$E_e = E^\circ + (RT/z\mathbf{F}) \ln a_o/a_r \qquad [8]$$

where a_o and a_r are the activities of oxidized and reduced species. Approximating activities by molarities c_o and c_r,

$$i_f = [z^2\mathbf{F}^2V(c_o + c_r)/4RT] \operatorname{sech}^2 [z\mathbf{F}(E - E^\circ)/2RT](dE/dt) \qquad [9]$$

As long as $E - E^\circ \leq -0.078/z$ volt, so that $c_o/(c_o + c_r) \leq 0.05$, Eq. [9] may be approximated within 10% by the simpler expression

$$i_f = [z^2\mathbf{F}^2V(c_o + c_r)/RT] \exp [z\mathbf{F}(E - E^\circ)/RT](dE/dt) \qquad [10]$$

which has the same potential dependence as the current for the metal-metal ion reaction. A similar approximation is valid when E is sufficiently greater than E°.

It will be noted that no kinetic parameters appear in these expressions for i_f since these unbuffered faradaic processes are assumed in effect to be infinitely fast. If, as is often the case, i_o is large and dE/dt is not, the limitations introduced by such an assumption are probably less serious than those brought about by the neglect of mass transport phenomena. Quantitative considerations including diffusion and forced convection are prohibitively complex, but qualitatively it is apparent that inhomogeneity in the electrolyte may have a considerable effect, since then only the volume of electrolyte nearest the electrode remains in virtual equilibrium with it during a change in potential.

Potential-Time Relations

With an appropriate choice of current-potential relations, potential-time relations during open-circuit decay may be determined for any electrode. As a specific example, the decay of hydrogen overpotential at a metal electrode in a well-stirred acid electrolyte free from oxygen and other reducible material will be considered, so that the reactions which take place during the decay are $2H^+ + 2e^- \rightarrow H_2$ and $M \rightarrow M^{z+} + ze^-$. The unbuffered metal-metal ion reaction is assumed to be at equilibrium at all times.

Near the equilibrium hydrogen potential.—For this metal electrode in a potential region such that hydrogen evolution is occurring at a rate given by Eq. [2], Eq. [1], [2], and [7] give

$$i_{ext} - i_o n\mathbf{F}(E - E_e^h)/RT - (z^2\mathbf{F}^2V/RT) \exp [z\mathbf{F}(E - E^\circ)/RT](dE/dt) = C_{dl}(dE/dt) \qquad [11]$$

where E_e^h is the equilibrium hydrogen potential. It is apparent that in a steady-state condition ($dE/dt = 0$), no current is carried by the metal-

metal ion reaction and only the first two terms are finite.

On opening the circuit, $i_{ext} = 0$ and integration yields

$$C_{dl} \ln [(E - E_e^h)/(E_0 - E_e^h)] + (z^2\mathbf{F}^2V/RT) \exp [z\mathbf{F}(E_e^h - E^\circ)/RT] \times \{Ei[z\mathbf{F}(E - E_e^h)/RT] - Ei[z\mathbf{F}(E_0 - E_e^h)/RT]\} = -(i_0 n\mathbf{F}/RT)t \quad [12]$$

where $Ei[x]$ is the exponential integral of x, t is the time on open circuit, and E_0 is the potential at the moment of opening the circuit ($t = 0$). If the circuit is opened from a steady-state condition in which the external current is i_i, Eq. [11] shows that $i_0 n\mathbf{F}/RT$ may be replaced by $i_i/(E_0 - E_e^h)$.

If $E^\circ >> E_e^h$, the second term in [12] may be neglected and $\ln (E - E_e^h)$ becomes a linear function of time during the decay with a slope of $-i_0 n\mathbf{F}/C_{dl}RT$. Under this condition, the fraction of the current from the hydrogen evolution reaction used during the decay in forming metal ions is negligible, and a plot of $\ln(E - E_e^h)$ vs. t may be used in the determination of C_{dl}. If the measured potential at the moment of interruption of current is in error because of an ohmic potential drop in the solution between the electrode and the reference electrode, such a plot also provides a means of determining E_0. This type of behavior, which corresponds to the discharge of a capacitor through an ohmic resistance, has been predicted (9), observed experimentally (18), and used in the determination of capacitance (13).

On the other hand, when a negligible fraction of the current from the hydrogen evolution reaction is used in changing the charge in the electrical double layer, the first term of [12] may be neglected, and $Ei[z\mathbf{F}(E - E_e^h)/RT]$ is a linear function of t. When $z\mathbf{F}(E_0 - E_e^h)/RT$ is small, the difference between exponential integrals may be approximated by $\ln [(E - E_e^h)/(E_0 - E_e^h)]$, so that the relation between $\ln(E - E_e^h)$ and t is again linear. However, the slope is now $-(i_0 n/z^2\mathbf{F}V) \exp [z\mathbf{F}(E^\circ - E_e^h)/RT]$ and is unrelated to the capacitance of the electrical double layer.

In Fig. 1, $\log (E_e^h - E)$ is plotted against t during the open-circuit decay of hydrogen overpotential at a 1 cm² metal electrode whose ions are divalent. As parameters typical of such a system, $i_0 = 10^{-5}$ amp, $n = 1$, and $C_{dl} = 20$ μf were chosen, and the volume of solution was taken to be 10^{-5} liter. Three cases are shown, each originating at the same value of $E_e^h - E_0 = 0.026$ v, but with different values of $E^\circ - E_e^h$.

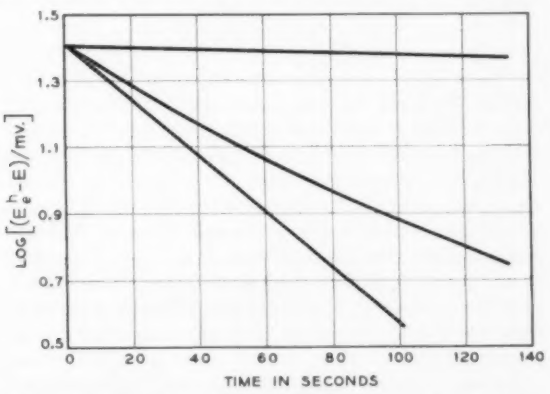

Fig. 1. Decay of hydrogen overpotential at a 1 cm² electrode of a metal whose ions are divalent ($z = 2$). $i_0 = 10^{-5}$ amp, $n = 1$, $C_{dl} = 20\mu f$, $V = 10^{-5}$ liter, $E_e^h - E_0 = 0.026$ v. Lower curve, $E^\circ - E_e^h \geqq 0.313$ v; middle curve, $E^\circ - E_e^h = 0.254$ v; upper curve, $E^\circ - E_e^h = 0.195$ v.

The most rapid decay corresponds to $E^\circ - E_e^h \geqq 0.313$ v. In this case, the second term of Eq. [12] is less than 1% of the first term so that the slope of $\log (E_e^h - E)$ vs. t is a measure of C_{dl}. The least rapid decay corresponds to $E^\circ - E_e^h = 0.195$ v. For this and any smaller values, the second term of [12] is at least 100 times the size of the first term so that the fraction of the current from the hydrogen evolution reaction changing the charge in the electrical double layer is negligible. The middle curve corresponds to $E^\circ - E_e^h = 0.254$ v, an intermediate case.

While the theory on which these plots are based is limited by the approximations made in its derivation, the large capacitative effect shown by faradaic process involving the metal-metal ion couple should be strongly emphasized. It can be shown readily that the oxidation of a metal in contact with a solution containing m moles of divalent metal ion corresponds to an apparent capacitance of the order of $1.5 \times 10^{13}\, m$ μf, and even in extremely dilute solutions this may easily exceed the capacitance of the electrical double layer.

In the Tafel region.—For the same metal electrode in a potential region where the current for hydrogen evolution is given by Eq. [3],

$$i_{ext} + i_0 \exp [\alpha\mathbf{F}(E_e^h - E)/RT] - (z^2\mathbf{F}^2V/RT) \exp [z\mathbf{F}(E - E^\circ)/RT](dE/dt) = C_{dl}(dE/dt) \quad [13]$$

On opening the circuit, $i_{ext} = 0$, and integration yields

$$C_{dl}\{\exp [\alpha\mathbf{F}(E - E_e^h)/RT] - \exp [\alpha\mathbf{F}(E_0 - E_e^h)/RT]\} + [\alpha z^2\mathbf{F}^2V/(\alpha + z)RT] \exp [z\mathbf{F}(E_e^h - E^\circ)/RT]\{\exp [(\alpha + z)\mathbf{F}(E - E_e^h)/RT] - \exp [(\alpha + z)\mathbf{F}(E_0 - E_e^h)/RT]\} = (i_0\alpha\mathbf{F}/RT)t \quad [14]$$

If $E^\circ >> E_e^h$, the second term in [14] may be neglected because a negligible fraction of the current from hydrogen evolution is used in forming metal ions. In this case, the equation may be rewritten

$$E = E_0 + (RT/\alpha\mathbf{F}) \ln \{1 + (\alpha\mathbf{F}i_0 t/RTC_{dl}) \exp [\alpha\mathbf{F}(E_e^h - E_0)/RT]\} \quad [15]$$

If the circuit is opened from a steady state in which the external current is i_i, Eq. [13] indicates that [15] may be simplified by replacing $i_0 \exp [\alpha\mathbf{F}(E_e^h - E_0)/RT]$ by $-i_i$.

If C_{dl} is independent of potential, the ratio i_0/C_{dl} is determined solely by the composition of the system, and Eq. [15] shows then that, at sufficiently large values of t, all decays in a system of constant composition become coincident, regardless of E_0 and electrode area. Furthermore, when t is large, the potential is a linear function of $\ln t$ with a slope of $RT/\alpha\mathbf{F}$.

Since Baars (1) and Bowden and Rideal (2) in 1928, many workers have observed such behavior. The experiments of Fedotov (19) are of particular interest, for the values of C_{dl} which he determined from measurements of the decay of hydrogen over-

potential on mercury agree well with the a-c determinations of capacitance at the same potentials. In certain cases, successive potential-time curves starting from different values of E_o have been observed to cross by Hickling and Salt (20) and Kolotyrkin (21). This has been ascribed by the latter to changes in surface area, but this explanation is clearly inapplicable under the conditions in which Eq. [15] applies.

If a negligible fraction of the current from the hydrogen evolution reaction is used in changing the charge in the electrical double layer, the first term in Eq. [14] may be neglected and the equation may be rewritten

$$E = E_o + [RT/(\alpha + z)\mathbf{F}]\ln\{1 + [i_o t(\alpha + z)/z\mathbf{F}V] \times \exp[\alpha\mathbf{F}(E_e^h - E_o)/RT]\exp[z\mathbf{F}(E^\circ - E_o)/RT]\} \quad [16]$$

which corresponds to the result obtained by Lukovtsev and Temerin (15).

The similarity in form between Eq. [15] and [16] is striking and clearly indicates that in the Tafel region capacitative effects resulting from faradaic processes may well be indistinguishable from the capacitance of the electrical double layer. The essential difference is that the slope exhibited by a plot of E vs. ln t at large values of t is $RT/(\alpha + z)\mathbf{F}$ rather than $RT/\alpha\mathbf{F}$. It is interesting to note that in this case, a crossing of decay curves can be ascribed to changes in surface area, since the resulting change in i_o is uncompensated by a corresponding change in V. The discrepancies observed by Hickling and Salt (20) between decay slopes and the negatives of the Tafel slopes measured by a direct method lend additional weight to this explanation of such behavior.

In Fig. 2, $E_e^h - E$ is plotted against log t during the open-circuit decay of hydrogen overpotential at the same 1 cm² metal electrode illustrated in Fig. 1. Again, typical parameters for such a system were chosen: $i_o = 10^{-6}$ amp, $C_{dl} = 20$ μf, and the volume of solution containing divalent metal ions in equilibrium with the electrode was taken to be 10^{-3} liter. The transfer coefficient α was chosen to be ½, so that the Tafel slope is −0.118 v/tenfold change in current. Three decays are shown, each from the same value of $E_e^h - E_o = 0.592$ v, but with different values of $E^\circ - E_e^h$.

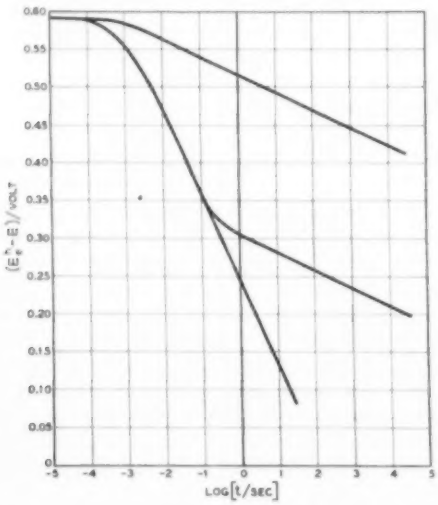

Fig. 2. Decay of hydrogen overpotential at a 1 cm² electrode of a metal whose ions are divalent ($z = 2$). $i_o = 10^{-6}$ amp, $\alpha = ½$, $C_{dl} = 20$ μf, $V = 10^{-3}$ liter, E_e^h-$E_o = 0.592$ v. Lower curve, E°-$E_e^h = 0.183$ v; middle curve, E°-$E_e^h = -0.080$ v; upper curve, E°-$E_e^h = -0.344$ v.

The most rapid decay corresponds to $E^\circ - E_e^h = 0.183$ v, in which case Eq. [15] is applicable, since the second term of Eq. [14] is no more than about 1% of the first term and may be neglected. The least rapid decay corresponds to $E^\circ - E_e^h = -0.344$ v, and in this case the relative magnitudes of the terms are reversed. The middle curve is for $E^\circ - E_e^h = -0.080$ v, an intermediate case, and is of particular interest because of the relatively sharp transition it exhibits. In the initial portion essentially all the current from the hydrogen evolution reaction goes to change the charge in the electrical double layer and the decay coincides with the decay curve for $E^\circ - E_e^h = 0.183$ v. The later part of the decay is parallel to the decay for $E^\circ - E_e^h = -0.344$ v and like it, results from the capacitative effect shown by the metal-metal ion couple. It is apparent that in this intermediate case, observations of the potential at times greater than 1 sec or of decays from values of $E_e^h - E_o$ of less than about 0.31 v will not include any capacitative effects due to the electrical double layer.

While it is doubtful that experimental conditions corresponding exactly to the approximations introduced in the derivation of Eq. [14] are ever attained in practice, it may be noted that Salkind (22) and Conway and Bourgault (23) have observed two-stage decays of potential analogous to that illustrated in Fig. 2 in studies of the decay of oxygen overpotential on nickel oxide electrodes. Similar considerations may well account for some of the anomalously large slopes observed during open-circuit decay measurements on oxygen-evolving platinum electrodes (8).

Analysis of Decay Measurements in the Tafel Region

From the discussion of the previous section and a comparison of Eq. [15] and [16], it is clear that any decay from a steady-state condition can be represented at least approximately by an equation of the form

$$E = E_o - b_t \ln(1 + t/t_o) \quad [17]$$

where b_t and t_o are parameters characteristic of the decay. Where a transition occurs, as illustrated in Fig. 2, values of b_t and t_o may be associated with each portion of the curve. In the simple case of the discharge of the electrical double layer illustrated in Eq. [15], t_o may be identified with the quantity $b_t C_{dl}/i_t$, and similar identifications may be made in more complex cases. Although numerical values of b_t and t_o can be determined by the analysis of measured decay curves, further information is necessary before physical meanings can be assigned to these parameters.

Where t_o can be identified with $b_t C_{dl}/i_t$, the determinations of the ratio b_t/t_o is sufficient to determine C_{dl}, and from Eq. [17] this is given by the negative of the initial slope. A similar situation obtains when a faradaic process exhibits a capacitative effect. An

expansion of the logarithmic term of Eq. [17] shows that for small values of t the potential is a linear function of t, but in practice this linear region is sufficiently small that measurements of considerable sensitivity are required if the ratio b_t/t_0 is to be found with any degree of accuracy.

This becomes apparent if the initial slope is considered to be approximated by a line drawn between E_0 and a later value of E. It can be shown that this will differ from the true value $-b_t/t_0$ by more than 10% if the later value of E is more than $0.2b_t$ away. Since values of b_t of greater than ± 0.051 v are seldom observed, it is apparent that precise measurements of the decay must be made within about 0.010 v of E_0 to give b_t/t_0 to 10%.

It is worth noting that in the interrupter method developed by Hickling (24) and others for measuring overpotential when ohmic potential drops exist in the solution between the electrode and the reference electrode, use is made of this linear potential-time region to extrapolate open-circuit measurements of potential to $t = 0$ and thus to determine E_0. Although the values of E_0 are less sensitive than the values of b_t/t_0 to an erroneous assumption as to the range over which the linear region extends, it is clear that care must be exercised when such a linear extrapolation is made.

There are several methods by which b_t and t_0 may be separately determined from experimental data. Most obviously, an empirical choice of t_0 can be made such that E is a linear function of $\ln (1 + t/t_0)$. The slope of such a line is $-b_t$. This procedure is, however, likely to be somewhat more tedious and less accurate than a method not involving trial and error.

When t is much larger than t_0, the potential becomes a linear function of $\ln t$ with a slope of $-b_t$ as shown in Fig. 2. The equation of this linear function is

$$E = E_0 - b_t \ln (t/t_0) \qquad [18]$$

from which it is apparent that the function passes through the value $E = E_0$ at $t = t_0$. Thus a linear extrapolation of the latter part of the E vs. log t plot to E_0 gives t_0 directly. Since it has been noted that all decay curves for a given electrode coincide at large values of t regardless of the value of E_0, the quantity $E_0 + b_t \ln t_0$ is constant and t_0 has therefore been termed the time required for the potential to decay to E_0 from infinite potential (11).

Two considerations make this method of determining t_0 and b_t less attractive than it at first appears. If it is assumed possible to take an exact tangent to the E vs. $\ln t$ curve at any point and to use this tangent for the determination of b_t and t_0, it can be shown that the value of t_0 obtained will be in error by more than 10% unless the tangent is taken at a time greater than 46 t_0, which corresponds to a potential decay of more than 3.8 b_t. Consequently, the method cannot be used with accuracy unless the potential decay is observed over a sizable range. This requirement eliminates its use in that part of the Tafel region nearest the equilibrium potential because the decay must then be followed into a potential region in which Eq. [17] is no longer applicable.

A second important consideration in the application of this method arises from the assumptions made during the derivations leading to Eq. [17]. For small changes in potential, b_t and t_0 may be taken as constants to a good approximation; but over larger ranges such constancy may be seriously questioned, throwing doubt on the extrapolation to E_0.

The following method of analysis overcomes to a considerable extent the objections raised to the procedures described above. The inverse of dE/dt is, from Eq. [17],

$$\left(\frac{dE}{dt}\right)^{-1} = -\frac{t_0 + t}{b_t} \qquad [19]$$

so that dt/dE is a linear function of t with a zero intercept of $-t_0/b_t$ and a slope of $-1/b_t$. In practice, dt/dE may be approximated by $(t_{n+1} - t_n)/(E_{n+1} - E_n)$ and plotted against $(t_n + t_{n+1})/2$ without introducing significant errors, for it can be shown that the computed derivative is within 5% of the true value as long as $t_{n+1} - t_n$ is less than $1.2(t_n + t_0)$. This procedure is particularly attractive in that it can be used to determine t_0 and b_t from measurements over any small range in potential and is limited only by the accuracy with which E and t can be measured.

Acknowledgment

The author is indebted to J. F. Dewald and U. B. Thomas for many helpful discussions during the course of this work.

Manuscript received July 28, 1959. This paper was prepared for delivery before the Chicago Meeting, May 1-5, 1960.

Any discussion of this paper will appear in a Discussion Section to be published in the December 1960 JOURNAL.

REFERENCES

1. E. Baars, *Sitzber. Ges. Beford. ges. Naturw. Marburg*, **63**, 2.3 (1928).
2. F. P. Bowden and E. K. Rideal, *Proc. Roy. Soc.* **A120**, 59 (1928).
3. J. A. V. Butler, *Trans. Far. Soc.*, **28**, 379 (1932).
4. G. Armstrong, J. A. V. Butler, *Trans. Faraday Soc.*, **29**, 1261 (1933).
5. A. N. Frumkin, *Acta Physicochim. USSR*, **18**, 23 (1943).
6. A. N. Frumkin, *Discussions Faraday Soc.*, **1**, 57 (1947).
7. A. Hickling and F. W. Salt, *Trans. Faraday Soc.*, **38**, 474 (1942).
8. W. R. Busing and W. J. Kauzmann, *J. Chem. Phys.*, **20**, 1129 (1952).
9. J. O'M. Bockris and E. C. Potter, *This Journal*, **99**, 169 (1952).
10. D. C. Grahame, *J. Phys. Chem.*, **57**, 257 (1953).
11. H. B. Morley and F. E. W. Wetmore, *Can. J. Chem.*, **34**, 359 (1956).
12. W. A. Roiter, W. A. Juza, and E. S. Polujan, *Acta Physicochim. USSR*, **10**, 389 (1939).
13. S. Schuldiner and R. E. White, *This Journal*, **97**, 433 (1950).
14. W. T. Scott, *J. Chem. Phys.*, **23**, 1936 (1955).
15. P. D. Lukovtsev and S. A. Temerin, *Trudy Soveshchaniya Elecktrokhim. Akad. Nauk SSSR, Otdel. Khim. Nauk*, **1950**, 494 (1953).
16. D. C. Grahame, *J. Am. Chem. Soc.*, **63**, 1207 (1941).
17. J. O'M. Bockris, "Modern Aspects of Electrochemistry," Chap. 4, Academic Press, New York (1954).
18. J. O'M. Bockris and E. C. Potter, *J. Chem. Phys.*, **20**, 614 (1952).
19. N. A. Fedotov, *Zhur. Fiz. Khim.*, **25**, 3 (1951).

20. A. Hickling and F. W. Salt, *Trans. Faraday Soc.*, **37**, 450 (1941).
21. Ya. M. Kolotyrkin, *Zhur. Fiz. Khim.*, **20**, 667 (1946).
22. A. J. Salkind, "Investigation of the Sintered Plate Nickel-Cadmium Battery." Thesis, Polytechnic Institute of Brooklyn (1958).
23. B. E. Conway and P. L. Bourgault, *Can. J. Chem.*, **37**, 292 (1959).
24. A. Hickling, *Trans. Faraday Soc.*, **33**, 1540 (1937).

Glossary of Symbols

C_{dl} — Capacitance of the electrical double layer, dq_{dl}/dE, farads.
E — Potential measured with respect to an unpolarized reference electrode, v (Gibbs-Stockholm sign convention).
E_e — Equilibrium potential of a faradaic process, e.g., a metal-metal ion process ($i_f = 0$), v.
E_e^h — Equilibrium potential of the hydrogen gas electrode, v.
E° — Standard potential of the faradaic process, v.
E_0 — Potential at beginning of decay ($t = 0$), v.
dq_f — Amount of positive charge entering electrolyte from electrode by means of the faradaic process, coulombs.
q_{dl} — Amount of positive charge on electrode side of the electrical double layer, coulombs.
i_{ext} — Current intensity in external circuit, amp.
i_f — Current intensity corresponding to the faradaic process, dq_f/dt, amp.
i_s — Steady-state current intensity in external circuit at the moment of opening the circuit, amp.
i_o — Exchange current intensity for an activation-controlled electrode reaction, amp.
t — Time, also time on open circuit, sec.
t_o — Parameter of decay, sec.
n — Number of electrons passed in an activation-controlled reaction when the rate-determining step occurs once.
α — Transfer coefficient for an activation-controlled reaction.
z — Number of electrons passed by the faradaic process in one occurrence of the over-all reaction.
b_t — Parameter of decay, change in potential for an e-fold change in time when $t >> t_o$, v.
a — Activity.
a_o — Activity of oxidized species.
a_r — Activity of reduced species.
c_o — Molarity of oxidized species.
c_r — Molarity of reduced species.
V — Liters of electrolyte in equilibrium with the electrode.

Arsine Evolution and Water Reduction at an Arsenic Cathode

H. W. Salzberg and Bernard Goldschmidt[1]

Chemistry Department, City College, New York, New York

ABSTRACT

The effects of current density, temperature, acidity, and salt concentration on the evolution of arsine have been studied at arsenic and lead-arsenic cathodes. Analysis of the data indicates that the surface of the electrode is largely covered with chemisorbed hydrogen at current densities as low as 5-10 ma/cm², that arsine is formed by reduction of water molecules on the chemisorbed layer of hydrogen, that the rate-determining step is the disproportionation between adjacent surface hydrides, and that water molecule reduction takes place at the electrode even in 1M sulfuric acid at current densities at least as low as 1 ma/cm².

Previous work (1-4) on tin, lead, and antimony cathodes has shown that on these cathodes, when cathodic disintegration or hydride formation occurs, the water molecule, rather than the hydronium ion, is the immediate source of the hydrogen present in the hydride molecule. This water molecule reduction is observed at current densities at least as low as 20-30 ma/cm² in solutions of pH 2.5 or higher. To see if water molecules are reduced at lower current densities and in more acid solution, it was decided to investigate the arsenic-arsine system, since arsine is known to form at low current densities and because micro methods for its determination are known.

Apparatus, Method, and Materials

The apparatus was that of the previous work, with only minor changes (1). The arsine was absorbed in $HgCl_2$-$KMnO_4$-H_2SO_4 solution and determined colorimetrically by the standard molybdenum blue method (5).

The electrolytic solutions were made of C. P. materials dissolved in distilled water and usually pre-electrolyzed at c.d.'s between 10 and 500 ma/cm² for periods up to 24 hr. Check runs using different batches of solution made from different lots of material were in good agreement with each other.

Arsenic cathodes were prepared by plating arsenic out of concentrated solutions of $AsCl_3$ in glacial acetic acid, using the method of Audrieth (6). It is felt that the surfaces were pure arsenic since any zinc that leached out of the brass before plating started would not replate, due to the large differences in both potential and concentration between the zinc and the arsenic. In any event, each cathode immediately before use was cleaned in fresh concentrated HCl and then replated from fresh plating solution for about 10 min at about 3-6 ma/cm² to remove impurities and/or oxide film. The lead-arsenic surface was prepared simply by dipping a lead washer of appropriate size into an arsenic plating solution. No conclusions can be drawn concerning this surface except that it was a mixture of arsenic and lead.

Current densities were calculated on the basis of geometric area, which means that real current densities and real rates of arsine formation were lower than the figures given here. Also, due to different

[1] Present address: Department of Chemistry, University of Wisconsin, Madison, Wis.

histories, each cathode must have had a roughness factor at least slightly different from the others.

40°C runs were controlled to within 0.2°C, 25°C runs were controlled to within 1°C.

Potentials were not measured while arsine formation was being determined. Separate cells with a calomel reference were used. First the potential was measured directly at the desired apparent current density. Then the *IR* drop was measured, using a current interrupter technique, and subtracted from the total reading to give the potential of the cathode vs. the calomel. The interrupter was a mercury capillary relay activated by 60-cycle half-wave rectified house current. The make-break times were of the order of microseconds. The *IR* drop was obtained from the calibrated oscilloscopic trace of the potential.

The temperature coefficient was obtained by averaging temperature coefficients for several different cathodes. This procedure was followed because differences in roughness caused different apparent rates at each temperature for the various cathodes whose temperature coefficients, however, were in agreement.

In order to guard against false rates due to changes in surface, each cathode was run first at 25°C, then at 40°C, at 25°C again, at 40°C again, etc, and the temperature coefficients were calculated from values in agreement with each other. Results were then averaged among all other cathodes used in the temperature coefficient experiments. Also, different batches of solution were used with the same cathodes, and the same solutions were used with different cathodes. Whenever results were not self-consistent they were discarded.

As an additional check, after 2 years had elapsed, temperature coefficients were re-run with different materials, different cells, and a different cathode system. The cathode was a 10 cm^2 cone of silver-plated brass which had been plated with arsenic to a thickness of several millimeters. Solutions were made with conductivity water. Solids were CP materials recrystallized from conductance water. The scouring gas was electrolytic hydrogen passed over a palladium catalyst to remove oxygen and then passed over activated carbon at solid CO_2-acetone temperature. Pre-electrolysis was carried out for periods of time up to 5 days. Although apparent c.d. and rates differed from those of the original work, temperature coefficients were in substantial agreement with the original.

In spite of the elaborate precautions discussed above, the results were often disheartenningly irreproducible. To a great extent this was due to differences in surface. Each cathode had a slightly different shape, area, position in the cell, arsenic thickness, arsenic roughness, a different time lapse between the original plating and use, and a different plating current. Results therefore varied from cathode to cathode. Curves obtained with different cathodes were shifted slightly along the axis, although the shapes of the curves were the same. However, differences between curves for different cathodes were minor compared to differences resulting from changes in pH. Also, by the nature of the reaction, the surface of any cathode must have changed during each run, thus giving rise to further irreproducibility.

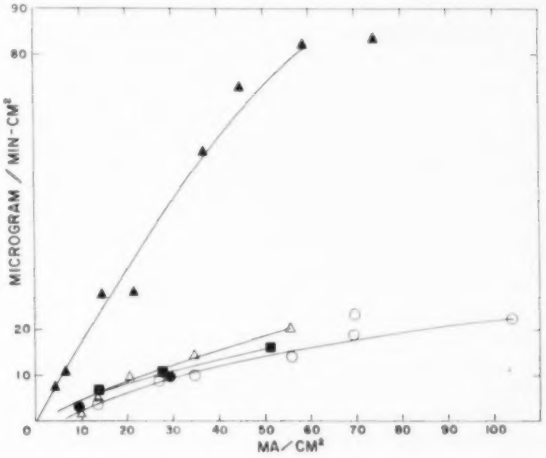

Fig. 1. Rate of arsine evolution vs. current density, ▲, 1M Na_2SO_4, △, 0.1M H_2SO_4; ○, 1M H_2SO_4; ●, 1M H_2SO_4-Grube's data; ■, 1M H_2SO_4 on Pb-As cathode.

Nevertheless by discarding the results of those cathodes that gave erratic results and by purifying and re-purifying solutions, results were finally obtained that were self-consistent and valid.

Experimental Results

Figure 1 shows the rate of arsine production plotted against apparent current density. The efficiency of arsine formation is low, only about 10% of the current going into arsine in neutral solution and about 1-2% in acid. Increased acidity lowers the rate of arsine formation. Arsine is formed at current densities less than 1 ma/cm^2. At high current densities, the rate falls off, probably due to a high pH around the cathode. The rate of arsine production at an arsenic-lead surface in molar acid is definitely higher than at an arsenic surface in the same solution. The fact that the two points taken from Grube's work (7) fit so well is fortuitous, since there would have been a slightly different curve using another cathode. Nevertheless, the agreement is good. Curves obtained, but not plotted here, for mixtures of acid and salt, would fall between those for pure acid and pure salt solutions. Curves obtained, but not plotted here, using cathodes that had accumulated a layer of surface oxide by standing in the laboratory for varying periods of time, gave results that were both higher and more erratic. Results using cathodes that had been deliberately given an oxide coating were also higher.

Figure 2 shows the overvoltage curves for arsenic and arsenic-lead surfaces in acid solution and the *voltage* curve for arsenic in neutral solution. Potentials are higher in neutral solution. Lead-arsenic potentials in acid are more than with arsenic in acid but less than for arsenic in neutral solution. The 25° and 40°C curves in neutral solution correspond at low current densities but diverge above current densities of about 30 ma/cm^2, with the 25°C curve being slightly higher. Each curve has two regions

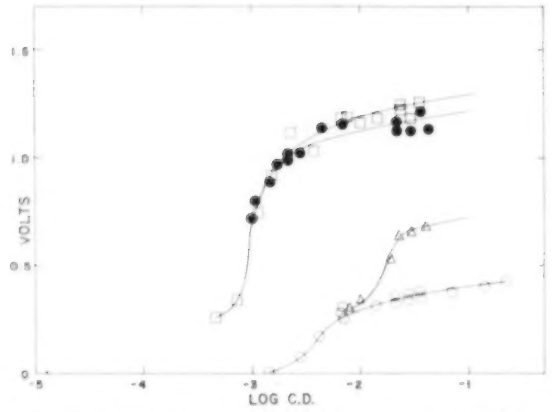

Fig. 2. Potential vs. current density curves. ○, overvoltage on arsenic in H_2SO_4 at 25°C; △, overvoltage on lead-arsenic in acid at 25°C; □, voltage on arsenic in neutral solution at 25°C; ●, overvoltage on arsenic in neutral solution at 40°C.

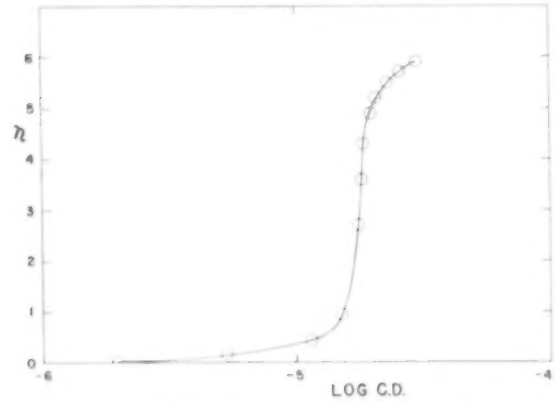

Fig. 3. Overvoltage vs. current density. Data taken from Grube's work on arsenic in acid solution.

corresponding to a build-up of potential at low current densities and a leveling off at higher current densities. The slopes observed at higher current densities are about those values generally observed at high hydrogen overvoltage, but in view of the crudeness of the apparatus, with a rather large experimental error. The leveling off at high current densities is in agreement with the results reported by Lloyd (8) and the general shape of the curve is that reported by Grube (7) as shown in Fig. 3. This graph shows that Grube's values differ from ours but that his curve has the same shape. Noteworthy also is the fact that at very low current densities his slope is about 0.03.

Table I gives some temperature coefficients. Within experimental error, they are all the same.

Discussion

Coverage of the surface by hydrogen.—The overall mechanism must proceed by way of a disproportionation between two adjacent arsenic-hydrogen groups. The probability of a simultaneous reaction between three adjacent As-H groups and of three consecutive electrochemical reductions at one site for each arsine molecule is negligible. This disproportionation would then occur between an arsenic-monohydrogen and an arsenic-dihydrogen group.

Since, in neutral solution, about 10% of the current goes into arsine production via adjacent arsenic hydrogen groups, at least 20% of the surface is covered by hydrogen atoms, even at 1 ma/cm² (Fig. 1). Yet the combination of surface hydrogen atoms in the unadsorbed or physically adsorbed state is extremely rapid (9). For such a large fraction of the surface as 20% to be covered by hydrogen, the heat of adsorption would be at least 23 kcal/mole, using the calculations of Salzberg and Schuldiner (9). This means that the hydrogen would be chemisorbed in the form of a surface hydride. Actually, arsenic and hydrogen do form a strong covalent bond whose energy is estimated by Pauling (10) to be 47 kcal/mole.

The arsenic-dihydrogen group mentioned above is either an adsorbed molecule or a surface dihydride. The latter would have to be extremely unstable since no such substance has been reported. On the other hand, since the bond energy of the hydrogen molecule is about 104 kcal/mole and that of two As-H bonds would be about 94 kcal/mole, an adsorbed hydrogen molecule would not be likely to break down into two hydrogen atoms which then form covalent bonds with an arsenic atom, i.e., disproportionate into an arsine molecule. Rather, the process would go the other way. Two hydrogen atoms held by covalent bonds to the same arsenic atom would combine to form a molecule of hydrogen. Since the radius of an arsenic atom is 1.25Å and that of the hydrogen atom is 0.37Å there would be plenty of room for two hydrogen atoms to be bound to one surface arsenic atom. The dihydrogen group would therefore be AsH_2, a surface hydride, formed either by a second hydrogen atom being produced at a site which already has a hydrogen atom [(a) in Fig. 4] or by a disproportionation between two adjacent AsH groups [(b) in Fig. 4]

In Fig. 4, the large circles represent arsenic atoms, the small ones hydrogen atoms. Step (a) is an electrochemical reaction; step (b) is also an electrochemical reaction; step (c) is a disproportiona-

Table I. Temperature coefficients at constant current

Solution	Cathode	Rate at 40°C/ rate at 25°C
1M H_2SO_4	As	1.3 ± 0.2
1M H_2SO_4	As-Pb	1.2 ± 0.3
1M Na_2SO_4	As	1.2 ± 0.2

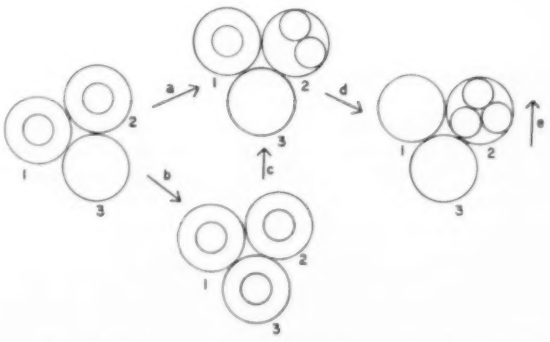

Fig. 4. Diagram of possible reaction paths. Large circles are arsenic atoms, small circles are hydrogen atoms.

tion between two adjacent monohydride molecules forming a dihydrogen molecule; step (d) is a disproportionation forming an arsine molecule; and step (e) is the desorption of the arsine from the surface.

In either event, whether the dihydride is formed electrochemically as in (a) or by disproportionation as in (c) arsine formation must be preceded by the formation of adjacent As-H groups. Since the dihydrogen molecule must be unstable, breaking down rapidly into molecular hydrogen and arsenic, most of the dihydride formed would go directly into molecular hydrogen. An over-all 10% yield of arsine implies that much more than 10% of the current goes into the formation of the unstable dihydrogen hydride and therefore that the surface would be largely saturated with monohydrogen hydride.

The rate-determining process.—The rate-determining step in arsine formation in both neutral and acid solution is (d) in Fig. 4, the disproportionation between As-H and AsH_2. Also, the water molecule, rather than the hydronium ion is the immediate source of the hydrogen found in arsine. These ideas follow from the facts that : (*a*) arsine production falls off as acidity is increased and in acid solution increases as sodium sulfate is added; (*b*) even in acid solutions, the potential at current densities where arsine is produced is high enough to reduce water molecules; (c) the temperature coefficient of arsine production at constant current is positive and the same in both acid and neutral solution. The import of this last statement may not be immediately obvious and so some elaboration is required.

The rate of a reaction is directly proportional to the number of reactant particles which possess a total energy equal to that of an activated complex. The energy of the activated complex is relatively independent of temperature. (For example, if the activated complex in this case is a molecule consisting of a surface arsenic atom and two adsorbed hydrogen atoms, there are no degrees of translational freedom, one degree of rotational freedom, and one degree of vibrational freedom less than the normal $3N$-6. The heat capacity at constant volume, according to classical theory, is at most 10 cal/mole-degree. Over a 15 degree range at constant pressure, the energy of the activated complex would change by about 170 cal at most.) Consequently, the reaction products at the moment of formation all have about the same energy regardless of the temperature at which the reaction occurs. After formation, inelastic collisions result in thermal equilibrium and so at higher temperatures the reaction products will have a greater energy. Nevertheless, at the moment of formation, the products have an energy independent of temperature.

One exception to this, however, is the case of electrochemical reactions involving an overvoltage. To speed up these reactions, electrical energy is supplied to the reacting particles, thus increasing the number that have the required energy. If the overvoltage is α, the electrical energy added per equivalent is $\alpha n\mathbf{F}$, where α is a fraction whose value is usually about ½ and **F** is the faraday. The rest of the electrical energy supplied to the system $(1-\alpha)n\mathbf{F}$ goes to the products of the rate-determining step. (This is obvious since this fraction of the expended energy does not influence the rate of reaction.) So, for these reactions, the energy of the reaction products is greater than that of the activated complex by $(1-\alpha)n\mathbf{F}$ until thermal equilibrium is reached. This means that the higher the overvoltage, the greater the energy of the products, since more electrical energy must be supplied. The products of water molecule reduction, which occurs at a higher voltage, will have a greater energy than the products of hydronium ion reduction. The higher the current, the greater the energy of the products, since the voltage is greater. Finally, the higher the temperature, the lower the overvoltage of the reaction and the less the energy of the reaction products at the moment of formation. With this in mind we can get down to cases.

The positive temperature coefficient, at constant current, eliminates an electrochemical, rate-determining step (RDS) since at constant current an electrochemically formed activated complex would be produced at a rate independent of temperature. The RDS then involves neutral products of electrochemical steps, i.e., the RDS is either (c), or (d) or (e) in Fig. 4.

The positive temperature coefficient also eliminates an RDS between electrochemical reaction products that react immediately, before they undergo collisions with solvent molecules and reach thermal equilibrium. The energy of newly formed products of an electrochemical step would decrease, if anything, with increased temperature and decreased overvoltage and hence the temperature coefficient of an RDS involving newly formed reactants would not be positive.

On the other hand, if all of the participants in the RDS had reached equilibrium, there would be no difference in the rates in neutral and in acid solution, since the energies of the reactants would depend only on temperature and not on pH. This eliminates the desorption of arsine [reaction (e)] as the RDS.

The only possibilities left are the two disproportionation reactions which could occur between one newly formed hydrogen atom and either one or two previously formed atoms that had already reached thermal equilibrium, that is either (c) or (d) in Fig. 4. Of these the formation of dihydrogen hydride (c) can be dismissed as the RDS. If the movement of the newly formed high-energy hydrogen atom from position 3 to position 2 is slow, the movement of the previously formed, and therefore lower energy, hydrogen atom from position 1 to position 2 should be even slower. But this would make (d) slower than (c) and so (c) could not be the RDS.

By elimination, therefore, the RDS is the disproportionation between the AsH and a newly formed electrochemically produced AsH_2 group, step (d).

The rate of this reaction obviously depends on the energy of the AsH_2. If this is formed by reduction of a water molecule at a high overvoltage, its energy would be higher than if it were formed from a hydronium ion at a lower overvoltage. But, since

the temperature coefficient is the same in both acid and neutral solution, the dihydrogen hydride must be formed with the same energy in both cases. This means that the hydride would be formed by reduction of water molecules, since presumably neutral solutions would not have sufficient hydronium ion present at the surface to maintain the reaction. The difference in rates between the acid and neutral solutions is the result of fewer water molecules being reduced in acid solutions.

The dihydrogen hydride formed from hydronium ion reduction would not have enough energy to form arsine but would break down to molecular hydrogen. Since the ion is more easily reduced than the water molecule, in acid before water molecule reduction can start, a critical current density must be reached at which the surface hydronium ion concentration is too small to support the current. The shape of the curve supports this idea. The greater the acidity, the more hydronium ion initially present, and the higher the neutral salt concentration the fewer hydronium ions initially present at the surface. The data show that increased acidity and decreased neutral salt concentration lowers the rate of arsine formation.

The production of arsine at a lead-arsenic cathode would follow the same mechanism as at an arsenic cathode, since in acid solution the temperature coefficient is the same, the shape of the overvoltage curve is the same, the shape of the rate curve is the same, and the rates and potentials both fall between those of arsenic in neutral solution and in acid solution.

The evolution of hydrogen, as distinct from the formation of arsine, has several different rate-determining steps, depending on the current density. At very low current densities, the surface is not saturated with hydrogen and the RDS is the combination of atoms to form molecules. The initial slope of Fig. 3 is about 0.03, within experimental error, and the overvoltage is less than about 40 mv.

Above about 10^{-5} ma/cm^2, Grube's results indicate that the surface starts to become saturated and the potential increases to that required for production of hydrogen on an arsenic hydride surface. This steep rise also shows up in the first portion of the curves in Fig. 2.

At about 5-10 ma/cm^2, the surface is saturated with monohydrogen hydride and the slope of the overvoltage curve levels off to about the 0.12 value expected for the reduction of a water molecule or the slow or retarded discharge of a hydronium ion. The fluctuations at higher values, especially in neutral solution, are either due to changes in the surface produced by arsine formation or to increase in pH.

The same mechanism of hydrogen production applies to the case of the lead-arsenic cathode except that here water reduction probably occurs at a lower current density than on pure arsenic.

Conclusions

It must be re-emphasized that uncertainty as to the true surface area makes the rate and current density data valid only as an upper limit. Also, use of tank hydrogen and ordinary distilled water in the earlier work could have lead to serious errors. However, the checks run with conductance water and a hydrogen purification train were in good enough agreement to indicate that the results were valid.

These conclusions stem from an analysis of the present work and from consideration of the data of Grube (Fig. 3).

1. Arsine is formed by reduction of water molecules on an arsenic surface covered with chemisorbed hydrogen in the form of a covalent hydride.
2. The rate-determining step in arsine formation is the disproportionation between an AsH and an adjacent AsH_2 group or molecule.
3. Water reduction takes place even in 1M acid at current densities at least as low a 1 ma/cm^2.
4. The reactions at a lead-arsenic surface are the same as at an arsenic surface except that in acid solution water reduction starts at lower current densities on the arsenic-lead cathode. Consequently, at a given current density, the voltage and therefore the amount of arsine formed is greater at the lead-arsenic surface.
5. At current densities below 1-2 x 10^{-5} amp/cm^2 in acid solution, the formation of hydrogen atoms is reversible. The rate-determining step in hydrogen evolution at this low current density is the combination of hydrogen atoms. The heat of activation is at least about 23 kcal/mole.
6. The saturation of the surface with chemisorbed hydrogen is virtually complete at current densities of about 10^{-2} amp/cm^2.

This work has implications for the general problem of hydrogen overvoltage. It shows, we believe, that water molecules are reduced at cathodes in acid solution at current densities well below those required for cathode disintegration. This is in agreement with the work of Schuldiner (11) and Schuldiner and Hoare (12) who showed that on palladium and platinum water molecules are reduced at low current densities at pH 0.8 and 1.4, respectively. In both cases the voltage required for water reduction was less than that which is commonly observed at high overvoltage cathodes, such as mercury and lead.

Perhaps the best summary of the position is that concentration polarization at the surface occurs at current densities much lower than that previously expected and that therefore water molecule reduction occurs.

Acknowledgment

This work was made possible only by the aid of the Office of Naval Research. The authors wish to thank Sr. Sigmund Schuldiner for advice and encouragement and Dr. Saul Berman for administrative assistance.

Manuscript received Jan. 31, 1958.

Any discussion of this paper will appear in a Discussion Section to be published in the December 1960 JOURNAL.

REFERENCES

1. F. Mies and H. W. Salzberg, *This Journal*, **105**, 64 (1958).

2. H. W. Salzberg, *ibid.*, **100**, 146 (1953).
3. L. W. Gastwirt and H. W. Salzberg, *ibid.*, **104**, 701, (1957).
4. H. W. Salzberg and A. J. Andreatch, *ibid.*, **101**, 528 (1954).
5. Sandel, "Colorimetric Determination of Traces of Metals," Interscience Publishers, New York (1950).
6. L. F. Audrieth and C. W. Stilwell, *J. Am. Chem. Soc.*, **54**, 472 (1932).
7. G. Grube and H. Kleber, *Z. Elektrochem.*, **30**, 517 (1924).
8. W. Lloyd, *Trans. Faraday Soc.*, **26**, 15 (1930).
9. H. W. Salzberg and S. Schuldiner, *This Journal*, **104**, 319 (1957).
10. L. Pauling, "Nature of Chemical Bond," Cornell University Press (1940).
11. S. Schuldiner, *This Journal*, **101**, 426 (1954).
12. S. Schuldiner and J. P. Hoare, *ibid.*, **102**, 488 (1955).

Technical Notes

Creeping Silver Sulfide

T. F. Egan and A. Mendizza

Bell Telephone Laboratories, Incorporated, Murray Hill, New Jersey

An effect was observed when a silver specimen coated with a porous gold electroplate was exposed to sulfur vapor. Silver sulfide formed at the pore sites as would be expected, but in addition it spread radially and rapidly on the gold surface, to which it was strongly adherent.

For a preliminary investigation of this effect, a silver panel was prepared, one half of which was heavily gold plated to produce a silver-gold junction. The cleaned specimen was suspended in air saturated with sulfur vapor at 60°C at which temperature the vapor pressure of sulfur is 0.0001 mm (1). After an overnight exposure (17 hr) silver sulfide had crept over the gold surface along the entire bimetallic boundary.

Figure 1 depicts the appearance of the sulfided surfaces at the conclusion of the test (165 hr). Periodic measurements were made at a point of maximum creepage and are shown in Fig. 2. A cross section of the specimen at the gold-silver junction is shown in Fig. 3. It is apparent that the cavity was produced by migration of silver ions needed for the formation of the sulfide on the gold. It is also evident that the sulfide coating on the gold is of the same order of thickness as that on the silver. However, it tapers rather abruptly to a thin film which at the leading edge exhibits interference colors (Fig. 1).

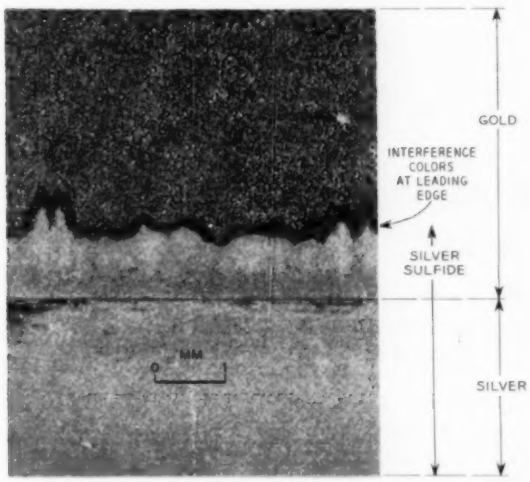

Fig. 1. Advance of silver sulfide on gold after 165 hr in sulfur vapor at 60°C. Leading edge very thin, exhibits interference colors.

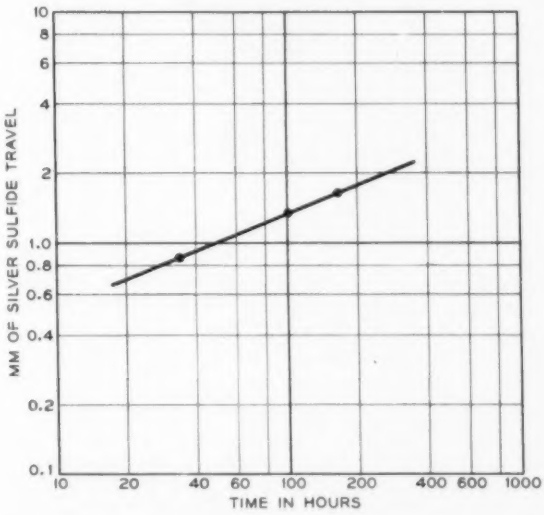

Fig. 2. Creepage silver sulfide on gold-sulfur vapor at 60°C.

The same experiment was performed using rhodium and silver. Direct microscopic examination revealed needles of silver sulfide at the bimetallic juncture but no creepage of silver sulfide on the rhodium surface. Figure 4 is a photomicrograph of a

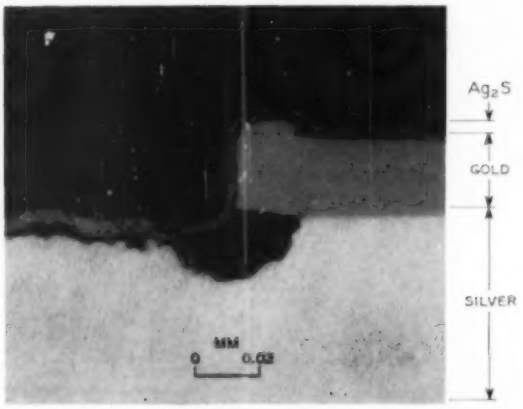

Fig. 3. Cross section of specimen showing cavity in silver and sulfide film on silver and on gold plate.

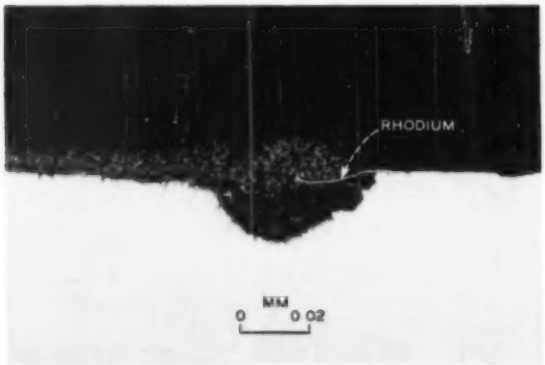

Fig. 4. Cross section of rhodium plated silver showing cavity resulting from silver sulfide needle growth.

cross section of this specimen. It shows what might appear to be a slight amount of creeping of the silver sulfide on the rhodium. This, however, is unlikely since the relatively thick sulfide coating ends abruptly. If creeping had occurred, one would expect the sulfide on the rhodium to taper out to an extremely thin film as had occurred in the case of the gold. The silver sulfide on the rhodium probably resulted from a collapse of the needles during the molding operation. The cavity, which undercuts the rhodium, indicates the quantity of silver required to form the silver sulfide needles. A similar experiment with silver and palladium also failed to produce spreading of silver sulfide.

At the present time there is no completely adequate explanation for the behavior of silver sulfide on the metals studied.

A recent (2) paper discusses a similar effect involving tantalum partly coated with silver and exposed to iodine vapors at 174°C. Silver iodide formed not only on the silver but spread rapidly over the uncoated tantalum surface. The spreading mechanism postulated for this effect assumes local cell action, enhanced by relative ease of flow of ions and electrons in different phases. In this instance spreading of the corrosion product is favored by the ease of flow of silver ions in the iodide and the ease of flow of electrons in tantalum. The same effect was obtained with silver on platinum and on graphite. While this theory appears to be operative in the case of the spreading of silver sulfide on the gold, it is not clear why the same phenomenon does not occur when rhodium or palladium is substituted for the gold, at least at the temperature employed (60°C).

From the practical point of view this phenomenon is of considerable importance. Silver-gold combinations are fairly common in electrical contact design. Some of the usual fabrication methods are electroplating, overlays, and inlays. Silver solder is also used to attach gold to other metals. In all cases, it should be realized that whenever a junction of silver and gold exists in a sulfiding atmosphere, the gold surface will be contaminated with silver sulfide. In these experiments, silver sulfide was more adherent to gold than to silver (Fig. 3) which would indicate that it would be more difficult to remove by contact wipe. Therefore, while silver sulfide is always undesirable on electrical contacts, it may be even more detrimental on gold.

Acknowledgment

The authors are indebted to Mr. E. E. Thomas for the photomicrographs.

Manuscript received Oct. 14, 1959.

Any discussion of this paper will appear in a Discussion Section to be published in the December 1960 JOURNAL.

REFERENCES

1. K. Neumann, *Z. Phys. Chem.*, **A171**, 416 (1934).
2. Christa Ilschner-Gensch and C. Wagner, *This Journal*, **105**, 198 (1958).

A New Method for Preparing Hydroxide-Free Alkali Chloride Melts

Donald L. Maricle[1] and David N. Hume

Department of Chemistry and Laboratory for Nuclear Science, Massachusetts Institute of Technology, Cambridge, Massachusetts

Molten salts have been used extensively in recent years as solvents for electrochemical processes and investigations. Alkali metal chlorides in particular offer excellent thermal stability, good solvent properties, and a wide potential span between anodic and cathodic decomposition limits. However, the difficulty of removing the last traces of residual moisture from the salts has often necessitated rather arduous drying procedures (1-3). If the moisture is not removed, hydrolysis occurs upon fusion as indicated by Eq. [1]

[1] American Cyanamid Co. Fellow 1958-1959. Present address: American Cyanamid Co., Stamford, Conn.

$$Cl^- + H_2O \rightarrow HCl\uparrow + OH^- \qquad [1]$$

The hydroxide ion thus produced precipitates metal ions, attacks glass, and is reduced more easily than the alkali metals, thus diminishing the usable potential range of the solvent.

Laitinen, *et al.* (4) have studied the preparation of a hydroxide-free, 59-41 mole % lithium chloride-potassium chloride eutectic by measuring the hydroxide ion concentration polarographically in the melt. Lithium salts are particularly difficult to dry, and polarography is sensitive to low concentrations of hydroxide ions. As a result they found it necessary to use a procedure involving vacuum treatments and fusion under hydrogen chloride which, until it was developed into a routine operation, required several days to complete. By such means they were able to obtain melts with low polarographic residual currents and with little tendency to etch glass apparatus.

The authors have made a polarographic study of drying procedures for the equimolar sodium chloride-potassium chloride melt 740°C, using a tungsten micro-electrode 0.8 mm in diameter and 5 mm long and a platinum-platinum (II) reference electrode. It was found that if the ordinary dry salts were fused and flushed with pure argon for 20 min to remove dissolved oxygen, only a small hydroxide reduction wave was found. Using a standard addition method for calibration, the hydroxide concentration of such a melt was estimated to be 0.17 millimolal, or 3 x 10^{-4}% expressed as water. If rigorously dried hydrogen chloride is bubbled through the melt for 20 min before the argon flush, even this small hydroxide ion impurity is removed. Typical polarograms with and without hydrogen chloride treatment are shown in Fig. 1. This is in considerable contrast to the lithium chloride-potassium chloride eutectic which will contain gross amounts of hydroxide ions if fused without special drying procedures and in which dry hydrogen chloride is not effective for removing hydroxide ions.

A new and better method of removing hydroxide impurities from both melts has been developed in

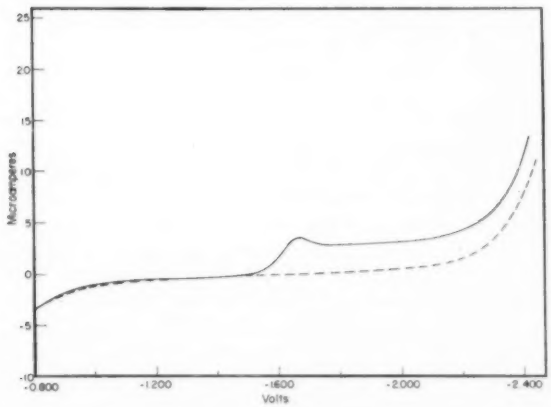

Figure 1. Residual polarographic currents in the NaCl-KCl melt before (solid line) and after (dotted line) removal of hydroxide ion impurity.

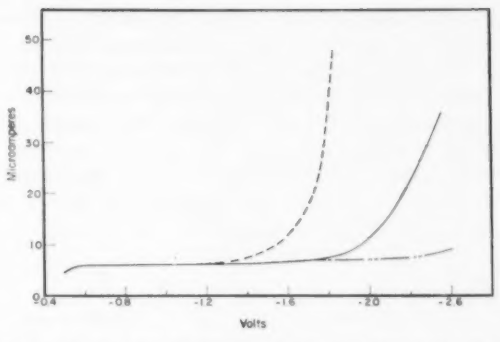

Figure 2. Residual polarographic currents during the purification of the LiCl-KCl eutectic. - - - - - Before treatment; ———— after 20 min chlorine and 20 min argon; ——— - - ——— after 40 min chlorine and 20 min argon.

the present investigation. This method eliminates the need for pre-drying any salts and can be carried out easily and rapidly. It consists simply of passing chlorine through the melt immediately after fusion of the undried salts. The reaction, presumably, is that of Eq. [2].

$$2OH^- + 2Cl_2 \rightarrow O_2\uparrow + 2HCl\uparrow + 2Cl^- \qquad [2]$$

The hydroxide ion is thus removed without contamination of the melt with any extraneous nonvolatile species. The oxygen and hydrogen chloride gases are swept out by the chlorine, and the chlorine is easily removed by flushing argon through the melt. After 20 min of treatment with chlorine followed by a 20 min argon flush, the hydroxide ion concentration in a sodium chloride-potassium chloride melt was reduced below the level detectable polarographically. Polarograms recorded before and after the chlorine treatment are shown in Fig. 1. For treating this melt, chlorine has the advantage of being much easier to dry than hydrogen chloride. An additional drawback to the use of hydrogen chloride is its characteristic of altering the fluid characteristics of the melt in such a way that splashing and spattering occurs with consequent deposition of melt at unwanted places in the apparatus.

The use of chlorine is extremely advantageous for drying lithium-ion-containing melts. Figure 2 shows polarograms obtained before and after chlorine treatments in the 59-41 mole % lithium chloride-potassium chloride eutectic at 450°C with a tungsten micro-electrode and a platinum foil used as an anode and reference electrode. It is apparent that after 40 min of chlorine treatment, the hydroxide ion concentration has been reduced below the level detectable polarographically. This was found to be true even if the salts were taken directly out of the bottle, with no pre-drying. A 20-min flush with argon was sufficient to remove the chlorine from this melt also. Therefore, if chlorine is used to purify the melt, the procedure takes only about 1 hr, in contrast with previously used procedures requiring up to several days.

While this method has been used by the authors to purify only the two melts mentioned above, it is

presumed that chlorine could be used to remove hydroxide impurities from other alkali metal and alkaline earth chlorides. However, it is interesting to note that if the temperature of the lithium-chloride-potassium chloride eutectic was raised from 450° to 740°C, reaction [2] did not occur to any appreciable extent, and the color of the chlorine solution changed from nearly colorless to red-brown. The sodium chloride potassium chloride melt exhibits a deep red-brown color when saturated with chlorine at 740°C. It appears as if higher temperatures favor the formation of a chlorine species which has a sufficiently diminished oxidizing power that it cannot oxidize the hydroxide ion in lithium-ion-containing melts.

Acknowledgment

This work was supported in part by the United States Atomic Energy Commission under Contract AT(30-1)-905.

Manuscript received Nov. 18, 1959.

Any discussion of this paper will appear in a Discussion Section to be published in the December 1960 JOURNAL.

REFERENCES

1. S. Senderoff and A. Brenner, *This Journal*, **101**, 16 (1954).
2. H. J. Gardner, C. T. Brown, and G. J. Janz, *J. Phys. Chem.*, **60**, 1458 (1946).
3. G. J. Hills, O. Inman, and L. Young, Proc. Intern. Comm. Electrochem. Thermodynam. and Kinet. 8th meeting, **90** (1958).
4. H. A. Laitinen, W. S. Ferguson, and R. A. Osteryoung, *This Journal*, **104**, 516 (1957).

Brief Communications

Location of Diffused pn-Junctions on Germanium by Electrodeposition of Copper

Reinhard Glang

Diamond Ordnance Fuze Laboratories, Washington, D. C.

The delineation of diffused junctions on silicon by chemical deposition or electroplating of metals has been described frequently in recent publications and can be achieved in various ways. Germanium, however, offers difficulties. It seems to be impossible to sharply define a junction on germanium by chemical displacement reactions (1). Electroplating methods of locating grown junctions on germanium crystals have been reported occasionally (2, 3), but apparently no procedure has been published for defining *diffused* junctions on germanium with metals. The technique described below makes it possible to delineate the junction between p-type germanium and thin diffused n-type layers.

A small piece of a diffused germanium wafer is angle lapped (4) as shown in Fig. 1 in order to expose the junction. The lapping is done against a glass plate, using an alumina abrasive 0.3μ in particle size, in order to avoid deep scratches on the beveled region. The surface is cleaned carefully with organic solvents and distilled water.

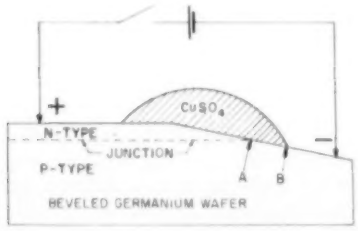

Fig. 1. Copper plating of diffused germanium wafer for delineation of junction.

The plating solution is prepared by dissolving approximately 20 g of $CuSO_4 \cdot 5H_2O$ in 80 ml of water and adding about 1 ml of concentrated (49%)HF. The hydrofluoric acid is intended to keep the germanium surface free from oxide. A small drop of this solution is placed on that part of the beveled surface where the junction is believed to be located. This is done carefully with a capillary pipette, so that the droplet does not flow over the edges of the germanium sample. Two adjustable metal probes are then brought into contact with the surface, one on the beveled p-region and the other on the non-beveled n-region. A small d-c voltage is applied between the probes, and the p-type region serves as the cathode. During these operations, the surface of the sample must be protected from strong light in order to avoid a photovoltage across the junction and consequent deposition of a thin film of copper on the n-region of the wafer. The circuit supplying the voltage is closed at 20-sec intervals for periods of only about 1 sec. After the first pulse, a deposit of copper is usually visible over the whole area between point A and point B in Fig. 1. This layer of copper adheres firmly to the germanium surface.

As indicated above, the voltage is applied continuously for only about 1 sec. Longer applications yield anode reactions which result in an electrolytic etch of the n-region, dulling its surface, and thus interfering with subsequent junction depth meas-

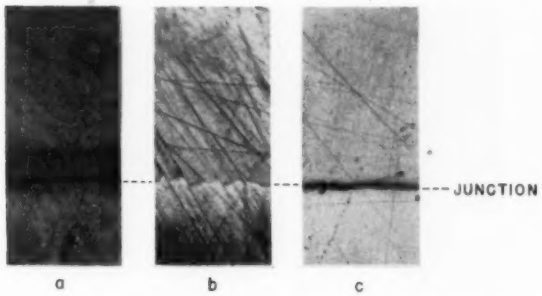

Fig. 2. Diffused pn-junctions in germanium. The lower thirds of the photographs show the copper-plated p-type region of the bevel. Lapping angles and junction depths: (a) 2°, 2μ; (b) ¾°, 2μ; (c) ¾°, 6.5μ. Magnification 300X before reduction for publication.

urements made with an interference microscope (4). The value of the voltage is critical and depends on the dimensions of the sample as well as on the sheet resistivity. On rectangular samples of width 2 mm, length 5-10 mm, junction depth 1-2μ, and sheet resistivity about 150 ohm, a voltage of 15 to 20 v and a current of about 30 to 50 ma adequately define the junction. Too high a voltage causes the copper to begin to spread over the n- as well as the p-region. A more common failure results from a voltage which is too low. In this case, copper tends to deposit from the edge of the drop nearest to the negative probe (i.e., point B, Fig. 1) while the region near the junction (i.e., point A Fig. 1) remains uncovered.

On samples having the previously specified dimensions, but sheet resistivities of 30 ohm or less and junction depths of 8 to 10μ, conditions are less critical; voltages as low a 5 v and currents of about 20 ma have proved effective.

Figure 2 shows samples of diffused germanium the lower thirds of which are the copper-plated p-type regions and the upper two thirds of which are the n-type regions. In Fig. 2a, the upper portion of the sample is not beveled, while in Fig. 2b and 2c the beveled n-region extends all the way to the upper edges of the photographs. Lapping angles and junction depths for these samples are as follows: (a) 2°, 2μ; (b) ¾°, 2μ; (c) ¾°, 6.5μ. As a consequence of the angle lapping procedure, the beveled surface areas are scratched. The surface damage accounts for minor irregularities in the junction delineation as clearly shown in Fig. 2b. On samples having a junction depth of only 1 or 2μ, irregularities in the copper-plated edge larger than those shown in Fig. 2b are occasionally observed, and these irregularities follow the surface profile. For example, when a scratch 1μ in depth was present on the sample's surface prior to diffusion, the junction depth was increased in this particular region.

For junction depths in the order of only 1μ it is advisable to use a lapping angle of 1° or smaller. A steeper bevel tends to permit extension of the copper plated area beyond the junction line, as occurred in Fig. 2a where the lapping angle was 2°. The surface damage which is done in the angle lapping procedure undoubtedly distorts the junction region and causes an apparent inaccuracy in its delineation. The larger the lapping angle the more serious this effect will be.

Considering the fact that the plating voltage biases the junction in the reverse direction, the currents between the probes are surprisingly high. Even in the absence of copper sulfate solution, these currents are of the same order of magnitude. Consequently, there must be a high leakage current, either through or by-passing the junction, but not through the drop. By etching 1 to 2μ deep into the beveled part of the surface, the leakage current can be reduced greatly. This is another indication of the disturbing influence of a damaged surface layer and explains why the voltage is so critical for effective plating. The voltage has to be sufficiently high to force through the droplet and into the diffused n-layer that fraction of the total current which is required to produce a visible deposit of copper. The main fraction of the current, however, will go from the p-type to the n-type region through the damaged surface layer, which offers a path of lower resistance across the junction.

Manuscript received Nov. 16, 1959.

Any discussion of this paper will appear in a Discussion Section to be published in the December 1960 JOURNAL.

REFERENCES

1. D. R. Turner, *This Journal*, **106**, 701 (1959).
2. H. E. Bridges, J. H. Scaff and J. N. Shive, "Transistor Technology," Vol. I, p. 288, D. van Nostrand Co., Inc., Princeton, N. J. (1958).
3. R. C. A. Laboratories, "Transistors" I, p. 130 (1956).
4. W. L. Bond and F. M. Suits, *Bell System Tech. J.*, **35**, 1209 (1956).

Magnetic Gradient at the Surface of Ferromagnetic Substances

S. Yamaguchi

The Institute of Physical & Chemical Research, Tokyo, Japan

The gradient of the magnetic field found at the surface of a magnet body has been measured by means of electron diffraction. This magnetic gradient was taken into consideration for elucidation of the Hedvall effect in catalysis and corrosion (1).

Experimental.— A flux of electrons spreads in passing through a magnetic field with a gradient. This phenomenon is observable in a diffraction pattern obtained from a ferromagnetic substance (Fig. 1).

A reduced iron catalyst[1] for practical ammonia synthesis and the sharp edge of a razor blade of

[1] This catalyst was produced by reducing blocks of iron oxide (Fe_3O_4) with hydrogen. The iron catalyst thus prepared kept the initial form of the oxide block.

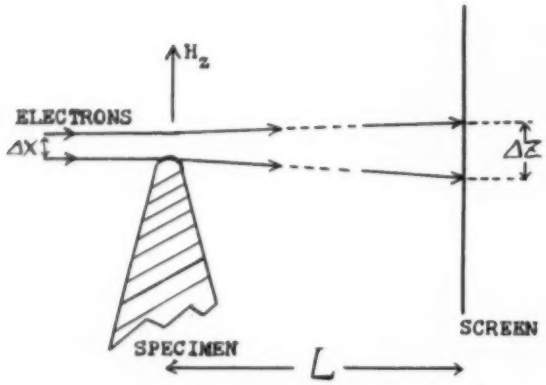

Fig. 1. Experimental arrangement

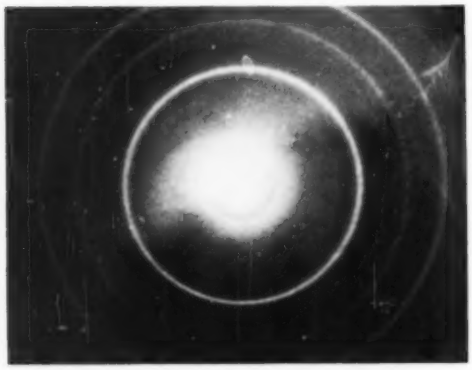

Fig. 2. Diffraction pattern from the edge of an iron catalyst. Wave length: 0.0308Å; camera length: 495 mm; positive enlarged 2.3 times.

hard steel were employed as objects for the experiment. The remanence of the former specimen was about 5000 gausses and that of the latter was about 10000 gausses. The surface (area: about 5 mm^2) of the catalyst was scanned with the electron beam (diameter: about 0.05 mm) in order to locate the maximum gradient of the magnetic field found at the catalyst surface. The electron beam grazed the sharp edge of the razor blade. Diffraction patterns obtained from the iron catalyst (size: 5 x 5 x 1 mm) and that from the razor edge (5 x 5 mm) are shown in Fig. 2 and 3. In these figures it is noticeable that the diffraction rings show a preferred orientation regarding the diffraction width, being diffuse in the direction of the magnetic field, but sharp in the direction perpendicular to the field. The relation between the field (H_z)and the spreading of the diffraction width of the (110) ring is illustrated in Fig. 4.

The central spot found in the diffraction pattern of Fig. 2 is enlarged 35 times in Fig. 5(a). It is noticeable here that the incident beam spreads along the direction of the magnetic field of the specimen. The cross section of the undistorted incident beam is shown in Fig. 5(b) with the same magnification as in Fig. 5(a). The amount of the magnetic spreading of the incident beam is measurable at the diffraction ring as well as at the central spot.

Measurement of the magnetic gradient.—The spreading ΔZ of the incident beam resulting from

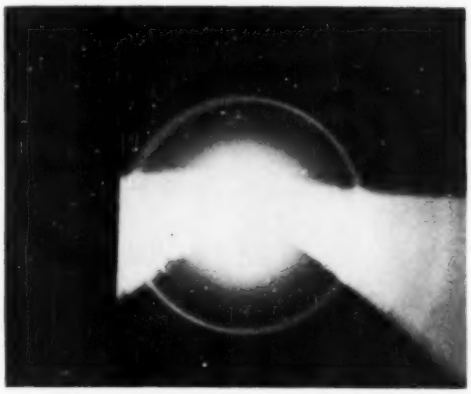

Fig. 3. Diffraction pattern from sharp edge of a razor blade. Wave length: 0.0309Å.

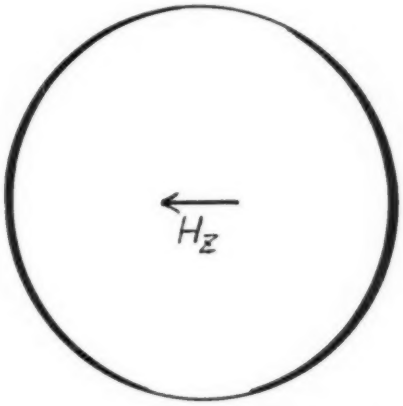

Fig. 4. Oriented spreading of the (110) ring in Fig. 2 and 3. H_z: the direction of the field.

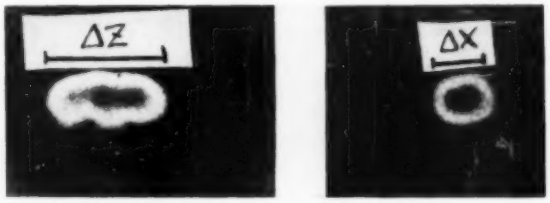

Fig. 5(a) (left). shows the central spot in Fig. 1. enlarged 35 times. It spreads along the direction of the field. Fig. 5(b) (right). shows the cross section of the undistorted incident beam; it is nearly circular.

the action of the magnetic gradient ($\partial H_z/\partial Z$) in the present conditions (Fig. 1) is given by

$$\frac{\Delta Z}{\Delta X} = e \left|\frac{\partial H_z}{\partial Z}\right| \cdot \frac{\lambda L l}{h} \qquad [1]$$

where e is the electron charge (1.6×10^{-20} emu), ΔX is the diameter of the flux of the undistorted incident beam, λ is the wave length of the electrons, h is Planck's constant (6.6×10^{-27} erg sec), L is the camera length (495 mm), and l is the magnetic path traveled by the electrons. In Fig. 2 or in Fig. 5(a) and (b) we measure $\Delta Z/\Delta X \cong 2.3$, and $\lambda = 0.0308$Å. If the magnetic path l is assumed tentatively to be 1μ we obtain

$$\frac{\partial H_z}{\partial Z} \cong 6 \times 10^5 \text{ gauss/cm}$$

as the maximum gradient according to Eq. [1]. This value of the magnetic gradient is not absolute because of the uncertainty in l.

In Fig. 3 we measure $\Delta Z/\Delta X \cong 3{,}4$, and $\lambda = 0.0309$A. Therefore, we obtain

$$\frac{\partial H_z}{\partial Z} \cong 9 \times 10^5 \text{ gauss/cm}$$

as the maximum gradient on the razor edge. This value is rather absolute, because the l-value here assumed is approximately equal to the minimum thickness of the truncated wedge of the razor blade (1μ).

Conclusion.—The maximum magnetic gradient is related to the lattice distortion or the magnetostriction found at the surface of the specimen. It is known that catalysis and corrosion of metals depend frequently on this lattice distortion. The magnetic Hedvall effect in catalysis and corrosion should be studied by scanning the magnet surface with a fine electron beam according to the present process.

Manuscript received Sept. 30, 1959.

Any discussion of this paper will appear in a Discussion Section to be published in the December 1960 JOURNAL.

REFERENCES

1. J. A. Hedvall, "Einführung in die Festkörperchemie," pp. 196-202, Fried. Vieweg & Sohn, Braunschweig (1952); H. H. Uhlig and A.de S. Brasunas, *This Journal*, **97**, 448 (1950).

Overtemperature in Metal Scaling

D. Caplan

National Research Council, Ottawa, Canada

Overtemperature resulting from the heat of reaction can affect the reaction kinetics of gases with metal surfaces. This has been discussed recently in the high-temperature oxidation of iron (1), iron-nickel (2), uranium (3), and molybdenum (4), and by the writer as a possible explanation for large differences in scaling rates of iron-chromium alloys with different surface preparations (5). To investigate the latter and because other measurements of overheating had been indirect, it was decided to determine the overtemperature directly with a thermocouple welded to the surface of the specimen.

The metals tested were high-purity vacuum melted iron, a pure Fe-26 Cr alloy, and a commercial Fe-30 Ni alloy (kindly supplied by R. T. Foley from material used in reference 2). Specimens in sheet form were used to provide an adequate surface/mass ratio. A chromel/alumel thermocouple was spot welded to the prepared metal surface. The assembly was lowered into the open top of a vertical tube furnace (on-off control) and the thermocouple output recorded on a strip chart potentiometer (L&N Speedomax G, full scale 50 mv pen travel in one second). Relevant details of six runs are listed in Table I.

The temperature/time curves are reproduced in Fig. 1. Runs 1 and 2 demonstrate that large over-

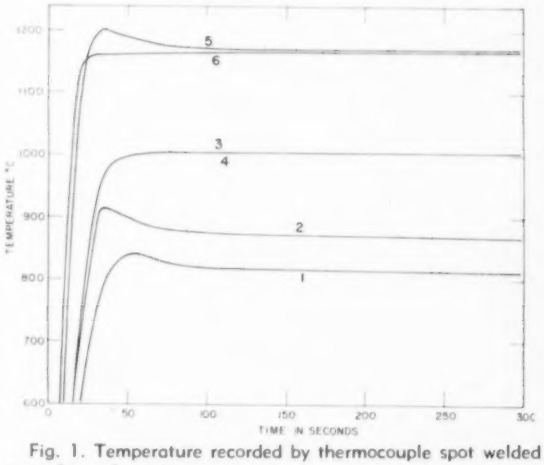

Fig. 1. Temperature recorded by thermocouple spot welded to surface of specimen.

temperatures can develop when iron is oxidized. A similar conclusion was reached by Schmahl, *et al.* (1), but quantitative comparison of the results is not possible because of the more positive attachment of the thermocouple and differences in the experimental conditions: overheating will be less if these conditions are such as to decrease the reaction

Table I

Run	Alloy	Size, cm	Weight, g	Surface prep.	Temp, °C	Atmosphere	Overtemp, °C
1	Fe	1 × 5 × 0.04	1.3	Electropolished	812	O_2, 200 ml/min	27
2	Fe	1 × 5 × 0.04	1.3	Electropolished	866	O_2, 200 ml/min	47
3	Fe-30 Ni	2 × 3.8 × 0.06	3.4	Etched as in ref. (2)	1005	still air	nil
4	Fe-30 Ni	2 × 3.8 × 0.06	3.4	Etched as in ref. (2)	1005	O_2, 100 ml/min	nil
5	Fe-30 Ni	2 × 3.8 × 0.06	3.4	Etched as in ref. (2)	1170	O_2, 100 ml/min	29
6	Fe-26 Cr	1 × 5 × 0.04	1.3	Electropolished	1165	O_2, 200 ml/min	nil

rate, increase the heat capacity of the specimen, or remove heat more efficiently from it.

The negative result in runs 3 and 4 with Fe-30 Ni at 1000° indicates that the deviation in the Arrhenius plot observed by Foley (2) was not due to overheating but rather to his alternative suggestion, that of a change in scaling mechanism. At 1170° the scaling rate is large enough to give sensible overheating (run 5).

No overtemperature in run 6 demonstrates that the relatively rapid initial scaling obtained with Fe-26 Cr alloys in the electropolished condition (5) is due to some cause other than overheating.

Manuscript received Dec. 21, 1959.

Any discussion of this paper will appear in a Discussion Section to be published in the December 1960 JOURNAL.

REFERENCES

1. N. G. Schmahl, H. Baumann, and H. Schenk, *Arch. Eisenhüttenw.*, **27**, 707 (1956).
2. R. T. Foley and C. J. Guare, *This Journal*, **106**, 936 (1959).
3. B. E. Hopkinson, *ibid.*, **106**, 102 (1959).
4. E. S. Bartlett and D. N. Williams, *Trans. Met. Soc. AIME*, **212**, 280 (1958).
5. D. Caplan, A. Harvey, and M. Cohen, to be communicated (presented at E.C.S. Columbus Meeting, 1959).

December 1960 Discussion Section

A Discussion Section, covering papers published in the January-June 1960 JOURNALS, is scheduled for publication in the December 1960 issue. Any discussion which did not reach the Editor in time for the June 1960 Discussion Section will be included in the December 1960 issue.

Those who plan to contribute remarks for this Discussion Section should submit their comments or questions in triplicate to the Managing Editor of the JOURNAL, 1860 Broadway, New York 23, N. Y., *not later than September 1, 1960*. All discussion will be forwarded to the author(s) for reply before being printed in the JOURNAL.

FUTURE MEETINGS OF
The Electrochemical Society

Chicago, Ill., May 1, 2, 3, 4, and 5, 1960

Headquarters at the Lasalle Hotel
Sessions will be scheduled on
Electric Insulation (including a symposium on "Electrolytic Capacitors"), Electronics (including Luminescence and Semiconductors), Electrothermics and Metallurgy (including symposia on Refractory Metals, "High-Purity Vanadium—Its Preparation, Properties, and Alloys," and on Rhenium, and a round table on "Methods of Reducing Iron Ores"), Industrial Electrolytics, and Theoretical Electrochemistry (general sessions, and a Symposium on "Electrochemical Engineering" co-sponsored by the Theoretical and Industrial Electrolytic Divisions)

★ ★ ★

Houston, Texas, October 9, 10, 11, 12, and 13, 1960

Headquarters at the Shamrock Hotel
Sessions probably will be scheduled on
Batteries, Corrosion, Electrodeposition, Electronics (Semiconductors), and Electrothermics and Metallurgy

★ ★ ★

Indianapolis, Ind., April 30, May 1, 2, 3, and 4, 1961

Headquarters at the Claypool Hotel

★ ★ ★

Detroit, Mich., October 1, 2, 3, 4, and 5, 1961

Headquarters at the Statler Hotel

Papers are now being solicited for the meeting to be held in Houston, Texas, October 9-13, 1960. Triplicate copies of each abstract *(not exceeding 75 words in length)* are due at Society Headquarters, 1860 Broadway, New York 23, N. Y., *not later than June 1, 1960* in order to be included in the program. *Please indicate on abstract for which Division's symposium the paper is to be scheduled and underline the name of the author who will present the paper.* Complete manuscripts should be sent in triplicate to the Managing Editor of the JOURNAL at 1860 Broadway, New York 23, N. Y.

Papers submitted for presentation at the meeting become the property of The Electrochemical Society and may not be published elsewhere, in whole or in part, unless permission is requested of and granted by the Society. Papers already published elsewhere, or submitted for publication elsewhere, are not acceptable for oral presentation except on invitation by a Divisional program Chairman.

The Electrochemical Society

INSTRUCTIONS TO AUTHORS OF PAPERS

Address all correspondence to the Editor, JOURNAL OF THE ELECTROCHEMICAL SOCIETY, 1860 BROADWAY, NEW YORK 23, N. Y.

FORM

Manuscripts submitted for publication should be in triplicate to expedite review. They should be typewritten, double-spaced, with 2½-4 cm (1-1½ in.) margins.

Title should be brief, followed by the author's name and his business or university connection.

Abstract of about 100 words should state the scope of the paper and give a brief summary of results.

ILLUSTRATIONS

Drawings will be reduced to column width, 8.3 cm (3¼ in.), after reduction should have lettering at least 0.15 cm (1/16 in.) high. Original drawings in India ink on tracing cloth or white paper are preferred. Curves may be drawn on coordinate paper only if the paper is ruled in blue. All lettering must be of lettering-guide quality. See sample drawing on reverse page.

Photographs must be glossy prints and mounted flat.

Captions for all figures must be included on a separate sheet. Captions and figure numbers should not appear in the body of the figure.

General—Figures should be used only when necessary. Omit drawings or photographs of familiar equipment. Figures from other publications are to be used only when the publication is not readily available, and should always be accompanied with written permission for reprinting.

SYMBOLS

If more than a few symbols are used, these should be defined in a list at the end of the paper, for example:

$a, b \ldots$ = empirical constants of Brown equation
f_i = fugacity of pure ith component, atm
D_v = bulk diffusion coefficient, cm^2/sec

REFERENCES

Literature and patent references should be listed at the end of the paper on a separate sheet, in the order in which they are cited. They should be given in the style adopted by *Chemical Abstracts*. For example:

R. Freas, *Trans. Electrochem. Soc.*, **40**, 109 (1921).

H. T. S. Britton, "Hydrogen Ions," Vol **1**, p. 309, D. Van Nostrand Co., New York (1943).

H. F. Weiss (To Wood Conversion Co.), U. S. Pat. 1,695,445, Dec. 18, 1928.

UNITS OF MEASUREMENT

Metric units should be used throughout but, where desirable, English units may be given in parentheses.

Corrosion rates in the metric system should preferably be expressed as milligrams per square decimeter per day (mdd), and in the English system as inches penetration per year (ipy).

In reporting electrode potentials, the sign of the standard Zn/Zn^{++} electrode potential should be taken as negative; Cu/Cu^{++} as positive.

ABBREVIATIONS

Abbreviations should conform with the American Standards Association's list of "Abbreviations for Scientific and Engineering Terms."

GENERAL

Authors should be as brief as is consistent with clarity, and must omit all material which can be regarded as familiar to specialists in the particular field.

The use of proprietary names, trade-marks, and trade names should be avoided if possible. If used, these should be capitalized so that the owner's legal rights are not jeopardized.

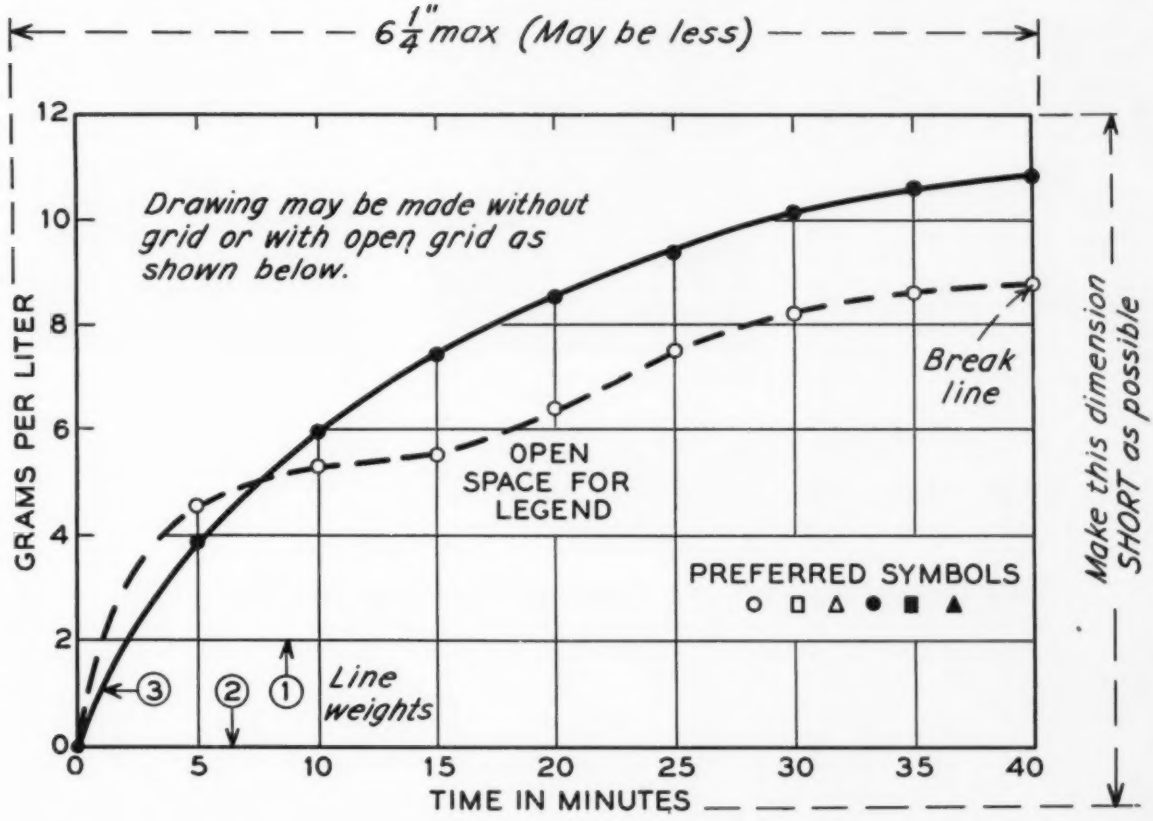

Remarks: Line weight 2 is used for borders and zero lines. When several curves are shown, each may be numbered and described in the caption. Lettering shown is approximately ⅛ in. In plotting current or potential as ordinate, increasing negative values should go down.

SAMPLE CURVE DRAWING FOR REDUCTION TO ½ SIZE

Current Affairs

Schaefer and Hamer to Take Office in Chicago

As a result of the recent annual election, in which the voting is by mail ballot, Ralph A. Schaefer has been elected the new President (1960-1961) of The Electrochemical Society, and Walter J. Hamer has been elected third Vice-President (1960-1963). They will take office at 8:00 A.M. on Thursday, May 5, 1960, in Chicago, Ill., at the Spring Annual Meeting of the Society.

R. A. Schaefer

W. J. Hamer

Dr. Schaefer, director of research and product development, processing engineering, and inspection functions of the Bunting Brass and Bronze Co., Toledo, Ohio, replaces William C. Gardiner, manager research engineering, Research and Development Dept., Industrial Chemicals Division, Olin Mathieson Chemical Corp., Niagara Falls, N. Y. Dr. Gardiner, as Past President, will continue as a member of the Board of Directors.

Walter J. Hamer, chief of the Electrochemistry Section of the National Bureau of Standards, Washington, D. C., will start the first year of his three-year term as Society Vice-President, and will serve with the two previously elected Vice-Presidents, Henry B. Linford and Frank L. LaQue.

Plans Completed for the Chicago Meeting, May 1-5, 1960

All arrangements now have been made for the Spring Meeting of The Electrochemical Society to be held at the LaSalle Hotel in Chicago, Ill., from May 1 through 5, 1960. The program, including general information and 75-word abstracts of papers to be presented, appeared in the March JOURNAL, pp. 47C-79C.

Changes in Program

There have been some changes, in times of presentation, meeting rooms, titles of papers, and authors, since the program was published in the March issue.

The correct program will be listed in the program booklet which will be available at the Chicago Meeting.

Members of the Chicago Local Committee are: Ernest L. Koehler, General Chairman; H. T. Francis, Advisor; Ralph Hovey, Hotel Arrangements; Ralph Wehrmann, Finance and Registration; C. A. Hampel, Entertainment; Sheldon Evans, Host Committee; Ladies' Program—Mrs. E. L. Koehler, Chairman; Mrs. C. A. Hampel, Advisor and Vice-Chairman; and Mrs. R. Hovey.

The Convention Committee has taken a "giant step" to insure you of the finest entertainment available in this, the largest convention city of the world. Highlighting our Society Luncheon will be guest speaker Bill Veeck, colorful president of the Chicago White Sox. Special arrangements have been made for Wednesday night with the world-famous Chez Paree, entertainment mecca of the Midwest. A cocktail hour in the Gold Key Club and dinner in the main dining room will be topped by a show featuring the nation's leading entertainers.

And for the Ladies

Plenty of time for shopping at Marshall Field—a must for every visitor. On Monday afternoon, a private smörgasbord which includes the wonderful delicacies of Swedish cuisine; and a visit to the Miniature Grand Opera at the Kungsholm Opera House for a rare and beautiful performance of Carmen. Wednesday luncheon will be at Fritzels, the restaurant which catered Michael Todd and Elizabeth Taylor's party celebrating the premiere of Smell-O-Vision. Chartered buses will then take you to the Oriental Institute of the University of Chicago. A specially conducted tour of the Institute and the Rockefeller Memorial Chapel has been arranged. And, if you have time, just a few blocks away is the Museum of Science and Industry. Get-together coffee hours at the LaSalle Hotel also have been planned.

International Flavor

Chicago is a gourmet's delight. Within minutes you can be dining in

E. L. Koehler

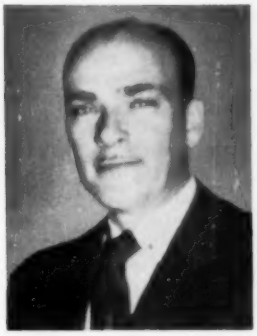
R. J. Hovey

Ralph Wehrmann

Sheldon Evans

"old world" atmosphere. Enjoy the Cantonese-style cookery of Chicago's Chinatown. Browse in the many interesting curio shops. For an authentic setting of enchanting Japanese Tea Houses and Garden surroundings with Geisha girls serving tempura, teriyaki, and sukiyaki cooked at your table, visit the Naka-No-Ya restaurant of the House of Azuma, both only a short ride from the hotel. The Athens, the Hellas, and the Pantheon feature Hellenic dishes and traditional Greek dancing. Cafe Bohemia is strongly recommended for fans of game food. Brand your own choice sirloin at the Stock Yard Inn. And for French, German, Italian, Jewish, Mexican, and Russian cooking, fine restaurants are plentiful. So just choose the cuisine—and your Host Committee will be happy to recommend the finest restaurant to you.

View from the Top

Enjoy a panoramic view of Chicago while sipping a cocktail at the Top of the Rock in the Prudential Building. From this vantage point, you can see most of the sites you may want to visit: world-famous collections of paintings, prints, and sculptures; the Adler Planetarium on the Lakefront; the famed Museum of Natural History; the Museum of Science and Industry; the Oriental Institute; the Aquarium; Orchestra Hall; the Civic Opera Building; the Miracle Mile of Shopping on Michigan Blvd.; the Chicago Public Library and the John Crerar Library.

Entertainment

There are five legitimate theaters and numerous motion picture theaters in the Loop area. A complete list of shows and films, including foreign films, will be available at the Host Committee desk. For jazz enthusiasts, the Blue Note, the London House, Jazz Ltd., the Cafe Continental are just a few of the clubs featuring leading jazz artists. Leading entertainers are featured at the many night spots, which include the famous Mr. Kelly's, the Empire Room of the Palmer House, the Camellia Room at the Drake, the Cloisters, and the Blue Angel. A good cup of coffee, along with poetry readings, folk singing, and the like, can be enjoyed in Chicago's many Espresso Houses.

Red Carpet Treatment

And there's lots more. . . . The Host Committee cordially welcomes you to Chicago and will be on hand to insure that your stay in Chicago will be most rewarding and pleasant.

Chicago's front door—Grant Park on the shore of Lake Michigan. Built entirely on land reclaimed from Lake Michigan, this mile-and-a-half-long showplace is one of Chicago's most magnificent vistas. Already included in its facilities are a great yacht basin, an outdoor concert amphitheater, a seaplane base, and a variety of recreational features. The Park's latest asset is an immense underground public parking garage.

Section News

Detroit Section

One of the high lights of the program year for the Detroit Section is the joint meeting with the Detroit Branch of the American Electroplaters' Society. On January 8, with Dr. James P. Hoare of The Electrochemical Society acting as Technical Chairman, approximately 100 persons were privileged to hear Dr. Allan T. Gwathmey, of the University of Virginia, talk on "A Study of Chemical Properties of Metals Using Large Single Crystals."

Dr. Gwathmey explained how single crystals may be used to understand the chemistry of metallic surfaces, accompanying his talk with fine electron photomicrographs of the growth and corrosion of metals. A time-lapse movie, in color, of the changes occurring on a copper single crystal, was especially interesting.

The next meeting of the Section, to be held on February 18, will be a joint meeting with the Detroit Section of the National Association of Corrosion Engineers, with Dr. H. T. Francis, of the Armour Research Foundation, as the speaker.

News from India

Scientific Instruments Organization in India.—At the instance of the Planning Commission, the Governing Body of the Council of Scientific and Industrial Research is setting up a Central Scientific Instruments Organization for promotion and development of indigenous manufacture of scientific instruments of all categories needed for teaching, research, and industry.

Refresher Course in Corrosion at the CECRI.—The Central Electrochemical Research Institute held a five-week refresher course on "Corrosion and Its Prevention," commencing November 9, 1959 at Karaikudi. The subjects for the course included corrosion processes, economics of corrosion, and prevention measures.

Aluminum Industry Expands in India.—With the formation of Hindustan Aluminium Corp. Ltd., a joint venture of Kaiser Aluminum and Chemical Corp., U.S.A., and the Birlas, the well-known industrial magnates, initial plans have been nearly completed for the establishment of an integrated aluminum-producing plant at Rihand in Uttar Pradesh State.

Technical Training Course in Batteries.—A short course in Technical Training in Batteries was arranged by the CECRI, Karaikudi, beginning February 1, 1960, aimed at technical personnel employed in industries manufacturing lead-acid batteries, as well as representatives of large consumers of the batteries, and organizations engaged in the testing of batteries according to the IS: specification. Topics for the eight-week course included: fundamentals of electrochemistry and metallurgy; lead-acid batteries: fabrication, uses, and recent advances, testing, battery plant layout, other types of storage batteries, primary batteries, fuel cells, solar and atomic batteries.

Electroplating and the ISI.—The Indian Standards Institution (ISI) set up, in 1953, a Sectional Committee to prepare Indian Standards covering the field of electroplating.

As a result of deliberations of the Sectional Committee (ETDC 12), the following Indian Standards already have been published: (*a*) IS: 1067-1958, Specification for Commercial Silver Plating; (*b*) IS: 1068-1958, Specification for Copper, Nickel, and Chromium Electroplated Coatings; (*c*) IS: 1337-1959, Specification for Hard Chromium Plating on Steel (Under Print); (*d*) IS: 1359-1959, Specification for Electro-Tin Plating (Under Print); (*e*) IS: 1378-1959, Specification for Oxidized Copper Finishes (Under Print). Specifications for the following also have been finalized and are likely to be available in printed form by June 1960: (*a*) Cadmium Plating, (*b*) Zinc Plating.

The Committee also is engaged in preparing a detailed code of practice for electroplating.

The subject of chemicals for electroplating is being handled through the appropriate committee of the Chemicals Division of ISI and the position of work in that field is as under: Standard Published: (*a*) IS: 330-1951, Specification for Chromic Acid; (*b*) IS: 331-1951, Specification for Chromic Salt. Work is in hand on the following: (*a*) Nickel Salts for Electroplating, (*b*) Sodium Cyanide, (*c*) Potassium Cyanide, (*d*) Zinc Cyanide, (*e*) Copper Cyanide, (*f*) Cadmium Cyanide, (*g*) Zinc Sulfate for Electroplating.

Seminar in Electrochemistry.—A Seminar in Electrochemistry was held by the CECRI, Karaikudi, during March 1960. It included the entire field of fundamental and applied electrochemistry, and personal experiences in the operation of electrochemical plants.

New Patrons, India Section.—T. I. Cycles of India, Ambattur, near Madras, and Kohinoor Electro Gilders, Bombay, have joined the India Section of the Society as Life Patrons.

T. L. Rama Char,
India Correspondent

Ontario-Quebec Section

The second meeting of the 1959-1960 season was held in the Laurentien Hotel, Montreal, on January 29, 1960. Two excellent papers were presented: "Problems and Advantages of High-Capacity Mercury Chlorine Cells" by M. Zundel, technical manager of Vickers Krebs Ltd., Montreal, and "Recent Developments in the Strategic Udy Smelting Process" by Leonard E. Olds, of Strategic Udy Processes Inc., Niagara Falls, N. Y. Technical Chairman was A. C. Holm, superintendent of the Shawinigan East Division of Shawinigan Chemicals Ltd., Shawinigan, Que.

E. R. Landry,
Secretary-Treasurer

Electronics Division Enlarged Abstracts, Spring 1960

The Electronics Division will again print an "Enlarged Abstracts" booklet containing 1000-word abstracts of papers to be presented before the Division's symposia on Luminescence, Semiconductors, and General Electronics at the Chicago Meeting of The Electrochemical Society, May 1-5, 1960.

The booklets will contain about 300 pages and are expected to be ready for distribution two weeks before the meeting.

The price will be $3.50 with a discount of $00.50 per copy for orders accompanied by payment and requiring no invoicing. Orders requiring invoicing will be charged the full price even though payment does accompany the order.

Checks should be made payable to: Electronics Division, The Electrochemical Society, and should be sent to:

Austin E. Hardy
Secretary-Treasurer
c/o Radio Corp. of America
New Holland Pike
Lancaster, Pa.

Extra copies, if any, will be on sale at the convention in Chicago.

Texas Section

The officers of the Texas Section (formation of which was approved at the May 1959 Society Board of Directors Meeting) are:

Chairman—R. G. Post, P. O. Box 535, Richardson, Texas
Vice-Chairman—L. G. Dean, Bldg. B-1404, Plant B, Dow Chemical Co., Freeport, Texas
Secretary-Treasurer—R. M. Hurd, Texas Research Associates, 1703 Guadalupe St., Austin 1, Texas
Councilor-Dallas Area (1 yr)—T. C. Franklin, Chemistry Dept., Baylor University, Waco, Texas
Councilor-Houston Area (2 yr)—C. S. Templeton, 3737 Bellaire Blvd., Houston 25, Texas

Roy G. Post, *Chairman*

New Members

In February 1960, the following were elected to membership in The Electrochemical Society by the Admissions Committee:

Active Sustaining Members

P. F. Grieger, Thomas A. Edison Research Lab., Div. of McGraw-Edison Co., Watchung Ave., West Orange, N. J. (Battery, Electric Insulation, Electrodeposition, Electro-Organic, Theoretical Electrochemistry)

H. G. Verner, Mallinckrodt Chemical Works, 3600 N. Second St., St. Louis, 7, Mo. (Electronics)

Active Members

Henri André, Yardney Electric Corp.; Mail add: 5 rue des Carrières, Montmorency (S&O), France (Battery)

R. J. Barton, Wright Air Development Div.; Mail add: 4968 Cobb Dr., Dayton 31, Ohio (Theoretical Electrochemistry)

J. F. Brauning, National Carbon Co.; Mail add: 230 N. Michigan Ave., Chicago 1, Ill. (Industrial Electrolytic)

D. K. Bray, Jr., General Abrasive Co., Inc., Niagara Falls, N. Y. (Electrothermics & Metallurgy)

J. E. Eby, Sylvania Lighting Products, 60 Boston St., Salem, Mass. (Electronics)

G. V. Elmore, Kettering Foundation, 150 E. South College, Yellow Springs, Ohio (Battery)

F. G. Gilbert, Canadian Carborundum Co.; Mail add: 2599 Ralph Ave., Niagara Falls, Ont., Canada (Electrothermics & Metallurgy)

A. F. Harter, General Aniline & Film Corp.; Mail add: 311 Eastern Parkway, Newark 6, N. J. (Industrial Electrolytic)

H. L. Henneke, Texas Instruments, Inc.; Mail add: 2822 Maple Dr., Garland, Texas (Electronics)

E. M. King, Union Carbide Consumer Products Co.; Mail add: 194 Barberry Dr., Berea, Ohio (Battery)

H. T. Knight, Fansteel Metallurgical Corp., North Chicago, Ill. (Electronics)

B. D. Lichter, Air Force Cambridge Research Center; Mail add: 183 Lexington St., Watertown 72, Mass. (Corrosion, Electronics)

J. P. Malloy, Electric Storage Battery Co.; Mail add: 7624 Front St., Cheltenham, Pa. (Battery)

R. E. Marlatt, Diamond Research Center, P. O. Box 348, Painesville, Ohio (Electrodeposition, Electrothermics & Metallurgy, Theoretical Electrochemistry)

E. M. Marski, P. R. Mallory & Co., Inc.; Mail add: 1203 Orchard Lane, Franklin, Ind. (Battery, Corrosion, Electric Insulation, Electrodeposition, Electronics, Electro-Organic, Electrothermics & Metallurgy, Industrial Electrolytic, Theoretical Electrochemistry)

L. J. Noga, General Electric Co.; Mail add: 45 Delwood Rd., Kenmore 17, N. Y. (Electronics)

G. S. Oxrieder, Kaiser Aluminum & Chemical Corp., P. O. Box 6217, Hillyard Station, Spokane 28, Wash. (Electrothermics & Metallurgy)

C. E. Paden, American Zinc Co. of Illinois, P. O. Box 495, East St. Louis, Ill. (Electronics)

H. H. Paproth, National Cash Register Co.; Mail add: 503 Peach Orchard Rd., Dayton 19, Ohio (Corrosion, Electronics)

J. F. Pudvin, Bell Telephone Labs. Inc., 555 Union Blvd., Allentown, Pa. (Electronics)

Indra Sanghi, Central Building Research Institute; Mail add: Hindustan Trust Ltd., 68 Dariyagunj, Delhi 7, India (Battery, Corrosion, Electrodeposition, Industrial Electrolytic)

D. J. Valley, Allegheny Electronic Chemicals Co.; Mail add: 160 South Ave., Bradford, Pa. (Electronics)

M. C. Vanik, W. R. Grace & Co., Clarksville, Md. (Electronics)

J. V. Vaughen, Stetson University, Deland, Fla. (Corrosion)

By action of the Board of Directors of the Society, all prospective members must include first year's dues with their applications for membership.

Also, please note that, if sponsors sign the application form itself, processing can be expedited considerably.

Student Associate Member

R. I. Bickley, Washington Singer Labs., University of Exeter, Prince of Wales Rd., Exeter, England (Corrosion)

Transfer from Associate to Active Membership

W. D. Goode, Jr., Battelle Memorial Institute, 505 King Ave., Columbus 1, Ohio (Electrothermics & Metallurgy)

Transfer from Student to Active Membership

E. P. Schwartz, Western Reserve University; Mail add: 315 N. Buchanaan St., Fremont, Ohio (Electrodeposition, Theoretical Electrochemistry)

Reinstatement to Active Membership

J. M. Finn, Jr., National Carbon Research Labs., P. O. Box 6116, Cleveland 1, Ohio (Industrial Electrolytic)

Deceased Members

R. A. Horst, Syracuse, N. Y.
H. S. Lukens, Ventnor City, N. J.

Personals

Harold T. Clark has been appointed to the newly created position of administrative director, Research and Development Dept., for Jones & Laughlin Steel Corp., Pittsburgh, Pa. In his new position, Dr. Clark, who formerly was director of research, will be responsible for supervising general administrative affairs of the department, patent matters, long-range planning of departmental objectives and facilities, and other technical assignments.

W. W. Heilman has been named plant manager of the Niagara Plant of Union Carbide Metals Co. Mr. Heilman had been assistant plant manager since May 1959.

Howard E. Kremers has been appointed district manager of market development for American Potash & Chemical Corp. Dr. Kremers will be responsible for all corporate market development activities assigned to the eastern district. His headquarters will be in the company's eastern general sales office in New York. Previously, he was manager of market development for the company's Lindsay Division.

Aleksandrs Martinsons, formerly of Boulder City, Nev., has taken a position with Columbia-Southern Chemical Corp. in Barberton, Ohio.

John D. Mettler, of the Technology Dept. of the Union Carbide Metals Co., Niagara Falls, N. Y., has been named to a newly created position, manager-economic appraisals. He will be responsible for assessing available technical and business information on selected research and development topics. The resulting economic feasibility analyses will be used to aid management in decision-making.

Lester L. R. Phillips, of the Hurlbut Paper Co., South Lee, Mass., is now in Los Angeles as a representative of the company on the West Coast.

Ralph A. Schaefer, director of research and development at the Bunting Brass and Bronze Co., Toledo, Ohio, has been named director of an enlarged department of engineering and research. In the expanded department which he will head, Dr. Schaefer will be in charge of research development, processing engineering, and inspection functions of the company.

Milton Stern, formerly with the Union Carbide Metals Co., Niagara Falls, N. Y., is now associated with Linde Speedway Labs., a division of Union Carbide Corp., Indianapolis, Ind.

Georges Destriau

George Destriau, discoverer of the phenomenon of electroluminescence, died in Cauderan, France, on January 20, 1960 at the age of 57. He had been in poor health for a long time.

Professor Destriau was born on August 1, 1903 in Bordeaux, France. He attended the Sorbonne and the Ecole Centrale des Arts and Manufactures, both in Paris, and received the engineering degree from the latter institution. He was awarded the doctorate in 1936 by the Sorbonne.

Since his discovery of electroluminescence in 1936, Professor Destriau continued his work in the field as a Westinghouse consultant. He also made several notable contributions in the fields of alpha particle scintillations, x-ray therapy, radiography, optics, and the properties of thin metal films.

He was a member of The Electrochemical Society, Société Francaise de Physique, Société Francaise de Chemie-Physique, Société Francaise des Electriciens, and the American Physical Society.

Book Reviews

Continuous Analysis of Chemical Process Systems, by Sidney Siggia. Published by John Wiley & Sons, Inc., New York, 1959. xiii + 381 pages; $8.50.

The author very accurately describes this book as ". . . a compilation of the existing information concerning available instruments for continuous analysis of components in chemical process systems." He essentially has reproduced the instrument manufacturers' current brochures covering a range of analytical methods: refractive index, density, viscosity, spectrometry (u.v., visible, i.r., x-ray, mass), electrochemical, thermal, and some more specialized procedures.

A brief discussion of the operating principles of commercially available instruments in a given group is followed by specifications so detailed as to list dimensions, weight, description of cabinet finish, etc., in many cases. "Example Applications" are also listed for *each* instrument of a single group. As a result, the subject matter becomes very repetitious and bulky. For example, the 31 pages of Chapter 17 contain some 11 descriptions of closely similar operating principles of 11 manufacturers' thermal conductivity instruments. The example applications listed for each of these instruments are similar in many respects. Surely a two- or three-page composite table listing instruments for measurement of thermal conductivity, and their minor differences in design and application, would have sufficed and yet have been just as useful for selection among them.

Apparently the text is directed toward groups concerned ". . . with the establishment of plant control facilities." The book may spare such groups the necessity of writing directly to manufacturers for current information, although this is doubtful in view of the rapid developments occurring in instrument design. However, these groups will not gain much assistance from the book in selecting either the proper class of control instruments or the specific instrument in a given class. A critical analysis or discussion of the comparative merits of different methods and different instruments is carefully avoided by the author. In fact, he states, "I do not compare instruments of different manufacturers since this cannot readily be done except in terms of a specific application." And, yet, it is just such critical evaluations which are required in practice and which must be made by process control groups for specific applications.

The value of this book could be enhanced greatly by adding chapters on the theoretical and practical bases for selection of a particular analytical method, on the general methods of adapting and modifying available equipment for specific applications, and on the similarities and differences between the listed instruments. Such treatment, coupled with elimination of repetitious material, would elevate the book from catalog to handbook and reference level.

Joseph Greenspan

Electrolytic Conductance, by Raymond M. Fuoss and Filippo Accascina. Published by Interscience Publishers, Inc., New York, 1959. ix + 279 pages; $8.00.

Many textbooks on physical chemistry give a creditable derivation of the Debye-Hückel equations for ionic activity coefficients. Few of them do more than discuss the various factors which enter into the treatment of conductance, eventually remarking that the constants of the Debye-Hückel-Onsager equation can be calculated from theory. This book shows why such is the case: conductance is a nonequilibrium process, the treatment of which requires more mathematical knowledge and ability than most graduate students of chemistry can muster easily, and also requires long and tedious manipulation which is dull and uninspiring to most students (and teachers). The authors state that the book was planned as a source book for part of a course on electrochemistry for first-year graduate students. This reviewer cannot recommend it for that purpose except for a very few well-prepared students. It may be more appropriate for some advanced groups which have special incentives to study it carefully.

The material included here has been scattered throughout the literature, and a prime purpose of the book was to make the story available in one logical sequence. The authors have succeeded admirably in their presentation of a fascinating tale. Most of the pages are devoted to mathematical development of the conductance equations, but many readers will find it worth while just to follow the interspersed story. It

is pointed out that the Onsager equation $\Lambda = \Lambda_0 - (\alpha \Lambda_0 + \beta) C^{1/2}$ does not apply to any real data but is the correct tangent to the conductance curve at $c = 0$. The Fuoss-Onsager equation $\Lambda = \Lambda_0 - Sc^{1/2} + Ec \log c + Jc$ is based on exactly the same theory but uses the ion size (the crystallographic value may be used), and includes satisfactory approximations of the "horribly complicated functions" encountered so that the equation fits real experimental data, Λ_0 being the only parameter which must be estimated from the data.

It is disappointing to learn that this equation, the culminating result of years of study, or its modified forms when ion pairs or covalent molecules are present, cannot be expected to hold if κa exceeds 0.2, or c exceeds 2×10^{-4} D for 1, 1 salts, which means about $0.016N$ in water or lower values in other solvents. The authors argue that at higher concentrations the Debye-Hückel model is no longer valid; the distance $1/\kappa$ is less than 4 or 5 ionic diameters and the Boltzmann distribution is too simple. Application to 2, 2 salts is limited to much lower concentrations, and unsymmetrical electrolytes cannot even be treated. The authors consider that the next breakthrough in conductance must come by way of fused salts, where nearest neighbors are about one ionic diameter apart; followed by a study of gradual dilution with solvent.

While introductory chapters are entitled Electrostatics and Vectors, Hydrodynamics, Statistical Mechanics, and Thermodynamics, these are the briefest of reviews, serving only to call attention to portions of these topics which are used later. It is too bad that a glossary of symbols is not included; the book cannot be read at one sitting, and the memory needs refreshing. Unfortunately, some symbols have several meanings: f may mean function, activity coefficient or even mole fraction; γ is used for activity coefficient here, fraction dissociated there; ρ usually means electrical density, but may mean distance.

The last chapters deal with ion association, starting with Bjerrum's crude but clever treatment and the classic work of Kraus and Fuoss published in 1933. On page 263, we find the conclusion that ion clustering of high degree must occur at low dielectric constant until in the limit the system will separate into two phases, one of practically pure electrolyte, the other of practically pure solvent. It is comforting to find this modern theoretical explanation of something which most chemists approach from the opposite direction—salts are insoluble in nonpolar solvents! It is, however, surprising that the authors do not cite the experimental findings of very high molecular weights for salts in solvents of low dielectric constant.

Cecil V. King

Tantalum and Niobium, by G. L. Miller. Published by Butterworths Scientific Publications, London. 767 pages; price, 120 shillings.

Until this new monograph was published, information on tantalum and niobium was scattered between some old textbooks and some new symposia. Now, Miller, the author of a well-known book on zirconium, has sorted out the existing material and presented it in coherent and masterly fashion. In addition, he has not hesitated, as a producer of these metals, to present his own opinions, even at the risk of mistakes.

The monograph comprises 12 chapters with the following titles and number of pages: History and Occurrence (17), Consumption and Uses (50), Extraction from the Ores (23), Separation and Purification (89), Production (66), Consolidation (74), Fabrication (28), Physical and General Properties (50), Mechanical Properties (35), Corrosion (113), Alloy Systems (162), plus an appendix on chemical analysis, metallography, and thermodynamic data. The literature data are as complete as needed for the description, and the author does not feel any language barrier, as Americans frequently do, in discussing his foreign references.

It is comforting to find a writer who cares for the history of a metal. Miller does, and, with a few exceptions, reports the individual advances and names of the investigators correctly. He omits to mention the final failures of tantalum when tried out as filaments in incandescent lamps, in surgical instruments, in fountain pens, and battery chargers. Also, the historical review of arc melting could be expanded somewhat.

In the chapter on uses, the main advantage of niobium over titanium in steel welds has not been stressed. The much more active titanium burns out rapidly, while niobium is protected to a large extent by silicon and manganese.

The chapters on ore extraction and separation-purification would be easier to understand if better organized. The author should have summarized the chemical properties as an introduction in a separate section. As it is, there are more than 200 pages on physical metallurgy, while the chemistry is dispersed in the text concerned with extraction and separation.

The most important steps in the extraction, purification, reduction, sintering, and melting of both metals are quite adequately reported. This concerns the Marignac and liquid-liquid separation, the fusion electrolysis and the sodium reduction of tantalum double fluoride, the carbide reduction of niobium oxide, the requirements and equipment for vacuum sintering, the results obtained in this operation as to purification as well as in electron beam melting. Possible alternatives are discussed, perhaps even too extensively, and the author evidently enjoys presenting the case in detail. The huge work on alloys and equilibrium diagrams, taken from the literature, is very well condensed.

In writing a book of this kind, an author has to make choices and to decide on the allocation of space to various topics. In doing so, Miller has fortunately not followed too far the modern line of cramming the text with physical chemistry. He has broadly described methods, equipment, and techniques. Thanks to this, his book is most interesting reading and it should not be omitted from the library of anybody working with rare metals.

W. J. Kroll

Notice to Members and Subscribers
(Re Changes of Address)

To insure receipt of each issue of the JOURNAL, please be sure to give us your old address, as well as your new one, when you move. Our records are filed by states and cities, not by individual names. The Post Office does not forward magazines.

News Items

New ECS Sustaining Members

The following recently became Sustaining Members of The Electrochemical Society:

American Smelting and Refining Co., Central Research Labs., South Plainfield, N. J.

Radio Corp. of America, RCA Victor Record Division, Indianapolis, Ind.

Tungsten for High-Temperature Coatings

High-purity tungsten now can be plated easily on metal surfaces by using a vapor deposition process which the National Bureau of Standards[1] has developed for the Navy. The method, devised by W. E. Reid and Abner Brenner of the Bureau's electrodeposition group, involves reducing gaseous tungsten hexafluoride with hydrogen by passing it over the heated object to be plated. At temperatures above 300°C, tungsten is deposited on the hot surface, and the only other reaction product, hydrogen fluoride, passes out with the excess of hydrogen.

Method

Tungsten hexafluoride was selected for use in the vapor deposition process for two reasons. First, the compound is a gas at room temperatures and therefore convenient to use. Second, tungsten apparently forms only one compound with fluorine—WF_6. Thus, the reactions are straightforward, uncomplicated by many products or side reactions.

The object to be plated is placed inside a cylinder of ceramic material and the air pumped out and replaced by hydrogen. A controlled temperature induction furnace heats this object to about 650°C. Then the two gases, tungsten hexafluoride and hydrogen, are passed through ordinary glass flowmeters into the reaction chamber. When the gaseous mixture comes in contact with the heated object, tungsten is deposited on the hot surface. The by-product of this reaction, hydrogen fluoride, is absorbed in a suitable trap.

Nature of the Deposit

Spectrochemical examination shows that the tungsten obtained by vapor deposition is purer than ordinary commercial tungsten. Silicon is the only impurity present in a concentration of 0.1% or more. Then, too, the deposited metal has the theoretical density of pure tungsten, 19.3 g/cm,[3] which is higher than that of tungsten compacts produced by powder metallurgy or by flame spraying. The hardness of the deposits obtained at 650°C is about 475 VHN or about the hardness of ordinary commercial tungsten.

The adhesive bond between the tungsten coating and various basic materials was investigated. Adhesion to molybdenum and to nickel was good; to copper, somewhat weaker; and to iron, rather poor. The tungsten-graphite bond was about as strong as the graphite itself. Tungsten deposited on ceramics also showed good bonding.

Deposits 1/16 in. thick were obtained by vapor deposition in 1 hr. The maximum thickness of deposit that can be obtained by the vapor method has not been determined, but would depend on the permissible roughness of the surface. Because of the rapidity of deposition, this process lends itself to the continuous production of tungsten-coated strips or wires.

[1] A similar method has been developed independently by the Bureau of Mines.

National Electronics Conference Call for Papers

The National Electronics Conference will be held at the Hotel Sherman, Chicago, Ill., on October 10, 11, and 12, 1960.

Authors of papers are invited to submit abstracts of 100-150 words (for publication in program) and either a 400 or 500 word summary or the completed paper for review. Please submit papers by May 1, 1960 to: Professor Thomas F. Jones, Jr., NEC Program Chairman, School of Electrical Engineering, Purdue University, Lafayette, Ind.

In addition to receiving the NEC Proceedings, authors of accepted papers are eligible for an annual NEC Award of $500.

Technical areas typical of those covered at the Conference include: adaptive servomechanisms; antennas and propagation; audio; circuit theory; communication systems; computers; information theory; instrumentation and telemetry; masers; microminiaturization, microwaves; millimeter waves; parametric amplifiers; plasma research; radar and radio navigation; radio astronomy; servomechanisms; signal-matched filters; solid-state circuits; solid-state devices and materials; space electronics, communications, and navigation; television; transistors; value engineering.

M.I.T. to Conduct Fundamental Research in Materials Sciences

Extensive fundamental research in the materials sciences will be conducted at the Massachusetts Institute of Technology under two grants, totaling $599,200, announced recently by the National Science Foundation.

At a time of increasing space age demands for new materials, the research is expected to provide resources in basic knowledge from which to create advanced working substances.

The studies will be carried out through collaboration of several branches of science and technology in the new Laboratory of Chemical and Solid State Physics, a group specially created at M.I.T. for research in the materials sciences.

In scope, the new work will be encompassed in the larger modern concept of materials and materials research held by scientists today. Of concern are those substances—such as metals, concrete, textiles—commonly thought of as applicable to structures or fabrics, as well as unusual metals and alloys, single crystals, ceramics, and compounds that have useful electrical, magnetic, and other properties. Transistors and plastics are two products of the new study of materials.

The M.I.T. work will be directed by Dr. John C. Slater, Institute professor and director of the Laboratory of Chemical and Solid State Physics. Staff members from the physics, metallurgy, chemistry, and mechanical engineering departments will participate in the work.

Glidden Co. Lectures in Chemistry to be Continued

Continuation of a lecture program in chemistry at several of the nation's top colleges and universities has been announced by Dr. William von Fischer, vice-president in charge of research for The Glidden Co.

Established three years ago to stimulate a greater interest in chemistry and chemical engineering, the program, known as "The Glidden Company Lectures in Chemistry," has been so enthusiastically received that Glidden will continue this activity during the current academic year. Lectures will be sponsored at the Johns Hopkins University, University of Florida, University of Minnesota, Lehigh University, Polytechnic Institute of Brooklyn, and Case Institute of Technology. Speakers, topics, and dates will be announced later by the individual schools.

Some of the lecturers in previous years have been Professor Linus Pauling of California Institute of Technology, Professor George B. Kistiakowsky of Harvard, Dr. Paul J. Flory of Mellon Institute, and Professors M. J. S. Dewar and C. K. Ingold of the University of London.

Alcoa and Westinghouse Develop New High-Capacity Silicon Rectifier

A three-year joint effort by Aluminum Co. of America and Westinghouse Electric Corp. has resulted in the development of a compact ac-to-dc silicon conversion unit believed to have greater efficiency and to offer more power output for its size

than any other large silicon rectifying equipment in the world.

Over-all efficiency of the new unit exceeds 97%. Use by the aluminum industry of the new unit would permit the production of up to 4% more primary aluminum per unit of electricity consumed.

Rated 10,000 amp at 600 v, the unit is comparable in physical size to previous silicon rectifiers having only half the output. The new high-capacity rectifier delivers 6000 kw of power from only 312 silicon cells, considerably more power per cell than ever before obtained in large silicon rectifiers.

Use of high-efficiency rectifying devices in the new unit reduced the number of cells needed to build the rectifier, and eliminated the need for elaborate apparatus to discharge heat generated by the ac-to-dc conversion. As a result, Westinghouse was able to contain the equipment in a cubicle measuring only 9 ft wide by 5 ft deep by 10 ft high. The unit requires about one third as much floor space as other types of rectifying equipment having similar ratings.

The 10,000-amp rectifier has been installed at Alcoa's Badin, N. C., smelter, where it is supplying power for the aluminum smelting process. A prototype 5000-amp silicon rectifier built by Westinghouse has been successfully operated at Badin since early 1958. Operating experience with this prototype unit provided technical background for development of the present design.

In addition to being a new tool for the aluminum industry, the rectifier represents the most comprehensive use of aluminum to date in the construction of large rectifiers. Approximately 60% of the entire weight of the assembled rectifier is Alcoa aluminum; uses include all conductors, heat sinks, hardware, and the cubicle enclosure. Among the advantages provided by this extensive use of aluminum was a reduction in weight commensurate with the reduced size of the unit.

Joint participation by Alcoa and Westinghouse to advance the science of the generation and rectification of electrical energy began in the 1880's. Alcoa used the world's first rotary converter, designed by George Westinghouse and built in 1890. The ignitron mercury-arc rectifier also was devised by Westinghouse and first used by Alcoa.

Ionics, Inc., to Build New Plant in Waltham, Mass.

New headquarters offices and manufacturing and research facilities for Ionics, Inc., will be constructed on a 7¾-acre site in Waltham, Mass., it was announced recently by Edwin R. Gilliland, president of the corporation.

"Preliminary land development to accommodate an 80,000-square-foot building is expected to begin soon, with plant construction scheduled to start in late 1960," he said. "The new plant will provide for expansion of production and research and development activities made necessary by a rapidly increasing work load."

The company is the world's largest producer of "electric membrane" plants which remove minerals or "desalt" brackish water to make it fit for human consumption. More than 40 such installations are now in operation around the world. Ionics' research division also holds many government and private industry research and development contracts in the fields of atomic energy, chemistry, and life support systems for submarines and manned space vehicles.

Vitro International to Design Radiation Laboratory in India

Vitro International, a division of Vitro Corp. of America, has been awarded a contract by the Indian Government for the design of a $4,000,000 high-level radiation laboratory at Trombay, India.

The laboratory, to be located at the Indian Atomic Energy Dept. nuclear center, will have more than 100,000 square feet of floor area. It will be one of the largest integrated radioactive research facilities in the world.

Edward D. Stone has been retained by Vitro to act as architectural consultant for the radiation laboratory. Mr. Stone designed the United States Pavilion at the Brussels World's Fair, the Museum of Modern Art (in association with Philip Goodwin), and the United States Embassy building in New Delhi.

The radioactive laboratory will include facilities for radiochemistry, radioisotope, and hot-metallurgy operations. A special feature will be a number of hot-cell areas for radiation experiments with plutonium and other highly toxic materials. Special shielding windows will provide for safe observation of experiments. Master slave manipulators will be installed for remote operations with radioactive materials and and a remote-operated overhead crane provided for transfer of materials from cell to cell. Movable dust control doors will be provided between the cells. Maintenance, service areas, laboratories, and offices will be included in the facility.

Allis-Chalmers Produces Film on Fuel Cell

A new 16-mm 7-min sound color film describing work involved in obtaining electrical energy from fuel cells has been produced by the Allis-Chalmers audio-visual section.

The film shows Allis-Chalmers researchers as they tested and hand-built the fuel cell equipment first applied in a tractor for demonstration purposes.

Although the basic theory of fuel cells has been known for 120 years, refinements of the original concept by Allis-Chalmers research laboratories has made practical this method of producing electricity from a chemical reaction.

Prints of the film, "The Fuel Cell

Brief Communications

The JOURNAL accepts short technical reports having unusual importance or timely interest, where speed of publication is a consideration. The communication may summarize results of important research justifying announcement before such time as a more detailed manuscript can be published. Consideration also will be given to reports of significant unfinished research which the author cannot pursue further, but the results of which are of potential use to others. Comments on papers already published in the JOURNAL should be reserved for the Discussion Section published biannually.

Submit communications in triplicate, typewritten double-spaced, to the Editor, Journal of The Electrochemical Society, 1860 Broadway, New York 23, N. Y.

Tractor," are available for showing before interested groups from Allis-Chalmers sales offices.

Announcements from Publishers

"Growth of Crystals, Vol. II," papers reporting Soviet research since the first Conference on the Growth of Crystals. Published by Consultants Bureau, Inc., New York, 1959. Clothbound; 189 figures, 12 tables, 229 literature citations; $16.00.

"Compilation of Standards on Electrical Insulating Materials, D-9." Published by American Society for Testing Materials, Philadelphia, 1959. Hard cover; 792 pages; $8.75.

"Thermoelectricity Abstracts," two volumes: PB 151657,* May 1959, 112 pages, $2.50; and PB 151810,* Aug. 1959, 81 pages, $2.25.

"Analytical Program for Processing Stainless Steel Uranium Dioxide Reactor Fuel Elements," Oct. 1959. AEC Report IDO-14493,* 24 pages; 75 cents.

"A Method of Specimen Corrosion Protection for High Temperature Creep Testing," Oct. 1959. AEC Report IS-48,* 17 pages; 50 cents.

"Electrolytic Disintegration of Zircaloy-2 in Nitric Acid Solutions," no date. AEC Report ORNL-2824,* 20 pages; 75 cents.

"Micro-Electrophoretic Determination of the Zeta Potential of Thorium Oxide," no date. AEC Report ORNL-2836,* 22 pages; 75 cents.

"Characterization of Surfactants in Aluminum-Uranium Fuel Reprocessing Solutions," Oct. 1959. AEC Report IDO-14489,* 21 pages; 75 cents.

"Sulfex Process: Depassivation of Stainless Steel," no date. AEC Report ORNL-2785,* 14 pages; 50 cents.

"Recovery of Uranium and Plutonium from Sulfuric Acid Decladding Solutions," no date. AEC Report ORNL-2830,* 68 pages; $1.50.

"Isomerization of Stilbenes," Sept. 1959. AEC Report UCRL-8883,* 117 pages; $2.50.

"Metal-Water Reactions: II—An Evaluation of Severe Nuclear Excursions in Light Water Reactors," June 1959. AEC Report GEAP-3178,* 34 pages; $1.00.

"Metal-Water Reactions: III—Fuel Element Stresses During a Nuclear Accident," July 1959. AEC Report GEAP-3191,* 25 pages; 75 cents.

"Electrodeposition of Plutonium at a Mercury Cathode," June 1959. AEC Report DP-388,* 13 pages; 50 cents.

* Order from Office of Technical Services, Business and Defense Services Administration, U. S. Dept. of Commerce, Washington 25, D. C.

Literature from Industry

Four-Layer Diode Multivibrator Circuits. Detailed information on the design and operation of high-speed flip-flop and multivibrator circuits employing four-layer diodes is given in Application Data publication No. AD-6.

Shockley Transistor Corp., Customer Engineering Dept., Stanford Industrial Park, Palo Alto, Calif., offers single copies of AD-6, additional information if desired, and suggestions on specific applications.

Porous Stainless Steel Filters. Revised literature, Release M-212A, on porous stainless steel filters is available. Included is information on properties of porous stainless steel. Full specifications are given on standard filters manufactured by the company, and a number of new filter types and sizes are presented.

For copies, write to Micro Metallic Div., Pall Corp., 30 Sea Cliff Ave., Glen Cove, N. Y.

"Magnetostriction in Cobalt and Cobalt Alloys." The introductory section of this 60-page compilation outlines the reciprocal and nonreciprocal mechanical and magnetic effects on ferromagnetic materials produced by magnetization. More than 125 references to magnetostriction effects in cobalt and cobalt alloys are listed, covering technical literature from 1874 through mid-1959.

The publication is available to persons who address requests on company letterhead to the Cobalt Information Center, c/o Battelle Memorial Institute, 505 King Ave., Columbus 1, Ohio. Requesters from abroad should write to Centre d'Information du Cobalt, 35 rue des Colonies, Brussels, Belgium.

Advertiser's Index

American Brass Company 96C
General Motors Research Laboratories 97C
Electric Storage Battery Company 111C
Great Lakes Carbon Corp., Electrode Division ..... Cover 2
National Carbon Company 111C
Republic Aviation 111C
E. H. Sargent & Company 92C
Stackpole Carbon Company ..... 93C and 111C
Sylvania Electric Products Inc. 95C
John Wiley & Sons, Inc. 98C

Employment Situations

Position Wanted

Chemical Engineers—M.S. Thirteen years' diversified experience in process and production control, assistant plant manager, process design, plant start-up, and trouble shooting in chloro-alkali industry. Desires responsible position in production or development. *Reply to Box 367, c/o The Electrochemical Society, 1860 Broadway, New York 23, N. Y.*

Positions Available

Three challenging research positions for experienced surface chemists in fully equipped laboratory devoted to research and development on aluminum and copper alloys involving:

—electrochemical kinetics, adsorption, and oxide film structure investigations related to finishing processes

—mechanisms of interfacial reactions of organics, solders, and brazes with metal and metal oxide surfaces

—mechanism of chemical and electrochemical reactions involved in corrosion of aluminum and copper alloys in various environments.

Pleasant living with access to major university. Interviews may be arranged for May ECS meeting. Reply to E. R. Patterson, Employment Manager, Olin Mathieson Chemical Corp., 125 Munson St., New Haven, Conn.

Research Chemist—Preferably with experience in electrochemistry, to work on theoretical and physicochemical aspects of nonaqueous electrolytes. Long-established company located near Philadelphia. *Reply to Box A-282, c/o The Electrochemical Society, 1860 Broadway, New York 23, N. Y.*

ELECTROCHEMICAL ENGINEER

Recent graduate with B.S. or M.S. in Chemical Engineering or Chemistry for technical service and product development on electrolytic anodes. Position requires strong interest in electrochemistry as well as an outstanding scholastic background.

After an initial assignment of one or two years with our research and development staffs, permanent job location will be New York City.

Send resumes to:
W. W. Palmquist,
National Carbon Company,
Division of Union Carbide Corporation,
P.O. Box 6087, Cleveland 1, Ohio.

UNION CARBIDE

MATERIALS TECHNOLOGIST

The Applied Research & Development Division of Republic Aviation has an important position available for a Senior Research Scientist. PhD preferred (MS acceptable) with record of accomplishment in bench-scale process and product development. Must be capable of conducting investigations and assuming supervision of laboratory programs for production of sample prototype quantities of advanced materials in these and similar areas: semiconductor refractories, phosphors, coating compositions, cermets and electro deposits.

Facilities at Republic are among the finest and include a new $14,000,000 Research Center in Farmingdale, Long Island, which is scheduled to open late this Spring. The Center will add a highly sophisticated environment making possible wider technical investigations, as well as stimulating entirely new avenues of scientific experiment.

Send resume in confidence to:
Mr. George R. Hickman
Technical Employment Mgr., Dept. 40-D
REPUBLIC AVIATION
Farmingdale, Long Island, New York

PHYSICIST or PHYSICAL CHEMIST

for Basic Research on
Electrical Contacts and Brushes

One of the country's oldest and largest manufacturers of carbon, graphite, & metal powder products has opportunity for top-ranking scientist in a fundamental field where professional activities and technical papers are encouraged.

Work involves surface phenomena and the fundamental physical processes associated with friction and commutation. Work will be done in association with Dr. Ragnar Holm, a leading authority on contacts, in fully-equipped, new labs.

Company offers the usual fringe benefits and enjoyable living in the mountains of Pennsylvania. School and hospital facilities are excellent. Any age or degree of experience will be considered and salary will be in proportion. All replies held in strictest confidence. Send resumes to:

Dr. E. I. Shobert, II, Mgr. of Research
STACKPOLE CARBON COMPANY
St. Marys, Pa.

Physical Chemist,
Electrochemist or Physicist

Required for Fundamental Research
in
Surface Chemistry
and
Electrochemistry

Must have Advanced Degree
(Ph.D. or M.S.)
Knowledge of Instrumentation and Electronics helpful

Dr. Paul Ruetschi, Head
Electrochemistry Division

The Carl F. Norberg Research Center
of
The Electric Storage Battery Company
19 West College Avenue
Yardley, Pennsylvania

Monographs of The Electrochemical Society

ECS Series

The following are books developed and sponsored by The Electrochemical Society and published by John Wiley & Sons, Inc., 440 Fourth Ave., New York 16, N. Y. Members of The Electrochemical Society can receive a 33 1/3% discount by ordering volumes from Society Headquarters, 1860 Broadway, New York 23, N. Y. Book and invoice will be mailed by John Wiley & Sons. Nonmembers (including subscribers) should order direct from Wiley.

Corrosion Handbook. Edited by Herbert H. Uhlig. Published 1948, 1188 pages, **$16.00**

Modern Electroplating. Edited by Allen G. Gray. Published 1953, 563 pages, **$8.50**

Abstracts of the Literature on Semiconducting and Luminescent Materials and Their Applications. Compiled by Battelle Memorial Institute.

Vol. I, 1953 Issue—published 1955, 169 pages, **$5.00** (soft cover)

Vol. II, 1954 Issue—published 1955, 200 pages, **$5.00** (soft cover)

Vol. III, 1955 Issue—Edited by E. Paskell; published 1957, 322 pages, **$10.00** (hard cover)

Vol. IV, 1956 Issue—Edited by E. Paskell; published 1959, 456 pages, **$12.00** (hard cover)

Vol. V, 1957 Issue—Edited by C. S. Peet; published 1960, 449 pages, In press

Electrochemistry in Biology and Medicine. Edited by Theodore Shedlovsky. Published 1955, 369 pages, **$11.50**

Vapor Plating (The Formation of Metallic and Refractory Coatings by Vapor Deposition), by C. F. Powell, I. E. Campbell, and B. W. Gonser. Published 1955, 158 pages, **$5.50**

High-Temperature Technology (Materials, Methods, and Measurements). Edited by I. E. Campbell. Published 1956, 526 pages, **$15.00**

Stress Corrosion Cracking and Embrittlement. Edited by W. D. Robertson. Published 1956, 202 pages, **$7.50**

Arcs in Inert Atmospheres and Vacuum. Edited by W. E. Kuhn. Published 1956, 188 pages, **$7.50**
(Papers Presented at the Symposium on Arcs in Inert Atmospheres and Vacuum of the Electrothermics and Metallurgy Division of The Electrochemical Society, April 30 and May 1, 1956, San Francisco, Calif.)

Technology of Columbium (Niobium). Edited by B. W. Gonser and E. M. Sherwood. Published 1958, 120 pages, **$7.00**
(Papers Presented at the Symposium on Columbium—Niobium of the Electrothermics and Metallurgy Division of The Electrochemical Society, May 15 and 16, 1958, Washington, D. C.)

The Structure of Electrolytic Solutions. Edited by Walter J. Hamer. Published 1959, 441 pages, **$18.50**
(Based on a Symposium held in Washington, D. C., in May 1957, sponsored by The Electrochemical Society, New York, and The National Science Foundation, Washington, D. C.)

Mechanical Properties of Intermetallic Compounds. Edited by J. H. Westbrook. Published 1959, 435 pages, $9.50
A Symposium, Sponsored by the Electrothermics and Metallurgy Division of The Electrochemical Society, May 4, 5, and 6, 1959, Philadelphia, Pa.)

Vacuum Metallurgy

Vacuum Metallurgy, third printing, 1958. Edited by J. M. Blocher, Jr.; 216 pages; **$5.00,** less a 20% discount to ECS members only. Available from Electrochemical Society Headquarters, 1860 Broadway, New York 23, N. Y.

(Papers Presented at the Vacuum Metallurgy Symposium of the Electrothermics and Metallurgy Division of The Electrochemical Society held in Boston, Mass., October 6 and 7, 1954)

The Electrochemical Society

Patron Members

Aluminum Co. of Canada, Ltd.,
Montreal, Que., Canada

International Nickel Co., Inc.,
New York, N. Y.

Olin Mathieson Chemical Corp.,
Niagara Falls, N. Y.
Industrial Chemicals Div., Research
and Development Dept.

Union Carbide Corp.
Divisions:
Union Carbide Metals Co.,
New York, N. Y.
National Carbon Co., New York, N. Y.

Westinghouse Electric Corp., Pittsburgh, Pa.

Sustaining Members

Air Reduction Co., Inc.,
New York, N. Y.

Ajax Electro Metallurgical Corp.,
Philadelphia, Pa.

Allen-Bradley Co., Milwaukee, Wis.

Allied Chemical & Dye Corp.
General Chemical Div., Morristown, N. J.
Solvay Process Div., Syracuse, N. Y.
(3 memberships)

Allied Research Products, Inc.,
Detroit, Mich.

Alloy Steel Products Co., Inc., Linden, N. J.

Aluminum Co. of America,
New Kensington, Pa.

American Metal Climax, Inc.,
New York, N. Y.

American Potash & Chemical Corp.,
Los Angeles, Calif. (2 memberships)

American Smelting and Refining Co.,
South Plainfield, N. J.

American Zinc Co. of Illinois,
East St. Louis, Ill.

American Zinc, Lead & Smelting Co.,
St. Louis, Mo.

American Zinc Oxide Co., Columbus, Ohio

M. Ames Chemical Works, Inc.,
Glens Falls, N. Y.

Auto City Plating Company Foundation,
Detroit, Mich.

Basic Inc., Maple Grove, Ohio

Bell Telephone Laboratories, Inc.,
New York, N. Y. (2 memberships)

Bethlehem Steel Co., Bethlehem, Pa.
(2 memberships)

Boeing Airplane Co., Seattle, Wash.

Burgess Battery Co., Freeport, Ill.
(4 memberships)

Canadian Industries Ltd., Montreal, Que.,
Canada

Carborundum Co., Niagara Falls, N. Y.

Catalyst Research Corp., Baltimore, Md.

Chrysler Corp., Detroit, Mich.

Ciba Pharmaceutical Products, Inc., Summit,
N. J.

Columbian Carbon Co., Brooklyn, N. Y.

Columbia-Southern Chemical Corp.,
Pittsburgh, Pa.

Consolidated Mining & Smelting Co. of
Canada, Ltd., Trail, B. C., Canada
(2 memberships)

Continental Can Co., Inc., Chicago, Ill.

Cooper Metallurgical Associates, Cleveland,
Ohio

Corning Glass Works, Corning, N. Y.

Diamond Alkali Co., Painesville, Ohio
(2 memberships)

Dow Chemical Co., Midland, Mich.

Wilbur B. Driver Co., Newark, N. J.
(2 memberships)

E. I. du Pont de Nemours & Co., Inc.,
Wilmington, Del.

Eagle-Picher Co., Chemical Div., Joplin, Mo.

Eastman Kodak Co., Rochester, N. Y.

Thomas A. Edison Research Laboratory, Div.
of McGraw-Edison Co., West Orange, N. J.

Electric Auto-Lite Co., Toledo, Ohio
C & D Division, Yardley, Pa.

Electric Storage Battery Co., Philadelphia, Pa.

Englehard Industries, Inc., Newark, N. J.
(2 memberships)

The Eppley Laboratory, Inc., Newport, R. I.
(2 memberships)

Erie Resistor Corp., Erie, Pa.

Exmet Corp., Tuckahoe, N. Y.

Fairchild Semiconductor Corp., Palo Alto,
Calif.

Food Machinery & Chemical Corp.
Becco Chemical Div., Buffalo, N. Y.
Westvaco Chlor-Alkali Div., South
Charleston, W. Va.

Foote Mineral Co., Paoli, Pa.

Ford Motor Co., Dearborn, Mich.

General Electric Co., Schenectady, N. Y.
Chemistry & Chemical Engineering
Component, General Engineering
Laboratory
Chemistry Research Dept.
General Physics Research Dept.
Metallurgy & Ceramics Research Dept.

General Instrument Corp., Newark, N. J.

(Sustaining Members cont'd)

General Motors Corp.
Brown-Lipe-Chapin Div., Syracuse, N. Y. (2 memberships)
Guide Lamp Div., Anderson, Ind.
Research Laboratories Div., Detroit, Mich.
General Transistor Corp., Jamaica, N. Y.
Gillette Safety Razor Co., Boston, Mass.
Globe-Union, Inc., Milwaukee, Wis.
Gould-National Batteries, Inc., Minneapolis, Minn.
Grace Electronic Chemicals, Inc., Baltimore, Md.
Great Lakes Carbon Corp., New York, N. Y.
Hanson-Van Winkle-Munning Co., Matawan, N. J. (2 memberships)
Harshaw Chemical Co., Cleveland, Ohio (2 memberships)
Hercules Powder Co., Wilmington, Del.
Hill Cross Co., Inc., New York, N. Y.
Hoffman Electronics Corp., Evanston, Ill.
Hooker Chemical Corp., Niagara Falls, N. Y. (3 memberships)
Hughes Aircraft Co., Culver City, Calif.
International Business Machines Corp., Poughkeepsie, N. Y.
International Minerals & Chemical Corp., Skokie, Ill.
ITT Laboratories, Nutley, N. J.
Jones & Laughlin Steel Corp., Pittsburgh, Pa.
K. W. Battery Co., Skokie, Ill.
Kaiser Aluminum & Chemical Corp.
Div. of Chemical Research, Permanente, Calif.
Div. of Metallurgical Research, Spokane, Wash.
Kennecott Copper Corp., New York, N. Y.
Keokuk Electro-Metals Co., Keokuk, Iowa
Libbey-Owens-Ford Glass Co., Toledo, Ohio
M. & C. Nuclear, Inc., Attleboro, Mass.
Mallinckrodt Chemical Works, St. Louis, Mo.
P. R. Mallory & Co., Indianapolis, Ind.
McGean Chemical Co., Cleveland, Ohio
Merck & Co., Inc., Rahway, N. J.
Metal & Thermit Corp., Detroit, Mich.
Minnesota Mining & Manufacturing Co., St. Paul, Minn.
Monsanto Chemical Co., St. Louis, Mo.
Motorola, Inc., Chicago, Ill.
National Cash Register Co., Dayton, Ohio
National Lead Co., New York, N. Y.
National Research Corp., Cambridge, Mass.
National Steel Corp., Weirton, W. Va.
New York Air Brake Co., Kinney Vacuum Div., Boston, Mass.
Northern Electric Co., Montreal, Que., Canada
Norton Co., Worcester, Mass.
Olin Mathieson Chemical Corp., Niagara Falls, N. Y.
High Energy Fuels Organization (2 memberships)
Peerless Roll Leaf Co., Inc., Union City, N. J.
Pennsalt Chemicals Corp., Philadelphia, Pa.
Phelps Dodge Refining Corp., Maspeth, N. Y.
Philco Corp., Philadelphia, Pa.
Philips Laboratories, Inc., Irvington-on-Hudson, N. Y.
Pittsburgh Metallurgical Co., Inc., Niagara Falls, N. Y.
Poor & Co., Promat Div., Waukegan, Ill.
Potash Co. of America, Carlsbad, N. Mex.
Radio Corp. of America
Tube Div., Harrison, N. J.
RCA Victor Record Div., Indianapolis, Ind.
Ray-O-Vac Co., Madison, Wis.
Raytheon Manufacturing Co., Waltham, Mass.
Reynolds Metals Co., Richmond, Va. (2 memberships)
Rheem Semiconductor Corp., Mountain View, Calif.
Schering Corporation, Bloomfield, N. J.
Shawinigan Chemicals Ltd., Montreal, Que., Canada
Speer Carbon Co.
International Graphite & Electrode Div., St. Marys, Pa. (2 memberships)
Sprague Electric Co., North Adams, Mass.
Stackpole Carbon Co., St. Marys, Pa.
Stauffer Chemical Co., New York, N. Y.
Sumner Chemical Co., Div. of Miles Laboratories, Inc., Elkhart, Ind.
Sylvania Electric Products Inc., Bayside, N. Y. (2 memberships)
Tennessee Products & Chemical Corp., Nashville, Tenn.
Texas Instruments, Inc., Dallas, Texas
Three Point Four Corp., Yonkers, N. Y.
Titanium Metals Corp. of America, Henderson, Nev.
Tung-Sol Electric Inc., Newark, N. J.
Udylite Corp., Detroit, Mich. (4 memberships)
Universal-Cyclops Steel Corp., Bridgeville, Pa.
Upjohn Co., Kalamazoo, Mich.
Victor Chemical Works, Chicago, Ill.
Western Electric Co., Inc., Chicago, Ill.
Wyandotte Chemicals Corp., Wyandotte, Mich.
Yardney Electric Corp., New York, N. Y.